New luminescent iridium (III) complexes containing NCN cyclometallated ligands: synthesis, photophysical properties and emission tuning

PIERPAOLO BRULATTI

New luminescent iridium (III) complexes containing NCN cyclometallated ligands: synthesis, photophysical properties and emission tuning

Pierpaolo Brulatti

Department of Chemistry
University of Durham

A thesis submitted in part-fulfilment for the degree of Doctor of Philosophy

2010

Abstract

New luminescent iridium(III) complexes containing N^C^N cyclometallated ligands: synthesis, photophysical properties and emission tuning

Pierpaolo Brulatti

The luminescence properties of cyclometallated iridium(III) complexes render them of interest, for example, as phosphorescent dopants in organic light-emitting devices (OLEDs), as photoactive units in solar energy conversion, and as biosensors. The vast majority comprise three bidentate ligands, archetypal examples being $Ir(ppy)_3$ and $[Ir(ppy)_2(bpy)]^+$ (ppy = 2-phenylpyridine; bpy = 2,2'-bipyridine).

The work described here explores the chemistry of iridium(III) complexes that contain a *terdentate* cyclometallating ligand. Most of the complexes studied have the general formula Ir(N^C^N)(N^C)X, where N^C^N represents a terdentate ligand based on 1,3-di(2-pyridyl)benzene; N^C a bidentate ligand such as ppy; and X is a monodentate ligand such as chloride, cyanide, thiocyanate or an acetylide. The synthetic methodology developed involves reaction of the N^CH^N proligand with iridium(III) chloride to give a dimer of the form $[Ir(N^C^N)Cl(\mu\text{-}Cl)]_2$, which is cleaved upon treatment with a bidentate N^CH ligand. The one remaining chloride ligand can then be exchanged for other monodentate ligands through silver-catalysed metathesis.

Most of these complexes are highly luminescent, with quantum yields in degassed dichloromethane at room temperature between 0.2 and 0.9. The effect of substituents in both the aryl and pyridyl rings of the terdentate and bidentate ligands has been investigated, together with the influence of X. The emission energy has been shown to vary over a very wide range, from the blue to red regions (λ_{max} = 456 to 667 nm). The trends have been partially rationalised using time-dependent density functional theory and cyclic voltammetry. Some complexes have been incorporated into multi-layer OLEDs that display unusually high efficiency, particularly for the red-emitting devices.

Selected rhodium(III) analogues have been prepared, together with related iridium(III) complexes incorporating bidentate N^N (bpy) ligands. A preliminary investigation into the utility of these complexes for the construction of multimetallic assemblies has been made, through the introduction of bridging ligands into position X.

Declaration

The work described herein was carried out in the Department of Chemistry at the University of Durham between October 2006 and December 2009. This thesis is the work of the author, unless otherwise stated, and no part of it has been submitted for a degree at this or any other university.

Statement of Copyright

Acknoledgments

Firstly my most sincere thanks are for my supervisor Dr. Gareth Williams for his guidance, encouragement and help for all the duration of my PhD.

I also must thanks the Depatment of Chemistry, Durham University and the EPSRC for the financial support support for this work.

A special thanks to all the present and past members of William's group, in particular, Will, Lisa, Louise, Stephanie, Victoria, Gemma, James and all the 4th years students of the last years who have worked with us.

The staff in the chemistry department, stores, the glass blowers, the workshops and the lab technicians. All the services, in particular the Dr. Alan Kenwright and all the staff of the NMR service, Dr. Mike Jones, Jackie Mosely and Lara Turner for mass spectrometry, Jarika Dorstal and Judith Magee for elemental analysis. Dr. Massimo Cocchi and Dr. Valeria Fattori for the OLEDs and the period spent in CNR in Bologna.

Most of all I thank my mother for all the support and love that she gave me during her life and my father for his love and the constant encouragement to achieve my goals. All my best friends in Italy: Paco, Giorgio, Giacomo, Maurizio, Marco e Daniela. I also want to thank the wonderfull people that I have met in my time in Durham and during these years, specially Armindo, Maddalena, Elena, Pavlos, Andrea, Reyes, Vanessa, Alvaro, Michele, Nick, Silvia, Maria, Matt, Claude-Stephanie.

Table of contents

Chapter 1 **1**

1. Introduction **2**

1.1 Luminescence in metal complexes **3**

1.1.1 Absorption 3

1.1.2. Charge transfer transitions 5

1.1.3. Emission 6

1.1.4. Fluorescence 8

1.1.5. Phosphorescence 8

1.2 Coordination complexes containing polypyridyl ligands **9**

1.2.1. Ruthenium(II) complexes with bidentate polypyridyl ligands 9

1.2.2. Ruthenium (II) complexes with terdentate polypyridyl ligands 11

1.2.3. Ruthenium(II) complexes containing cyclometallated ligands 13

1.3. Iridium(III) complexes **14**

1.3.1. Iridium polypyridyl complexes 15

1.3.1.1. Iridium(III) complexes with two bidentate (N,N) ligands, $[IrL_2Cl_2]^{n+}$ 15

1.3.1.2. Iridium(III) complexes with three bidentate (N,N) ligands, $[IrL_3]^{n+}$ 17

1.3.1.3. Iridium(III) complexes with one terdentate ligands (N,N,N) ($IrLCl_3$ species) 18

1.3.1.4. Iridium(III) complexes with two terdentate ligands (N,N,N) ($[IrL_2]^{3+}$ species) 19

1.3.2. Iridium complexes containing bidentate cyclometallating ligands 24

1.3.3. Iridium complexes containing terdentate cyclometallating ligands 27

1.4. Nature of excited states in Iridium Cyclometallated Complexes and their modifications **30**

1.4.1. Emission tuning 31

1.4.1.1. Yellow and red-shifted emission 32

1.4.1.2. Blue-shifted emission 35

1.5. Applications of luminescent metal complexes **38**

1.5.1. OLED applications 39

1.5.2. Oxygen sensing 44

1.5.3. Solar energy harnessing and photocatalytic water splitting 45
1.5.4. Bioanalytical applications 46
1.5.5. Light-emitting Electrochemical Cells (LECs) 46
1.6. Rhodium complexes 48

Chapter 2 51
Synthesis of mononuclear Iridium(III) and rhodium(III) complexes 52
2.1 Background and objectives of the work 52
2.2. Synthesis of Ligands 58
2.2.1. Synthesis of terdentate N^C^N ligands 58
2.2.1.1. Synthesis of N^C^N ligands via Stille cross-coupling 61
2.2.1.2. Synthesis of N^C^N ligands via Miyaura cross-coupling 66
2.2.2. Synthesis of bidentate N^C ligands 70
2.3. Synthesis of iridium complexes 72
2.3.1. Synthesis of intermediate iridium di-chlorobridged dimers 72
2.3.2. Synthesis of Ir(N^C^N)(N^C)Cl complexes 73
2.3.2.1. X-ray crystallography 82
2.3.2.2. Synthesis of complexes Ir(N^C^N)(N^C)Cl with substituents on the pyridyl rings of the ligands 86
2.3.2.3. Synthesis of Ir(N^C^N)(ppyz)Cl 89
2.3.3. Synthesis of $[Ir(N^C^N)(N^N)Cl]^+$ complexes 90
2.3.4. Synthesis of $[Ir(N^C^N)(N^C^N)']^+$ complexes 92
2.3.5. Complexes with pyridylbenzimidazole as bidentate ligand, Ir(N^C^N)(pbi)Cl and $[Ir(N^C^N)(Me\text{-}pbi)Cl]^+$ 94
2.3.6. Metathesis reaction of monodentate ligand 102
2.4. Rhodium complexes 110
2.4.1. Synthesis of rodium di-chloro-bridged dimers 110
2.4.2. Synthesis of Rh(N^C^N)(N^C)Cl complexes 111
2.5. Concluding remarks 114

Chapter 3 116
3. Photophysics, electrochemistry, DFT and OLEDs 117
3.1. Ir(N^C^N)(N^C)Cl complexes 117
3.1.1. Theoritical studies based on DFT calculations 117

3.1.2. Electrochemistry 119
3.1.3. Ground state absorption 121
3.1.4. Emission from complexes in solution 121
3.1.5. Ir(N^C^N)(N^C)Cl complexes of series 1 and 2 in OLEDs, and photochemistry in polymer matrices 131
3.2. Strategies for further emission tuning of the Ir(N^C^N)(N^C)Cl complexes 136
3.2.1. Effect of the substituents in the pyridyl ring of the N^C^N ligand 137
3.2.2. Effect of substituents in bidentate ligands 145
3.2.3. Emission tuning through the ancillary ligand 150
3.2.3.1. Complexes Ir(N^C^N)(N^C)CN and Ir(N^C^N)(N^C)SCN 150
3.2.3.1.1. DFT calculations 150
3.2.3.1.2. Photophysical studies 151
3.2.3.2. Ir(N^C^N)(N^C)(acetylide) complexes 157
3.3. $[Ir(N^C^N)(N^N)Cl]^+$ complexes 160
3.3.1. DFT calculations and electrochemical studies of $[Ir(N^C^N)(N^N)Cl]^+$ complexes 160
3.3.2. Photophysical properties of $[Ir(N^C^N)(N^N)Cl]^+$ complexes 161
3.4. Ir(N^C^N)(pbi)Cl and $[Ir(N^C^N)(Mepbi)Cl]^+$ complexes 165
3.4.2. Photophysical studies 165
3.5. Concluding remarks 168

CHAPTER 4 170
4. Multimetallic complexes with cyclometallated Ir(III) units containing terdentateligands 171
4.1. Background and previous work 171
4.2. Synthesis of multimetallic complexes using acetylide and tetrazolate-based bridging ligands 178
4.2.1. Synthesis of the bridging ligands 179
4.2.2. Synthesis of homo-metallic dinuclear complexes 182
4.3. Electrochemistry and preliminary assessment of photophysical properties 187
4.3.1. Electrochemical studies 187
4.3.2. Ground state absorption 188

4.3.3. Emission and excited states 189
4.4. Concluding remarks 192

Chapter 5 193
5. Experimental 194
5.1. Synthetic procedures and characterisation 194
5.2. Photochemical and photophysical measurements 195
5.3. Electrochemical measurements 197
5.4. Density functional theory calculations 197
5.5. X-ray crystallography 197
5.6. Synthesis of bidentate ligands (N^C) 199
5.7. Synthesis of terdentate ligands (N^C^N) 207
5.8. Synthesis of bridging ligands 218
5.9. Synthesis of Iridium di-chloro bridged dimers 221
5.10. Synthesis of rhodium di-chloro bridged dimers 226
5.10. Synthesis of iridium complexes 229
5.11. $[Ir(N^C^N)(N^C^N)]^+$ and $[Ir(N^C^N)_2]^+$ complexes 245
5.12. Complexes with pyridylbenzimidazole as bidentate ligand 247
5.13. Ligand metathesis 252
5.14. Synthesis of Rhodium complexes 269
5.15. Synthesis of multimetallic complexes 272

Chapter 6 276
Bibliography 277

Abbreviations

A1	1,3-trifluoromethyl-phenylacetylide
A2	1-phenylacetylide
A3	1-(4-methoxy)phenylacetylide
A4	1-(4-dimethylamino)phenylacetylide
A5	1-(4-benzonitrile)acetylide
Abs	absorbance
AgOTf	Silver triflate
ASAP	Athmospheric Solids Analysis Probe
bphA	4,4'-diehynylbiphneyl
br-OMepy	2-bromo-4-methoxypyridine
brphtr	5-(2-bromophenyl)tetrazole
btiqH	2-(1-benzo[b]thiophene) iso-1-quinoline
btrph	4,4'-tetrazolylbiphenyl
bpy	2-2'-bipyridine
bpybH	1,3-di(2-pyridyl)benzene
COSY	correlation spectroscopy
CT	charge transfer
CTTS	charge transfer to solvent
dFppyH	2-(4,6-difluoro-phenyl)-pyridine
DCM	dichloromethane
DFT	density functional theory
dFpMepyH	2-(2,4-difluorophenyl)-4-methylpyridine
dFpOMepyH	2-(2,4-difluorophenyl)-4-methoxypyridine
dFppyH	2-(2,4-difluorophenyl)pyridine
$dinpyH_2$	2,6-bis(indolyl)pyridine
DME	1,2-dimethoxy ethane
DMF	dimethylformammide
DMSO	dimethyl sulfoxide
dpymbH	5-methyl-1,3-di(2-pyridyl)benzene
$E_{1/2}^{ox}$	half wave oxidation potential
$E_{1/2}^{red}$	half wave reduction potential

E^p	peak potential for irreversible processes
EI	Electron Ionisation
EPA	diethyl ether-isopentane-ethanol
ES	Electro Spray
H**L1**	1,3-di-(2-pyridyl)-4,6-dimethyl-benzene
H**L2**	1,3-di-(2-pyridyl)-4,6-di-fluoro-benzene
H**L3**	1,3-di-(2-pyridyl)-4,6-di-(trifluoromethyl)benzene
H**L4**	1,3-bis-(4-(trifluoromethyl)-2-pyridyl)-4,6-bis-(trifluoromethyl)benzene
H**L5**	1,3-di-(4-methoxy-2-pyridyl)-4,6-di-fluoro-benzene
H**L6**	1,3-bis(4-dimethylamino)pyridine-4,6-difluoro-benzene
HRMS	High Resolution Mass Spctrometry
HSQC	heteronuclear single quantum correlation
IC	internal conversion
ISC	intersystem crossing
ILCT	intra-ligand-charge transfer
ITO	indium tin oxide
$k_Q^{O_2}$	bimolecular rate constant for quenching by oxygen
k_r	radiative rate constant
LC	ligand-centred
LEC	Light Emitting Electrochemical Cells
LLCT	ligand-to-ligand-charge transfer
LMCT	ligand-to-metal-charge transfer
m-CPBA	m-chloro-peroxy-benzoic acid
MALDI	Matrix Assisted Laser Spectrometry
Mebib	bis(N-methylbenzimidazolyl)benzene
Me-pbi	2-(2-pyridyl-N-methyl)bezimidazole
MLCT	metal-to-ligand-charge transfer
MC	metal-centred
MO	molecular orbital
mp	melting point

MS	mass spectrometry
n-BuLi	n-butyl lithium
NMR	nuclear magnetic resonance
NOESY	nuclear Overhauser effect spectroscopy
OLED	Organic Light Emitting Device
phbpyH	6-phenyl-2,2'-bipyridine
phen	1,10-phenanthroline
PPV	poly (phenylenevynilene)
pbiH	2-(2-pyridyl)bezimidazole
pha	1-phenylacetylide
phtr	5-phenyltetrazole
pic	2-picolinic acid
ppyH	2-phenylpyridine
ppyz	1-phenylpyrrazole
S_0	ground singlet state
S_n	n^{th} excited singlet state
SBLCT	sigma-bond-to-ligand charge transfer
SOC	spin-orbit coupling
THF	tetrahydrofuran
TMSA	trimethylsilyl acetylide
tpy	2,2':6',2''-terpyridine
ttpy	4'-(*p*-tolyl)-2,2':6',2''-terpyridine
Φ_{lum}	emission quantum yield
λ_{max}^{em}	maximum emission wavelength
Σk_{nr}	sum of non-radiative rate constants
τ	emission lifetime

CHAPTER 1

INTRODUCTION

1. Introduction

The increased interest in studying and synthesising novel coordination compounds containing transiton metals is due to the wide range of possible applications that have been found which exploit their properties. "The metal-ligand interaction can lead to properties of dual nature, the metal-ligand synergy is weak enough to permit the presence of the intrinsic properties of metal and ligands simultaneously, but also strong enough to show new properties, characteristic of coordination compounds."[1] Particular attention is deserved to be given to the photochemical, photophysical and electrochemical properties of metal complexes containing conjugated ligands, which have attracted the attention of a large number of scientists over the past decades[2]. Of crucial importance in this field, being known since its early stages as *Inorganic Photochemistry*, is how metal complexes interact with visible and ultraviolet light, mainly but not exclusively in solutions and for a large number of cases at room temperature.[2]

A great deal of attention has been focused on complexes of transition metals with polypyridyl ligands, one of the first examples of investigation being $[Ru(bpy)_3]^{2+}$[2], which was reported in 1959 by Paris and Brandt. $[Ru(bpy)_3]^{2+}$ attracted interest primarily as an excited-state electron-transfer agent, before being largely studied as the main reference example of low-lying metal-to-ligand charge-transfer (MLCT). The reason for the popularity of this complex among inorganic chemists lies in the fact that it is easily prepared and relatively stable towards photodecomposition.[3] Moreover complexes containing polypyridyl and related cyclometallating ligands can display intense phosphorescence following excitation.[4]

New application, in light-emitting devices, luminescent probes and sensors rapidly evolved which maintained the interest in developing the knowledge of such kind of materials and, most likely, will be maintained in the future.[5] As anticipated, numerous efforts were made in investigating the properties and synthesising new complexes containing metal centres such as Ru(II), as well as Os(II) and Re(I).[6-9] Only more recently, interest has extended widely to other types of metals, such as

Rh(III), Ir(III), Pt(II) and Pd(II); nevertheless these too show very promising and in some cases superior photochemical and electrochemical properties.[10]

1.1 Luminescence in metal complexes

1.1.1. Absorption

Absorption of light by a molecule in the visible or ultraviolet regions results in formation of excited electronic states of the molecule. Each excited state has its own characteristic energy relative to the ground state. Atoms in their absorption spectra show very sharp lines, each of which is related to a transition to a different electronic state. In the case of polyatomic molecules, because of vibrational and rotational energy in every electronic state, we observe that absorption spectra manifest the transitions involved with a different appearance, as broad bands.[11] This can be explained considering that the Frank-Condon principle, in its classical form, states that since absorption is “instantaneous”, a molecule is formed in its excited state with the size and shape of its ground state, and therefore has vibrational excitation.[11] Since the nuclei are much heavier compared to the electrons, the electronic transition is much faster than the possible response of the nuclei.[12, 13] Therefore the size and shape of the molecule beeing different in each of the electronic states, according to the Frank-Condon principle, absorption is presented in the spectrum as broad bands[2, 14]. (Figure 1.1)

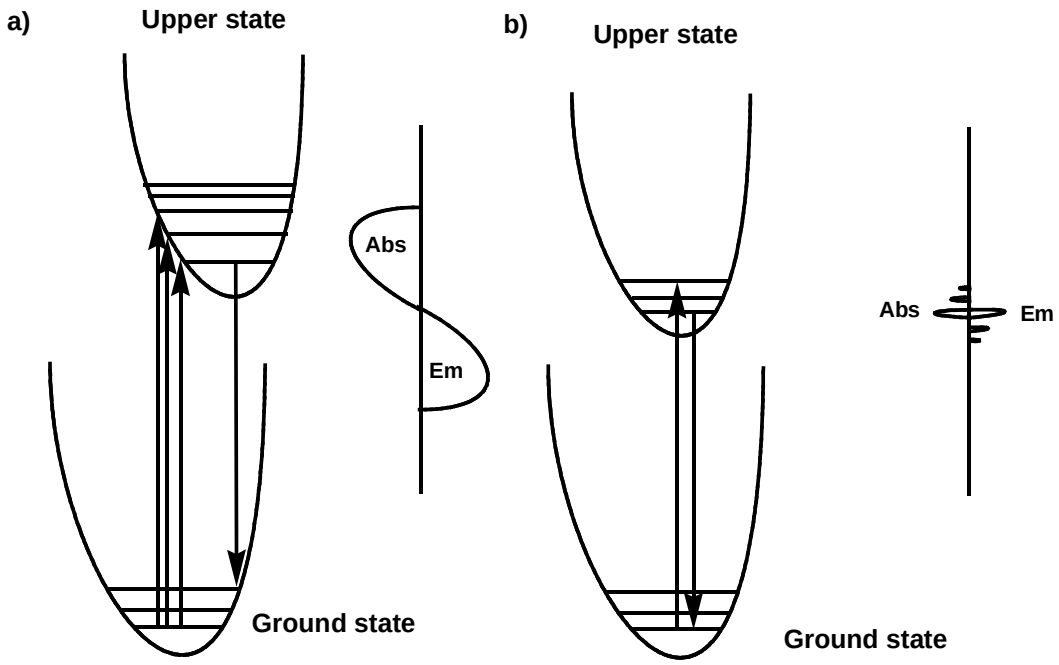

Figure 1.1: Franck-Condon effect for absorption and emission (a) for excited state and ground state having different internuclear distances and (b) for excited state and ground state of the same geometry and size.

In general terms absorption is defined by the Beer-Lambert law, which can be written as:

$$Abs = \log_{10}(I_0/I_t) = \varepsilon cl$$

In the above equation, Abs is the absorbance, *l* is the light path length through the absorbant material, *c* is the concentration of the absorbant. I_o and I_t are respectively incident and transmitted light intensities.[11] The molar exctinction coefficient is referred to as the molar absorptivity, a function of incident light. In absorption, extinction coefficients are related to the nature of the transition. If the transition is forbidden by the principles of quantum mechanics, the extinction coefficient results to be small. On the other hand, if the transition is allowed, the extinction coefficient is larger.[11] The integrated extinction coefficient for one band in the absorption spectrum is related to the probability of a transition from the lower ground state to the upper excited state. The reciprocal of the transition

probability is the lifetime of the upper state before it spontaneously reverts to the ground state by emitting a photon.

1.1.2. Charge transfer transitions

Metal complexes are susceptible to absorbtion of light, which in some cases may lead to the transfer of an electron (or at least negative charge) from the ligand to the d orbitals or from the d orbitals to the ligands. In these transitions, called cherge transfer, electrons move over a notable distance within the molecule. Since metal complexes have complicated electronic structures, the presence of both metal and ligand orbitals leads to a wide range of available excited states. Molecular orbitals (MOs) comprise of several atomic orbitals and can be described as being of predominantly metal or ligand character, depending upon which atomic orbitals have the most similar energy to the MO of interest.[15-17] When radiation is absorbed, an electronic transition between two molecular orbitals occurs and the resulting excited state can be characterised approximately by the molecular orbitals involved.[18] The assignment of the various bands which appear in the absorption spectra of transition metal complexes is often a very difficult task to solve because the absorption spectra reflect the complexity of the electronic structure of the molecule.[1] Charge transfer (CT) involves displacement of the electronic charge from the ligands to the metal or *vice versa* and can be itself of a number of types (Figure 1.2). In metal complexes the transitions that occur in absorption can often be classified to a first approximation as charge transfer, intraligand or metal centred.[19, 20] For example, metal to ligand charge transfer (MLCT) is an appropriate description when an electron is promoted from a *d* orbital of the metal to a π^* orbital of the ligand, or LMCT when the charge transfer can be regarded as an electronic transition from an orbital of the ligand to an orbital of the metal. Similarly electronic transitions can take place by promotion of an electron between two orbitals both localized on the ligand such as π-π^* transitions (LC, ligand-centred or intraligand transitions). Also metal centred transitions (MC) may be observed in which the participating MOs are localised predominantly on the metal centre and involve electron promotion between two orbitals of the metal.[2, 14] The transitions localised on the central metal ion are of the $d \rightarrow d$ type, usually observed in fluid solutions and relatively weak.[21]

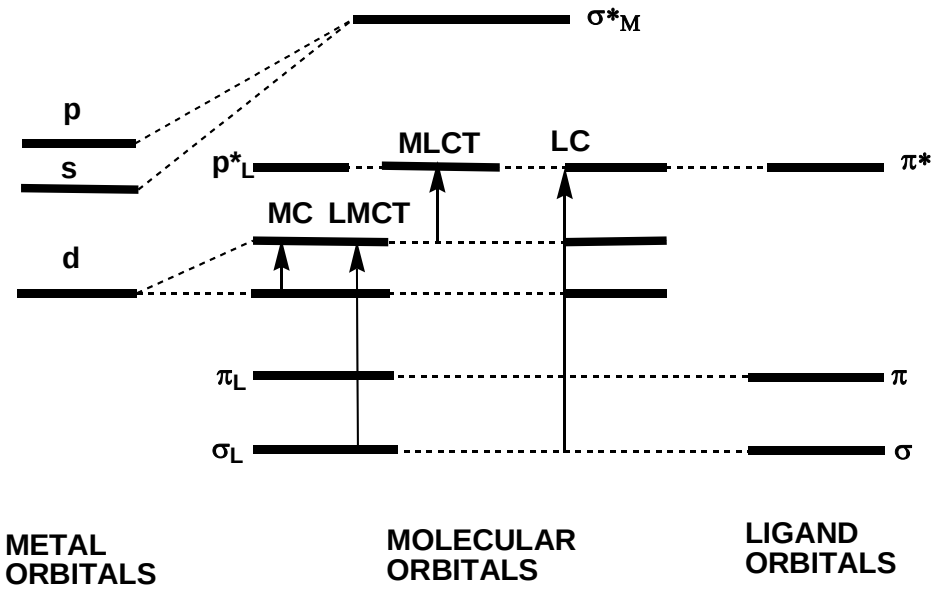

Figure 1.2: Schematic energy-level diagram for an octahedral transition metal complex. The various kinds of electronic transitions are also indicated.

Also some less frequently encountered types of transitions exist, including those that involve transitions from a metal centred orbital to an orbital localised on the solvent (*charge transfer to solvent,* CTTS) and *ligand-to-ligand charge transfer,* LLCT where the transition is betwen two orbitals localised on different ligands coordinated to the same metal centre.

1.1.3 Emission

The energy acquired by a molecule during the formation of an excited state can be released following different ways. The process of radiative decay involves the molecule dispersing its energy by emitting photons. A more common way consists instead of non radiative decay, when the excess of energy is transferred to other molecules as vibrational, rotational or translational energy, either within the same molecule or to other molecules or solvent in the local enviroment. Also thermal degradation can occur, in other words the energy can be trasfered to the

enviroment as heat. Molecules in their excited states can also take part in a variety of chemical reactions.

In order to observe emission by a molecule, excitation has to occur in the first place, in other words the excited state needs to be populated, and if the energy required comes from absorbed light, then the subsequent emission of a photon by a molecular system is referred as photoluminescence[22]. Upon absorption of a photon of light of suitable wavelength, an electron is promoted to a higher energy orbital, producing a singlet excited electronic state (S_n). This process, termed excitation, is denoted by the orbital that the electron originated from, and the orbital to which it is promoted, e.g. π–π *. In a singlet excited state (S_n); the orientation of the spin of the excited electron is anti-parallel to that of the ground state electron. According to Kasha's rule the excited molecule undergoes rapid relaxation via a non-radiative pathway to the lowest singlet excited state (S_1), this process is much faster than the competing radiative process.[23]

It is possible to identify two different types of emission. In Figure 1.3 these two different types of emission, termed phosphorescence and fluorescence, are schematically shown with a Jablonski diagram for a d^6 complex (e.g. Ir(III)).

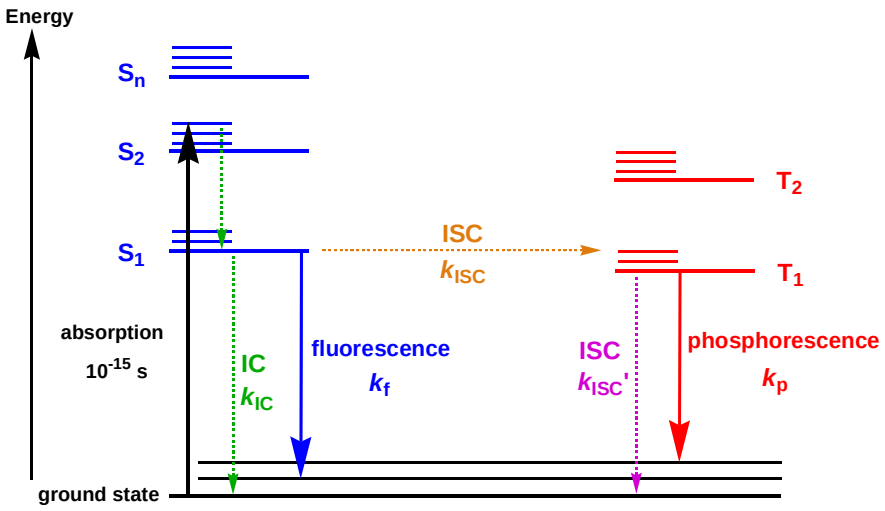

Figure 1.3[24]: processes involved in absorption and emission for d^6 complex (Ir(III)).

1.1.4. Fluorescence

Once the initial absorption promotes the molecule to its electronic excited state, the molecule can undergo internal conversion, which is a very fast non-radiative process that can occur for upper electronic excited states to revert spontaneously to lower excited states or to the ground state, the difference in energy being converted into vibrational energy and then to heat. It is called fluorescence when radiative relaxation from a S_n excited state to the singlet ground state S_0 occurs, in other words fluorescence is a process that does not involve a change in spin multiplicity (Figure 1.3). Fluorescence happens at lower frequencies compared to the exciting radiation because the emissive transition takes place after the energy is partially dispersed to the environment as vibrational energy. In fact many fluorescent materials absorb in the UV and blue region and emit in the visible region as green or orange light.

1.1.5. Phosphorescence

On the other hand, sometimes spontaneous crossing from the initially formed excited state to a second excited state of different spin occurs, a process named *intersystem crossing* (shown in figure 1.3).[25] Intersystem crossing occurs when the energy curve of the singlet and triplet excited states cross each other, therefore conversion from ↑↓ to ↑↑ of the electronic spins is possible and the molecule enters an excited triplet state.

The corresponding radiative transition back to the ground state, which is called *phosphorescence*, involves a change of spin quantum number. Being spin-forbidden, phosphorescence is normally characterized by a longer natural lifetime whilst non-radiative processes are much faster at room temperature. Triplet-singlet transitions become more favoured when spin-orbit coupling is relatively strong.[12], for example, in heavy metal complexes. Here, the process is accelerated by the strong spin-orbit coupling of the metal atoms that promotes the triplet-to-singlet transition by introducing a mixed character of singlet and triplet states and provoking a breakdown of the selection rules[2]. In this situation, the spin quantum number thus becomes an inaccurate description of the system, and

promotion of the spin-forbidden triplet-to-singlet radiative pathway increases the rate constant of phosphorescence to the point that it becomes competitive with the spin-allowed processes.[26] Since the triplet excited states are always lower in energy than singlet excited states according to Hund's rules, phosphorescent emission is lower in energy than the corresponding fluorescent emission.

The efficiency with which a compound emits light can be quantified in terms of the luminescence quantum yield, which is the number of photons that are emitted per photon absorbed by the system.

A metal complex in an excited state can also lead to a wide range of photochemical reactions due to the change in the electronic distribution caused by absorption. Thus the excited molecule is characterized by a different reactivity compared to that of the ground state situation, and a large number of processes caused by molecular excitation are known. For instance, the most common photochemical reaction for a complex is represented by replacement of a ligand by the solvent (e. g. water).[2]

1.2 Coordination complexes containing polypyridyl ligands

1.2.1. Ruthenium(II) complexes with bidentate polypyridyl ligands

$[Ru(bpy)_3]^{2+}$ (Figure 1.4) has certainly been one of the complexes containing polypyridyl ligands most extensively studied and most widely used in research laboratories.[27] Thanks to its stability, photochemical and redox properties, this complex has attracted the attention of many researchers, first on this molecule itself and then on several of its derivatives.[28-30] The great deal of interest in studying this class of complexes has stimulated the growth of several branches of pure and applied chemistry.[31-33] In particular, the Ru(II) polypyridine complexes have played a key role in the development of, not only photochemistry and photophysics, but also electrochemistry, photoelectrochemistry, chemi- and electrochemi-luminescence, and electron and energy transfer.

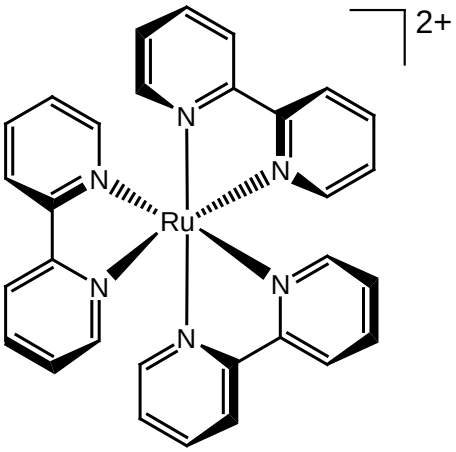

Figure 1.4: structure of $[Ru(bpy)_3]^{2+}$.

The synthesis of $[Ru(bpy)_3]^{2+}$ (Figure 1.4) was reported in 1959 by Paris and Brandt. The emission of $[Ru(bpy)_3]^{2+}$ was firstly assigned as being fluorescence from a singlet ^{1}MLCT, d→π*, excited state.[34] Only in a second instance was its emission described as spin-forbidden phosphorescence from a triplet ^{3}MLCT, d→π*, excited state. In fact deactivation of the upper excited states via non-radiative decay and the long luminescence lifetimes confirmed the latter assignment.[33, 35] The 2,2'-bipyridine ligand plays a role in the emission of the complex by acting as π-acceptor during the MLCT transitions due to the significant π backbonding between the Ru(II) and π * orbitals of bpy.[36]

The photochemical properties of polypyridyl Ru(II) complexes, but also the reversible oxidation of the metal and reduction of the ligand at accessible potentials, stability of the oxidation states and electronic stability in both the ground and excited state, allowed this class of complexes to offer the potential for a wide variety of applications as luminescent photosensitisers, photocatalysts and electron transfer reagents converting light to chemical energy.[27, 36-40] Another important feature of this class of complexes is the possibility of inserting ancillary ligands with adequate modifications, in order to modulate their properties. This aspect gives a fundamental importance to ligand design allowing a wide range of

different types of ligands to be part of the chemistry of the polypyridyl complexes of ruthenium.

1.2.2. Ruthenium (II) complexes with terdentate polypyridyl ligands

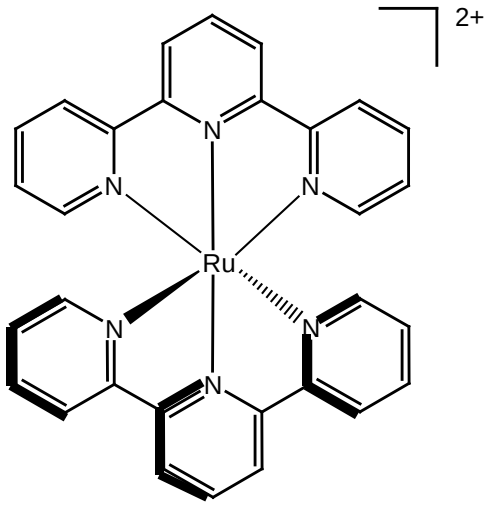

Figure 1.5: structure of $[Ru(tpy)_2]^{2+}$

Particularly advantageous, from a structural viewpoint at least, was the introduction of terdentate polypyridyl ligands in the coordination sphere of ruthenium polypyridyl complexes. Being achiral, complexes of the $[Ru(tpy)_2]^{2+}$ type present several synthetic and structural advantages over the chiral bpy-based systems.[41] Although tpy-based systems display less favourable photophysical properties, functionalisation on the 4' position of the terpyridine ligand opens up, together with their intrinsic achirality, the possibility of building linear arrays.[42-45] Even though intermolecular photochemical processes have been widely investigated and exploited, photoinduced processes in covalently-linked multicomponent systems are of great interest.[46, 47] Formation of multicomponent systems is achieved by assembly of suitable monometallic "building blocks". Complexes based on $[Ru(bpy)_3]^{2+}$ have been used, but are not geometrically ideal

due to their existence as a racemic mixture of Λ and Δ isomers. Thus when two or more complexes of this kind are linked together, stereoisomers are formed which are difficult to separate and may exhibit subtly different photophysical properties.[48, 49] The successful purification of geometrical isomers of monometallic ruthenium complexes, incorporating mono-functionalised bipyridine ligands, has achieved by selective precipitation from methylene chloride and preparative plate silica chromatography, as recently been reported by Fletcher *et al*. [50, 51] The isolation of such isomerically pure building blocks gives the possibility to investigate stereoselective synthesis of multicomponent systems.[24]

$[Ru(tpy)_2]^{2+}$ however is found to be not emissive at room temperature.[52] This can be explained by the weak ligand field splitting caused by the terpyridine ligands, allowing a favourable deactivation via non-radiative decay of the ^{3}MLCT to a higher-lying but a thermally accessible ^{3}MC level.[53, 54] Efforts were made to inhibit this non-radiative decay to the ^{3}MC level by attempting to increase the gap between the ^{3}MLCT and the ^{3}MC excited states. [55] (Figure 1.6) The strategies adopted to do so include the introduction of electron withdrawing groups in the 4' position of the terdentate ligand, more extended tpy-type ligands and the introduction of stronger σ-donor ligands such as cyclometallated ligands.[56-59]

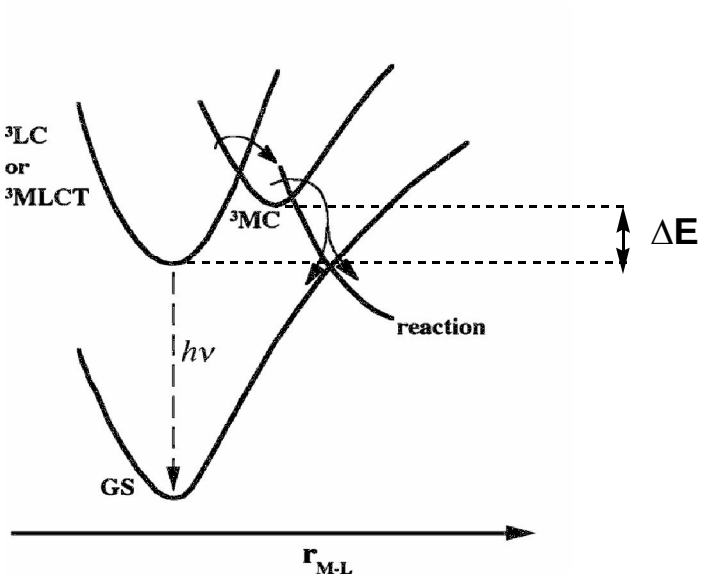

Figure 1.6[27]: Radiative versus non-radiative decay.

In order to avoid the non-radiative decay, successful notifications were made by Sauvage and collaborators in the 90s who found that $[Ru(4,4'\text{-dptpy})_2]^{2+}$ and $[Ru(tptpy)_2]^{2+}$ (Figure 1.7) were both emissive, in contrast to $[Ru(ttpy)_2]^{2+}$, which is non emissive at room temperature.[60]

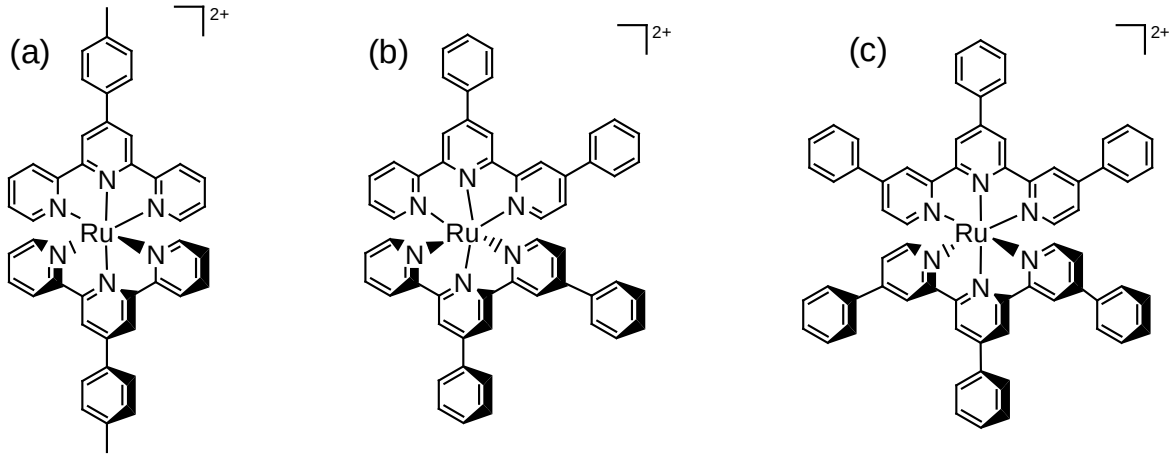

Figure 1.7[24]: Structure of (a) $[Ru(ttpy)_2]^{2+}$, (b) $[Ru(4,4'\text{-dtpy})_2]^{2+}$ and (c) $[Ru(tptpy)_2]^{2+}$.

This experimental data showed how, when the number of phenyl groups attached to the ligand is higher, the ligand's π-acceptor ability is enhanced and the ligand field splitting energy becomes wider. The increase in energy of the MC excited state and decrease in the MLCT state work synergistically to increase ΔE, enhancing luminescence.[60, 61]

1.2.3. Ruthenium(II) complexes containing cyclometallated ligands

Cyclometallating ligands, coordinating the metal centre by an anionic carbon through C-M bonds, are stronger σ-donors compared to the pyridyl rings. Therefore the induced ligand field is stronger and the electron density around the metal centre is higher. In this way the splitting of the ligand field energy becomes bigger leading to more intense luminescence, since the ^{3}MC is now at higher

energies compared to the ^{3}MLCT.[62] Examples of Ru(II) complexes containing cyclometallated ligands are $[Ru(bpy)_2(ppy)]^+$ and $[Ru(ttpy)(phbpy)]^+$ (see Figure 1.8), synthesised by Constable *et al.*[63, 64] These complexes show emission from ^{3}MLCT and red-shifted absorption compared to the bpy and tpy-based complexes due to the σ-donor effect of the anionic carbon coordinated to the metal centre.[65]

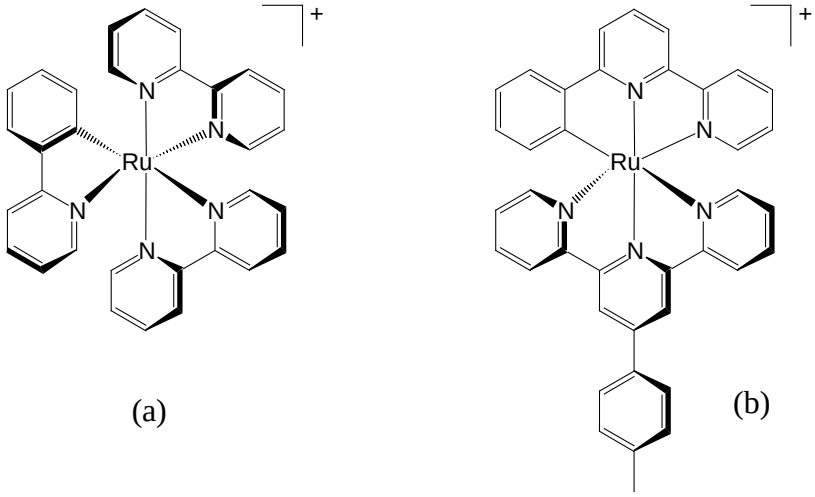

Figure 1.8[24]: Structure of (a) $[Ru(bpy)_2(ppy)]^+$ and (b) $[Ru(ttpy)(phbpy)]^+$

1.3. Iridium(III) complexes

Over the past 8 years, there has been a rapid expansion of the literature regarding luminescent complexes of iridium(III). In this work, we will particularly focus on the synthesis, properties and applications of iridium(III) complexes containing cyclometallated ligands as they are thought to be very promising for use in OLEDs (Organic Light Emitting Devices) and other applications that will be described further on. The main features that make iridium(III) complexes so appealing to researchers include their good stability, high photoluminescent quantum yields, ease of spectral tuning through synthetic modifications, short triplet-state lifetimes and ability to participate in outer sphere electron transfer reactions.[66-68] As ligands play an important role in changing the electron density localized on the

metal center and hence the energy of the excited states, we can distinguish between two different classes of complexes containing different classes of ligands.[69] At one extreme one type of complex contains three or four anionic ligating atoms such as chloride and/or cyclometallating aryl ligands; the complexes in this case typically have low-lying MLCT excited states since the charge compensation to the anions allows oxidation on the metal center. The class at the other extreme contains exclusively neutral ligands instead. In this kind of complex, less charge density is localized on the metal and the lowest-lying excited states are approximated as ligand centered (LC) since metal oxidation is thermodynamically unfavourable.[66] In early studies of luminescent iridium complexes, difficulties emerged for species such as $[Ir(bpy)_3]^{3+}$, $[Ir(phen)_3]^{3+}$ and other tricationic species due to the harsh conditions required for their synthesis and difficult purifications[66, 67]. On the other hand iridium(III) complexes containing cyclometallating ligands, such as *fac*-$Ir(ppy)_3$, have found interest in OLED applications as their emission from triplet MLCT states is found to be very efficient and also this type of complex is robust and features synthetic versatility and reversible electrochemistry. Between these two extremes are complexes containing only one or two anionic ligating atoms and five or four neutral ligands respectively, which may display excited states of intermediate (MLCT/LC) or quite different (e.g. LLCT) character.[70] All these characteristics have allowed iridium based complexes to displace complexes based on other metals in various applications.[68,71-74]

1.3.1. Iridium polypyridyl complexes

1.3.1.1. Iridium(III) complexes with two bidentate (N,N) ligands, $[IrL_2Cl_2]^{n+}$

During the first attempts to obtain $[Ir(bpy)_3]^{3+}$, De Simone *et al.* in 1969 reported the formation of $[Ir(bpy)_2Cl_2]Cl$ instead as undesired product by fusing $K_3IrCl_6*3H_2O$ with bpy at 270°C. Characterisation of the obtained complex by NMR revealed it to be the *cis* isomer.[66, 75] Similar types of complexes were shortly after synthesised, for instance in 1969 Chiswell *et al* prepared *cis*-$[Ir(phen)_2Cl_2]Cl$ (phen = 1,10-phenanthroline) starting from K_3IrCl_6 as well.[76] Broomhead presented a different synthetic method to obtain the same

phenanthroline based complex in 1971.[77] The synthesis was carried out following two steps, in the first $[Ir(phen)Cl_4]_2[phenH]^+$ was prepared from $(NH_4)_3IrCl_6 \cdot 2H_2O$ and 1,10-phenanthroline by reflux in acidic water for 2 hours. The second step consisted of heating the phenanthrolinium salt in refluxing glycerol for 1 hour to give *cis*-$[Ir(phen)_2Cl_2]Cl$ as a yellow solid. These early examples of iridium polypyridyl complexes reflected the synthetic difficulties and the harsh conditions needed when preparing even simple iridium(III) complexes.[66] A new synthetic method to synthesise this class of iridium(III) complexes was introduced by Brewer *et al.* in 1990, when complexes containing different types of polypyridyl bidentate chelates $[IrL_2Cl_2]^+$ (Figure 1.9) were obtained from $IrCl_3*3H_2O$ upon addition of two equivalents of the chelate L in a mixture of EtOH and H_2O.[78]

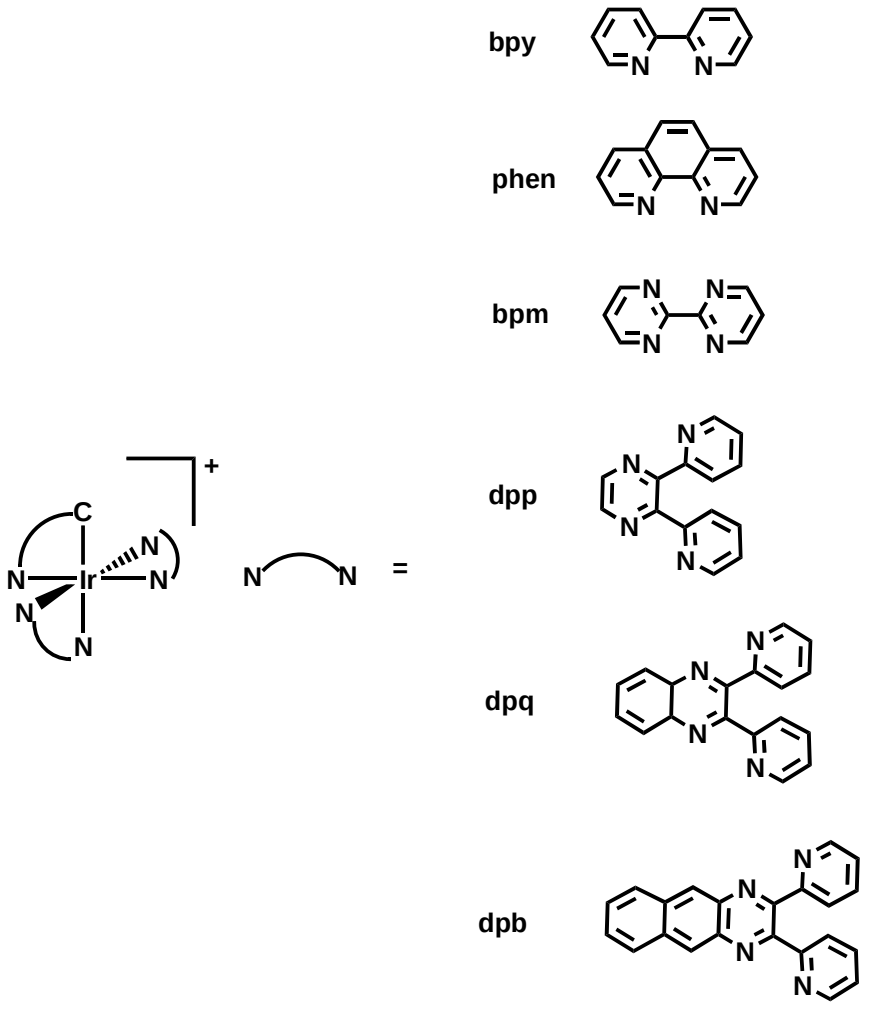

Fig. 1.9[78]: Representation of $[IrL_2Cl_2]^+$ complexes (L = bidentate chelate).

It was observed in electrochemical studies that in the $[IrL_2Cl_2]^+$ complexes the first two reduction steps were ligand based, which was in contrast to what was observed in the Rh(III) based complexes, where the first step in reduction was metal centred.[66, 78] The ligands bpm, dpb, dpq, and dpb (Figure 1.9) are all easier to reduce than bpy, and the first reduction potential for these $[IrL_2Cl_2]^+$ complexes is clearly related to the extent of electronic delocalisation over the ligand. After the uptake of two electrons by the ligand system, reduction is metal centred and involves displacement of the chlorine atoms from the coordination sphere of the metal generating a four coordinated Ir(I) complex. A noteworthy feature of the above reduction pattern is that the reduced two-electron $[IrL_2Cl_2]_2$ species are stable. The luminescence data at room temperature of this series of complexes reflect the emission expected from a MLCT excited state, in fact the following emission maxima were observed along the series of ligands respectively for bpy (510 nm), bpm (525 nm), dpp (562 nm) and dpq (634 nm).[78] The increase of the reduction potential of the complexes follows a similar pattern according to the emission.[66]

1.3.1.2. Iridium(III) complexes with three bidentate (N,N) ligands, $[IrL_3]^{n+}$

The first examples of $[IrL_3]^{n+}$ type of Ir(III) complxes were, $[Ir(bpy)_3]^{3+}$ which was firstly reported in 1958 by Martin *et al* and obtained from K_3IrCl_6 and bpy as an orange solid,[79] and $Ir(phen)_3^{3+}$ (Figure 1.10) in 1964 by Chiswell *at* al, but in this last case purity was not clearly achieved.[76] The procedure later described by Demas *et al* in 1974 led to better results, the complexes were synthesised by converting $K_3IrCl_6*3H_2O$ into a halide-free sulfate upon treatment with $K_2S_2O_8$ and $KHSO_4$ in boiling water, evaporation to dryness, and fusion in air above 250 °C for 30 min. Upon cooling it was mixed with bpy and fused under CO_2 at 230°C, leading to $[Ir(bpy)_3]^{3+}$.[80]

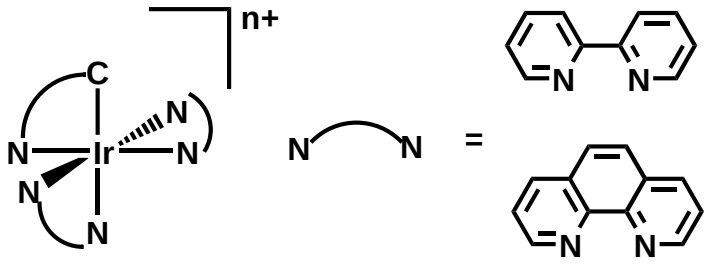

Fig. 1.10: Representation of $Ir(bpy)_3$ and $Ir(phen)_3$.

Treatment of *cis*-$[Ir(bpy)_2Cl_2]^+$ with trifluoromethanesulfonic acid in *o*-dichlorobenzene led to *cis*-$[Ir(bpy)_2(OSO_2CF_3)_2]^+$ in 95% yield, as reported by Meyer *et al.* in 1984.[81] This trifluoromethanesulfonate complex proved to be an excellent precursor to $[Ir(bpy)_3]^{3+}$, the substitution proceeding in 80% yield by heating with bpy in ethylene glycol for 5 h.

1.3.1.3. Iridium(III) complexes with one terdentate ligand (N,N,N) ($IrLCl_3$ species)

The first work that reported formation of a complex of the class $IrLCl_3$ (Figure 1.11) was that of Morgan and Burstall in 1937 by reaction of Na_3IrCl_6 in water with terpy to obtain formation of $Ir(tpy)Cl_3$.[82] Brewer *et al* in the 80s prepared the same complex by reacting $IrCl_3*13H_2O$ and tpy in ethylene glycol.[83]

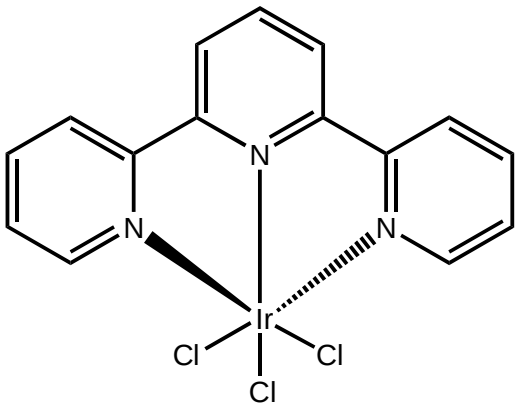

Figure 1.11: structure of $Ir(terpy)Cl_3$.

1.3.1.4. Iridium(III) complexes with two terdentate ligands (N,N,N) ($[IrL_2]^{3+}$ species)

Demas and co-workers presented a paper in 1990 reporting the synthesis of $[Ir(tpy)_2]^{3+}$.[84] The synthesis was performed in a similar way to that used for the preparation of $[Ir(bpy)_3]^{3+}$. Starting from K_3IrCl_6, the iridium sulfate formed after the first step was then reacted with tpy at reflux temperature in ethylene glycol. (Figure 1.12)

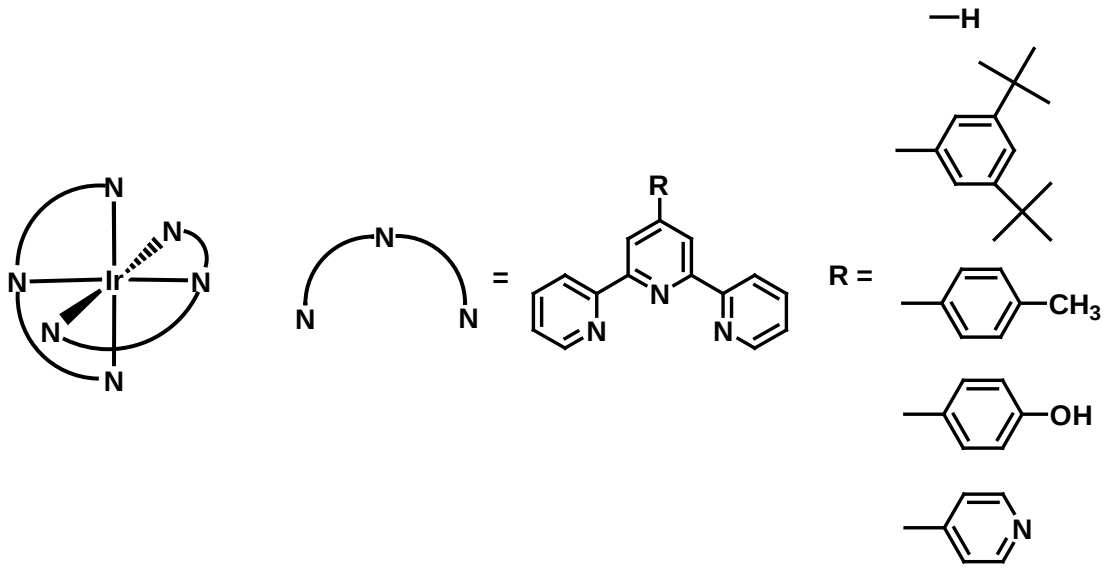

Fig. 1.12[66] Representation of bis-terpyridine complexes.

In the work of Sauvage *et al* a new synthetic pathway to prepare bis-terdentate iridium(III) complexes was carried out following two steps, the first being the formation under relatively mild conditions of $IrLCl_3$ as an intermediate from $IrCl_3*2H_2O$ and then its reaction with a second tpy-based terdentate ligand to give $(IrLL')^{3+}$ type of complexes [85] (Figure 1.13). Iridium bis-terpyridine complexes showed luminescence at room temperature, with emission at 458 nm for the complex bearing the unsubstituted terpyridine and above 500 nm for the ones

containing aryl-substituted terpyridines. The complexes showed a ligand centred emission with some extent of MLCT character in the aryl-substituted complexes and lifetimes of the excited states on the scale of microseconds.[85]

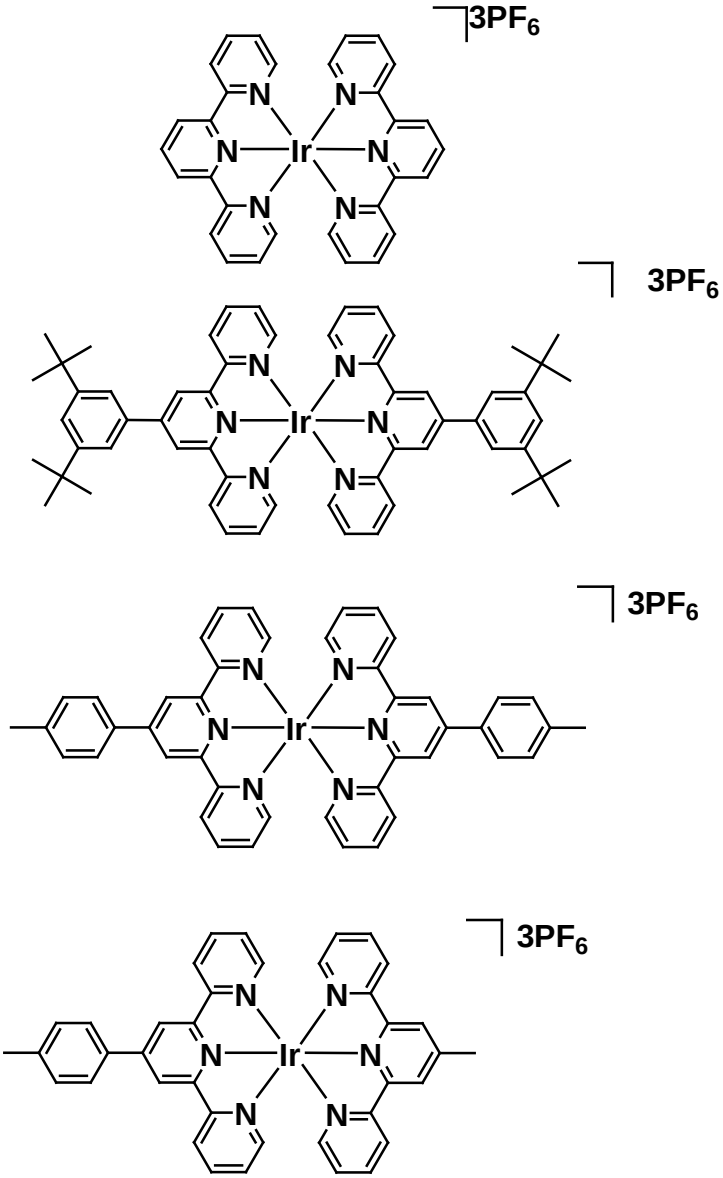

Figure 1.13[86]: Examples of $[(IrLL')]^{3+}$ complexes synthesised by Sauvage *et al*.

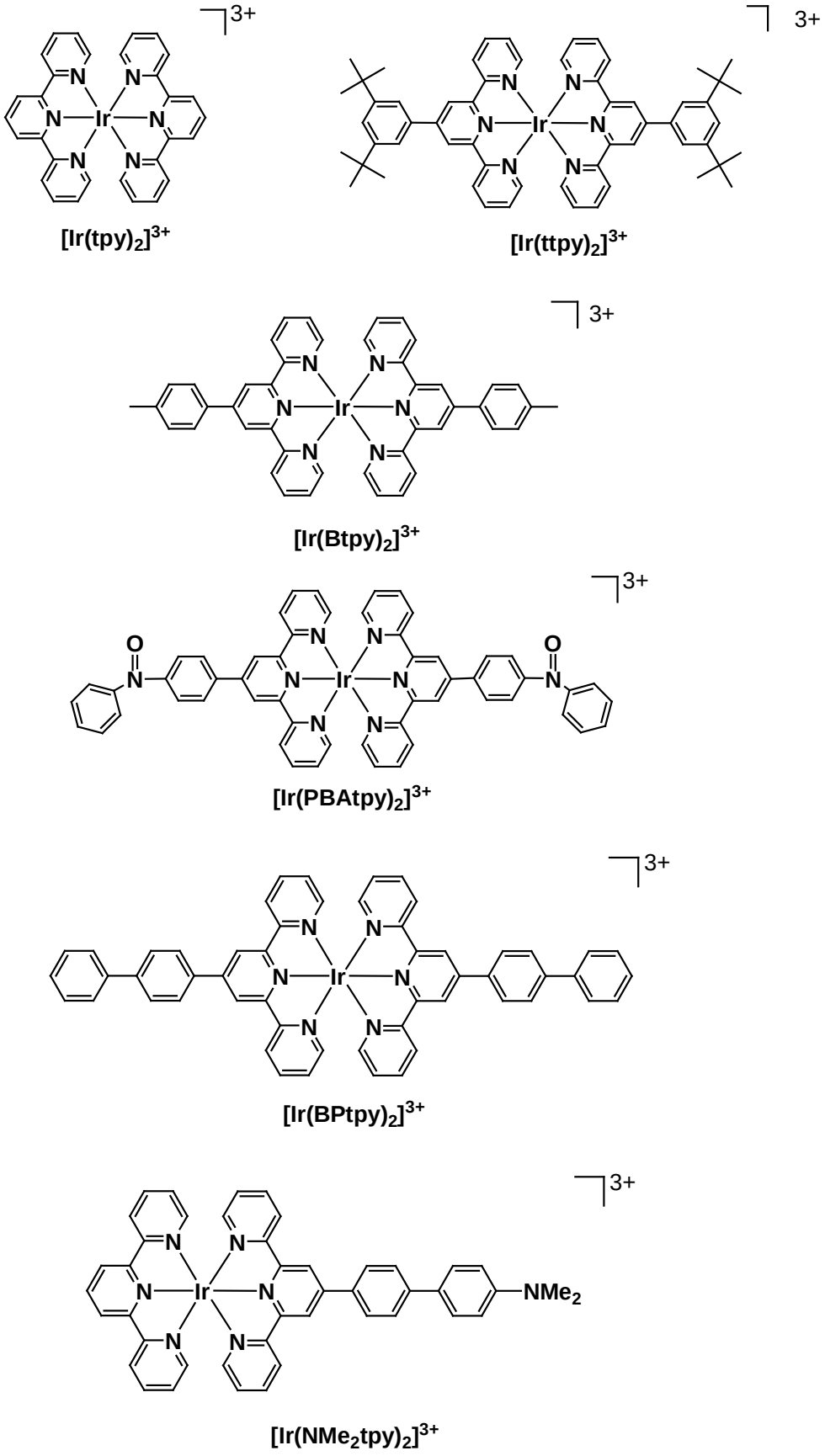

Figure 1.14[86]: Schematic structures of bis-terdentate complexes; the planes of the two terdentate units are roughly orthogonally each other.

The emission properties of this class of polypyridyl complexes can be varied depending on the substituents attached to the terdentate ligands. Along the series of Figure 1.14, the lowest-lying excited level, as monitored from the emission features, moves to lower and lower energy, a result mainly ascribable to an increasingly large ligand and more extensive conjugation. Interestingly, along this series the emission passes from a predominant ^{3}LC character for $[Ir(tpy)_2]^{3+}$, to a mixed ^{3}LC/^{3}MLCT character in $[Ir(ttpy)_2]^{3+}$ and $[Ir(tBtpy)_2]^{+}$, and finally to a predominant ^{3}MLCT character for $[Ir(PBAtpy)_2]^{3+}$. For $[Ir(BPtpy)_2]^{3+}$ the emission is best assigned to a ^{3}LC level, likely centered at the biphenyl moiety.(87) The changes in the nature of the emission display usual features. The emission profile of a ^{3}MLCT emission shows broad luminescence bands, while spectra characteristic of ^{3}LC emissions are generally narrower and well resolved; some representative cases are illustrated by the luminescence profiles of Figure 1.15.(87) Hypsochromic shift of the emission peak occurs on passing from room temperature to 77 K in frozen polar solvent (see Figure 1.15), and k_r value seems to be much smaller for ^{3}LC cases compared to those of ^{3}MLCT character.(88, 89) For $[Ir(terpy)(NMe_2tpy)]^{3+}$, an intraligand charge transfer state (ILCT, presumably from NMe_2 to tpy) is thought to be the lowest-lying excited state, resulting in very weak emission intensity for this complex. (Figure 1.15 spectra).(87)

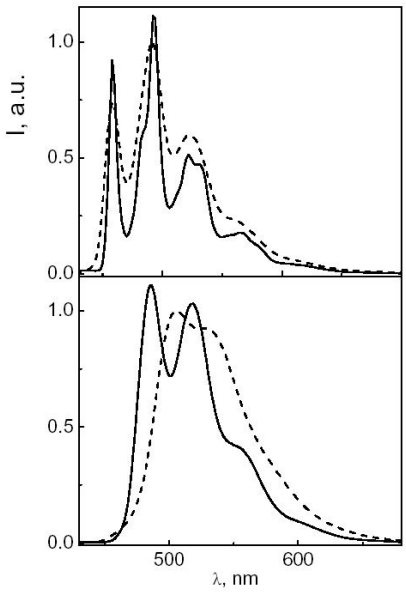

Figure1.15(27) Luminescence profiles at room temperature (dashed line) and at 77 K (full line) for a ^{3}LC emitter, $[Ir(tpy)_2]^{3+}$, and a mixed ^{3}LC/^{3}MLCT emitter, $[Ir(ttpy)_2]^{3+}$

A similar synthetic strategy was adopted by Williams *et al* to prepare complexes with pH sensitive groups on the ligands, showing how the luminescence of the complex changes from a predominantly LC character at higher pH to mainly MLCT at lower pH values, following protonation of the pyridine site [(90)] (Figure 1.16).

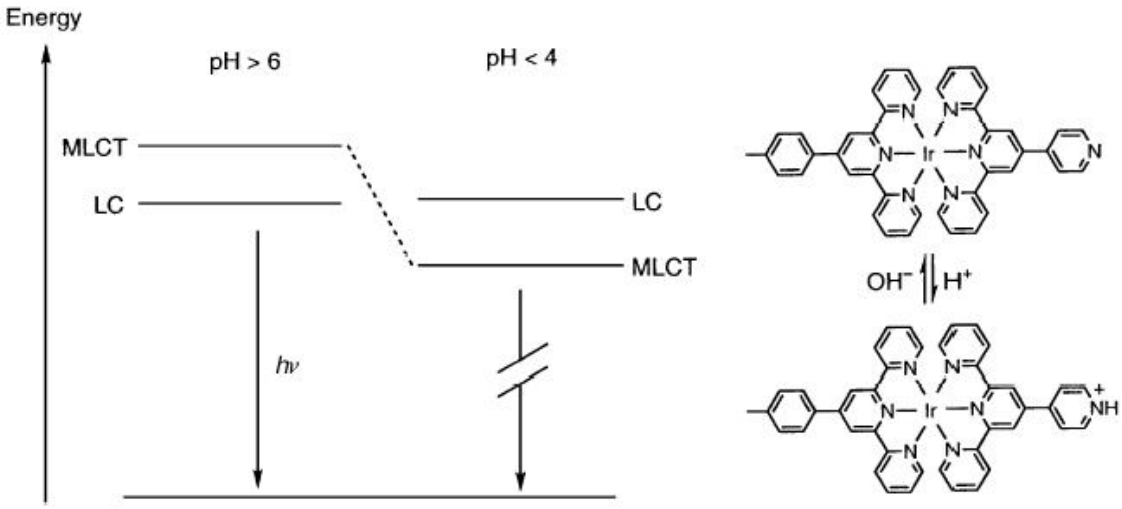

Figure 1.16[(66)] : pH-dependence of the luminescence of a pyridine-appended bis-terpyridine complex.

The $[Ir(tpy)_2]^{3+}$-type species have been devised for the building up of dyads and triads as models for photoenergy conversion schemes.[(25, 71, 87)] In this respect, $Ir(terpy)_2^{3+}$-type units offer also the possibility to create linear arrays with geometrically opposite photoactive and electroactive units, e.g. D and A, electron donor and acceptor units, respectively (thus allowing to prevent the well known problem of the geometrical isomers encountered for tris-bidentate arrangements[(91)]). This can be done by attaching suitable substituents at the 4'-position of the coordinated terpy's with the usually explored electrochemical potential range.[(71)]

1.3.2. Iridium complexes containing bidentate cyclometallating ligands

Ir(III) $5d^6$ complexes show several similarities with analogous complexes of Fe(II), Ru(II), Os(II) and Re(I), that are respectively $3d^6$, $4d^6$, $5d^6$ and $5d^6$. In an octahedral field, the *d* orbitals of the metal are split by a magnitude that is proportional to the strength of the ligand field. Cyclometallating ligands are located amongst the "strong" ligands in the spectrochemical series. In early studies of iridium(III) polypyridyl cyclometallating complexes, it was noticed that spontaneous cyclometallation could occur during the preparation of $[Ir(bpy)_3]^{3+}$ involving one of the bpy ligands[67], so that widespread use of ppy as a ligand was adopted, since a wide variety of complexes containing cyclometallating ligands could be deliberately synthesised. In further studies on complexes containing ppy ligands, it was noticed that the carbon atoms of the cyclometallating ligands were in mutually *cis* positions, which means that each one of them was in turn in a position *trans* to a nitrogen atom (*trans* effect of the Ir-C bonds).[92-94] Thus a complex such as $Ir(ppy)_3$ can exist as two different isomers as shown in Figure 1.17, namely facial (*fac*) or meridional (*mer*) configurations (Figure 1.17). This effect was clearly seen in the stepwise reaction of $Ir(acac)_3$ with ppy, where the ppy subsequently displaces the acac group until complete conversion to *fac*-$Ir(ppy)_3$.[95]

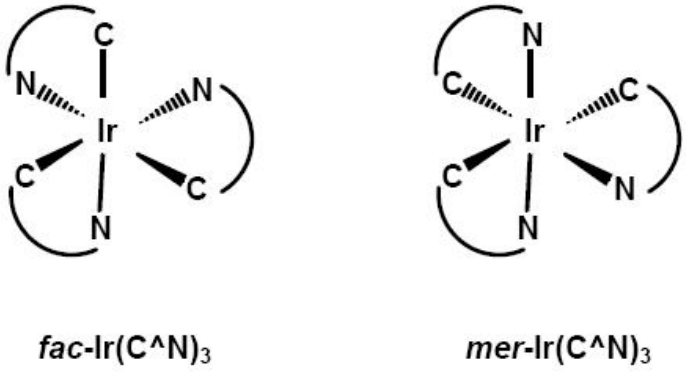

fac-Ir(C^N)$_3$ *mer*-Ir(C^N)$_3$

Figure 1.17[87]: *mer* and *fac* isomers in Ir(C^N)$_3$ complexes

The two isomers show different structural properties considering that in the *fac* isomer Ir-C and Ir-N bonds are nearly of the same length, for the *mer* isomer instead the bond situated in a *trans* position to the Ir-C bond is longer than those *trans* to a Ir-N bond. The two isomers can thus manifest different behaviour in terms of electrochemical and photophysical properties.[96] Most of the work reported to date on synthesis and photophysics of cyclometallated complexes of d^6 transition metals is relative to the facial isomers.[97-99] Originally Nanoyama in 1974 and succesively Watts and coworkers synthesised in 1984 di-chloro-bridged iridium dimers by refluxing $IrCl_3$ with the ligand in a 2-ethoxyethanol-water mixture (Figure 1.18) as the intermediate from which a series of tris-cyclometallated complexes were prepared that showed luminescence at room temperature. The redox processes on the iridium metal center were found to be tunable as a function of the type of the substituent attached to the cyclometallating ligands (electron-withdrawing or electron-donor agents having a different effect on the photophysical properties of the complexes).[66, 100-103] (Figure 1.18)

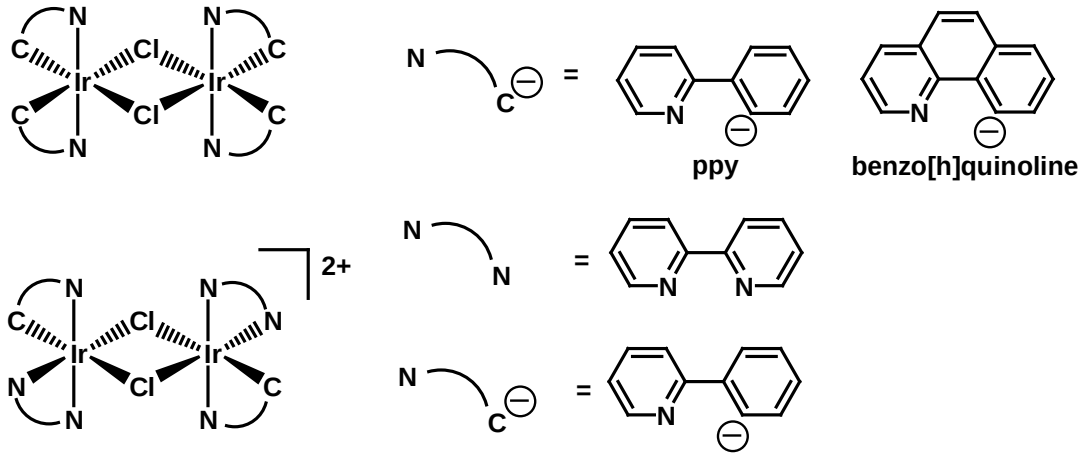

Figure 1.18[66]: representation of examples of di-chloro bridged iridium(III) dimers

In Tamayo and co-workers' work, new synthetic routes for isolation of either the facial or meridional isomers of tris-cyclometallated Ir(III) complexes and

conversion between them are shown. The meridional isomer is the kinetically favoured product while the facial isomer is the thermodynamic product obtained at higher temperatures. In Tamayo's work it is also described how the spectroscopic and photophysical properties of the two isomers have different features. It is reported in the literature that meridional isomers display red-shifted emission and decreased quantum efficiencies compared to their facial relatives, a fact that can be explained by the efficient bond breaking that occurs for the meridional isomer in the excited state acting as an effective quenching pathway and giving isomerization to the facial isomer.[96] The presence of three cyclometallating ligands on the metal centre induced a ^{3}MLCT character of the emission at room temperature. In 2000, in fact Thompson and coworkers published a paper reporting the first OLED based on $Ir(ppy)_3$.[104] Watts *et al.* also reported the synthesis and photophysical properties of complexes containing both cyclometallating and polypyridyl ligands (such as $[Ir(ppy)_2(bpy)]^+$, Figure 1.19).

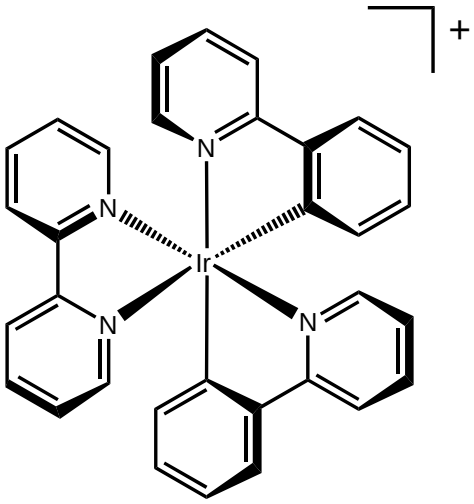

Figure 1.19: structure of $[Ir(ppy)_2(bpy)]^+$

$[Ir(ppy)_2(bpy)]^+$ displayed intermediate electrochemical and photophysical properties between the LC predominant character of $[Ir(bpy)_3]^{3+}$ and the MLCT character of $[Ir(ppy)_3]$.[105]

1.3.3. Iridium complexes containing terdentate cyclometallating ligands

Complexes containing terdentate ligands offer the possibility of creating linear arrays with photoactive and electroactive units avoiding the problems of geometrical isomers as seen in the case of units containing bidentate ligands. The approach adopted is usually functionalization on the aromatic "ends" of the complex structure by attaching substituents and building up multicentred systems by reacting different metal fragments. In particular, a good strategy to obtain linearly disposed multicentered complexes is by functionalization of the 4' position of the coordinated terpy.[91, 106] Moreover the introduction of terdentate ligands on the complex platform can help prevent molecular distortions during the formation of the excited states.[106]

The research group of Campagna and Mamo synthesised in 1997 the first Ir(III) complex with terdentate cyclometallating ligands. Preparation of complexes $[Ir(LH)(L^-)]^{2+}$ and $[Ir(L^-)_2]^+$ was reported by refluxing $IrCl_3*3H_2O$ in glycerol, where LH indicates 2,6-bis(7'-methyl-4'-phenyl-2'-quinolyl)pyridine[107] (coordinating as a N,N,N terdentate ligand) and L^- its deprotonated form (which can coordinate the iridium as N,N,C cyclometallating ligand) (Figure 1.20). Both complexes show low energy MLCT character in their emission due to the introduction of cyclometallating ligands in the coordination sphere of the metal centre.[107] However, the complex $[Ir(LH)(L^-)]^{2+}$ (*heteroleptic* monocyclometallated complex) showed lower luminescence intensity at room temperature compared to $[Ir(L^-)_2]^+$ (*homoleptic* bis-cyclometalated complex).[107] The investigation carried out by Williams and coworkers on mono-cyclometalated $[Ir(NCN)(NNN)]^{2+}$ complexes (Figure 1.21) explained the low luminescence intensity in terms of the higher degree of ligand-to-ligand charge transfer character and low metal contribution of the excited state in heteroleptic monocyclometallated complexes.[108, 109] On the other hand the higher luminescence observed in the homoleptic bis-cyclometallated complexes can be explained by a higher MLCT degree caused by

the increase of the σ-donor effect with the introduction of a second cyclometallating ligand.[107, 108]

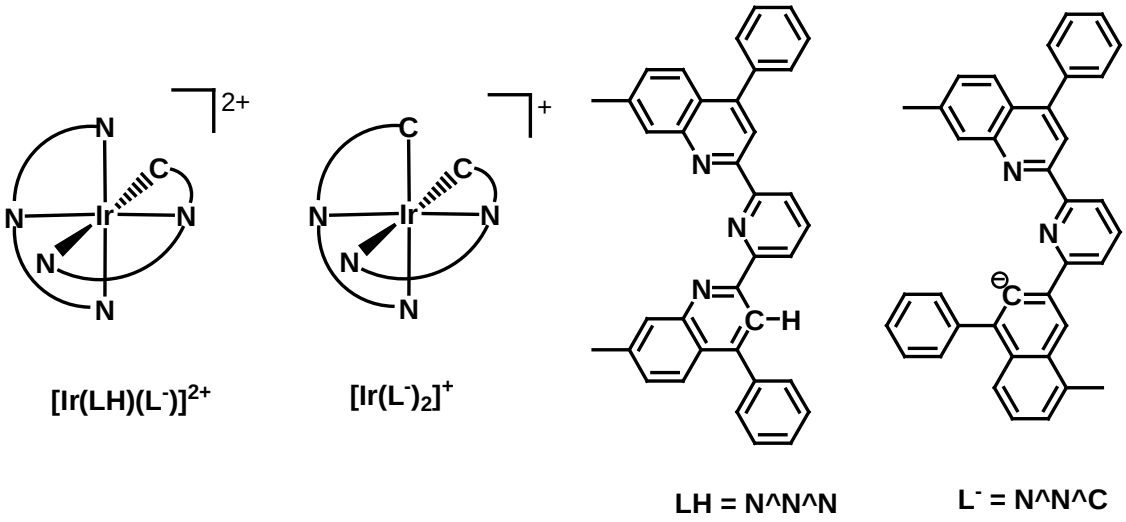

Figure 1.20[67]: representation of Mamo and Campagna's mono- and bis-cyclometallated complexes with terdentate ligands.

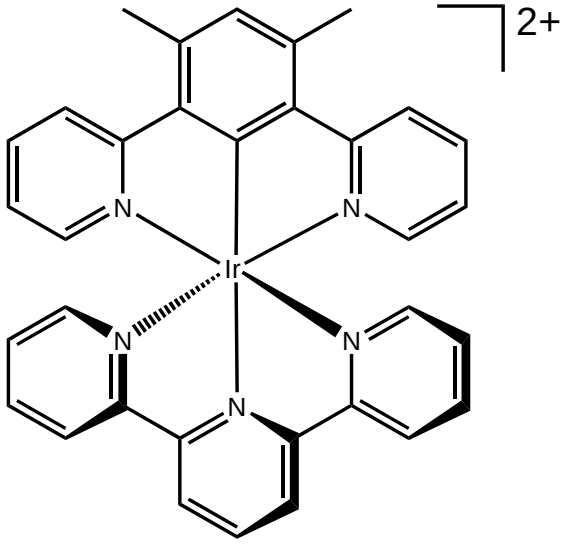

Figure 1.21: structure of a $[Ir(NCN)(NNN)]^{2+}$ complex

Promotion of a higher degree of metal participation upon bis-cyclometallation is confirmed also in systems of the type $[Ir(N^C^N)(N^N^C)]^+$.[109] Moreover the fact that the cyclometallating carbons are part of a different terdentate ligand contributes to decrease the extent of the LLCT character.[107]

The increased contribution of the metal centre in the excited states of the complex within the passage from mono- to bis-cyclometallated platforms suggests that the introduction of a third cyclometallating site in the coordination sphere may increase the MLCT character of the emission even further.[107] The research group has been involved in the investigation of the synthesis and the photophysical properties of bis-terdentate coordinated complexes containing dipyridyl-xylene N^C^N ligand and a second terdentate ligand C^N^C or C^N^O-coordinating (Figure 1.22). The C^N^C-coordinating class of bis-terdentate complexes were manifesting promising emission properties with quantum yields comparable to those of the analogous tris-bidentate complexes (e.g. $Ir(ppy)_3$). The emission was described as ^{3}MLCT character, and, as confirmed by DFT calculations, the LUMO was mainly localised on the N^C^N ligand.[108, 109] The C^N^O-coodinating systems, on the other hand, exhibited low luminescence quantum yields. Despite the high luminescence, complexes bearing C^N^C ligands possess very low stability in solution, involved in photodissociation, leading to cleavage of one of the trans-disposed Ir-C cyclometallating bonds and probable fomation of the five coordinated species bearing a solvent molecule on the sixth coordination site.[107]

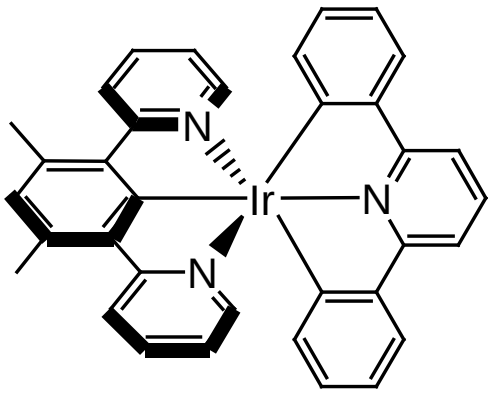

Figure 1.22[87]: example of Ir(N^C^N)(C^N^C) complex

1.4. Nature of excited states in Iridium Cyclometallated Complexes and their modifications

As noted previously, light absorption is associated with electronic transitions from a ground state to singlet levels of various electronic localization such as ligand centered (^{1}LC), metal centered (^{1}MC), metal-to-ligand charge transfer (^{1}MLCT) and ligand-to-metal charge transfer (^{1}LMCT),[110-113] whereas emission instead is nearly always associated with a process from the lowest lying triplet state (Figure 1.23).[114] Due to the separation of the energies of the d orbitals, Δ is large in iridium(III) complexes so that MC levels in such complexes do not participate in emission as they are hardly accessible in energy. This implies that an electron promotion occurs from the HOMO (Highest Occupied Molecular Orbital), which is localized on the metal center for the MLCT transition, to π* orbital LUMO (Lowest Unoccupied Molecular Orbital) located on the ligand, mainly on the pyridine rings.[115]

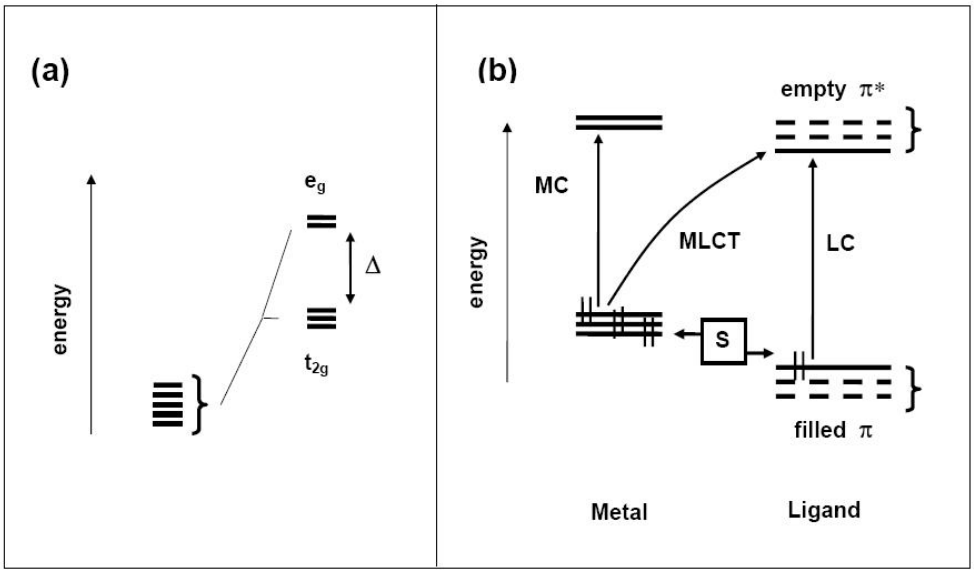

Figure 1.23[87]: a) orbitals in octahedral field; b) orbital description of MC, MLCT and LC transitions.

Iridium complexes containing cyclometallating ligands show two main emissive transitions in the long-lived excited states, namely in approximation they are associated with metal-to-ligand charge transfer (MLCT) and ligand centered transitions (LC) respectively. The formation, in Iridium(III) complexes, of a mixed emissive triplet excited state is enabled by the strong spin-orbit coupling associated with the metal centre which promotes intersystem crossing. In fact a combination of measurements, such as excited state lifetime measurements, time resolved luminescence and computational investigation, showed how the excited state involved in the emission of cyclometallated iridium(III) complexes is thought to be a mixed MLCT-LC character.[68, 116] This effect occurs when sufficient overlap is present between MLCT and LC states[116, 117]. Thus by changing the nature of the ligand and the substituents situated on them it is possible to tune the energy of the orbitals involved.[68] Also in some cases, transitions between cyclometallating ligands and ancillary ligands are feasible. On the other hand, when the contribution of the π^* orbitals is mainly of the cyclometallating ligands, both frotier orbitals are associated with them and the ancillary ligand plays a more passive role in the excited states but, by influencing the metal orbitals via inductive communication through σ bonds, even a non-participating ligand can adjust the energy of the MLCT transition by changing the degree of mixing of states.[116]

1.4.1. Emission tuning

In summary, tuning the energy of the excited states can be aproached in different ways, such as coordination of different types of ligands to the metal center. By selecting appropiate ligands, it is possible to tune the emission of the complexes, ranging over the visible spectrum from blue at high energies to red at low energies.[118-121] The energy of the excited states can be also modified by changing the degree of conjugation on the ligands in order to diffuse or reduce the coordination sphere of the complex, or even changing the level of aromaticity present on the ligands themselves. For example, recent investigations have shown that in iridium(III) complexes containing terdentate cyclometallating ligands, low-energy emission is achieved in cases of extended π systems.[122-124] The introduction of anionic ligands in the complexes stabilizes the MLCT states and decreases the possibility of an intraligand charge transfer transition. It is also

possible to tune the energy of the excited states of the complex by substituent effect, in order to change the electron density on the metal-ligand bonds and the energy of the orbitals involved. In particular electron-withdrawing substituents on the ligands such as –F and -CF_3, tend to stabilize the HOMO by lowering the electron density on the metal center or, on the other hand, electron-donating substituents such as –C(CH_3) or –OCH_3, lead to the opposite effect, and attached to the conjugated ligands they modulate the energy of the excited state.[68, 125]

1.4.1.1. Yellow and red-shifted emission

A wide range of colours obtained in electrogenerated chemiluminescence is reported for Ir(III) complexes as they move from green ($Ir(ppy)_3$) to yellow ($Ir(thpy)_3$) in neutral heteroleptic complexes of the structure $(C\hat{}N)_2Ir(LX)$, where the cyclometallating ligands are of various nature (Figure 1.24) and LX represents a monoanionic ligand such as acetyl acetone, picolinic acid or N-methyl salicylimmine (Figure 1.24).[126, 127] It has been observed by Thompson, Forrest and co-workers that variation of colour depends on the different types of cyclometallating ligand coordinated to the metal (Figure 1.25) ranging from 512 nm to 612 nm for bis-cyclometallated complexes bearing a bidentate anionic ancillary ligand, with quantum yields within the interval 0.1 and 0.4. In particular, as the size of the cyclometallating ligands increases (more delocalization of the electron density), the energy of the ligand-centred LUMO lowers, allowing the emission to change from green ($Ir(ppy)_3$) to yellow (e.g. $Ir(thpy)_2(acac)$) and then to red (e.g. $Ir(\alpha bsn)_2(acac)$), for the complexes that emit above 600 nm.[87, 126, 127]

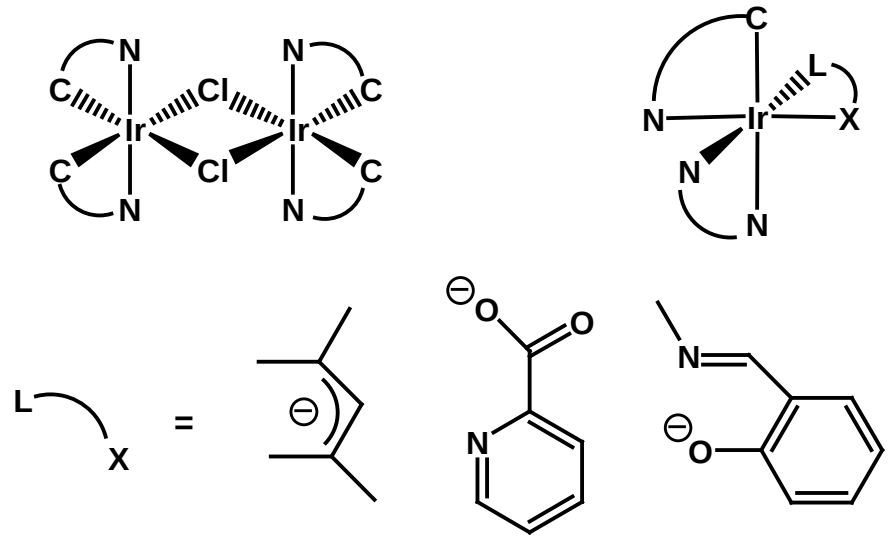

Figure 1.24[126]: neutral heteroleptic complexes of the structure $(C^N)_2Ir(LX)$

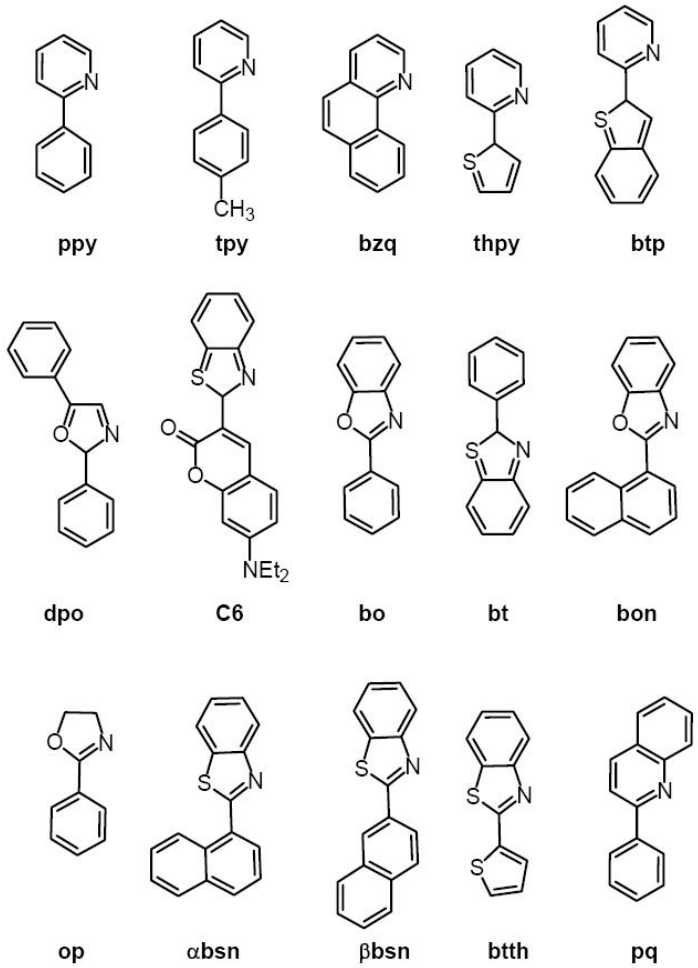

Figure 1.25[87]: different C^N ligands used in neutral heteroleptic complexes of the structure $(C^N)_2Ir(LX)$

Emission shift from green to red is shown with complexes of the structure *fac*-Ir(C^N)$_3$, in neutral homoleptic complexes, by varing the nature of the cyclometallating ligand coordinated to the iridium centre (figure 1.26).[86] This class of complexes shows emission properties similar to those of (C^N)$_2$Ir(LX) with quantum yields ranging from 0.08 to 0.4 and red-shifted emission until reaching 644 nm for the most red emitting complex of the series Ir(tiq)$_3$.[86]

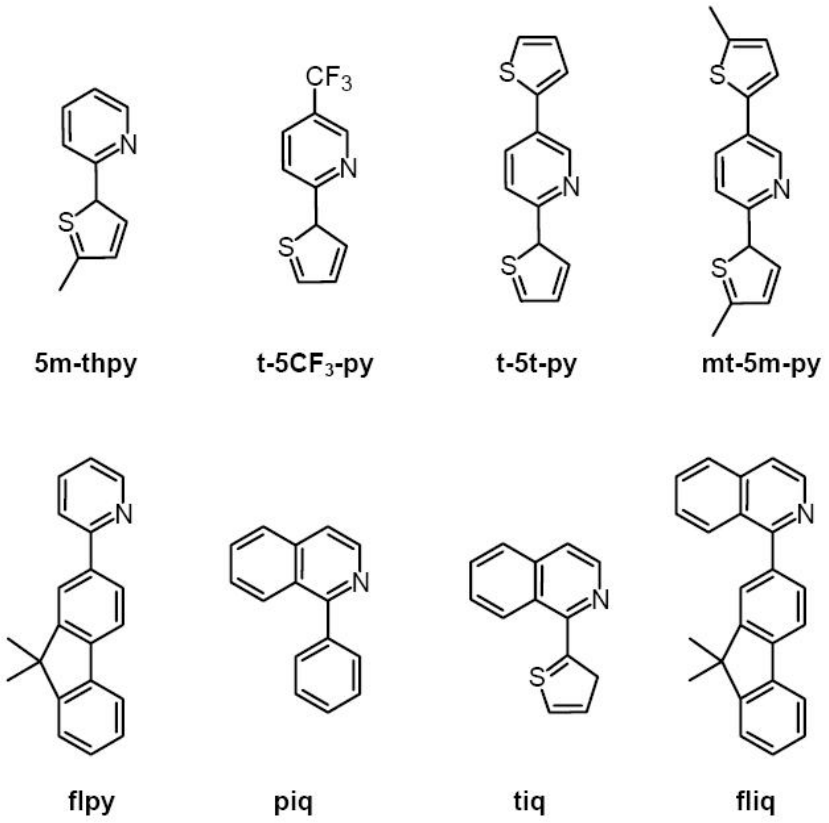

Figure 1.26[87]: examples of C^N ligands used in *fac*-Ir(C^N)$_3$ to have colour change from green to red

1.4.1.2. Blue-shifted emission

The excited states of Ir(III) complexes can be tuned to shift the emission to the opposite direction, to the blue and near UV, by adopting different strategies. In fact electron-withdrawing groups as substituents on the cyclometallating ring, such as fluorine, stabilize the HOMO level with little effect on the LUMO, provoking thus an increase in the HOMO-LUMO energy gap and finally leading to emission at higher energies.[96, 128, 129] In Figure 1.27 are reported examples of cyclometallating ligands used by Thompson and co-workers, [96] in which phenyl-pyrazole and tolyl -pyridine based ligands shift the emission to the blue with respect to the phenyl-pyridine based complexes. This effect is induced by the electro-withdrawing fluorine substituents on the phenyl rings and also by changing of the nature of the N^C fragment with the introduction of a pyrazole ring in the place of a pyridyl ring, which destabilises the LUMO. The emission for the complexes ranges from 492 nm for the *fac*-Ir(ppy)$_3$ to 450 nm for the *fac*-Ir(dfppy)$_3$, until 390 nm for *fac*-Ir(dfppz)$_3$.[96]

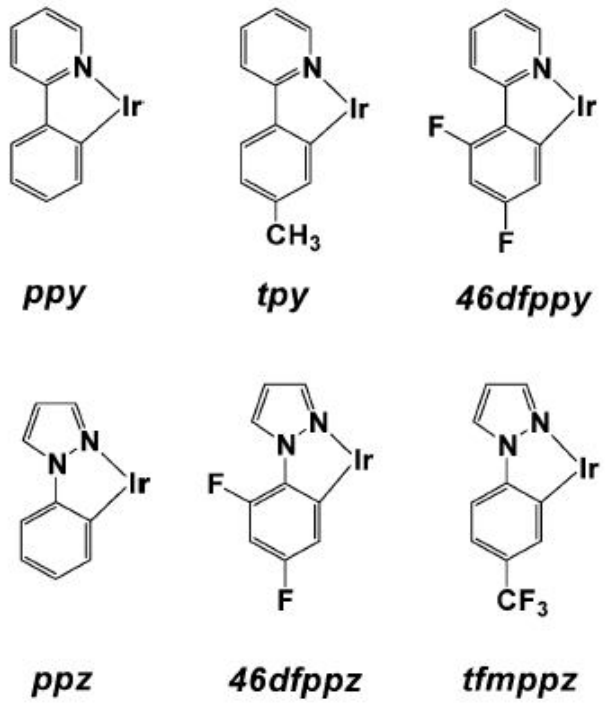

Figure 1.27[96]: Cyclometallating ligands used to prepare blue emitting Ir(*C^N*)$_3$ type of complexes.

On the other hand it has been found that ancillary bidentate ligands of the type LL or LX can also cause a blue shift in emission.[116, 129] Thompson and co-workers prepared a series of complexes of the type $Ir(N^C)_2(LL)$ and $Ir(N^C)_2(LX)$ that show bluer emission if compared to analogous complexes containing acac as ancillary ligand (Figure 1.28). Tuning the emission by ancillary effect can lead to significant shifts towards the blue region (e.g. from 512 nm for $Ir(tpy)_2(acac)$ to 458 nm for the complex $[(tpy)_2Ir(dppe)](CF_3SO_3)$).[116]

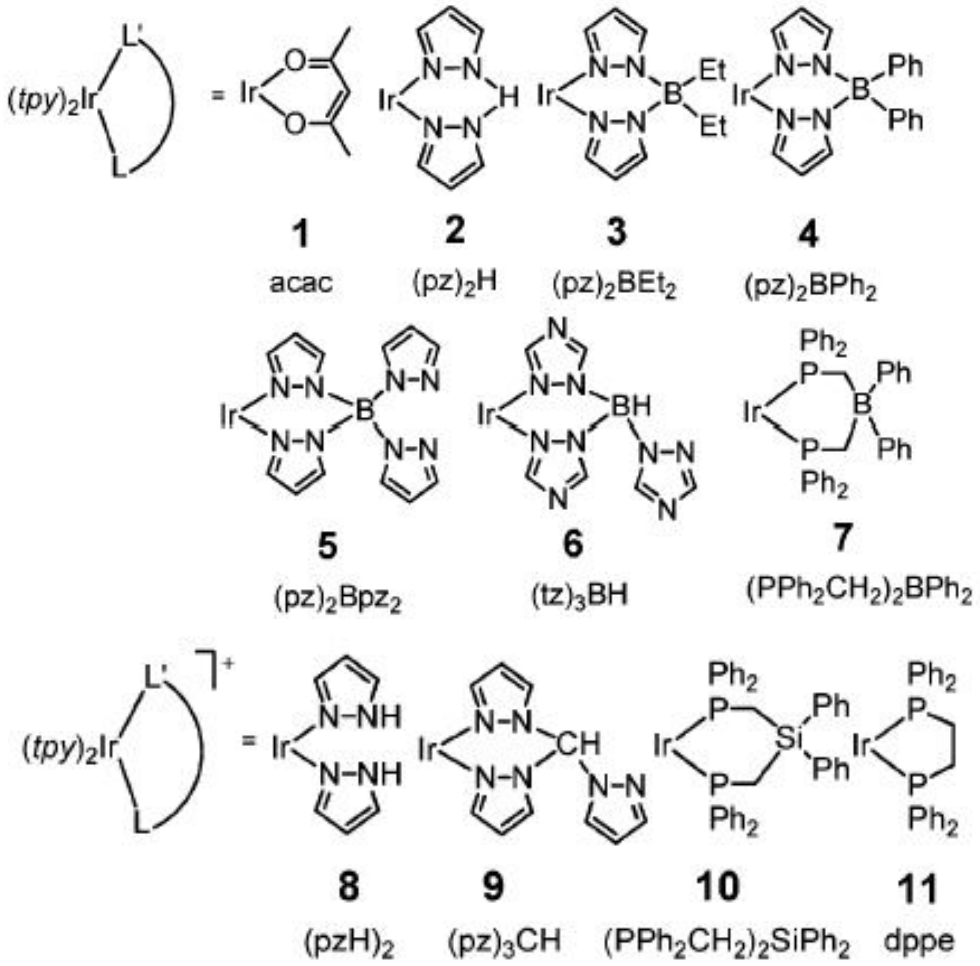

Figure 1.28[116]: LL ancillary ligand used from Thompson et al. for blue emitting complexes

Monodentate ancillary ligands such as cyanide and isocyanide can cause a blue shift in emission compared to that of *fac*-Ir(ppy)$_3$. This phenomenon can be rationalised by the fact that the cyanide and isocyanide are characterized by strong electron-withdrawing properties. In blue emitting complexes the degree of mixing of MLCT and LC character is decreased in the excited state. This happens because the iridium d orbitals, which participate the HOMO, are located at lower energies and only a little change is introduced in the energy of the LUMO.[107]

Another strategy to blue-shift the emission of iridium(III) complexes consists in destabilising the LUMO energy level rather than stabilising the energy of the HOMO, in order to increase the HOMO-LUMO energy gap.[130-135] Photochemical studies on complexes containing different heterocycles manifested significant shifts towards blue emission (e.g. Ir(dFppy)(ppz)$_2$ 390 nm and Ir(dFppy)$_2$(ppz) 380 nm, see Figure 1.29).[22] However luminescence quantum yields for this type of complxes was reported to be 2 orders of magnitude lower than for the pyridyl analogues (e.g. Ir(pmb)$_3$, Φ=0.04), probably due to the fact that the emission level lies at very high energies, thus a small ^{3}MLCT-^{3}MC energy gap characterises these complexes.[87, 129]

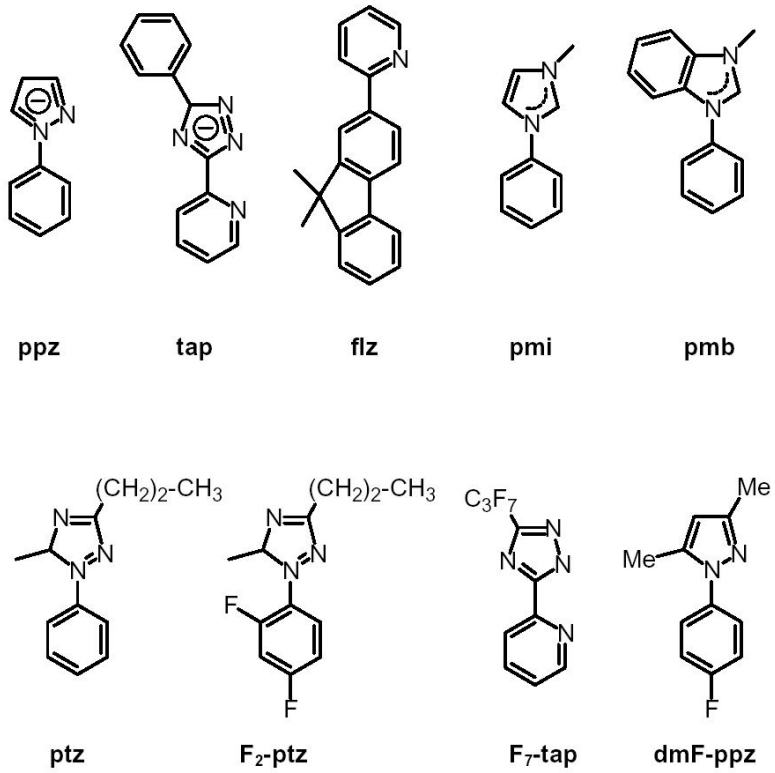

Figure 1.29[87]: examples of bidentate ligands for blue emitting complexes containing different heterocycles from pyridyl rings.

1.5. Applications of luminescent metal complexes

Luminescent metal complexes are attractive for diverse applications. The effectiveness of a complex in a specific role is determined by its excited-state properties and can be manipulated through synthetic modifications.[68] Early works in this field were predominantly focused on ruthenium(II) tris-diimine complexes, but a limitation of the material was the limited possibility of colour tunig caused by a non emissive thermally accessible metal centred state.[1] Iridium(III) complexes were found to be more suitable for many applications. In fact, Ir(III) complexes have a broad colour tuning possibility, due to an increased ligand-field stabilisation energy, therefore the ^{3}MC state is less accessible than in the case of Ru(II) complexes.[73, 74] But also, the reversible electrochemistry, synthetic versatility,

and robust nature of iridium (III) complexes render them appealing materials for a multitude of applications.

Consequently, the design of novel complexes for OLED applications has become a major synthetic goal in materials research.[127, 137] The usefulness and applicability of new luminescent materials can be assessed according to their stability, external quantum yield, excited-state lifetime, and emission energy. It is highly desirable to tailor transition-metal complexes that will emit across the visible spectrum and to produce molecules in which light emission predominates over nonradiative decay. These properties can be evaluated using both photo- and electroluminescent methods.[138]

1.5.1. OLED applications

Organic electroluminescence (EL) is the electrically driven emission of light from noncrystalline organic materials, which was first observed and extensively studied in the 1960s.[139] In 1987 Kodak introduced a double layer organic light-emitting device (OLED), which combined modern thin film deposition techniques with suitable materials and structure to give moderately low bias voltages and attractive luminance efficiency.[140] Shortly afterwards, in 1990 the Cambridge group of Friend announced a conducting polymer-based LED[141, 142]. Since then, the interest in research in this new field has been increased, and progress has been made in improving color gamut, luminance efficiency and reliability of the devices. The growing interest is largely motivated by the promise of the use of this technology in flat panel displays. The efficiency of an OLED is determined by charge balance, radiative decay of excitons, and light extraction. Enormous progress has been made recently in developing phosphorescent emitters via triplet–singlet energy transfer, and high-efficiency OLEDs with a wide range of different colours have been prepared and reported.[142] Current research activity is directed towards surface modifications that can increase light extraction efficiency, while the problem of light-trapping remains unsolved in terms of its application to displays. The most critical performance characteristic for OLEDs is the device operational lifetime. Continuous operation of OLEDs generally leads to a steady loss of efficiency and a gradual rise in bias voltages. Although OLEDs have

achieved long operational stability, the material issues underlying the EL degradation are not fully understood.[142]

An OLED has an organic EL medium consisting of extremely thin layers (<0.2 mm in combined thickness) sandwiched between two electrodes. In a basic two-layer OLED structure, one organic layer has the function of transporting holes and the other organic layer is specific for transporting electrons. The interface between the two layers provides recombination of the injected hole–electron pair resulting in electroluminescence.[13] When an electrical potential difference is applied between the anode and the cathode such that the anode is at a more positive electrical potential with respect to the cathode, injection of holes occurs from the anode into the hole-transport layer (HTL), while electrons are injected from the cathode into the electron-transport layer (ETL).[142] The injected holes and electrons both migrate towards the oppositely charged electrode, and upon recombination, energy is released as light. The heterojunction should be designed to facilitate hole-injection from the HTL into the ETL and to block electron injection in the opposite direction in order to enhance the probability of exciton formation and recombination near the interface region.[142]

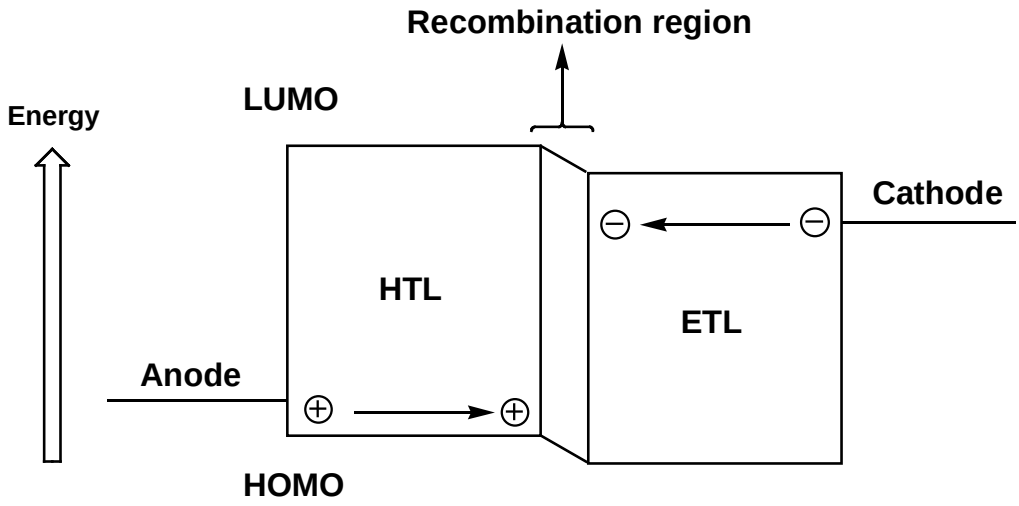

Figure 1.30: schematic recombination process in the Energy level diagram of a two-layer OLED.

As shown in Figure 1.30, the highest occupied molecular orbital (HOMO) of the HTL is slightly above that of the ETL, so that holes can enter into the ETL, while the lowest unoccupied molecular orbital (LUMO) of the ETL is significantly below that of the HTL, in order that electrons are trapped in the ETL. The simple structure of a two layer OLED can be modified to a three-layer structure, in which an additional luminescent layer is introduced between the HTL and ETL to function primarily as the site for hole–electron recombination and thus electroluminescence.[142] A great advantage of the three layer OLEDs is that the functions of the individual organic layers are distinct and can therefore be optimized independently. Thus, the luminescent layer can be chosen to emit a desired color as well as a high luminance efficiency. Moreover ETL and HTL can be optimized primarily for the carrier-transport property. The extremely thin organic EL medium offers reduced resistance, permitting higher current densities for a given level of electrical bias voltage. Since light emission is directly related to current density through the organic EL medium, the thin layers coupled with increased charge injection and transport efficiencies have allowed acceptable light emission to be achieved at low voltages.[142]

The composition of OLEDs consists of an organic matrix in which the luminescent chromophore is embedded, then the matrix (for example 4,4'-N-N'-dicarbazolylbiphenyl, CBP) is sandwiched between multiple layers of charge transport materials such as 2,9-dimethyl-4,7-diphenyl-1,10-phenanthroline, BCP and 4,4'-bis-[N-(naphthalyl-N-phenylamino)biphenyl, α-NPD (electron and hole transport materials respectively) and capped with a low work-function cathode (LiF/Al) and a transparent anode (indium-tin oxide.(Figure 1.31)[68]

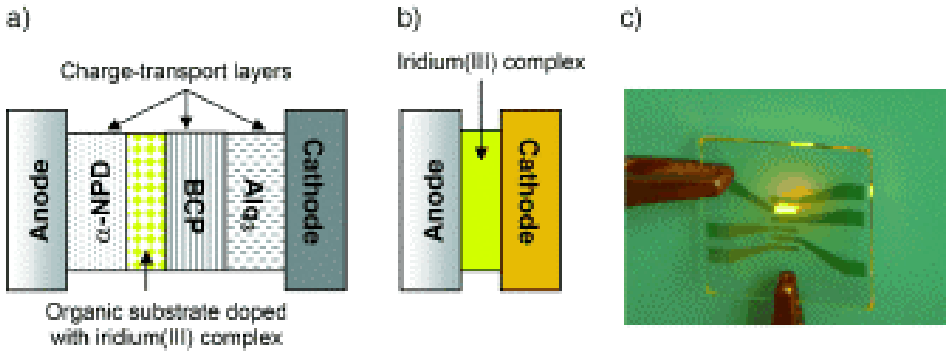

Figure 1.31[68]**:**a) A multilayer device ensemble involving an organic material (e.g., CBP) doped with a neutral or anionic iridium(III) chromophore. This matrix is sandwiched between hole- (e.g., α-NPD) and electron-injecting (e.g., Alq_3, q=8-hydroxyquinoline) layers as well as a hole blocking layer (e.g., BCP) and capped with a low work-function cathode (e.g., LiF/Al) and a transparent anode (e.g., ITO). b) Single-layer device geometry in which a cationic iridium(III) chromophore is spin-coated on an ITO substrate and capped with a gold electrode. c) Electroluminescence from $[Ir(ppy)_2(dtbbpy)](PF_6)$ in a single-layer, air-stable device (560 nm).

Transition metal-based organic light emitting diodes (OLEDs) are considered to be promising candidates for flat panel displays, due to their color versatility, low operational voltages and phosphorescence efficiency.[143, 144] Many efforts in this field have been made during the recent years to replace liquid crystal displays (LCDs).[143] Industrial interest was already attracted by SMOLEDs (Small Molecule OLEDs) and polymer-based OLEDs with some cases already available on the market.[142, 145, 146] The ongoing design of new material leads to higher efficiencies, enhanced brightness and improved lifetimes of optoelectronic devices.[142] Tang and Van Slyke in 1987 assembled the first OLED based on metal complexes by using an Alq_3 (q=8-hydroxyquinoline) which emits green light from a singlet excited state chromophore.[140] Since then altering the device characteristic through modifications on the chromophores has aroused large attention among scientists, specially by using heavy metal complexes such as those containing Ir(III), Ru(II), Os(II) and Pt(II).[141, 142, 147] Thanks to the strong spin-orbit coupling, singlet-triplet mixed states are generated in metal complexes and the spin-forbidden nature of the relaxation of the triplet state is removed so that high efficency electrophosphorescence is achieved in OLEDs containing heavy metal complexes (in figure 1.32 some examples are shown).[142]

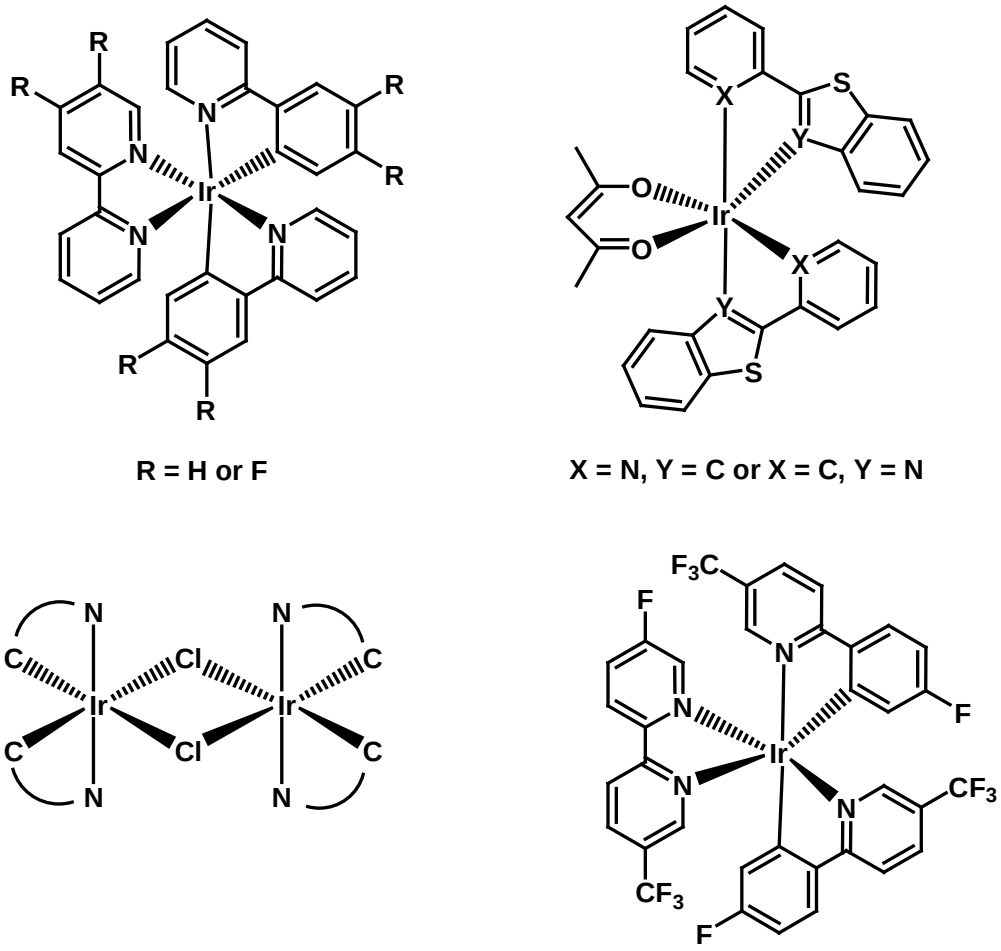

Figure 1.32[142, 148]**:** triplet emitting materials and related intermediates

The electrically generated excitons, produced when holes and electrons, after being injected, migrate through the thin film to the interface between the two layers recombine, can be either singlets or triplets.[149] Theoretical predictions and experimental measurements suggest a singlet-to-triplet ratio for the excitons of 1 to 3. The strong spin-orbit coupling due to the presence of heavy-metal complexes enhances therefore the efficiency of the emission.[147] In fact triplet emitters can have theoretical limit of emission efficiency of 100% against the about 25% of the singlet emitters such as organic molecules.[68] Thanks to their electroluminescence properties, iridium(III) complexes have been found to be

promising for use in OLEDs, as they are not subject to displacement effects under electrical fields[141] and neutral iridium(III) complexes have attracted a lot of attention in this field during the last decade. The interest shown towards Ir(III) metal complexes is also driven by the possibility of changing the emission energy in order to make possible a wide variety of colours, ranging from green for $Ir(ppy)_3$ to yellow, red and blue according to the ligand.[86, 133, 150, 151] In their work, Thompson and Forrest reported how, by changing the nature of the excited states, they observed emission from different regions of the visible spectrum.[150, 152] Holmes and Friend in a similar way tuned the electrochemiluminescence into green-blue emission by synthetic modifications and improved operational lifetimes of the devices by introducing less labile ancillary ligands on the complexes.[153] Anionic iridium complexes of the form $[Ir(ppy)_2X_2]$, where X can be CN^- or NCO^-, are found to show similar properties that can be exploited in OLED fabrication thanks to their improved stability[68]. Cationic iridium(III) complexes have recently emerged since they show ability to electrochemiluminesce from a single-layer of neat complex sandwiched between two air-stable electrodes.[68]

1.5.2. Oxygen sensing

Ir(III) cyclometallated complexes show high luminescence in degassed solution, with quantum yields of the order of 0.5 and even higher and lifetimes in the range of μs.[154, 155] In the presence of oxygen (aerated solutions) quantum yields and lifetimes can be quenched by a factor of even 60 times compared to the values in degassed solutions.[147] Thanks to their tunable excited state properties and relatively high stability in presence of singlet oxygen,[156] iridium(III) luminophores have found potential application as oxygen probes in various medicinal, chemical and environmental sensors.[157-159] This is due to the fact that an efficient energy transfer occurs to the triplet ground state of molecular oxygen that results in luminescence quenching of the complex and the formation of singlet state oxygen $O_2(^1\Delta_g)$.[68, 160] Oxygen concentration is then quantified according to the changes in the luminescence intensity and in the lifetime of the complex.[161] The biggest limitation to the successful application of solid state iridium(III) based sensors is due to the possibility of self-quenching between neighboring molecules.[68] Ongoing studies are focussing on trying to avoid such a limitation, which can be

done by separating the luminescent dyes by embedding them in oxygen permeable polymeric matrices with the intention of preventing dye aggregation, but the low loading concentration limits the sensitivity of the sensor.[68, 160]

1.5.3. Solar energy harnessing and photocatalytic water splitting

Of major interest for scientists is the possibility to convert solar irradiation into an usable form of energy.[68] Iridium(III) complexes can be used as photosensitisers in harnessing solar energy through a photocatalytic cycle to split water into oxygen and hydrogen that can provide a valid source of fuel.[68] In fact in such processes a transition metal is required as photosynthesiser in conjunction with an electron relay to collect and store radiant energy and then convert protons to hydrogen molecules.[68, 162-164] The process involved is composed of two half reactions; in one the water is oxidised into molecular oxygen and in the other reduced into molecular hydrogen.[68] The possibility of producing hydrogen attracts a big deal of attention into this process since hydrogen can represent a potential source of fuel. Due to the ease with which cyclometallated iridium(III) complexes may be involved in typical photoreduction schemes, they can serve as photosensitisers in combination with an electron relay used to collect and store radiant energy in order to transform protons into molecular hydrogen.[161, 162] In particular heteroleptic iridium(III) complexes are thought to be promising candidates for this type of application and recently have displayed significant improvements in terms of hydrogen production compared to the previously used $[Ru(dmphen)_3]^{2+}$ (dmphen=4,7-dimethyl-1,10-phenanthroline).[165] (Figure 1.33) The improvement in hydrogen production has been attributed to the fact that Ir(III) complexes are stronger reducing agents compared to ruthenium complexes, allowing an easier passage of electrons to the electron relay.[68]

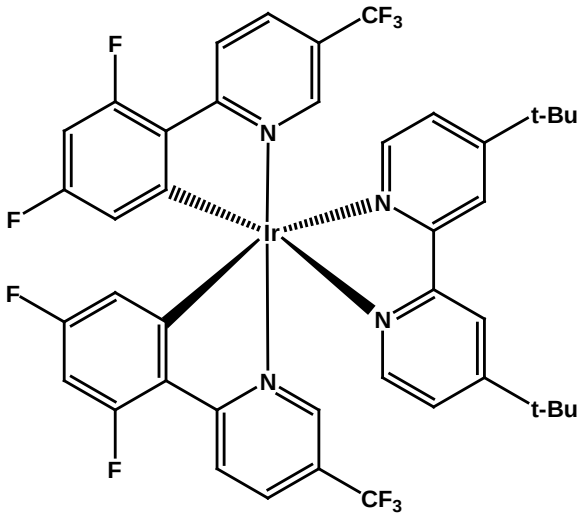

Figure 1.33[165]: heteroleptic Ir(III) complex synthesised by Bernhard *et al.* The complex showed improvements in hydrogen production compared to the standard $[Ru(dmphen)_3]^{2+}$ previously used.

1.5.4. Bioanalytical applications

Iridium(III) complexes can be good candidates for bioanalytical applications as well.[68] Intense emission and long-lived excited states are the properties that render them excellent materials for sensitive and time resolved detection.[166] The ability of suitably functionalised iridium complexes to bind biological substrates allows biological labelling applications.[68] The complexes can bind substrates in two different way, the complex can be bound covalently with, for example, aldehyde-amine cross linking or for example noncovalently by DNA intercalation.[167, 168] The complexes bound to the substrates exhibit different luminescence properties from their substrate-free forms, changing the features of their properties according to the different enviroment they are bound to. Therefore labels based on luminescent complexes can be used for monitoring bioconjugation reactions and the binding affinity to different substrates.[169]

1.5.5. Light-emitting Electrochemical Cells (LECs)

Light-emitting Electrochemical Cells (LECs) can potentially offer an alternative type of light emitting device to OLEDs.[170-174] Unlike conventional OLEDs in fact, LECs display some advantageous properties, in particular light emission with low threshold voltages. Moreover, the onset voltage has been found to be almost

independent of the film thicknesses. LECs exhibited signignificantly improved electroluminescence efficiencies compared with analogous OLEDs and proved to be fairly insensitive to the electrode work-function. Higher quantum efficiencies of the LECs have been attributed to a balanced electron and hole injection as well as the favourable location of the emissive layer in the centre of the organic medium. LECs are composed of an active polymer layer which contains both electronic and ionic conductors sandwiched between two electrodes.[172] A semiconducting polymer and a polyelectrolyte form an intimate blend with a phase-separated bicontinuous network morphology in which both ionic and electronic charge-carriers are mobile. (Figure 1.34a.) Upon a sufficiently high voltage being applied to the electrodes, near the cathode the polymer is reduced and at the anode is oxidised. In order to mantain charge neutrality, the positive-type (*p-type*) and negative-type (*n-type*) doped layers formed are stabilised by counter ions available in the ion conducting phase.(Figure 1.34b.) Under the influence of the applied field, these regions extend towards the centre of the layer, forming an electrochemically induced p-n junction, where the p-type carriers (holes) and n-type carriers (electrons) meet and recombine leading to emission of a photon.[174] (Figue 1.34c.)

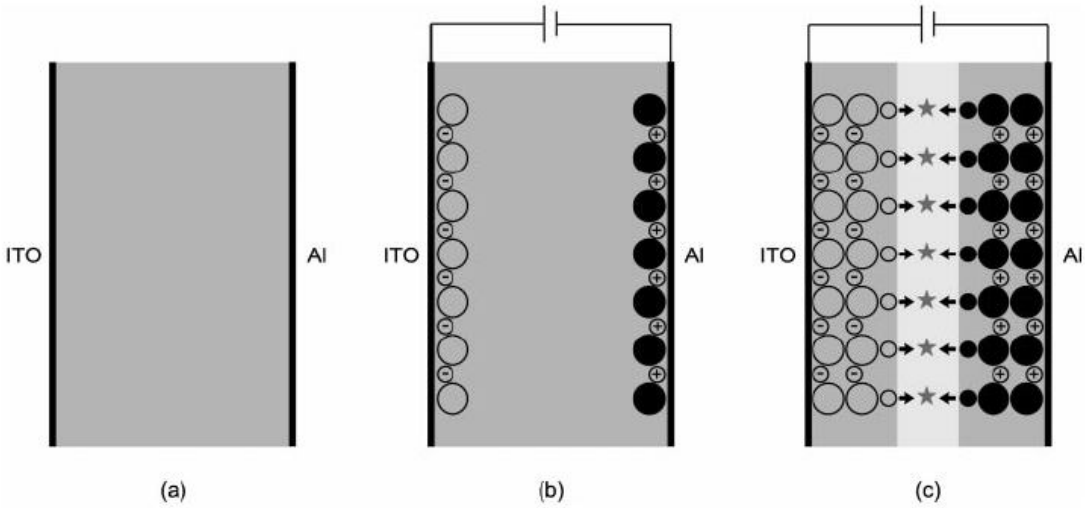

Figure 1.34[174]: schematic diagram showing the mechanism of charge recombination in LECs leading to emission of light.

De Cola and co-workers introduced devices containing metal complexes as charged species, in particular a combination of dinuclear $[Ru(bpy)_3]^{2+}$ complexes blended in PPV was used.[175] Even though most of the reported examples of LECs contain Ru(II) based complexes, and only few cases of Ir(III) complexes have been investigated, positively charged Ir(III) coplexes show promising characteristics to be exploited in this type of application. Liu, Pend and co-workers reported the application of cationic iridium(III) complexes in LECs in 2007.[176] (Figure 1.35)

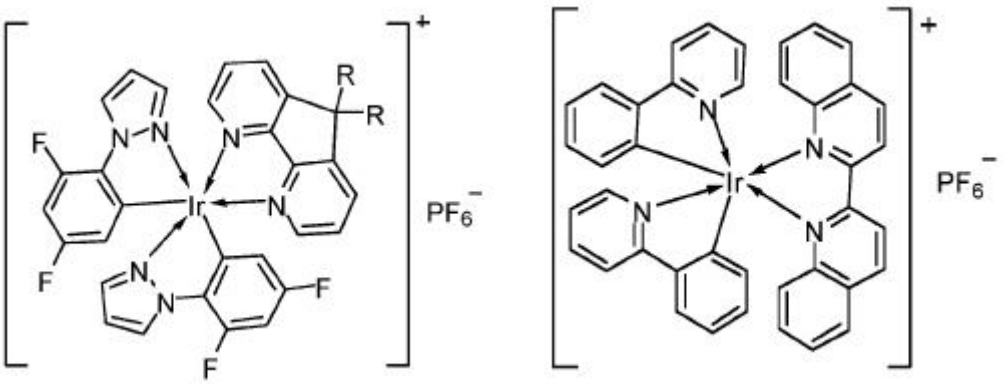

Figure 1.35[176]: cationic complexes used by Liu, Pend and co-workers in LECs

1.6. Rhodium complexes

Luminescent ruthenium(II) complexes have played a major role in inorganic photochemistry and less attention has been given to iridium(III) complexes, but even leser has probably been given to rhodium(III) complexes.[177] A possible explanation may be the fact that tri-cationic species present more synthetic and work-up difficulties if compared to dicationic Ru(II) based species.[178] Nevertheless Rh(III) complexes can find application in DNA and RNA biological

sensors and also in photomolecular devices.[179] In 1979 Demas *et al* synthesised $[Rh(bpy)_3]^{3+}$ with an analogous synthetic strategy to $[Ir(bpy)_3]^{3+}$.[180] The emission displayed by the bpy based Rh(III) was lower in intensity compared to the analogous Ir(III) and Ru(II) complxes and with shorter lifetimes. The emission of $[Rh(bpy)_3]^{3+}$ was described as being of a ^{3}LC character.[181] (Figure 1.36a))

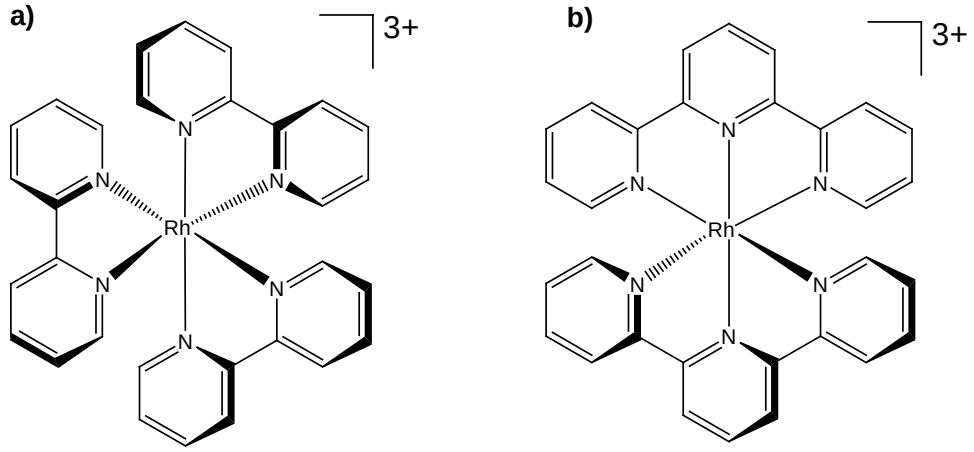

Figure 1.36: structure of $[Rh(bpy)_3]^{3+}$ and $[Rh(tpy)_2]^{3+}$

The complex, $[Rh(tpy)_2]^{3+}$ (Figure 1.36b)) containing two terpyridine terdentate ligands having a lower ligand field strength than three bipyridine only shows emission at 77 K from a MC excited state.[182] Rhodium complexes containing cyclometallating ligands were also synthesised. In fact *fac*- and *mer*-$[Rh(ppy)_3]$ were prepared adopting synthetic procedures similar to those reported for $[Ir(ppy)_3]$. However the emission was much weaker than that of the iridium analogue, being relatively weak for *fac*-$[Rh(ppy)_3]$ (Figure 1.37a)) in degassed solution at room temperarature.[183] The most commonly studied cyclometallated rhodium complexes are the bis-cyclometallated tris-bidentate complexes of the class $[Rh(ppy)_2(bpy)]^+$ (Figure 1.37b)) synthesised similarly to their iridium anologues (via di-chloro bridge dimer as an intermediate).[184] $[Rh(ppy)_2(bpy)]^+$ showed structured long-lived emission at low temperature from a predominantly ppy-based π– π*, LC excited state with a small amount of mixing with the MLCT

state associated with the ppy ligands.[24] This differs significantly from the iridium analogue, from which emission of MLCT character was observed.[185]

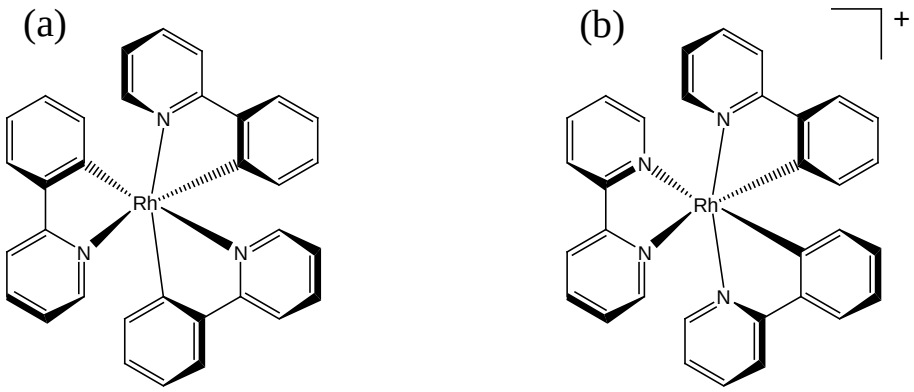

Figure 1.37[24]: Structure of (a) *fac*-[Rh(ppy)$_3$] and (b) [Rh(ppy)$_2$(bpy)]$^+$.

The photophysical properties of [Rh(NC)$_2$(NN)]$^+$ complexes can be modulated by varying or functionalising the NC and/or NN-coordinating ligands. The introduction of 2-thienylpyridine as N^C fragment leads to an increase of the emission intensity and lifetime at room temperature, which is thought to be due to the lower energy of emission and thus to reduce thermal deactivation of the emissive state by the higher-lying MC states.[186, 187]

CHAPTER 2

Synthesis of mononuclear Iridium(III) and Rhodium(III) complexes

2. Synthesis of mononuclear iridium and rhodium complexes

2.1 Background and objectives of the work

The research of the group has focused on assessing the influence of cyclometallation on the excited states of iridium(III) complexes. As mentioned in Chapter 1, the increased participation of the metal centre in the excited states of the complexes increases with the number of cyclometallation sites in the coordination spere. This is displayed by comparing the photophysical properties of complexes with a different degree of cyclometallation. Systems containing exclusively polypyridyl ligands with no cyclometallation sites have generally a ligand-centred emission. In those with one and two cyclometallating units, the participation of the metal centre in excited states increases progressively until being assigned as mainly MLCT in complexes with three cyclometallating ligands (Figure 2.1).[106]

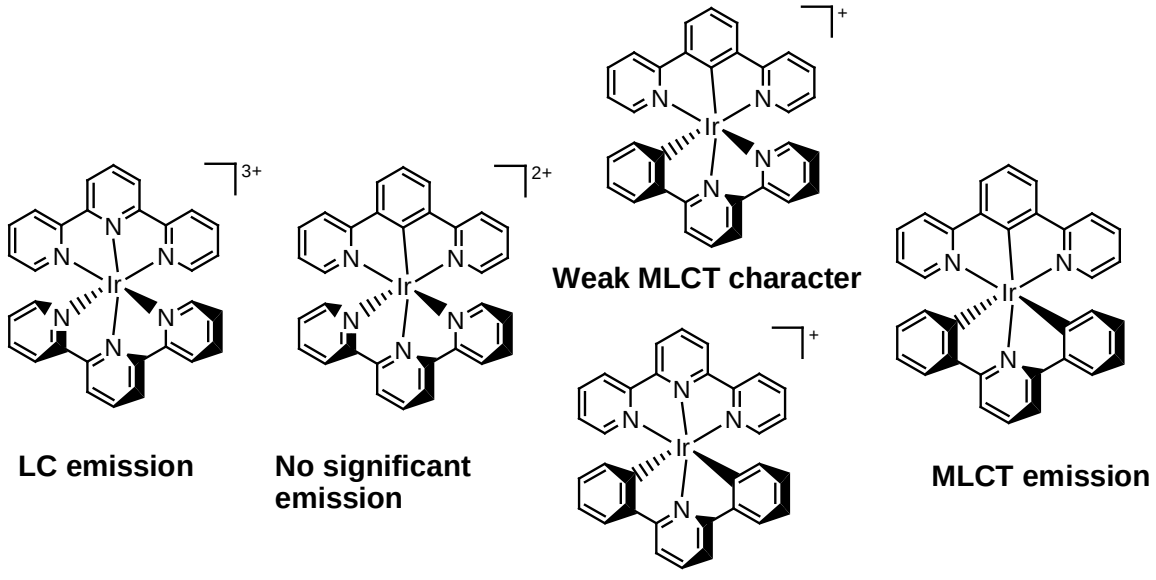

Figure 2.1: the role of the metal centre in the excited states is related to the number of cyclometallating sites in the coordination spehere, here bis-terpyridine, mono-, bis and tris-cyclometallated complexes are shown.

Within our research group, systems of the classes Ir(N^C^N)(C^N^C), Ir(N^C^N)(C^N^O) and Ir(N^C^N)(N^N^N) were previously studied, in which two terdentate ligands fullfilled the coordination sphere of the iridium(III) centre. In particular, tris-cyclometallated complexes containing terdentate ligands displayed photophysical properties similar to those of tris-bidentate analogues, such as $Ir(ppy)_3$, which is one of the most used green emitters for OLEDs applications. Despite the photophysical properties manifested by Ir(N^C^N)(C^N^C) complexes, very low stability in solution required the design of a new iridium(III) platform. To date, previous work within the research group on iridium (N^C^N)-coordinated complexes included the synthesis and photophysical properties of one complex of the form Ir(N^C^N)(N^C)Cl, containing two cyclometallating ligands, the second being phenyl-pyridine. This charge-neutral complex showed high luminescence quantum yield in solution and blue-shifted emission compared to that of Ir(N^C^N)(C^N^C) complexes.

In this work, particular attention is given to bis-cyclometallated complexes with the same general structure, but containing different types of N^C^N ligands, each of which is investigated in the presence of dFppy (2-(4,6-difluoro-phenyl)-pyridine) and ppy (2-phenyl-pyridine) as N^C bidentate ligands in the metal coordination sphere. The same ligand units were also introduced onto rhodium(III) metal centre. The synthesis of new iridium(III) bis-cyclometallated complexes is promising for OLED applications as charge-neutral complexes are generally preferred over charged compounds.[188] Also, introduction of bipyridine as bidentate ligand was investigated (complexes of the general structure $[Ir(N^C^N)(bpy)Cl]^+$), in order to compare the effect of a neutral ligand on the complex properties and its introduction offers an interesting point of comparison with the bis-cyclometallated analogues. Moreover, recent studies have pinpointed positively charged iridium(III) complexes as appealing candidates for LECs applications and the complexes $[Ir(N^C^N)(bpy)]^+$, being relatively highly luminescent, may match the properties required for such applications.

A new class of trans-bis-cyclometallated Ir(III) complexes have also been investigated, namely complexes of the form $[Ir(N^C^N)_2]^+$ and

$[Ir(N^C^N)(N^C^N)']^+$, their synthesis is discussed in this work, although the range of complexes of this type that have been possible to isolate in pure form has proved to be limited.

In general, the achiral structures introduced with the use of terdentate ligands in the iridium(III) coordination sphere offer advantages; in fact this new class of Ir(III) complexes can represent a possible candidate in creating multicentered systems in which the problem of geometrical isomerism is overcome.[87]

The generic pathway adopted to synthesize bis-cyclometallated complexes proceeds through two steps, each of which involves the coordination of a cyclometallating ligand to the metal center (Figure 2.2). The first synthetic step involves the coordination of an N^C^N ligand to the iridium(III) ion. The coordination of the terdentate ligand leads to the formation of a di-chloro-bridged iridium dimer which is then cleaved to yield a bis-cyclometallated complex by the addition of a second cyclometallating ligand (N^C^N or N^C).

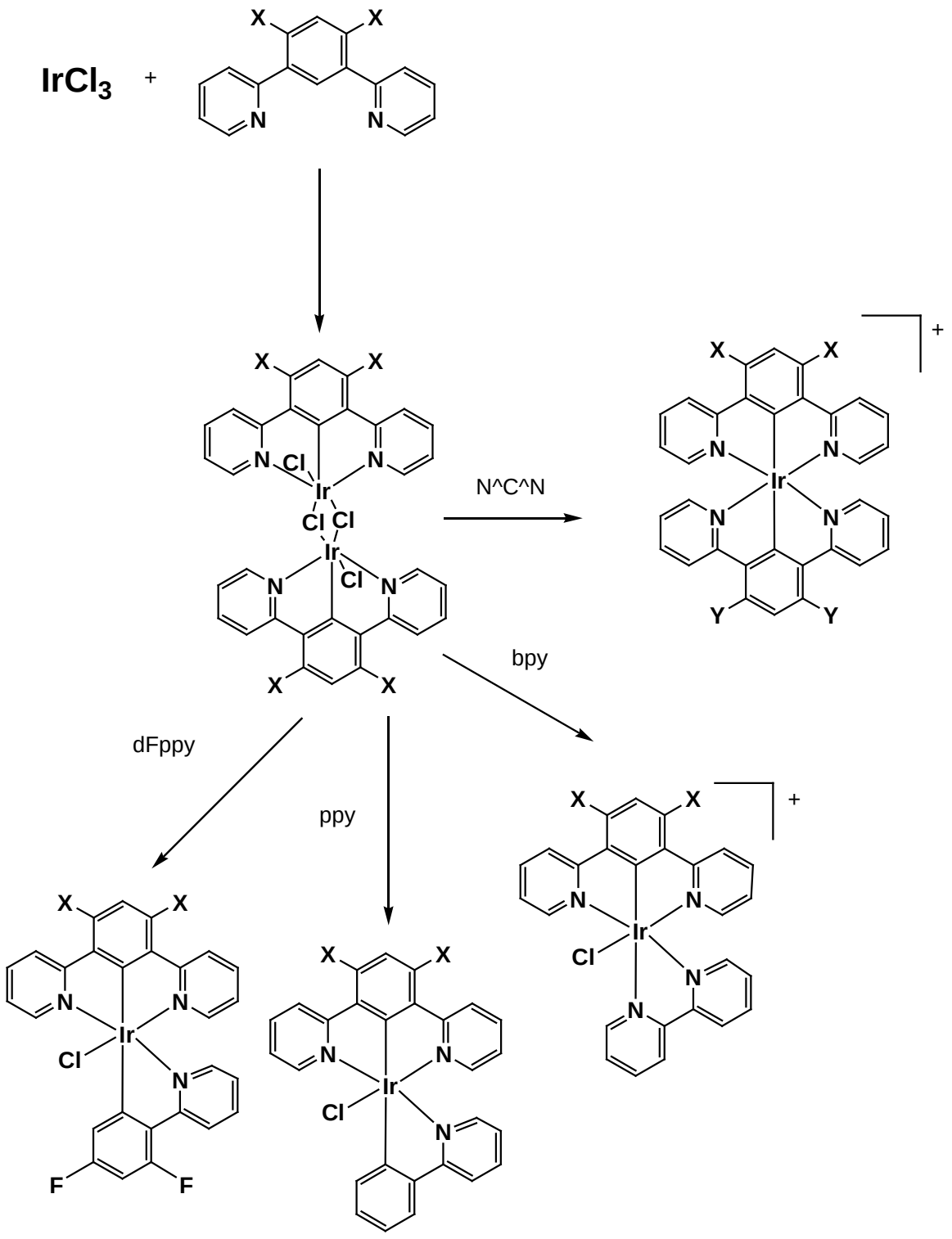

Figure 2.2: general scheme for the synthesis of bis-cyclometallated iridium complexes, where X = -CH_3, -CF_3, -F, Y = -CH_3, -F

In the formation of the di-chloro bridged iridium dimers, an important role is played by the substituents present in the 3 and 5 positions of the cyclometallating ring of the terdentate ligand. Their presence avoids the formation of different types of coordination modes of the cyclometallating ligand to the iridium centre, as shown in figure 2.3. In fact, since the C-C bonds connecting pyridyl and phenyl rings of the terdentate ligands are free to rotate, two different ways of coordination are possible in the absence of these substituents, since cyclometallating sites are also available at positions 3 and 5 of the cyclometallating ring. Coordination from the ligand can occur as a terdentate N^C^N when cyclometallation occurs on position 1 of the phenyl ring (Figure 2.3b)), but also, the same unsubstituted N^C^N ligand can aproach the iridium centre as a bidentate N^C ligand when cyclometallation occurs on positions 3 or 5, with the remaining pyridyl ring not coordinating to the metal center (figure 2.3a)).

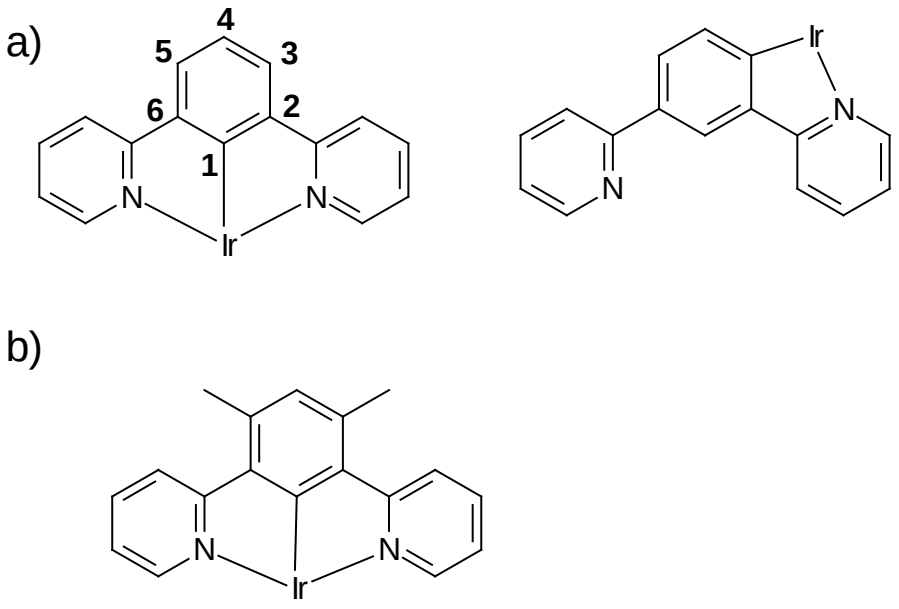

Figure 2.3: a) two different modes of coordination are possible with unsubstituted N^C^N units, in the absence of substituents in 3 and 5 positions of the phenyl ring; b) in the presence of only substituents the mode of coordination possible is as a terdentate ligand

The possibility of two cordination modes leads to a mixture of products, wich are difficult to separate, given the generally low solubility of iridium di-chloro bridged dimers. Two different aproaches can be adopted in order to avoid this problem. Design of ligands bearing substituents on the positions 3 and 5 of the phenyl ring of the N^C^N frame (e.g. the methyl groups as in Figure 2.3) prevents the formation of the undesired products with the N^C coordination mode of Figure 2.3 a). An alternative strategy to avoid the same problem, previously adopted by our research group, is also represented by synthesising ligands with a C_3 symmetry (Figure 2.4).[24]

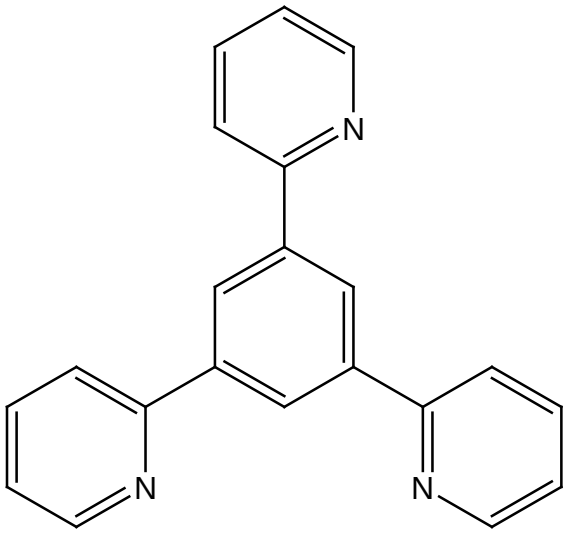

Figure 2.4: example of terdentate ligand in which all three potentially cyclometallating sites are equivalent, forming N^C^N coordination.

Complexes Ir(N^C^N)(N^C)Cl can undergo displacement of the Cl, leading to the introduction of a different ancillary ligand at the sixth site of the coordination sphere of the iridium centre. For instance, in this work is described introduction of CN, SCN and a variety of substituted and unsubstituted aryl acetylides, all of which are monodentate monoanionic ancillary ligands.

For each complex synthesized, characterization by mass spectrometry and NMR spectroscopy gave important information about the structural identity and purity of the target complexes. Particular attention was also given to new strategies in tuning the emission energy of the complexes. Substituents on both the N^C^N and the N^C ligand are proved to play a role in tailoring the energies of the frontier orbitals that determine the colour of the emission. The electron-withdrawing or electron-donating nature of the substituents plays a determinant role in shifting the emission over a wide range of colours, towards either the blue or the red region. The support of theoretical studies, such as DFT calculations, is fundamental in order to design ligands capable of varying the energy of the orbitals involved in the emission process, with the aim of affecting the HOMO-LUMO energy gap of the complexes.

2.2. Synthesis of Ligands

In this section the synthesis of two main types of ligands is discussed, depending on the mode with which they can coordinate the metal centre: ligands which are able to coordinate the metal centre as N^C^N monocyclometallating terdentate ligands and C^N monocyclometallating bidentate ligands.

2.2.1. Synthesis of terdentate N^C^N ligands

Coordination of polypyridyl ligands, such as 2,2′:6′,2″-terpyridine (tpy), to metal centres leads to formation of highly stable complexes whose formation is enforced by σ-donating nitrogen and π-accepting heterocycles.[109, 189-191] In addition, the use of terdentate fragments coordinating metal centres offers structural advantages (see Chapter 1). In this chapter, the synthesis of derivatives of 1,3-di(2-pyridyl)benzene (bpybH) as terdentate cyclometallating N^C^N ligands is described. This class of ligands is isoelectronic with tpy, but N^C^N ligands are anionic, due to the C-H unit that replaces the central N atom of the neutral ligand tpy.[109] The activation of the C-H unit is thus fundamental to give cyclometallation towards the metal centre (Figure 2.5).

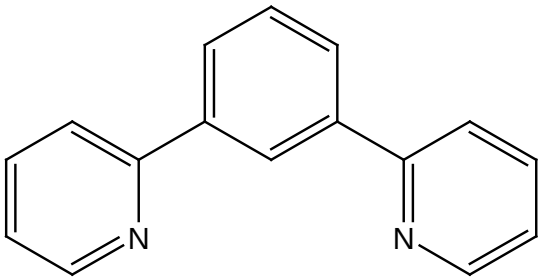

1,3-bis(2-pyridyl)benzene
bpybH

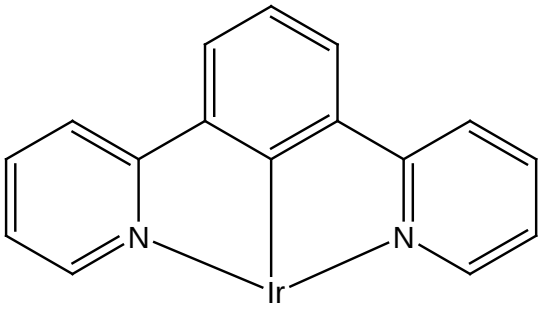

N^C^N-cyclometallated bpyb

Figure 2.5[109]: 1,3-di(2-pyridyl)benzene coordinating a metal centre upon activation of the C-H unit.

The first examples of N^C^N-coordinating bpyb were reported by Sauvage and Collin in the 1990s, using ruthenium and osmium.[109] The preparation of the N^C^N moieties was achieved by reaction of 1,3-dicyanobenzene with acetylene, under 10 atm pressure and at 130°C, the reaction being catalysed by Co(Cp)(COD) (where Cp=cyclopentadiene and COD=1,5-cyclooctadiene).[192, 193] (Figure 2.6) This synthetic pathway, even though leading to a high yield of the desired terdentate ligand, includes the use of acetylene, which is potentially explosive under pressure.[109]

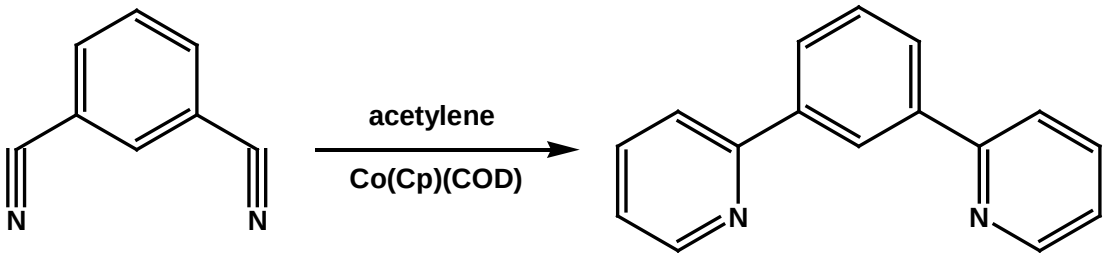

Figure 2.6[109]: cobalt-catalysed synthesis of 1,3-bis(2-pyridyl)benzene from 1,3-dicyanobenzene and acetylene.

More recently, palladium catalysed cross-coupling reactions have been widely used for the synthesis of polyaromatic ligands.[24] In particular, cross-coupling involving a 1,3-dihalogen aryl ring and 2-substituted pyridyl substrates represents a general scheme for the synthesis of terdentate N^C^N ligands (Figure 2.7). Stille cross-coupling conditions can produce the desired N^C^N systems, when -SnR_3 is the substituent attached onto the pyridyl ring.[194] Alternatively, py-ZnCl precursors were also used by Negishi for the synthesis of similar frames.[195] Suzuki cross-coupling[196] has also been reported as an advantageous procedure in the synthesis of dpybH type of ligands, borate substituted moieties being less toxic if compared to the analogous stannyl derivatives. However, owning to the instability of the pyridine-2-boronic acid, Suzuki cross-coupling is significantly troublesome in the synthesis of N^C^N ligands and Stille and Negishi's methods result thus to be more of an appealing choice.[109]

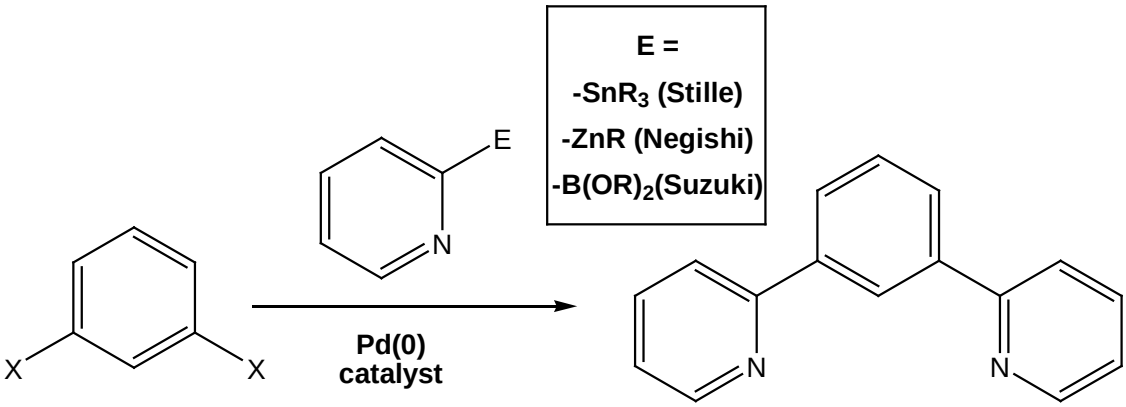

Figure 2.7[109] : summary of the synthetic pathways leading to fomation of bpybH ligands, Stille's method (E = -SnR_3 precursor), Negishi's method (E = -ZnR precursor) and Suzuki's method (E = -$B(OR)_2$).

2.2.1.1. Synthesis of N^C^N ligands via Stille cross-coupling

Even though Stille's method involves the use of rather undesirable toxic compounds, whilst good results are reported in the literatue for the synthesis of 5-methyl-1,3-di(2-pyridyl)benzene (dpymbH) by Negishi's coupling[197], during previous work within our research group poor yields were obtained by adopting Negishi's procedure.[197] Therefore Stille cross coupling is described in this Chapter as the main synthetic route towards preparation of N^C^N cordinating units, due to the availability of 2-tri-*n*-butyl-stannylpyridine. In 1999, Cardenas and co-workers reported the first example for the synthesis of dpybH via Stille's cross-coupling (Figure 2.7).[194] The reaction mechanism of the Stille's cross-coupling is summarised in Figure 2.8 and it involves in a first step the reduction of the palladium catalyst (compound **1** in Figure 2.8) to the active Pd(0) species **2**. This is followed by oxidative addition of the organohalide (**3**) to give a cis intermediate which isomerizes to the trans intermediate (**4)**. Then transmetallation with the stannane takes place (**5**) to form the intermediate shown (**7)**, which is finally converted into the desired product (**8**), and regenerating the active Pd(0) species **2,** by reductive elimination.[198]

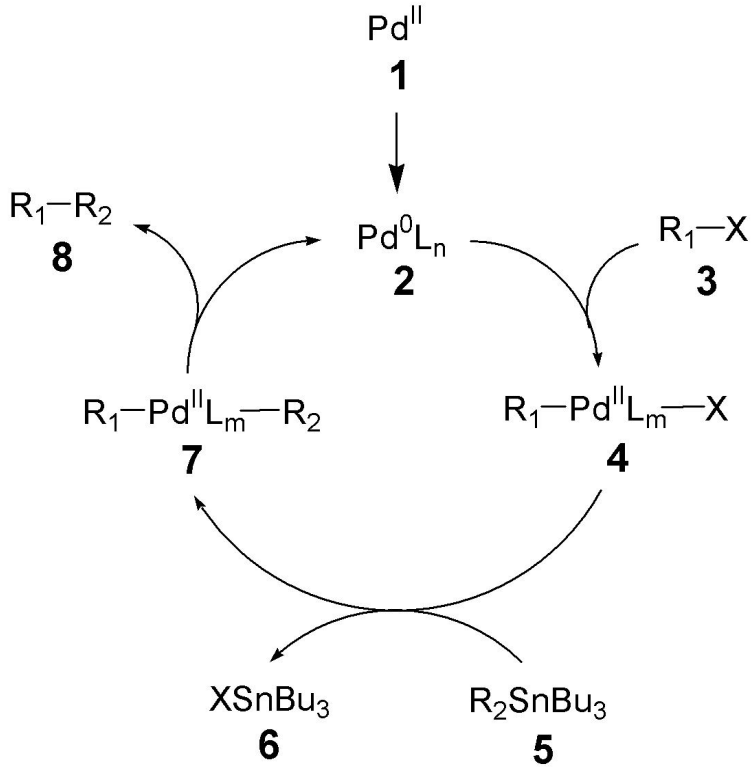

Figure 2.8[198]: general mechanism of Stille cross-coupling involving activation of the catalyst to Pd(0), followed by oxidative addition and reductive elimination to give the desired cross-coupled species.

In this work the synthesis of terdentate N^C^N ligands bearing substituents on the positions 3 and 5 of the phenyl ring has been carried out, owing to the previously discussed synthetic advantages which they offer during the preparation of the intermediate iridium di-chlorobridged dimers. Synthesis of 1,3-di-(2-pyridyl)-4,6-dimethyl-benzene (H**L1**) (Figure 2.9) was carried out in two steps: Dibromination of m-xylene was achieved upon reaction with excess bromine in the presence of a catalytic amount of iodine, giving 2,4-di-bromo-m-xylene with a yield of 22%.[199] (Figure 2.9a)) Stille's cross-coupling reaction[194, 200] then carried out by reacting this product with 2-tri-n-butyl-stannyl-pyridine in the presence of bis(triphenylphosphine)palladium(II) chloride as catalyst and lithium chloride, all under an inert atmosphere in toluene as a solvent at reflux for 3 days. (Figure 2.9b)) Purification of the final product was achieved by silica gel chromatography,

which separated the desired N^C^N system (yield=26%) from the starting material and the mono pyridyl-substituted benzene. Formation of the bis pyridyl-substituted benzene is confirmed by ^{1}H-NMR and mass spectrometry.[197]

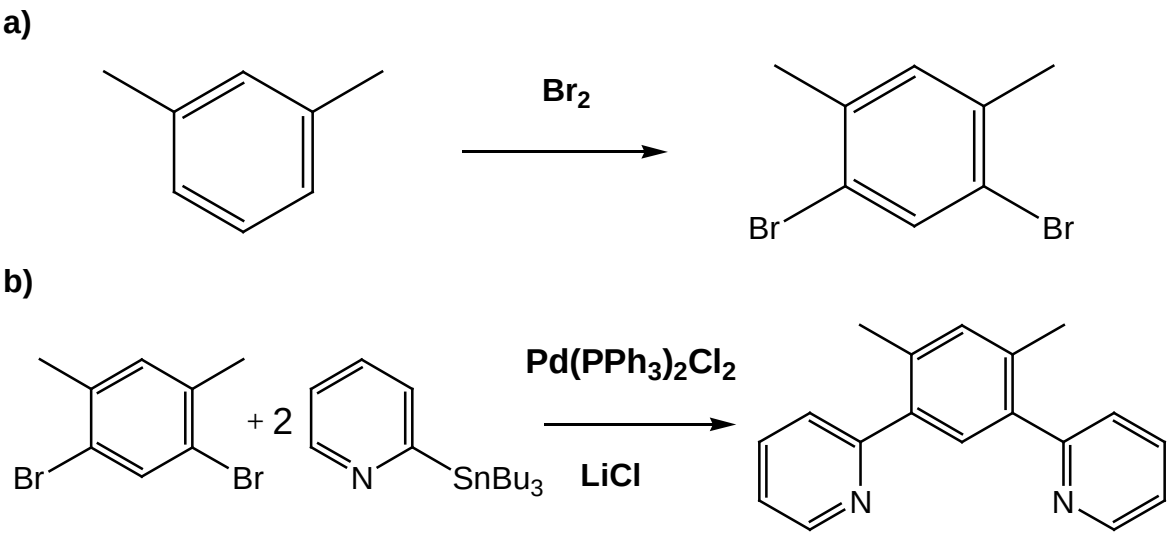

Figure 2.9: synthesis of H**L1**, **a)** bromination of m-xylene; **b)** Stille's cross-coupling

The synthesis via Stille's conditions of other 4,6-substituted N^C^N ligands is also reported, following preparation of the dihalogen precursors. Similarly to H**L1**, the ligand H**L2** (Figure 2.10), was prepared by a two step synthetic pathway. Bromination of 2,4-difluorobromobenzene gave 1,5-dibromo-2,4-difluorobenzene (yield=77%). (Figure 2.10a)) which was followed by Stille's cross-coupling to give the target N^C^N ligand with a yield of the order of 50-60% (Figure 2.10b)).

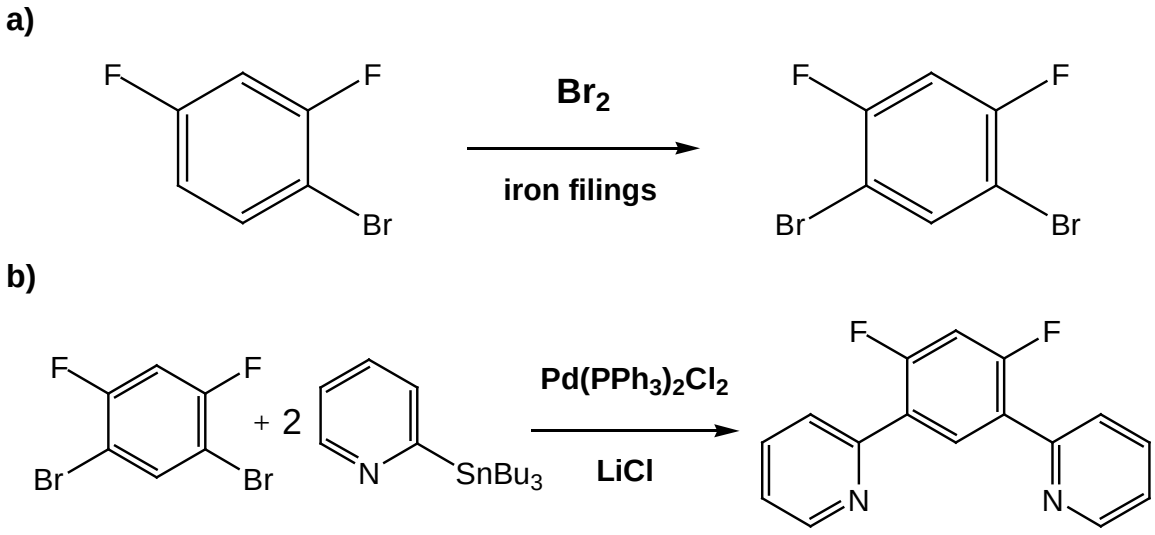

Figure 2.10: synthesis of H**L2** by **a)** bromination of 2,4-difluoro-bromobenzene and **b)** Stille's reaction to give the target product.

Synthesis of H**L3** was achieved by a three-step pathway. 3,5-Bis-trifluoro-methyl-aniline was dibrominated[201] (yield=77%) (Figure 2.11a)), then the amino group was removed from the 1,5-dibromo-2,4-bis-trifluoromethyl-aniline by treatment with sulfuric acid and sodium nitrite to yield 2,6-dibromo-3,5-bis-trifluoro-methyl-benzene[201] (yield=37%), (Figure 2.11b)) Finally, this compound was cross-coupled with 2-tri-n-butyl-stannyl-pyridine to obtain the N^C^N target ligand H**L3** (yield=25%) purified by silica gel chromatography (Figure 2.11c)).

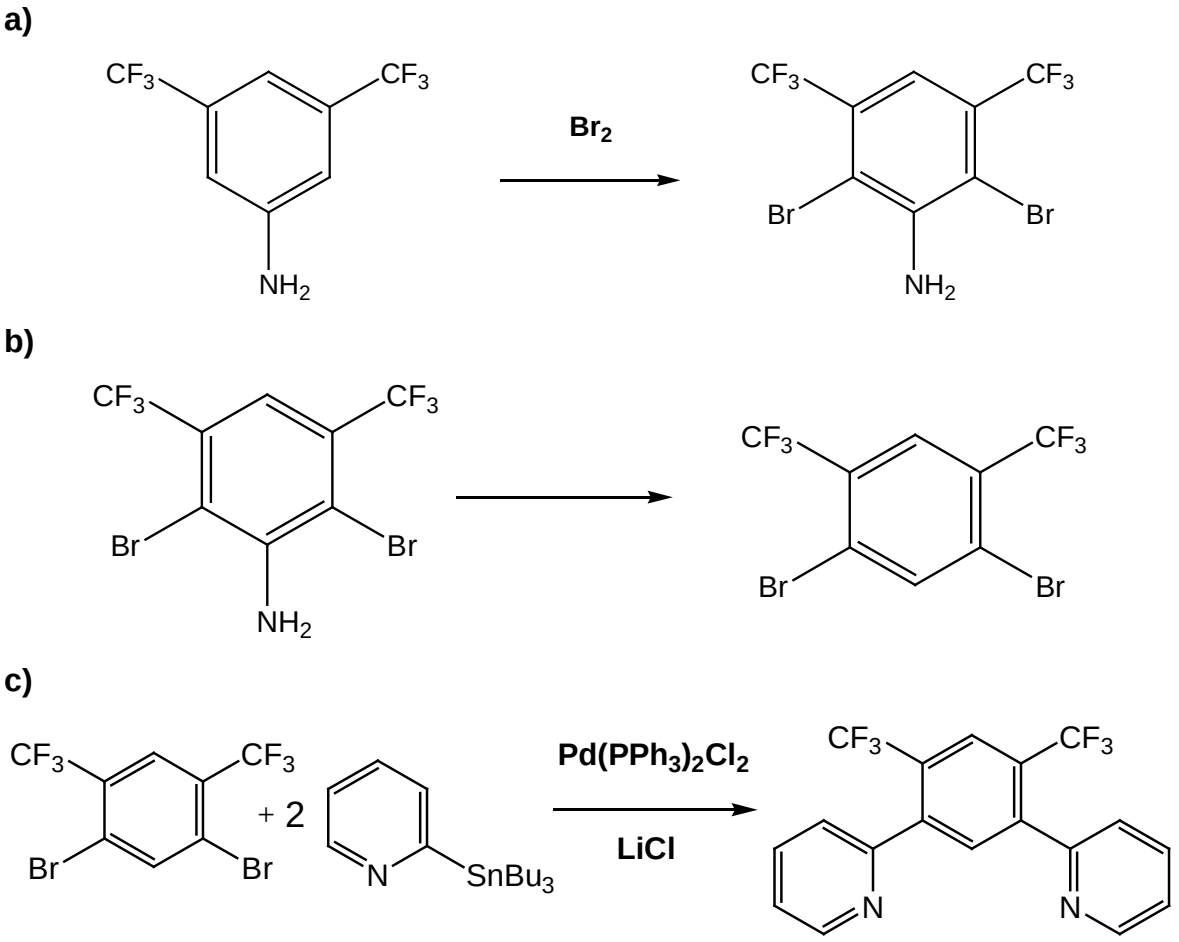

Figure 2.11: synthesis of H**L3**, **a)** bromination of 3,5-bis-trifluoromethyl-aniline; **b)** removal of $-NH_2$ and **c)** Stille's cross-coupling

As will be discussed in Chapter 3, it was also of interest to us to prepare N^C^N ligands incorporating substituents in the pyridyl rings, in addition to the phenyl rings. For this purpose, the appropriately substituted pyridines carrying a tributyltin group at the 2-position were required. They should be accessible by reaction of the 2-lithio derivatives with Bu_3SnCl.

Conventionally, halogen-lithium exchange is used. However, in this work, we made use of a reactant diverted ortho lithiation procedure, which avoids the need for the 2-halogen pyridine.[202]

For example, treatment of 4-(trifluoromethyl) pyridine with butyl lithium in dry THF in the presence of dimethylaminoethanol led directly to 2-lithio-4-(trifluoromethyl) pyridine which, upon treatment with Bu_3SnCl, gave the corresponding stannane

(Figure 2.12). Subsequent reaction with 1,3-dibromo-4,6-bis(trifluoromethyl) benzene gave ligand H**L4** (Figure 2.13).

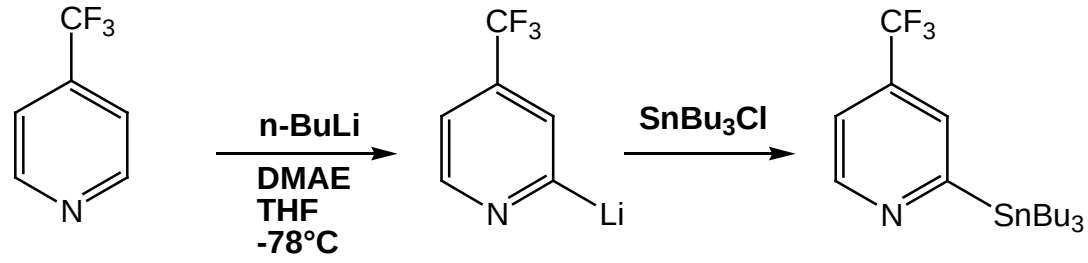

Figure 2.12: preparation of 2-tri-n-butylstannyl-4-(trifluoromethyl)-pyridine via ortho-diverted lithiation, where DMAE = dimethylamino ethanol

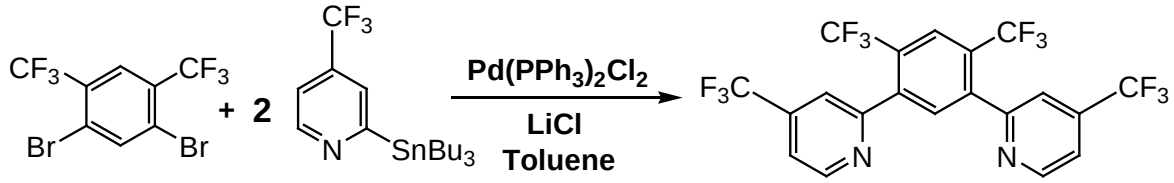

Figure 2.13: synthesis of H**L4** via Stille's cross-coupling.

2.2.1.2. Synthesis of N^C^N ligands via Miyaura cross-coupling

As shown in Figure 2.14, 1,3-benzenediboronic acid can be cross-coupled with 2-bromopyridine and to give bpyH derivatives.[109]

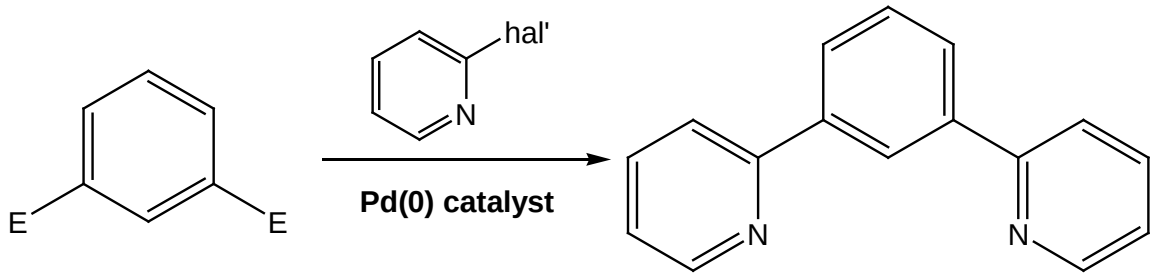

Figure 2.14: synthetic path leading to formation of bpybH ligands via Suzuki's method, where E = -$B(OH)_2$ and hal' = halogen

The mechanism of this type of reaction is illustrated in Figure 2.15.

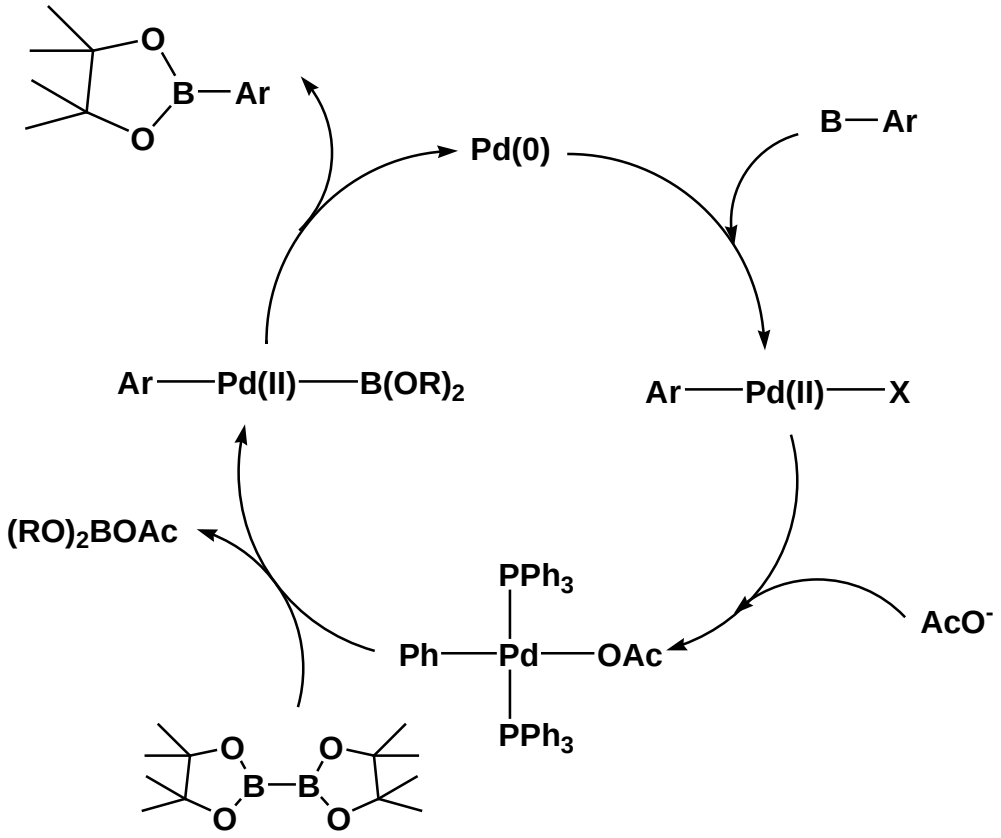

Figure 2.15[203]: generic mechanism of Suzuki-Miyaura cross-coupling of an aryl halide with boronic ester or acid.

This methodology can be exploited in order to synthesise bpybH systems bearing a larger variety of substituents on the position 4 of pyridyl rings avoiding the use of stannyl derivatives. In this section, the synthesis of such bpyb bearing –OMe and -NMe_2 in the pyridine rings is discussed. The synthesis of H**L5** (see Figure 2.18) involved prior preparation of the 4-methoxy substituted bromopyridine and of the aryl diboronate ester fragment, followed by Suzuki-Miyaura cross-coupling reaction.[204, 205] The synthesis of 2-bromo-4-methoxy pyridine was carried out in the four steps summarised in Figure 2.14, starting from 2-bromopyridine.

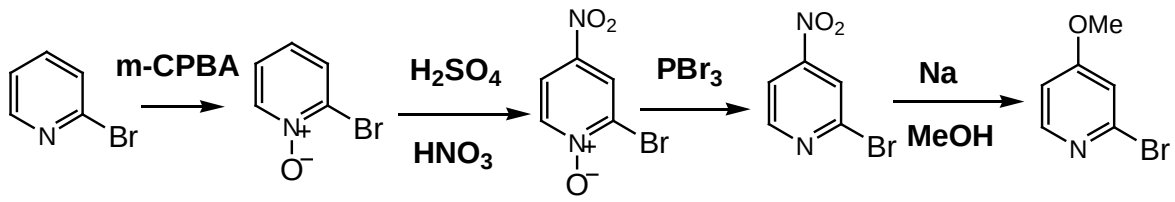

Figure 2.16: synthetic pathway to 2-bromo-4-methoxypyridine

The aryl fragment 1,3-di-(pinacolatoboron)-4,6-difluoro-benzene was prepared from 1,3-di-bromo-4,6-di-fluoro–benzene, by a Pd catalysed Miyaura reaction with bis(pinacolato)diboron. In line with the conditions originally defined by Miyaura for simple aryl halides, Pd(dppf)Cl_2 was used as a catalyst, in the presence of KOAc (Figure 2.17).[206] The diboronic ester was obtained in 80% yield following a simple work-up procedure. This is the first reported example of the utility of the Miyaura reaction in preparing 1,3 aryl diboronate esters incorporating flanking substituents. It should be noted that the classical procedure for boronic acid formation, involving lithiation and subsequent treatment with B(oipr)$_3$, is likely to be incompatible with the substitution pattern, owning to the subsceptibility of the C-F bonds to nucleophilic attack.

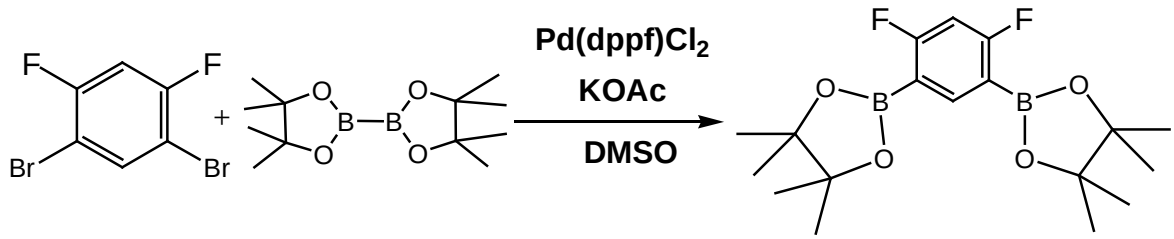

Figure 2.17: synthesis of the di-boronic ester 1,3-di-(pinacolatoboron)-4,6-di-fluoro-benzene

The di-boronic ester precursor is then reacted with the 2-bromo-4-methoxypyridine under inert atmosphere in Suzuki-Miyaura cross-coupling conditions, using dimethoxyethane as solvent and in presence of $Na_2CO_3.H_2O$ with $Pd(PPh_3)_4$ as a catalyst. H**L5** was thus obtained as a product (Figure 2.18).[207]

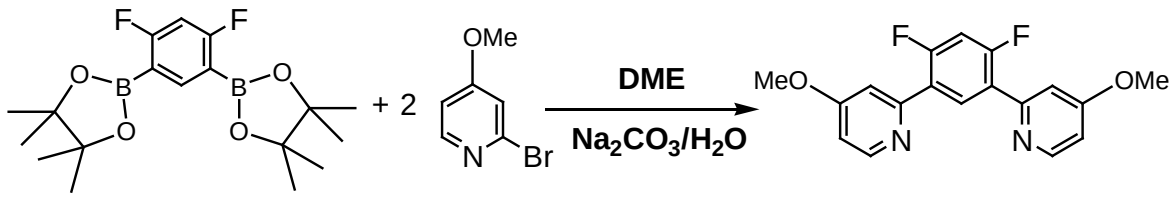

Figure 2.18: synthesis of H**L5**

Similarly, via Suzuki-Miyaura cross-coupling under analogous conditions, 1,3-di-(4-pinacolatoboron)-4,6-di-fluoro-benzene can also be reacted with 2-bromo-4-dimethylaminopyridine in order to synthesise 1,3-bis(4-dimethylamino)pyridine-4,6-difluoro-benzene (H**L6**).[207] Prior formation of 2-bromo-4-(dimethylamino)pyridine was achieved starting from 2-bromopyridine via diverted ortho lithiation followed by treatment with CBr_4 (Figure 2.19).[207]

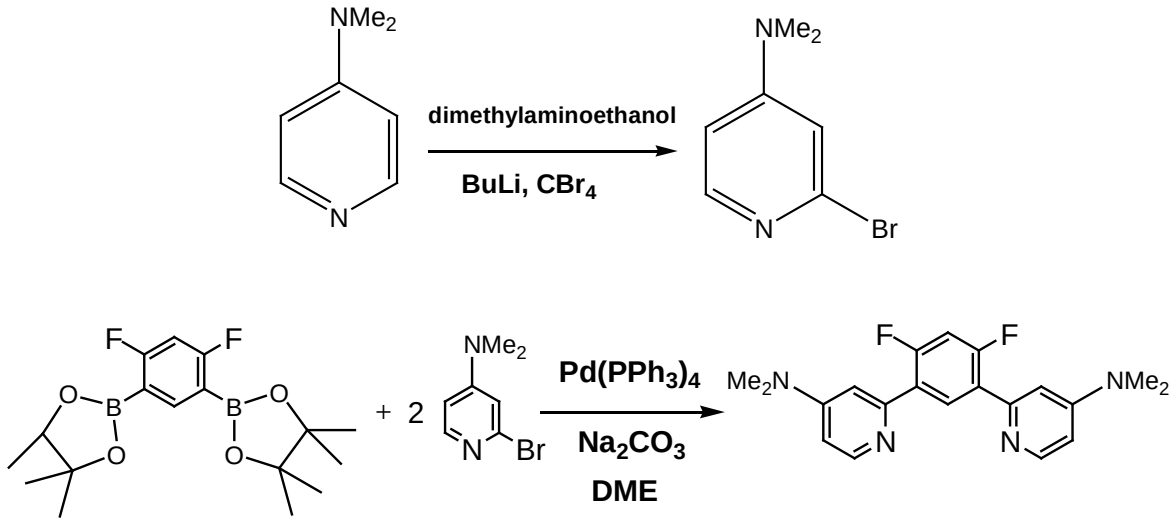

Figure 2.19: preparation of 2-bromo-4-dimethylaminopyridine and subsequent synthesis of H**L6** via Miyaura cross-coupling.

2.2.2. Synthesis of bidentate N^C ligands

As for the terdentate ligands, the bidentate phenylpyridines can be accessed by cross-coupling methods such as the Suzuki or Stille reactions of the appropiately substituted precursors. The synthesis of 2-(2,4-difluorophenyl)pyridine (dFppyH) involves a Suzuki cross coupling reaction of 2-bromopyridine with 2,4-difluorophenyl boronic acid (Figure 2.20).[208] The same method was employed to prepare 2-(2,4-difluorophenyl)-4-methoxypyridine (Figure 2.21).

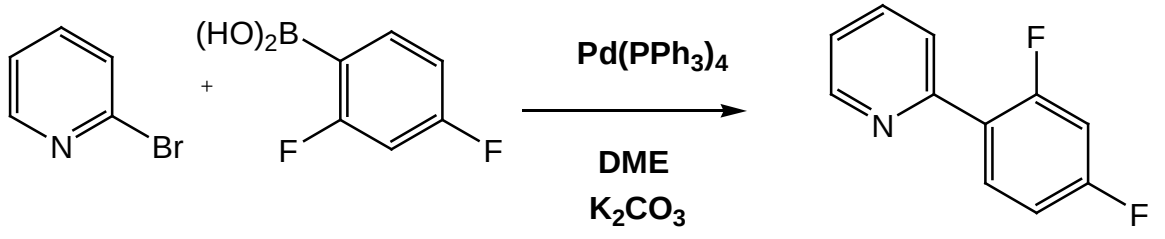

Figure 2.20: Suzuki coupling for the synthesis of N^C bidentate ligand 2-(2,4-difluorophenyl)pyridine (dFppyH)

The synthesis of 2-(2,4-difluorophenyl)-4-methoxypyridine (dFpOMepyH) was carried out adopting Suzuki croos-coupling procedure, giving better results (yield = 80%), Stille reaction for the synthesis of the same molecule, due the the poor stability of 2-(tri-butylstannyl)-4-methoxypyridine.

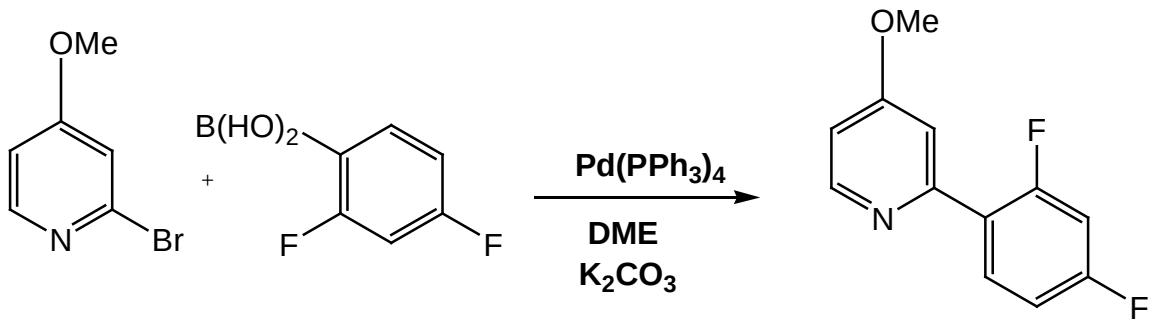

Figure 2.21: scheme for the synthesis of 2-(2,4-difluorophenyl)-4-methoxypyridine

In contrast, 2-(2,4-difluorophenyl)-4-methylpyridine (dFpMepyH) was prepared by a Stille coupling, as shown in Figure 2.22. The Stille reaction for the synthesis of this molecule has a yield of 74%, the good result here obtained is due to the tolerable stability of the 2-(tri-butylstannyl)-4-methylpyridine, if compared to the methoxy-substituted analogue.

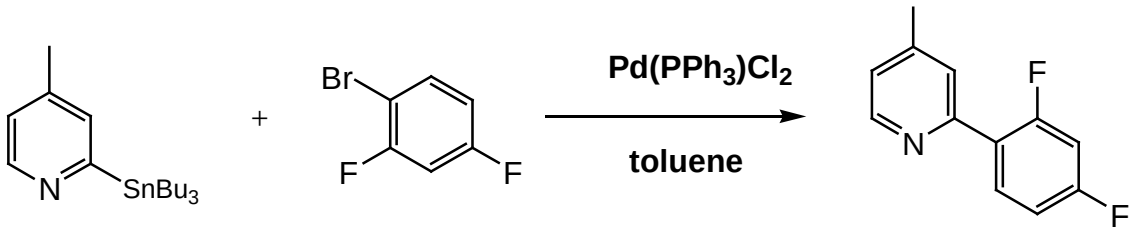

Figure 2.22: scheme for the synthesis of 1,3-di-fluoro-phenyl-4-methoxypyrydine.

The previous examples of Suzuki cross-coupling involved exclusively bromo substituted substrates. However, also chlorine substituted substrates are active in respect to this type of cross-coupling reactions when ortho to heterocyclic nitrogen atoms, allowing the possibility to obtain a wider variety of cyclometallating ligands. Such an example is the synthesis of 2-(1-benzo[b]thiophene) iso-1-quinoline (btiqH) (Figure 2.23).

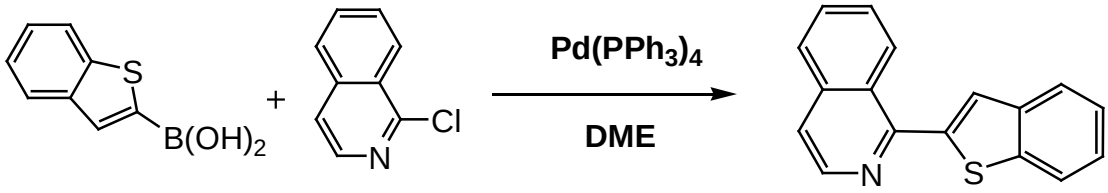

Figure 2.23: scheme for the synthesis of 2-(1-benzo[b]thiophene) iso-1-quinoline.

2.3. Synthesis of iridium complexes

2.3.1. Synthesis of intermediate iridium di-chlorobridged dimers

The synthesis of the target complexes involves the formation of an intermediate iridium dimer before coordination of the second cyclometallating ligand. The dimer formed is di-chloro bridged and its synthesis is relatively straightforward. Starting from $IrCl_3*3H_2O$ in a mixture of 2-ethoxyethanol and water (3:1 v/v), the terdentate ligand is added and the solution refluxed for one day[209]. Figure 2.24 shows the general synthetic route for the iridium(III) di-chlorobridged dimers, where X and Y represent different substituents attached on the N^C^N ligand. In this work, the different dimers were prepared following the same synthetic pathway: when Y = -H, all three dimers with X = $-CH_3$, -F and $-CF_3$ as substituents on the phenyl ring of the N^C^N frame were synthesised. When Y = $-CF_3$, X = $-CF_3$, and when X = -F, Y = OMe. After the reflux period the dimers are obtained as a precipitate from the reaction mixture. In most of the cases represented in Figure 2.24, the dimer formed is characterized by a very low solubility, precipitating from the solution.

However, those in which X = CF_3 do not form a precipite following the reaction period and are easily soluble in dichloromethane and chloroform (Figure 2.24).

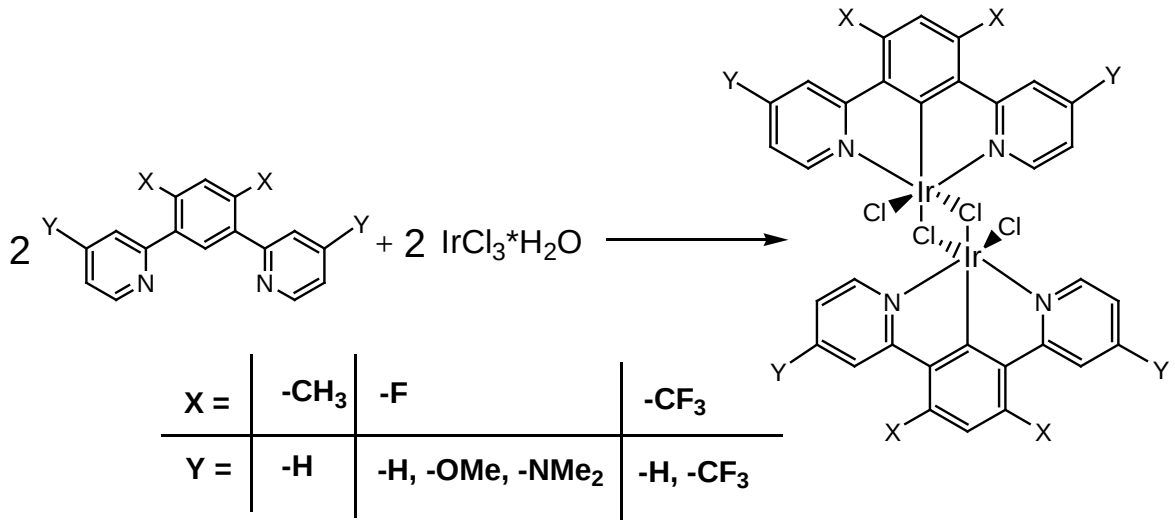

X =	-CH_3	-F	-CF_3
Y =	-H	-H, -OMe, -NMe_2	-H, -CF_3

Figure 2.24: iridium(III) di-chloro bridged dimer containing N^C^N ligand with substituents X on the 3,5 positions of the phenyl ring ligand and Y on the pyridyl rings of the N^C^N.

Due to the very low solubility of the dimers where the substituent X is $–CH_3$ or –F, the NMR characterization is performed in deuterated DMSO, which probably cleaves the dimer by replacing the chlorine bridging atoms in the sample to give the soluble mononuclear $[Ir(N^C^N)Cl_2(DMSO)]^+$ cation. The dimer containing –F groups on the N^C^N ligand presents a very low solubility and either does not undergo cleavage in DMSO, or the resulting complex is insoluble in DMSO. Therefore its NMR characterisation could not be carried out and the solid was used directly for the following reactions.

2.3.2. Synthesis of Ir(N^C^N)(N^C)Cl complexes

Upon reaction of di-chlorobridged dimers containing N^C^N ligands with a second N^C mono-cyclometallating bidentate ligand, formation of complexes of the class Ir(N^C^N)(N^C)Cl takes place, leading to neutral bis-cyclometallated complexes.

During previous work within the research group the synthesis of Ir(**L1**)(ppy)Cl (Figure 2.25) was reported by refluxing $[Ir(\mathbf{L1})Cl(\mu\text{-}Cl)]_2$ with an excess of ppyH in the presence of AgOTf, in ethylene glycol at 196°C for 1 hour.[106]

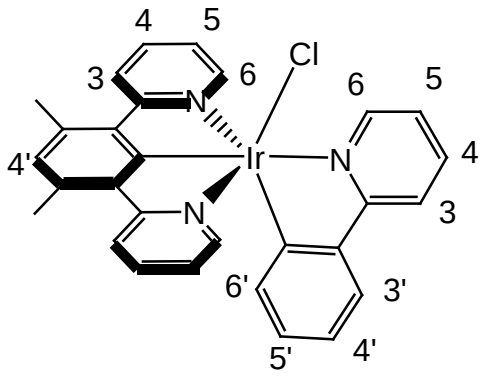

Figure 2.25[210]: structrue of Ir(**L1**)(ppy)Cl previously synthesised within the research group

In this work, we sought to synthesise Ir(L1)(dFppy)Cl **(1)** (Figure 2.26) in a similar manner, but using dFppyH in place of ppyH. However, the reaction gave a low yield compared to that from the synthesis of Ir(**L1**)(ppy)Cl. NMR spectroscopy also showed that the target complex was not obtained as a pure product since the unreacted dFppyH was not separated properly from the desired complex, so another methodology was adopted. The solvent was changed to toluene and the reaction mixture heated at 110°C overnight. The yield was found to be improved up to around 60% and purification of the target complex was achieved by silica gel chromatography. Initially, impurity due to chlorine loss from Ir(**L1**)(dFppy)Cl **(1)** was observed during the characterisation of the complex. Therefore during the work-up the reaction mixture was dissolved in dichloromethane and washed with a 1M aqueous solution of HCl, as a source of Cl^- ions, improving the yield up to 94%. The HCl wash also seems to remove excess ppyH as its hydrochloride salt.

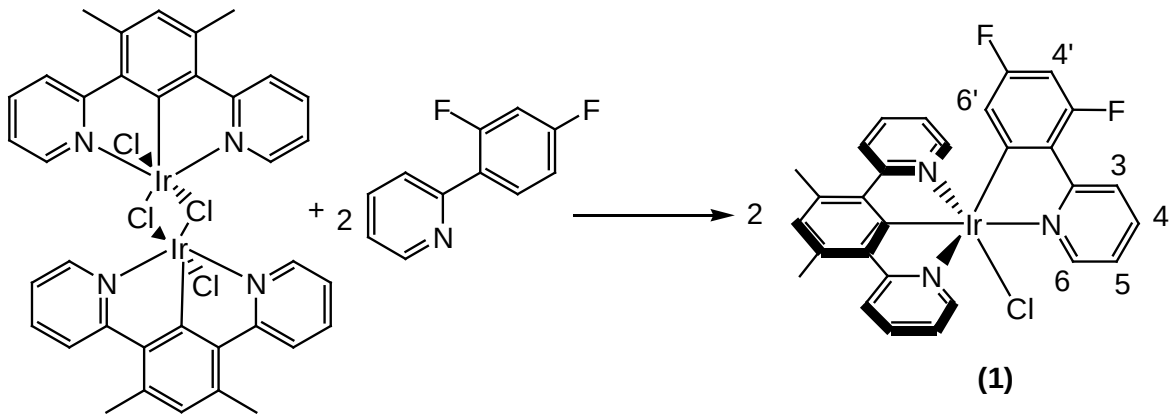

Figure 2.26: scheme for the synthesis of Ir(**L1**)(dFppy)Cl **(1)** and the atom numbering system for assignement of NMR

Formation of the complex was confirmed by electrospray mass spectrometry which showed signals for the $[Ir(\mathbf{L1})(dFppy)]^+$ parent ion, where no ancillary ligand occupied the sixth coordination site, and for $[Ir(\mathbf{L1})(dFppy)(CH_3CN)]^+$ due to the displacement of the Cl^- ion by acetonitrile present in the eluent of the spectrometer. Confirmation of formation of the complex containing the chlorine as ancillary ligand is given by elemental analysis. ^{1}H-NMR Spectroscopy (in deuterated acetonitrile and chloroform) also shows the formation of the target complex. In both solvents, also, the purity of the complex synthesised is confirmed by the pattern of the signals relative to the ligands coordinated, which is similar to that of the previously synthesised Ir(**L1**)(ppy)Cl. The spectrum displays doublets for the proton in position 6 of the N^C ligand and for the proton in position 6 of the N^C^N whose corresponding integrals are in a 1:2 ratio. Particularly indicative are the resonances at highest and lowest fields, respectively assigned to the protons in position 6 (typically between 9.50 ppm and 10.20 ppm) and 6' (typically between 5.20 ppm and 6.00 ppm) of the N^C ligand. In fact, the presence of isolated signals in these regions confirms the purity of the complex obtained (Figure 2.27).

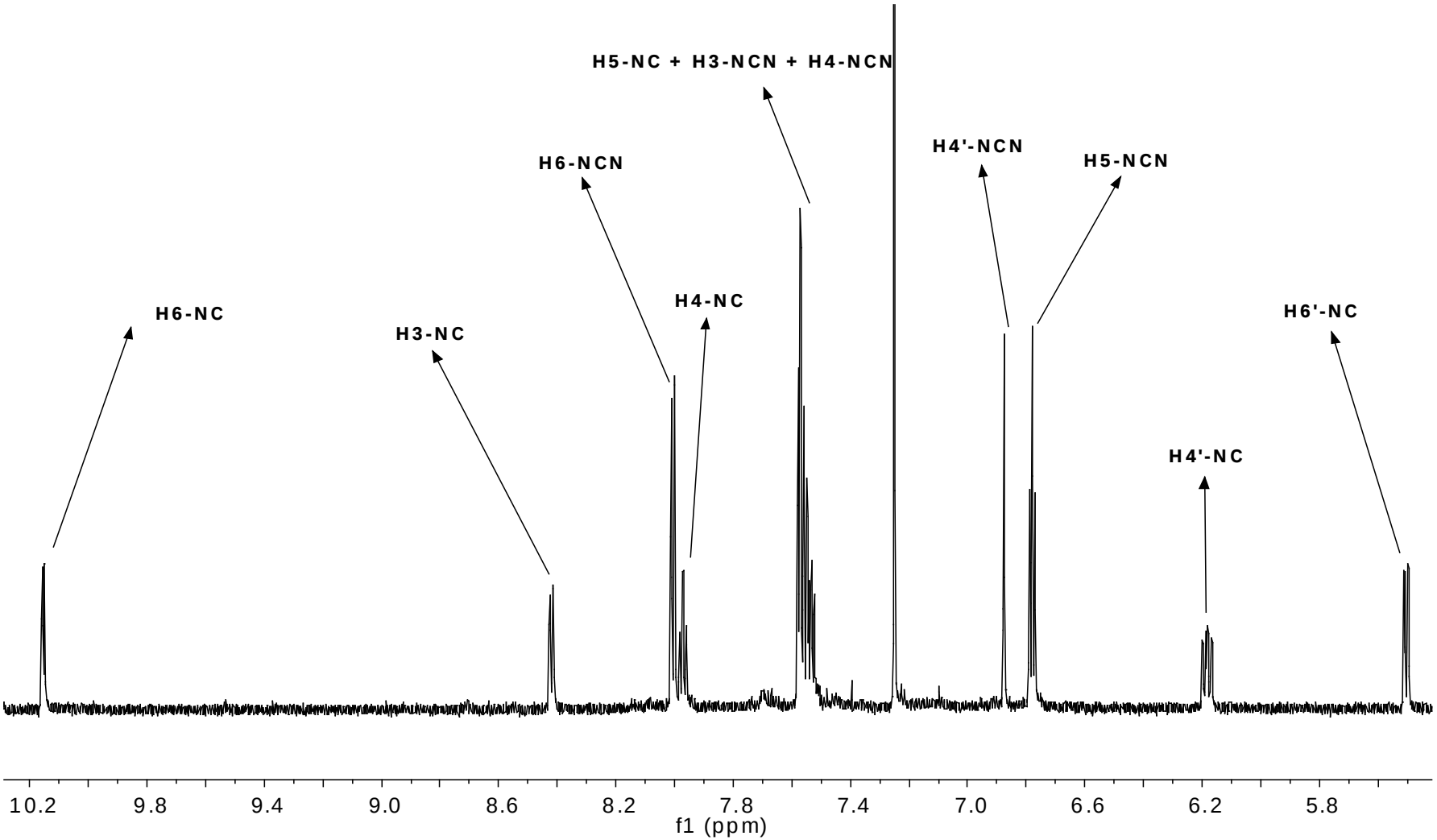

Figure 2.27: ^{1}H-NMR spectrum in $CDCl_3$ of Ir(**L1**)(dFppy)Cl **(1)**

2-D techniques such as COSY and NOESY also give information about the structure of the complex showing cross peaks between the proton in position 6-N^C and the protons 6-N^C^N and 5-N^C^N. Formation of a sole isomer is deduced namely the *C-trans-N* isomer (Figure 2.28) in which the cyclometallating carbons are not mutually trans to one another. There was no evidence for the formation of the *C-trans-C* isomer. Both isomers are meridional and no formation of facial isomer is considered to be possible due to the presence of the terdentate N^C^N ligand which is too rigid and resticted to coordinate as a facial ligand. The formation of the isomer with cyclometallating carbons not mutually trans to each other is thought to be the thermodynamically favoured product, in fact because of the high trans influence of the cyclometalated carbons the other isomer, where two carbon atoms are in trans position to each other, would be disfavoured (see Figure 2.28).

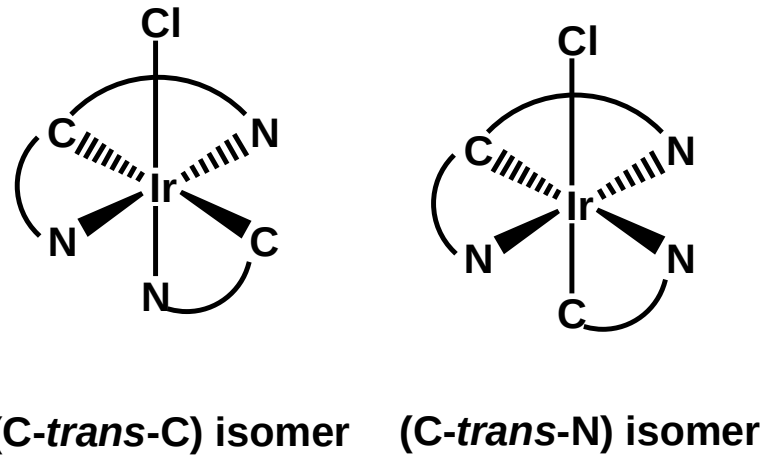

Figure 2.28: scheme of the two different isomers possible in principle for Ir(N^C^N)(N^C)Cl complexes

Formation of the *C-trans-N* isomer is confirmed conclusively by the X-ray crystallography on crystals of the complex obtained from dichloromethane/ethyl ether (10/90), which will be discussed in Section 2.3.2.1.

The complexes Ir(**L3**)(dFppy)Cl **(3)** and Ir(**L2**)(dFppy)Cl **(2)** are prepared in a similar manner (Figure 2.29), with comparable conclusions being drawn from mass spectrometry and ^{1}H-NMR spectroscopy. In this case, coupling of the protons of the cyclometallating ring of the N^C ligand leads to a more complicated pattern of resonances in the high-field region. ^{19}F-NMR offers a further probe (Figure 2.30). It reveals two mutually coupled signals for the F atoms of the bidentate ligand and one for the CF_3, consistent with the formation of a single complex with C_2 symmetry in the terdentate ligand only.

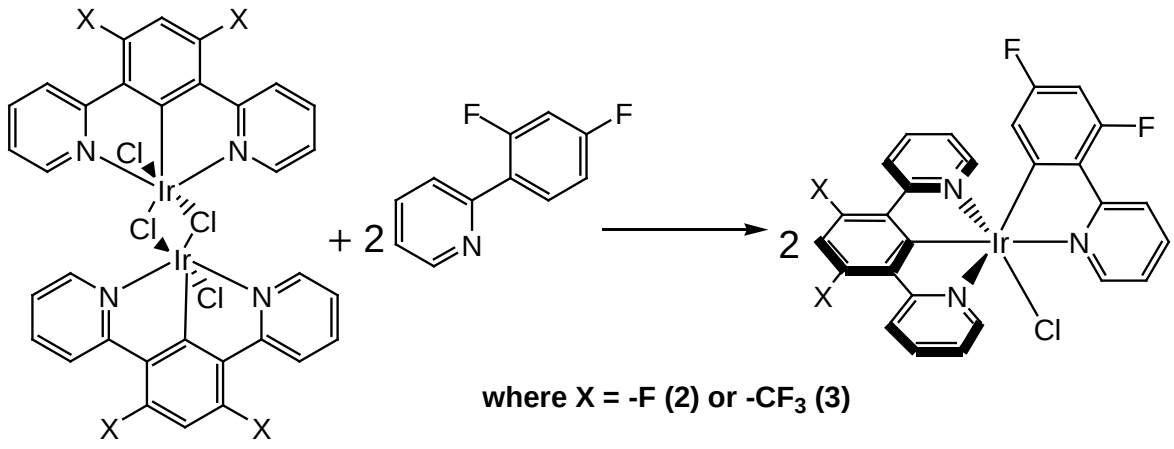

Figure 2.29: synthesis of Ir(**L3**)(dFppy)Cl **(3)** (X = -CF_3) and Ir(**L2**)(dFppy)Cl **(2)** (X = -F)

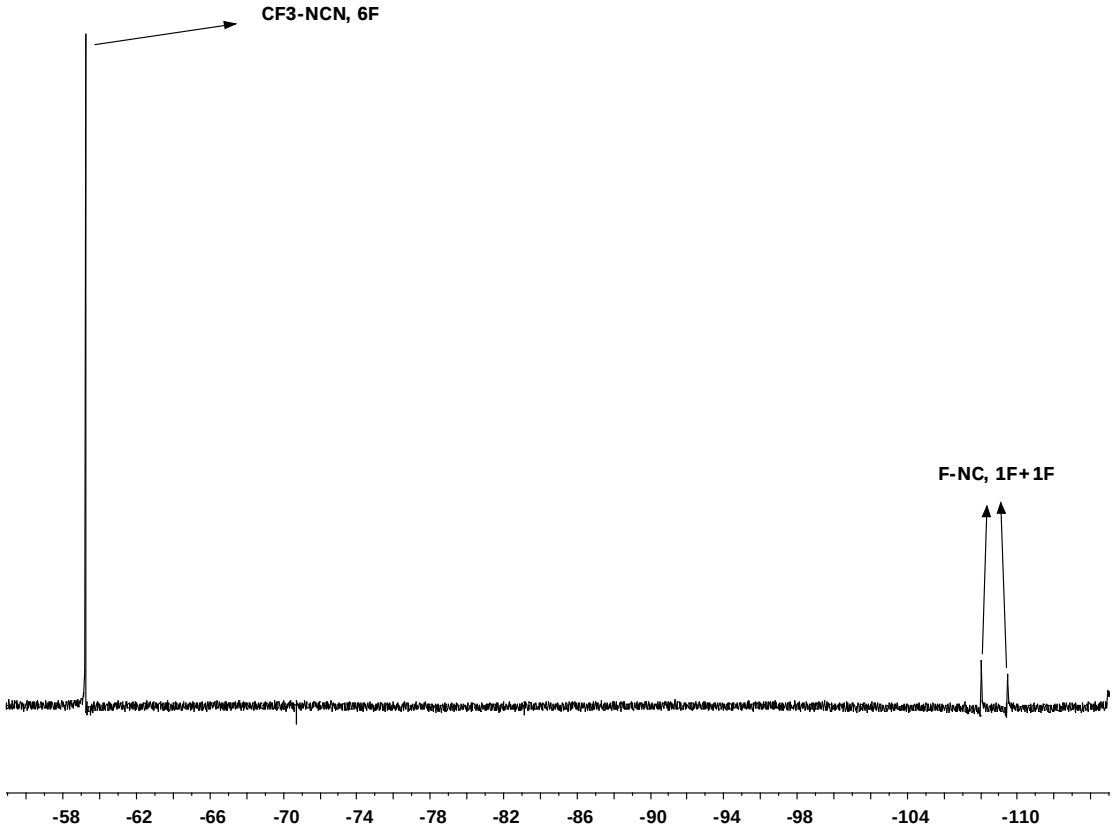

Figure 2.30: ^{19}F-NMR specrum of Ir(**L3**)(dFppy)Cl **(3)** in $CDCl_3$.

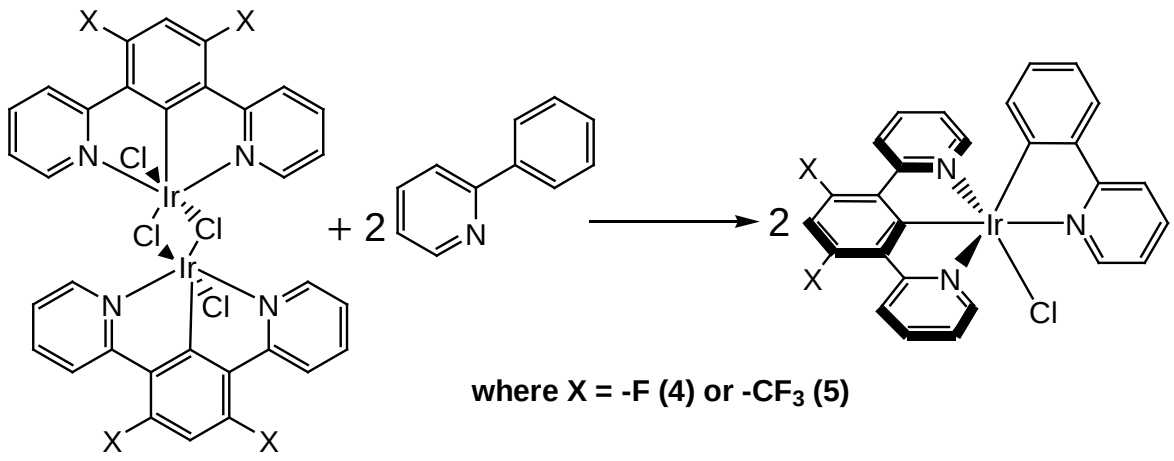

Figure 2.31: scheme for the synthesis of Ir(**L3**)(ppy)Cl **(5)** and Ir(**L2**)(ppy)Cl **(4)**

Ir(**L3**)(ppy)Cl **(5)** (Figure 2.31) was prepared using the same methodology adopted in the previous cases, giving a yield of 17%. In order to improve this value another strategy was then adopted, using ppyH as the solvent as well as the reactant. The di-chloro bridged iridium dimers containing respectively the **L2** and **L3** N^C^N ligand were added to 0.25 ml of 2-phenylpyridine and refluxed for one day (Figure 2.31). This second method gave a yield of 91% of the target product. X-ray crystallography confirmed the exclusive formation of the thermodynamically favoured C-trans-N isomer (see Section 2.3.2.1.).

Complex	Yield	Resonance of H^6-N^C ($CDCl_3$)/ppm	Resonance of $H^{6'}$-N^C ($CDCl_3$)/ppm	Resonance of H^6-N^C (CD_3CN)/ppm	Resonance of $H^{6'}$-N^C (CD_3CN)/ppm	Mass Spectrometry (ES+) *m/z*
Ir(L1)(dFppy)Cl (1)	94%	10.15	5.51	9.44	5.43	642 $[M–Cl]^+$, 682 $[M–Cl+CH_3CN]^+$
Ir(L3)(dFppy)Cl (3)	35%	10.17	5.21	10.02	5.20	791 $[M–Cl+CH_3CN]^+$
Ir(L2)(dFppy)Cl (2)	39%	9.52	5.44	-	-	691 $[M–Cl+CH_3CN]^+$
Ir(L1)(ppy)Cl	59%	10.12	6.00	-	-	606 ([M – Cl]+), 638 ([M –Cl+MeOH]+)
Ir(L3)(ppy)Cl (5)	91%	10.12	6.07	-	-	755 $[M-CH_3CN]$
Ir(L2)(ppy)Cl (4)	88%	10.12	6.07	-	-	655 $[M–Cl+CH_3CN]^+$

Table 2.1: ^{1}H-NMR and mass spectrometry characterisation of Ir(N^C^N)(N^C)Cl complexes

In Table 2.1 a summary of the ^{1}H-NMR and mass spectrometry characterisation of this class of complexes is presented. The NMR samples in deuterated acetonitrile of the complexes Ir(**L1**)(dFppy)Cl **(1)** and Ir(**L3**)(dFppy)Cl **(3)** displayed a signal pattern typical of the presence of a sole complex. These two complexes are relatively stable in acetonitrile. Whereas the complex Ir(**L2**)(dFppy)Cl **(2)** and the three complexes bearing ppy as a bidentate ligand showed, in their NMR spectra in CD_3CN, the presence of two species; one for the chlorine coordinated complex and the other for the complex formed upon loss of Cl in acetonitrile solution, presumably being $[Ir(N\hat{}C\hat{}N)(N\hat{}C)(CH_3CN)]^+$. NMR samples prepared in deuterated chloroform, on the contrary, showed, for all the six complexes, higher stability, and the presence of the solvent-coordinated species is not observed. However, if the complexes are in solution for relatively long times and exposed to daylight, loss of the ancillary chlorine is observed.

Comparing the NMR data in $CDCl_3$ of the complexes containing dFppy (see Table 2.1), the pattern of the signals appears similar for the three complexes, although some differences in the resonance of the most de-shielded and the most shielded signals are displayed. In fact, the resonance for $H^{6'}$-NCN of the **L3** coordinated complex appears at lower fields (5.21 ppm) compared to that of the complexes conataining **L1** and **L2**, which are located at respectively at 5.51 ppm and 5.44 ppm. Whereas the proton H^{6}-NCN of the **L2** coordinated complex displays a resonance of 9.52 ppm, which is located at lower fields in relation to those at 10.15 ppm and 10.17 ppm for the species bearing respectively **L1** and **L3**. Considering the series of the complexes containing ppy as bidentate ligand, on the other hand, the resonances of the protons $H^{6'}$-NCN and H^{6}-NCN are located at similar values for the three complexes.

2.3.2.1. X-ray crystallography

The molecular structures of the complexes Ir(**L1**)(dFppy)Cl **(1)** and Ir(**L3**)(ppy)Cl **(5)** in the crystals are shown respectively in Figures 2.32 and 2.33, and selected bond lengths and angles are collated in Tables 2.2 and 2.3. Bond lengths and angles involving the metal are essentially identical in the two cases, when the standard deviations are taken into account. Thus we shall consider the values for

only one complex, Ir(**L1**)(dFppy)Cl **(1)**. As expected, due to the geometric constraints associated with binding of a terdentate ligand that forms 5-membered chelating rings, the iridium centre exhibits a distorted octahedral geometry, with an N^{NCN}–Ir–N^{NCN} angle of 161.2(2)˚. The M–L bond lengths to the terdentate and bidentate ligands reveal significant differences. Thus, the Ir–C^{NCN} bond is shorter than the Ir–C^{NC} (1.940(6) and 2.005(6)Å respectively), presumably reflecting the constraints imposed on the former by binding of the two flanking pyridyl rings. The Ir–N^{NCN} bonds {average 2.042Å} are likewise shorter then the Ir–N^{NC} {2.156(5)Å}. The main factor in play here is almost certainly the fact that in the latter two cases, the N atoms are *trans* to cyclometallated carbon atoms, which have a very strong *trans* influence, whereas the N atoms of the NCN ligand are necessarily *trans* to one another.

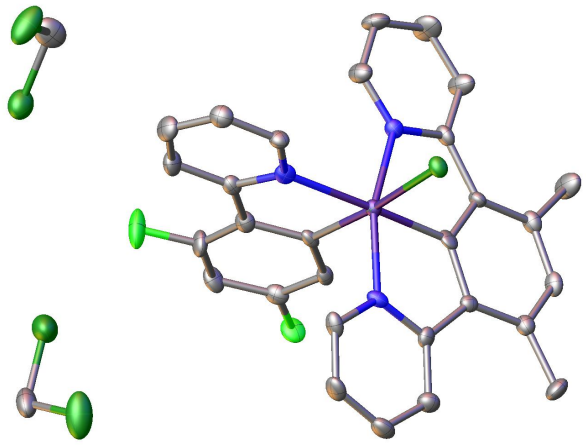

Figure 2.32: X-ray crystallography structure of the complex of Ir(**L1**)(dFppy)Cl **(1)**, co-crystallised with CH_2Cl_2, T = 120 K.

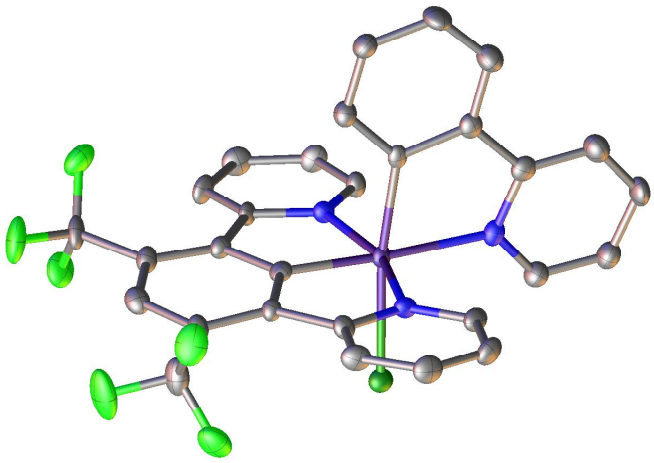

Figure 2.33: X-ray crystallography structure of the complex Ir(**L3**)(ppy)Cl **(5)**, T = 120 K.

Ir–N(1)	2.156(5)	N(13)-Ir-N(30)	161.2(2)
Ir–C(12)	2.005(6)	N(13)-Ir-C(24)	80.7(2)
Ir–N(13)	2.036(5)	N(30)-Ir-C(24)	80.5(2)
Ir–N(30)	2.048(5)	N(1)-Ir-C(24)	174.6(2)
Ir–C(24)	1.940(6)	C(12)-Ir-Cl	172.0(2)
Ir–Cl	2.461(2)	N(1)-Ir-C(12)	78.9(2)
		N(1)-Ir-Cl	93.2(2)
		C(24)-Ir-Cl	92.0(2)
		C(24)-Ir-C(12)	95.9(3)

Table 2.2: Selected bond lengths (Å) and angles (˚) for [Ir(**L1**)(dFppy)Cl **(1)**].

Ir–N(1)	2.156(3)	N(13)-Ir-N(30)	161.9(1)
Ir–C(12)	2.018(4)	N(13)-Ir-C(24)	80.7(1)
Ir–N(13)	2.049(3)	N(30)-Ir-C(24)	81.1(1)
Ir–N(30)	2.047(3)	N(1)-Ir-C(24)	176.4(1)
Ir–C(24)	1.930(4)	C(12)-Ir-Cl	172.2(1)
Ir–Cl	2.467(1)	N(1)-Ir-C(12)	79.4(1)
C(3)-Ir-C(12)	97.0(1)	N(1)-Ir-Cl	93.4(1)
		C(24)-Ir-Cl	90.2(1)

Table 2.3 Selected bond lengths (Å) and angles (˚) for [Ir(**L3**)(ppy)Cl] **(5)**.

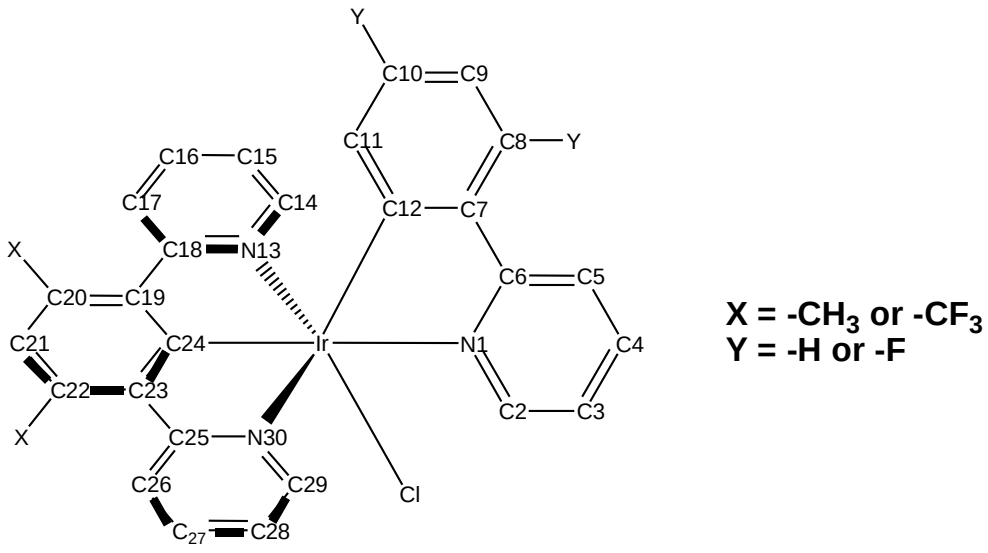

Figure 2.35: atom labelling used for the representation of the crystal structures

2.3.2.2. Synthesis of complexes Ir(N^C^N)(N^C)Cl with substituents on the pyridyl rings of the ligands

The synthesis of a new class of iridium(III) complexes of the same structure Ir(N^C^N)(N^C)Cl, but bearing additional substituents (-CH_3, -OMe or –NMe_2) on the pyridyl rings of both the terdentate and the bidentate ligands is here reported. An analogous synthetic pathway to that discussed in section 2.3.2. is carried out by reaction of the respective di-chloro bridged dimers with the bidentate moiety, in the presence of AgOTf and using toluene as the solvent. The synthetic scheme for complexes carrying methoxy or dimethylamino substitutents on the 4 position of the N^C^N pyridyl is illustrated in Figure 2.36 and 2.37 respectively and the synthesis summarised in Table 2.4. Formation of target complexes and purity was confirmed by mass spectrometry and by ^{1}H-NMR and ^{19}F-NMR spectroscopy in deuterated chloroform.

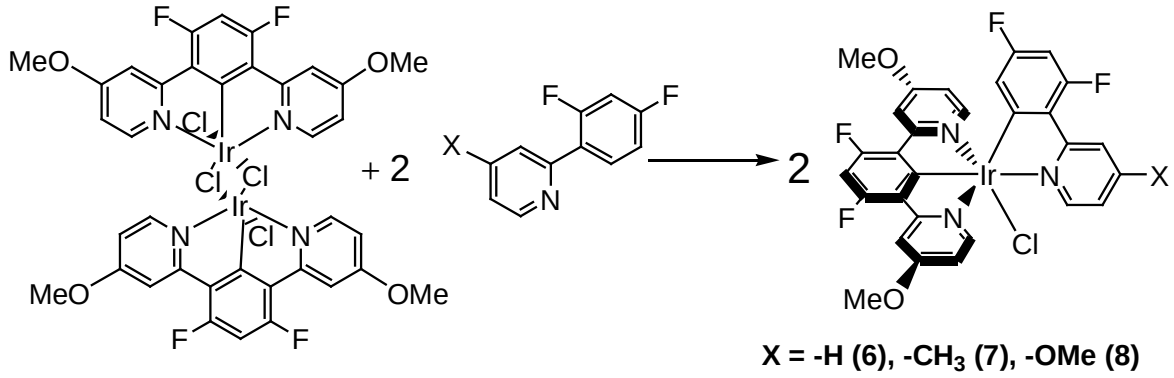

Figure 2.36: scheme for the synthesis of OMe substituted Ir(**L5**)(N^C)Cl, where X = -H, -CH_3 or –OMe.

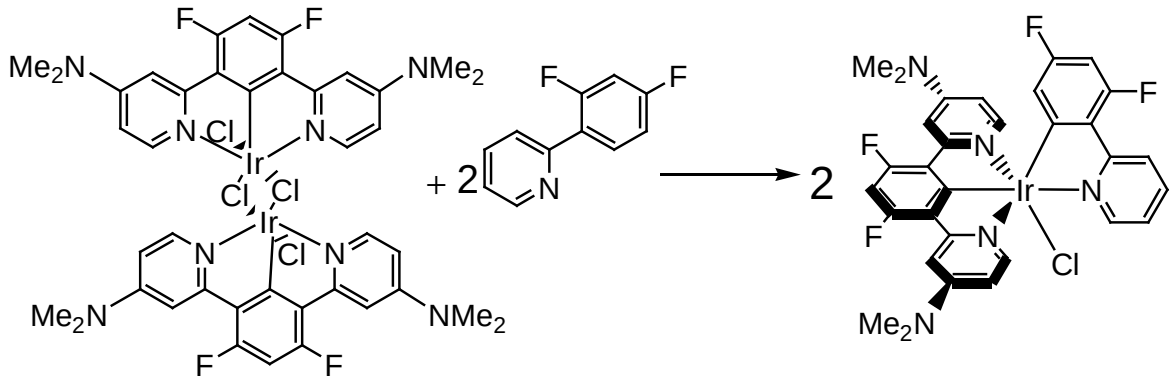

Figure 2.37: scheme for the synthesis of Ir(**L6**)(dFppy)Cl

Complex	Yield	Resonance of H^{6}-N^C ($CDCl_3$)/ppm	Resonance of $H^{6'}$-N^C ($CDCl_3$)/ppm	Mass Spectrometry (ES+) *m/z*
Ir(L5)(dFppy)Cl (6)	65%	10.11	5.56	751 $[M\text{-}CH_3CN]^+$
Ir(L5)(dFppic)Cl (7)	65%	9.96	5.58	759 $[M\text{-}H]^+$, 724 $[M\text{-}Cl]^+$
Ir(L5)(dfpOMepy)Cl (8)	26%	9.89	5.55	740 $[M\text{-}Cl]^+$, 775 $[M+H]^+$
Ir(L6)(dFppy)Cl[207]	81%	10.14	5.64	771 $[M\text{-}Cl]^+$

Table 2.4: ^{1}H-NMR ($CDCl_3$) and mass spectrometry characterisation of Ir(N^C^N)(N^C)Cl complexes carrying substituents on the N^C^N pyridyl ring.

Similarly to the synthesis of the previously discussed Ir(N^C^N)(N^C)Cl complexes, reaction of $[Ir(\mathbf{L4})Cl(\mu\text{-}Cl)]_2$ with ppyH leads to formation of the complex Ir(**L4**)(ppy)Cl **(9)** (Figure 2.38). Whereas $[Ir(\mathbf{L3})Cl(\mu\text{-}Cl)]_2$ with btiqH leads to formation of Ir(**L3**)(btiq)Cl **(11)** (Figure 2.38). Characterisation of these complexes by ^{1}H-NMR spectroscopy in $CDCl_3$ and mass spectometry leads to analogous conclusions regarding purity and structure to those relative to the other Ir(N^C^N)(N^C)Cl systems (Table 2.5).

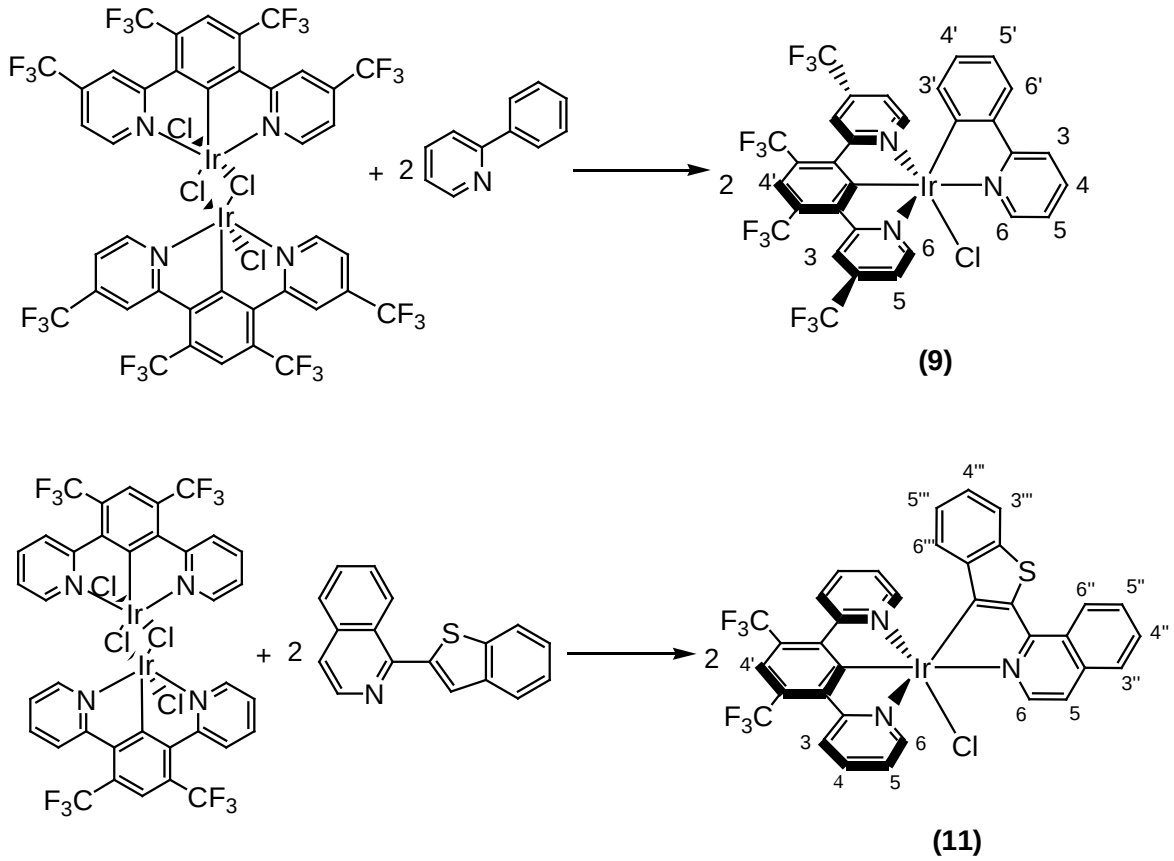

Figure 2.38: scheme for the synthesis of Ir(**L4**)(ppy)Cl **(9)** and Ir(**L3**)(btiq)Cl **(11)**.

Complex	Yield	Resonance of H^{6}-N^C ($CDCl_3$)/ppm	Resonance of $H^{6'}$-N^C ($CDCl_3$)/ppm	Mass Spectrometry (ES+) *m/z*
Ir(L4)(ppy)Cl (9)	40%	10.01	5.58	891 $[M\text{-}CH_3CN]^+$
Ir(L3)(btiq)Cl (11)	86%	10.12	5.99 *	855 $[M]^+$

Table 2.5: ^{1}H-NMR ($CDCl_3$) and mass spectrometry characterisation of Ir(N^C^N)(N^C)Cl complexes carrying substituents on the N^C^N pyridyl ring, for Ir(**L4**)(btiq)Cl **(10)** the resonance at lowest fields is that of $H^{6''}$-NC.

2.3.2.3. Synthesis of Ir(N^C^N)(ppyz)Cl

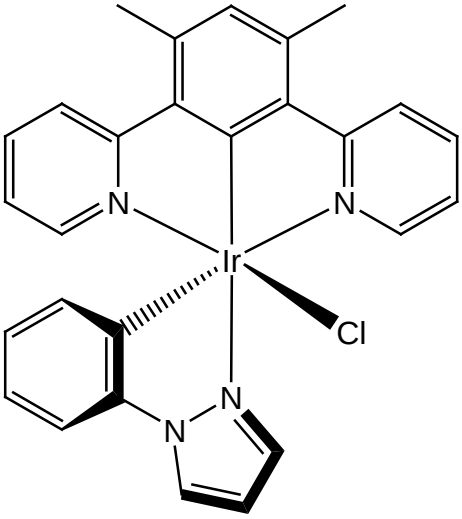

Figure 2.39[(122)]: structure of Ir(**L1**)(ppyz)Cl

A complex of the structure Ir(N^C^N)(N^C)Cl in which N^C is 1-phenylpyrazole, was previously synthesised by Whittle within our research group (Figure 2.39).[(122)] The reaction was carried out in refluxing ethylene glycol at 196°C and the product was obtained with a yield of 54%. In this work, Ir(**L2**)(ppyz)Cl **(12)** was prepared in a similar manner, upon treatment of $[Ir(\mathbf{L2})Cl(\mu\text{-}Cl)]_2$ with ppyzH in toluene at 110°C, in the presence of AgOTf (Figure 2.40).

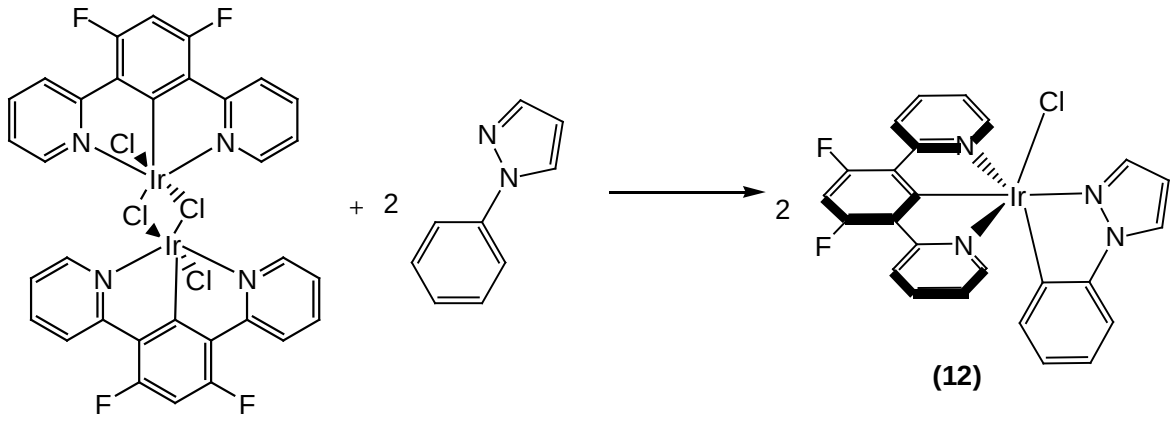

Figure 2.40: scheme for the synthesis of Ir(**L2**)(ppyz)Cl **(12)**.

2.3.3. Synthesis of $[Ir(N^C^N)(N^N)Cl]^+$ complexes

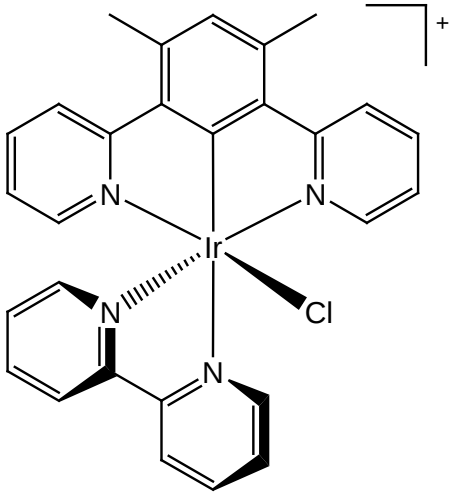

Figure 2.41[24]**:** structure of $[Ir(\mathbf{L1})(bpy)Cl]^+$

If di-chloro iridium(III) dimers are reacted with a neutral bidentate ligand, formation of positively charged mono-cyclometallated complexes is achieved, of the class $[Ir(N^C^N)(N^N)Cl]^+$. Previously within the research group the synthesis of $[Ir(\mathbf{L1})(bpy)Cl]^+$ (Figure 2.41) was achieved in 84% yield upon treatment of

$[Ir(\mathbf{L1})Cl(\mu\text{-}Cl)]_2$ with bipyridine (bpy) in ethylene glycol at reflux.[24] $[Ir(\mathbf{L3})(bpy)Cl]^+$ **(13)** and $[Ir(\mathbf{L2})(bpy)Cl]^+$ **(14)** (Figure 2.42) were prepared by a method identical to that used for $[Ir(\mathbf{L1})(bpy)Cl]^+$.

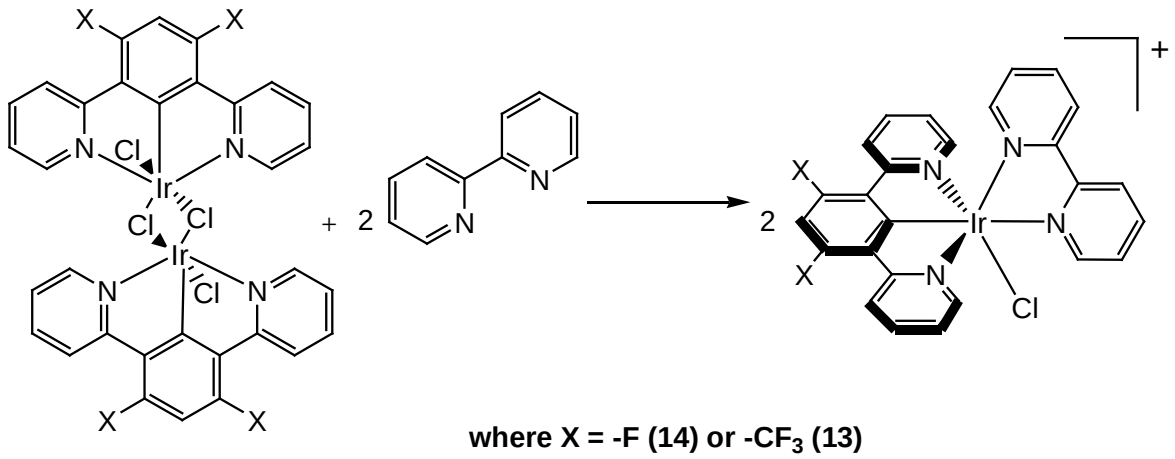

Figure 2.42: synthesis of $[Ir(\mathbf{L3})(bpy)Cl]^+$ **(13)** and $[Ir(\mathbf{L2})(bpy)Cl]^+$ **(14)**.

The positively charged complexes bearing bpy as bidentate ligand showed lower solubility in deuterated chloroform than the neutral bis-cyclometallated complexes. Their NMR characterisation is thus carried out in deuterated acetonitrile (Table 2.6). In fact, due to their positively charged nature, the Ir-Cl bond is stronger than that of the bis-cyclometallated analogues, so no loss of the chloride ligand is observed in acetonitrile. The proton H^6-NN resonates at 9.88 ppm for $[Ir(\mathbf{L3})(bpy)Cl]^+$ **(13)**, a value which, compared to that of H^6-NC of Ir(**L3**)(dFppy)Cl **(3)** in CD_3CN at 10.02 ppm, is located at lower fields.

Complex	Yield	Resonance of H^6-N^N ($CDCl_3$)/ppm	Mass Spectrometry (ES+) *m/z*
$[Ir(L3)(bpy)Cl]^+$ (13)	76%	9.88	751 $[M]^+$
$[Ir(L2)(bpy)Cl]^+$ (14)	62%	9.79	651 $[M]^+$

Table 2.6: ^{1}H-NMR (CD_3CN) and mass spectrometry characterisation of Ir(N^C^N)(N^N)Cl complexes

2.3.4. Synthesis of $[Ir(N^C^N)(N^C^N)']^+$ complexes

During previous work of the research group, different types of bis-cyclometallated irirdium(III) complexes containing exclusively terdentate ligands were synthesised, those in particular being of the structure Ir(N^C^N)(C^N^N), Ir(N^C^N)(C^N^C) or Ir(N^C^N)(O^N^C) (Figure 2.43).[106]

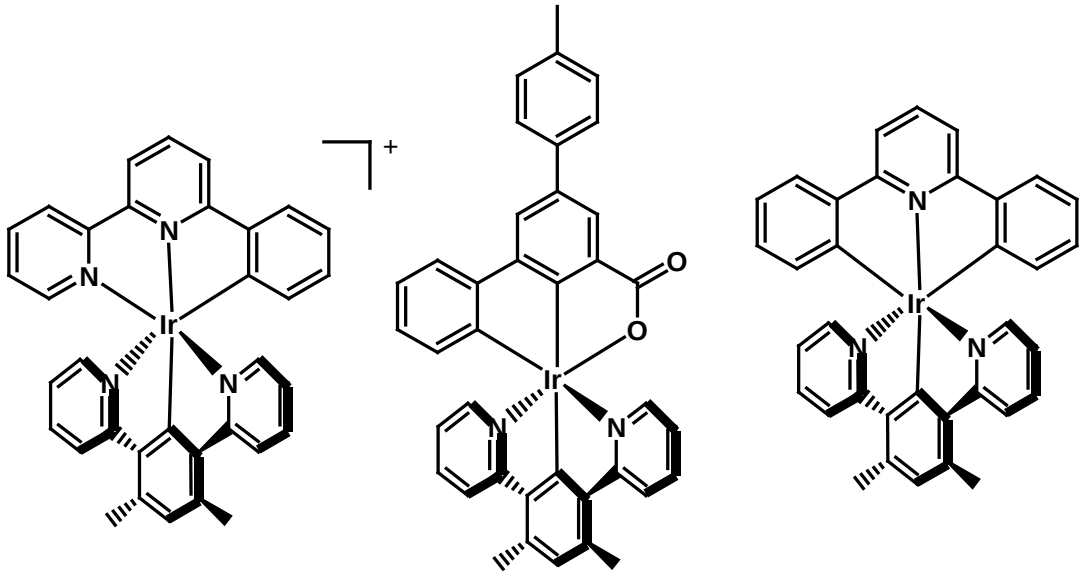

Figure 2.43[106]: examples of Ir(N^C^N)(C^N^N), Ir(N^C^N)(C^N^C) and Ir(N^C^N)(O^N^C) previously synthesised by the research group

The reason for using asymmetric terdentate cyclometallating ligands was based on avoiding the disposition, in bis-cyclometallated complexes, of cyclometallating sites in mutually trans position to each other. Due to the strong σ-donor effect of the cyclometallating phenyl rings, coordination leading to formation of trans bis-cyclometallated systems is in fact disfavoured. The coordination of two terdentate monocyclometallating ligands might however be facilitated, by using ligands whose structure forces the second cyclometallating site to be located in trans position with respect to the first one, and also by modulating the strength of the σ-donor effect through changing the substituents on the N^C^N ligands. This has been confirmed in the present work by the first reported formation of complexes of

the structure [Ir(N^C^N)(N^C^N)']$^+$. This class of complexes is new and was realised for two combinations of terdentate ligands. [Ir(**L2**)(**L1**)]$^+$ **(15)** and [Ir(**L2**)$_2$]$^+$ **(16)** (Figure 2.44) were synthesized, starting respectively from [Ir(**L1**)Cl(μ-Cl)]$_2$ or [Ir(**L2**)Cl(μ-Cl)]$_2$, upon treatment with respectively **L1** or **L2** in toluene with addition of AgOTf in the reaction mixture and reflux for one day. The yields were respectively 84% and 27%. The formation of both complexes was confirmed by mass spectrometry and ^{1}H-NMR Spectroscopy.

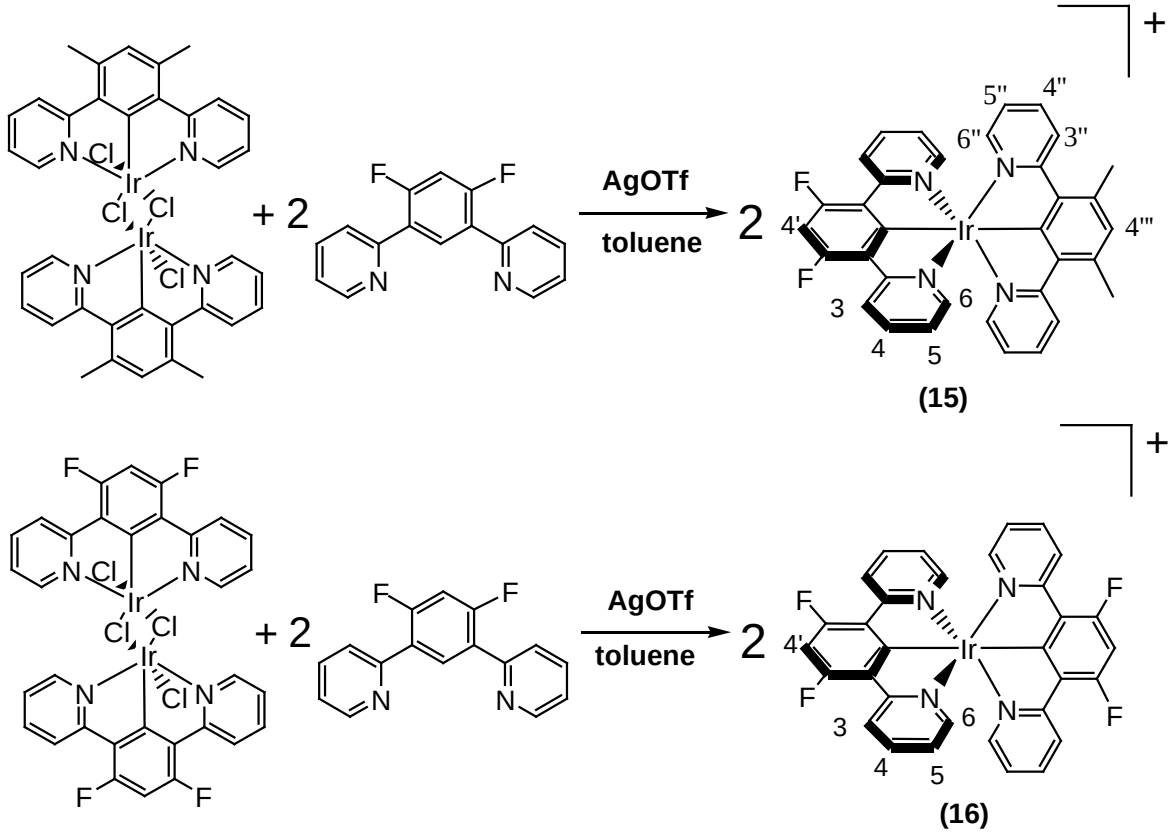

Figure 2.44: [Ir(N^C^N)(N^C^N)']$^+$ complexes synthesized

Attemps to synthesise [Ir(**L3**)$_2$]$^+$, [Ir(**L3**)(**L1**)]$^+$, [Ir(**L1**)$_2$]$^+$ and [Ir(**L3**)(**L2**)]$^+$ were also made, but the yield and purity of compounds obtained were very low, a fact that can probably be attributed to the high trans effect of the cyclometallating carbons. In fact the structure of the desired bis-cyclometallated complex with both N^C^N ligands bound terdentately in an octahedral configuration requires that two carbon atoms be in trans position to each other. For this reason, another mode of coordination of the second ligand as an N^C bidentate instead of the N^C^N mode

may be favourable as shown in Figure 2.45. This is confirmed by mass spectrometry, which displays peaks that can be related to the parent ion $[Ir(N^C^N)(N^C^N)Cl]^+$ and by ^{1}H-NMR showing a pattern of signals attributable to such complexes, in which the C_2 symmetry of one of the N^C^N ligands is broken.

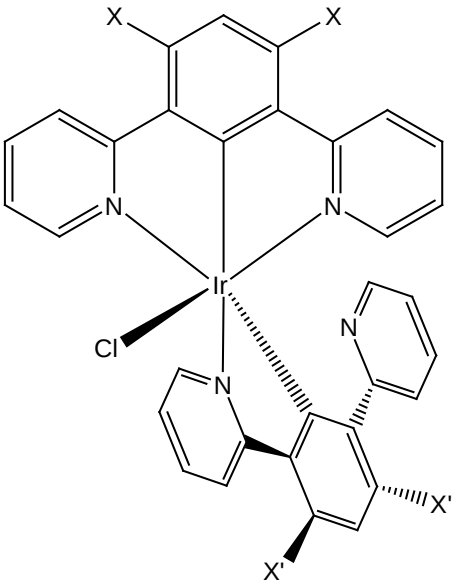

Figure 2.45: in the attempted preparation of $[Ir(N^C^N)(N^C^N)']^+$ the second ligand may coordinate as a bidentate N^C ligand.

In the cases of the two complexes successfully obtained, probably the electron withdrawing effect of the fluorine atoms on the cyclometallating ligands reduces the electron density at the metal centre, hence diminuishing the trans effect and making more feasible the coordination of the second N^C^N ligand.

2.3.5. Complexes with pyridylbenzimidazole as bidentate ligand, Ir(N^C^N)(pbi)Cl and $[Ir(N^C^N)(Me\text{-}pbi)Cl]^+$

Previous work was reported on systems incorporating 2,6-bis(indolyl)pyridine ($dinpyH_2$). It was found that coordination to the metal centre can occur in two different modes, [24] (Figure 2.46) which are thought to be dependent upon the

reaction conditions. Treatment of [Ir(**L1**)Cl(μ-Cl)]$_2$ with dinpyH$_2$ in the presence of $AgSO_3CF_3$ in acetic acid leads to deprotonation of the imidazolic proton and subsequent coordination of dinpy as a dianionic N$^-$^N^N$^-$ ligand, whereas the corresponding reaction carried out in the presence of K_2CO_3 in ethylene glycol leads to coordination of dinpy as a biscyclometallating C^N^C-coordinating ligand (Figure 2.46)

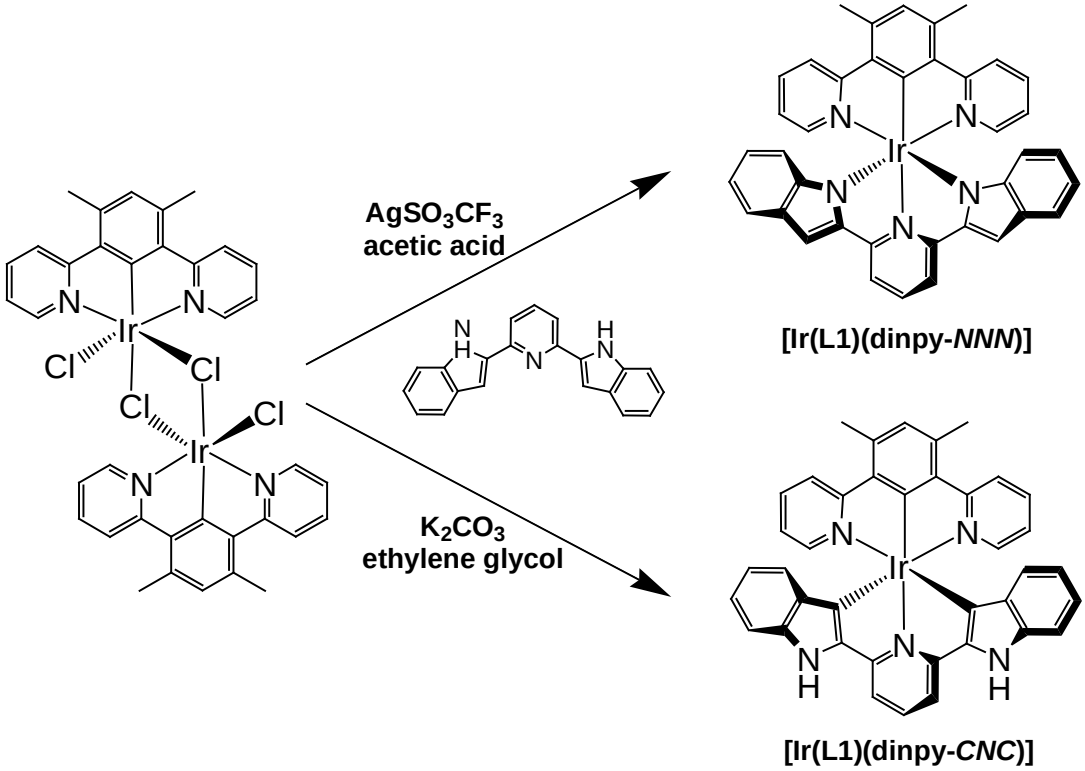

Figure 2.46[24]**:** scheme for the synthesis of [Ir(dpydmb)(dinpy-NNN)] and [Ir(dpydmb)(dinpy-CNC)]

For the Ir(N^C^N)(N^C)Cl complexes discussed so far in this chapter, the σ donor character of the cyclometallating site of the N^C^N ligand is believed to strongly influence the subsequent coordination of the bidentate ligand, similarly to the observed preference of tris(phenylpyridine) complexes to form facial rather than meridional isomers. As observed in the synthesis of the Ir(N^C^N)(N^C)Cl complexes, formation of the isomer where the (N^C^N) cyclometallating site and

the pyridyl N atom of the N^C ligand were in mutually trans position was favoured (Figure 2.47).

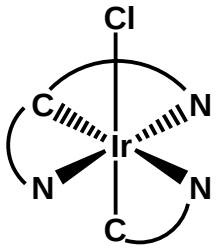

(C-*trans*-N) isomer

Figure 2.47: isomer favoured in Ir(N^C^N)(N^C)Cl complexes

The coordination of 2-(2-pyridyl)benzimidazole (pbiH) to $[Ir(ppy)_2]^+$ fragments was studied by our research group leading to in $Ir(ppy)_2(pbi)$ and $[Ir(ppy)_2(pbiH)]^+$ complexes (Figure 2.48). Reaction of $[Ir(ppy)_2(\mu\text{-}Cl)]_2$ with pbiH in DMF in the presence of K_2CO_3 as a base led to formation of $Ir(ppy)_2(pbi)$ (Figure 2.48a)) in which pbi is an anionic bidentate ligand. In contrast, reaction under milder conditions (DCM/MeOH at reflux) in the absence of a base gave $[Ir(ppy)_2(pbiH)]^+$, in which pbiH is a neutral bidentate ligand (Figure 2.48b)).

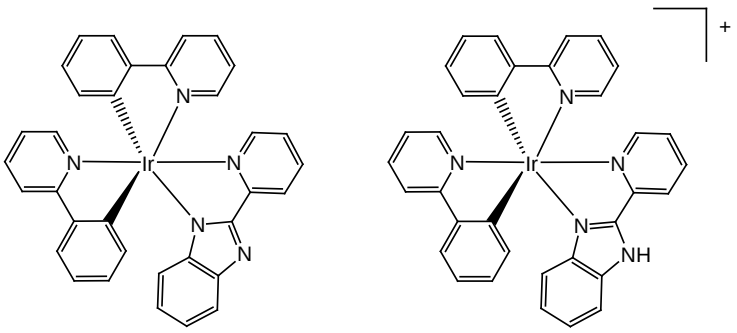

a) **b)**

Figure 2.48: a) $Ir(NC)_2(pbi)$ synthesised in DMF in the presence of K_2CO_3; **b)** $[Ir(NC)_2(pbiH)]^+$ synthesised in DCM/MeOH.

Aside from the ambidentate nature of pbi/pbiH, it is an asymmetric ligand, and so its coordination to an Ir (N^C^N) fragment can lead to formation of two different isomers. One is that in which the coordinating N atom of the imidazolic ring is positioned in trans position to the cyclometallating carbon of the N^C^N ligand, which will be referred to as *C-trans-N(imid)* isomer. The other isomer, where the N atom of the pyridyl ring is in trans position to the cyclometallating site, is named *C-trans-N(pyr)* isomer. (figure 2.49).

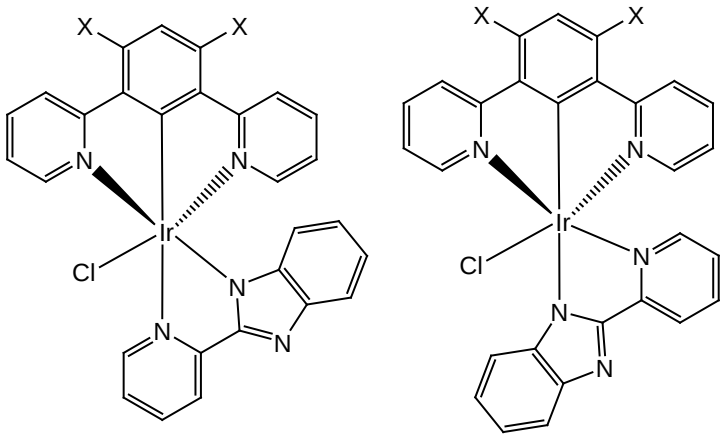

***C-trans-N(pyr)* isomer** ***C-trans-N(imid)* isomer**

Figure 2.49: two different modes of coordination of pbi to iridium(N^C^N) dimers

In summary, coordination of pbi as a bidentate ligand in N^C^N coordinated iridium complexes offers several points of interest since four possible coordination modes to the iridium centre are possible (figure 2.50).

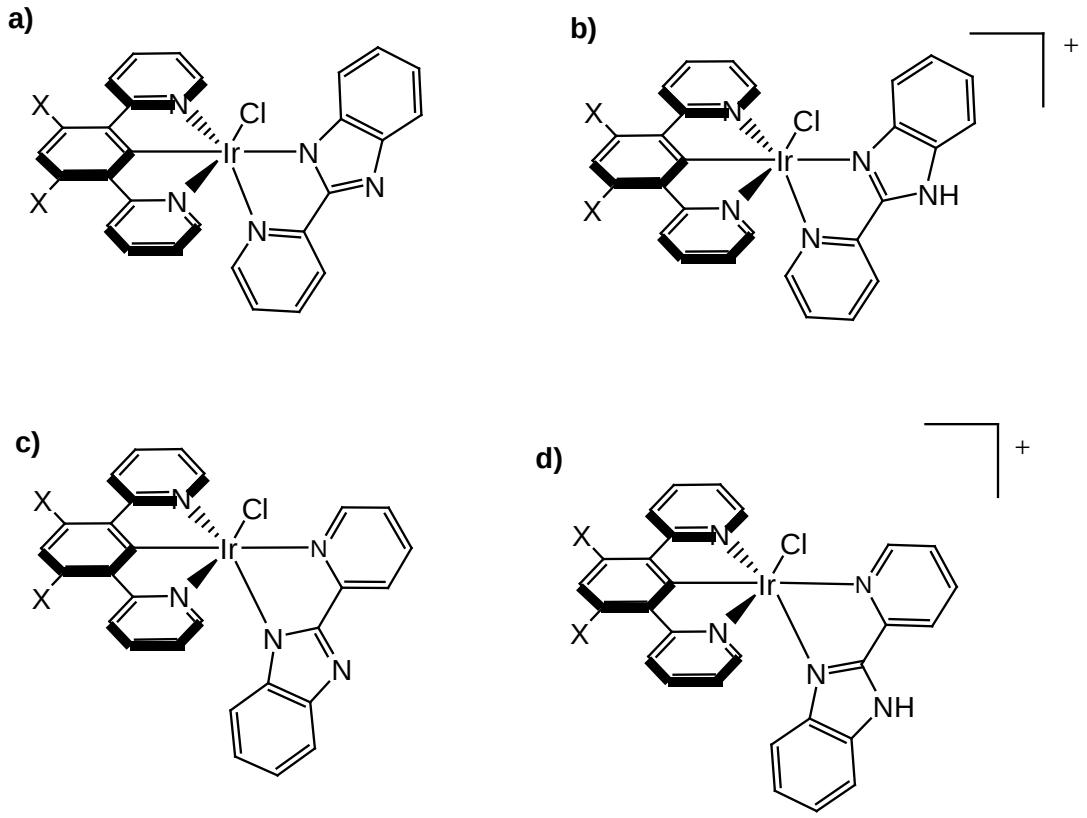

Figure 2.50: four possible modes of coordination of pbi to the metal centre: **a)** the pbi coordinates as an anionic ligand forming a *C-trans-N(imid)* complex; **b)** pbiH as a neutral ligand giving *C-trans-N(imid)*; **c)** pbi as a anionic ligand giving *C-trans-N(pyr)*; **d)** pbiH as a neutral ligand giving *C-trans-N(pyr)*.

In an attempt to obtain Ir(**L1**)(pbi)Cl **(17)** as a target complex, [Ir(**L1**)Cl(μ-Cl)]$_2$ was reacted wih pbi in DMF and in the presence of K_2CO_3. Formation of the target complex was not observed. However, the corresponding reaction in toluene in the presence of AgOTf led (Figure 2.51), after chromatography, to a yellow solid in 28%, for which the mass spectrum showed the signal of the parent ion [(Ir(**L1**)(pbi)Cl)+H]$^+$.

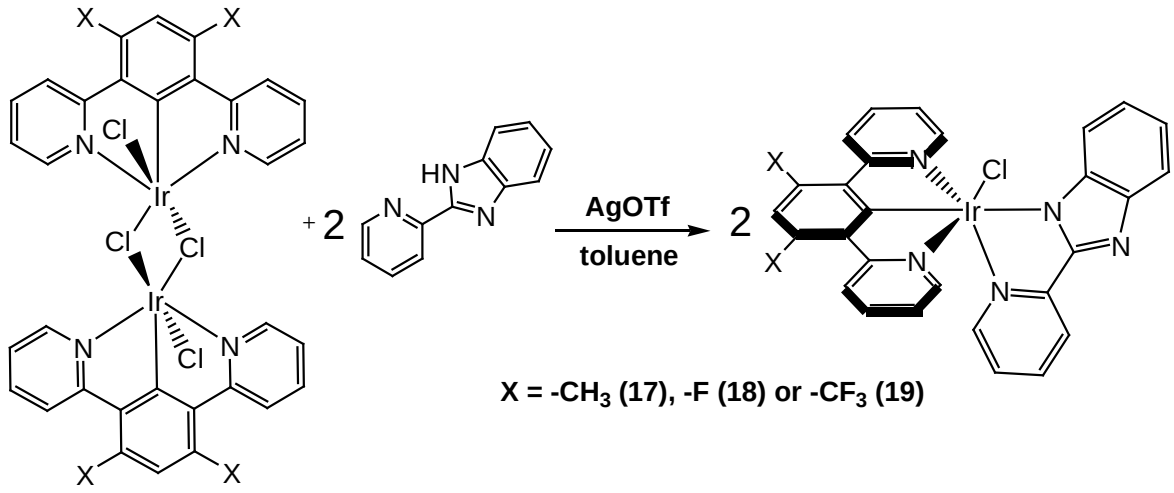

Figure 2.51: synthesis of Ir(**L1**)(pbi)Cl **(17)**, Ir(**L2**)(pbi)Cl **(18)** and Ir(**L3**)(pbi)Cl **(19)**.

Information provided from Mass Spectrometry and ^{1}H-NMR confirms that coordination of pbi to the iridium metal centre occured successfully, but it does not provide definitive proof of which of the four coordination modes illustrated in Figure 2.50 has occured. Definitive identification is fortunately provided by X-ray diffraction of crystals of the complex (Figure 2.52), which showed the absence of a counter ion, indicating a neutral complex, and that the deprotonated imidazolic nitrogen is trans to the carbon of the N^C^N ligand i.e. coordination mode (a).

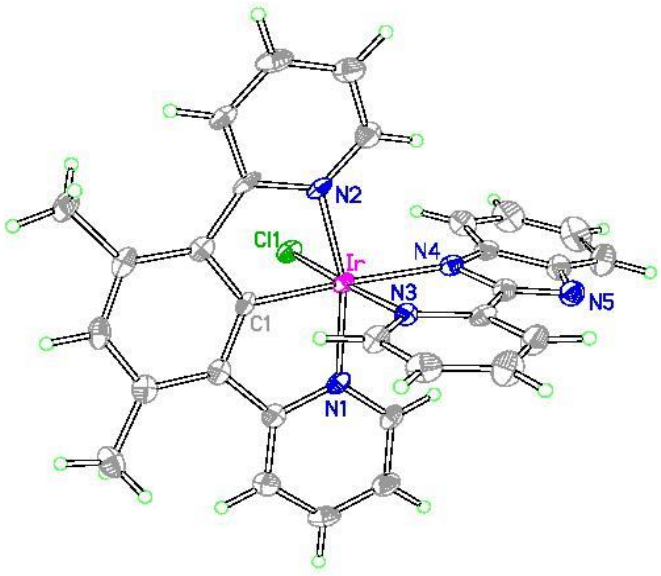

Figure 2.52: crystal structure of Ir(**L1**)(pbi)Cl **(17).**

In order to investigate the properties of the cationic analogues, in which binding occurs through the =N- atom, we chose to block deprotonation at the –NH- atom by methylation. Me-pbi was prepared by addition of NaH to pbiH in dry THF, followed by treatment with a solution of MeI in THF at room temperature over night (Figure 2.53).

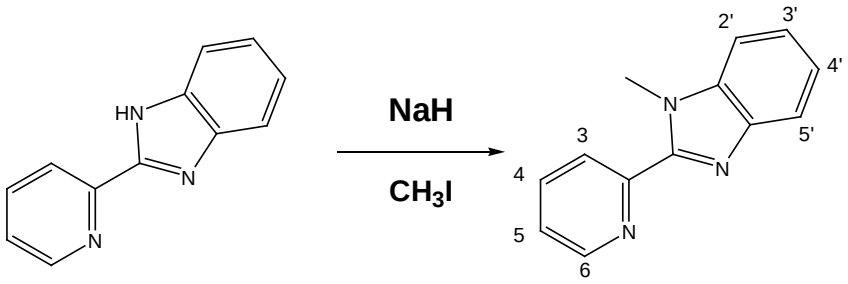

Figure 2.53: synthesis of Me-pbi

[Ir(**L1**)Cl(μ-Cl)]$_2$ was reacted with Me-pbi in toluene in the presence of AgOTf, leading to the cationic complex [Ir(**L1**)(Me-pbi)Cl]$^+$ **(20)** (Figure 2.54). The product was obtained by precipitation following addition of a saturated aqueous solution of KPF_6 and purification was achieved by chromatography giving a yellow solid with 53% yield.

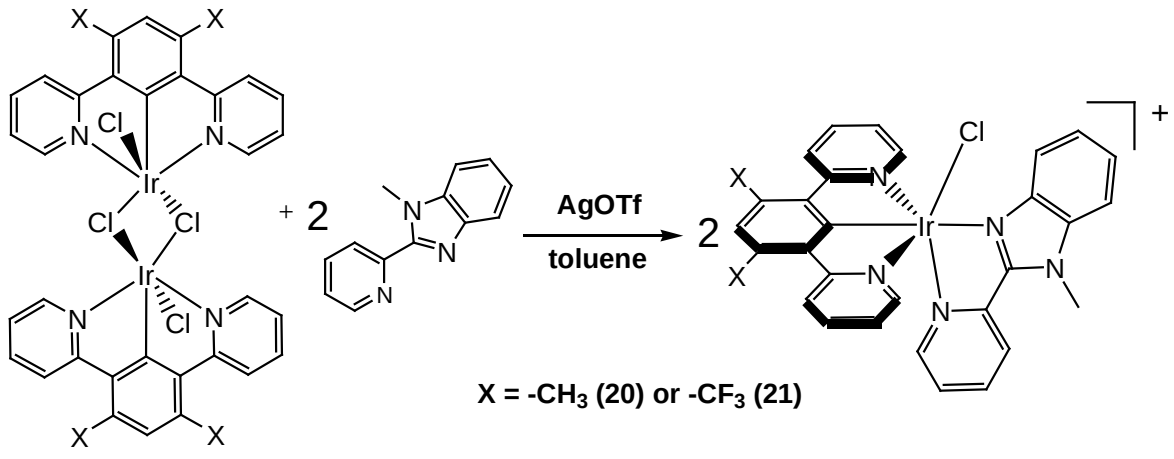

Figure 2.54: synthesis of [Ir(**L1**)(Me-pbi)Cl]$^+$ **(20)** and [Ir(**L3**)(Me-pbi)Cl]$^+$ **(21)**.

Ir(**L1**)(pbi)Cl **(17)**, Ir(**L2**)(pbi)Cl **(18)**, Ir(**L3**)(pbi)Cl **(19)**, [Ir(**L1**)(Me-pbi)Cl]$^+$ **(20)** and [Ir(**L3**)(Me-pbi)Cl]$^+$ **(21)** are obtained as sole isomers according to the ^{1}H-NMR spectra (data summarised in Table 2.7). A significant difference is observed between the resonance (8.73 ppm) of the most deshielded proton assigned to position 6 of the bidentate ligand in Ir(**L1**)(pbi)Cl **(17)** and the resonance of the proton in position 6 of Ir(**L2**)(pbi)Cl **(18)** (9.88 ppm). It is possible that this difference is related to the formation of the *C-trans-N(imid)* or the *C-trans-N(pyr)* isomer. The ^{1}H-^{1}H-NOESY of Ir(**L1**)(pbi)Cl **(17)** and [Ir(**L1**)(Me-pbi)Cl]$^+$ **(20)** shows the presence of cross peaks between the proton in position 6 of the pyridyl ring of the bidentate ligand and the protons in position 5 (observed only for Ir(**L1**)(pbi)Cl **(17)**) and 6 on the pyridyl ring on the terdentate ligand, suggesting formation of the *C-trans-N(imid)* isomer, whereas Ir(**L2**)(pbi)Cl **(18)** shows a weak cross peak between proton 6 of the pbi and proton 3 of the pyridyl ring of the N^C^N, suggesting possible formation of the isomer *C-trans-N(pyr)* for this complex. In the ^{1}H-^{1}H-NOESY of the complex Ir(**L3**)(pbi)Cl **(19)** and [Ir(**L1**)(Me-pbi)Cl]$^+$ **(20)**, cross peaks between the proton in position 6 and the protons in position 5'' and 6'' are not observed suggesting a possible formation of the *C-trans-N(pyr)*. The crystal structure of Ir(**L1**)(pbi)Cl **(17)** (Figure 2.52) indicates the formation of the *C-trans-N(imid)* isomer. Upon these observations it is possible to deduce that formation of different isomers can be influenced by the substituent groups on the phenyl of the N^C^N ligand. However, this evidence must be treated with caution as these assumptions are based on intuitive considerations of the fact that in the *C-trans-N(imid)* isomer, the H^6-pbi is closer in space to the proton 6 and 5 of the N^C^N, whereas in the *C-trans-N(pyr)* isomer, H^6-pbi is closer in space to H^3-NCN. A further evidence is that the crystals obtained might not represent the isomer present in the corresponding solution of the sample, owning to a different propencity, if formation of both was obtained, of the two isomers to form crystals.

Complex	Yield	Resonance of H^6-N^N ($CDCl_3$)/ppm	^1H-^1H-NOESY cross peaks
Ir(L1)(pbi)Cl (17)	28%	8.73	H^6-pbi with H^6 and H^5-NCN
Ir(L2)(pbi)Cl (18)	42%	9.88	H^6-pbi with H^3-NCN
Ir(L3)(pbi)Cl (19)	37%	9.79	-
$[Ir(L1)(Me\text{-}pbi)Cl]^+$ (20)	53%	10.06	H^6-pbi with H^6-NCN
$[Ir(L3)(Me\text{-}pbi)Cl]^+$ (21)	53%	10.01	-

Table 2.7: ^1H-NMR ($CDCl_3$), ^1H-^1H-NOESY and mass spectrometry characterisation of Ir(N^C^N)(pbi)Cl and $[Ir(N^C^N)(pbi)Cl]^+$ complexes.

2.3.6. Metathesis reaction of monodentate ligand

The bond Ir-Cl in the Ir(N^C^N)(N^C)Cl systems, as previously discussed, is relatively weak and, for some complexes, loss of chlorine upon exposure of light or only dissolving the complex in an appropriate solvent (i.e. acetonitrile) occurs. This phenomenon can be exploited in order to coordinate a different type of monoanionic ancillary in the place of chlorine. Synthesis of iridium complexes bearing a variety of monodentate ancillaries, starting from the corresponding halide species, is reported in various works in the literature, amongst those Haga *et al.* in 2006 reported the incorporation of a series of monoanionic ligands by displacing Cl in Ir(Mebib)(N^C)Cl systems (Mebib = bis(N-methylbenzimidazolyl)benzene.[154] In particular the monoanionic ligands used were –Br, -I, -CN, CH_3CN and –pha (Figure 2.55).

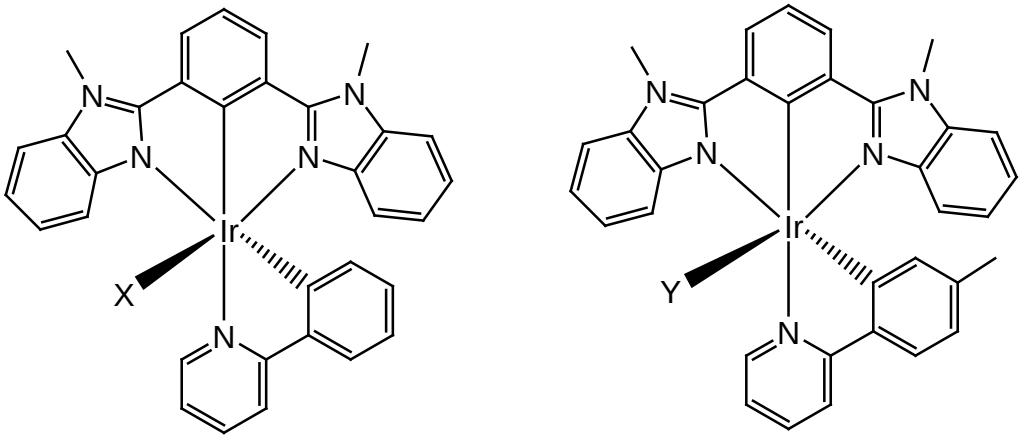

X = -Br, -I, -CN, -CNCH$_3$

Y = -CNCH$_3$, -pha

Figure 2.55: monoanionic ancillaries ligands used by Haga and co-workers for displacing the Cl in the sith position of the coordination sphere of Ir(Me-bib)(ppy)Cl and Ir(Me-bib)(Me-ppy)Cl

In this work, the synthesis of complexes in which the chlorine atom on the sixth coordination site of complexes of the structure Ir(N^C^N)(N^C)Cl is displaced by –CN, -SCN and different acetylides is described.

The complex Ir(**L1**)(dFppy)CN **(22)** (Figure 2.56) was synthesised, starting from Ir(**L1**)(dFppy)Cl **(1)** dissolved in methanol treated with AgOTf, which facilitates the removal of the Cl from the coordination sphere of the complex. The solution was refluxed for 4 hours to allow complete loss of Cl, then a solution of NaCN in 2 ml of water was added. The reaction led to the formation of mono-CN bridged dinuclear complex (Figure 2.56) as the main product. The reaction was then attempted by dissolving Ir(**L1**)(dFppy)Cl **(1)** in acetone and adding AgOTf, followed by addition of an excess of KCN in methanol. After allowing to react at room temperature, the excess of KCN was removed by extraction from DCM into water. The product was a yellow solid obtained with a yield of 68% (Figure 2.57).

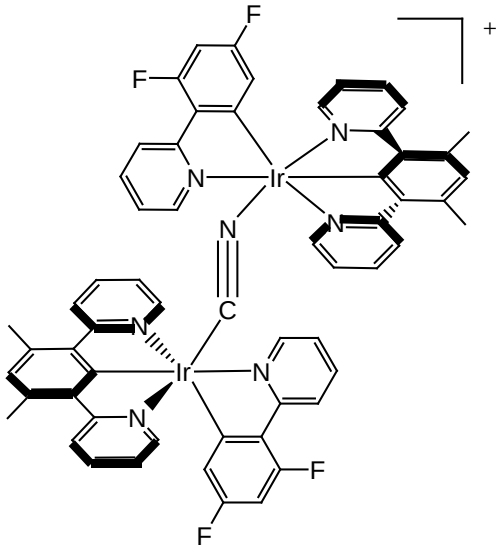

Figure 2.56: mono-bridged CN complex

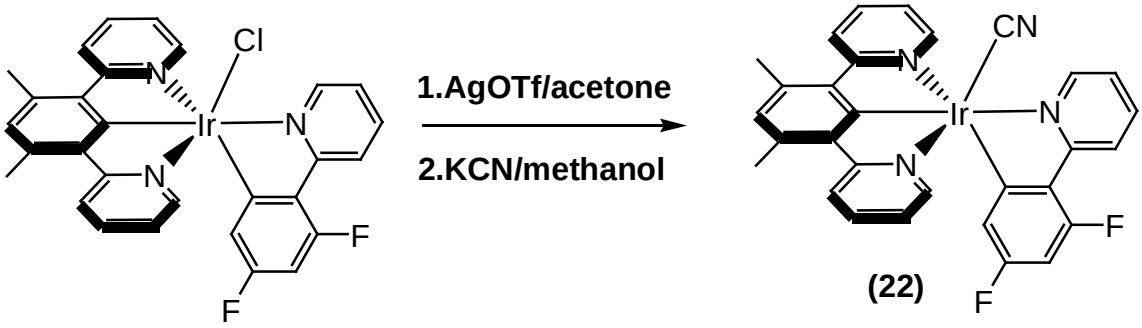

Figure 2.57: synthesis of Ir(**L1**)(dFppy)CN **(22)**.

The formation of the target product was confirmed by mass spectometry, showing the parent ions $[Ir(\mathbf{L1})(dFppy)]^+$ and $[Ir(\mathbf{L1})(dFppy)CN]^+$. The ^{1}H-NMR of Ir(**L1**)(dFppy)CN **(22)** and Ir(**L1**)(dFppy)Cl **(1)** display an identical pattern of signals. Same reaction method was then adopted to synthesise the complexes Ir(**L2**)(dFppy)CN **(23)**, Ir(**L2**)(ppy)CN **(24)**, Ir(**L3**)(dFppy)CN **(25)**, Ir(**L1**)(ppy)CN **(26)** and Ir(**L5**)(dFppy)CN.

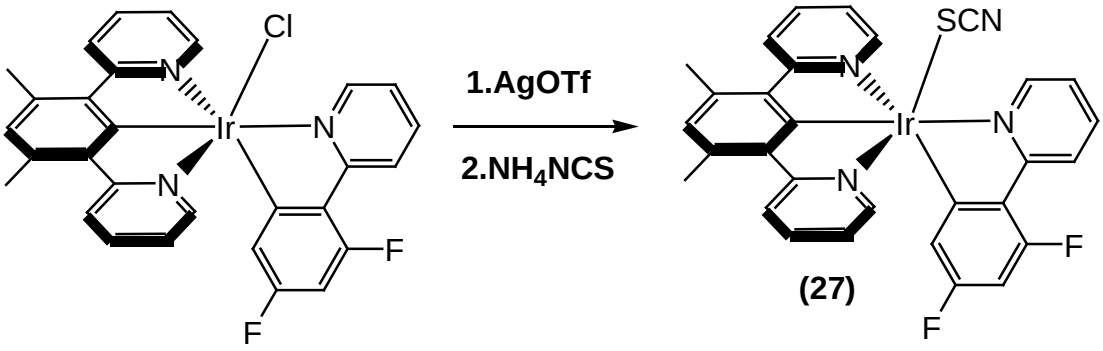

Figure 2.58: synthesis scheme of Ir(**L1**)(dFppy)NCS **(27)**.

The complex Ir(**L1**)(dFppy)SCN **(27)** (Figure 2.58) was synthesised by stirring Ir(**L1**)(dFppy)Cl **(1)** for 1 hour in acetone in the presence of AgOTf, followed by addition of an excess of NH_4SCN in methanol. The product was a yellow solid obtained with a yield of 95%. The formation of the target product was confirmed by mass spectometry, by the presence of the species $[Ir(\mathbf{L1})(dFppy)]^+$ and $[Ir(\mathbf{L1})(dFppy)SCN]^+$. Proton NMR displayed the presence of a sole product. Following same method also was achieved preparation of Ir(**L1**)(ppy)SCN **(28)** and Ir(**L2**)(ppy)SCN **(29)**.

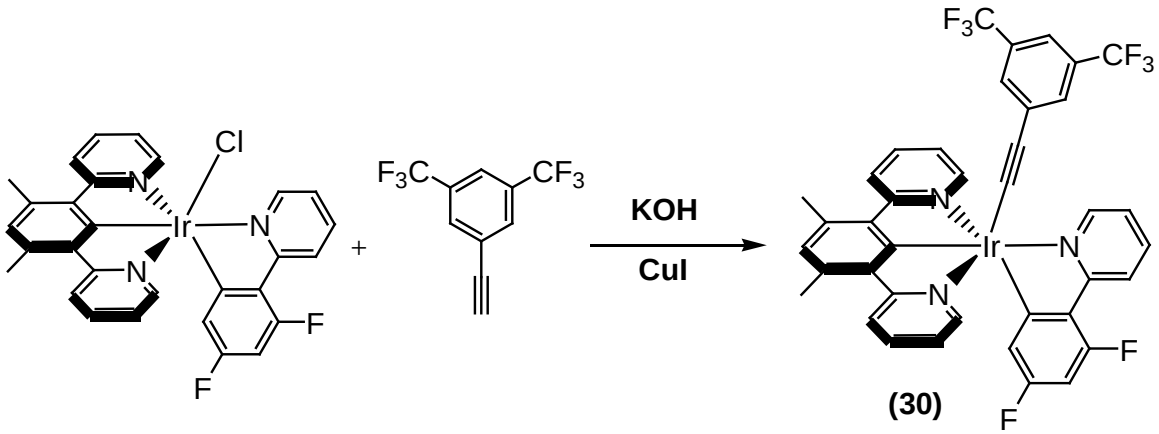

Figure 2.59: synthesis scheme of Ir(**L1**)(dFppy)(**A1**) **(30)**.

The synthesis of Ir(**L1**)(dFppy)(**A1**) **(30)** (**A1** = 1,3-trifluoromethyl-phenylacetylide) (Figure 2.59) was carried out by strirring for 4 hours dtfmba in a solution of KOH in methanol, followed by addition of Ir(**L1**)(dFppy)Cl **(1)** dissolved in methanol and then stirring the combined solutions overnight in presence of CuI as catalyst. The product formed as a yellow precipitate from the reaction mixture and was easily purified by washing the precipitate with methanol in order to wash out the remaining unreacted materials; a yield of 52% was obtained. The target product was identified by mass spectrometry and by ^{1}H-NMR due the presence of the signals assigned to the protons of the phenyl ring of the ancillary ligand. (Figure 2.60) Mass spectrometry showed precence of the ions [Ir(**L1**)(dFppy)Cl **(1)**]$^{+}$ and [Ir(**L1**)(dFppy)(**A1**)]$^{+}$.

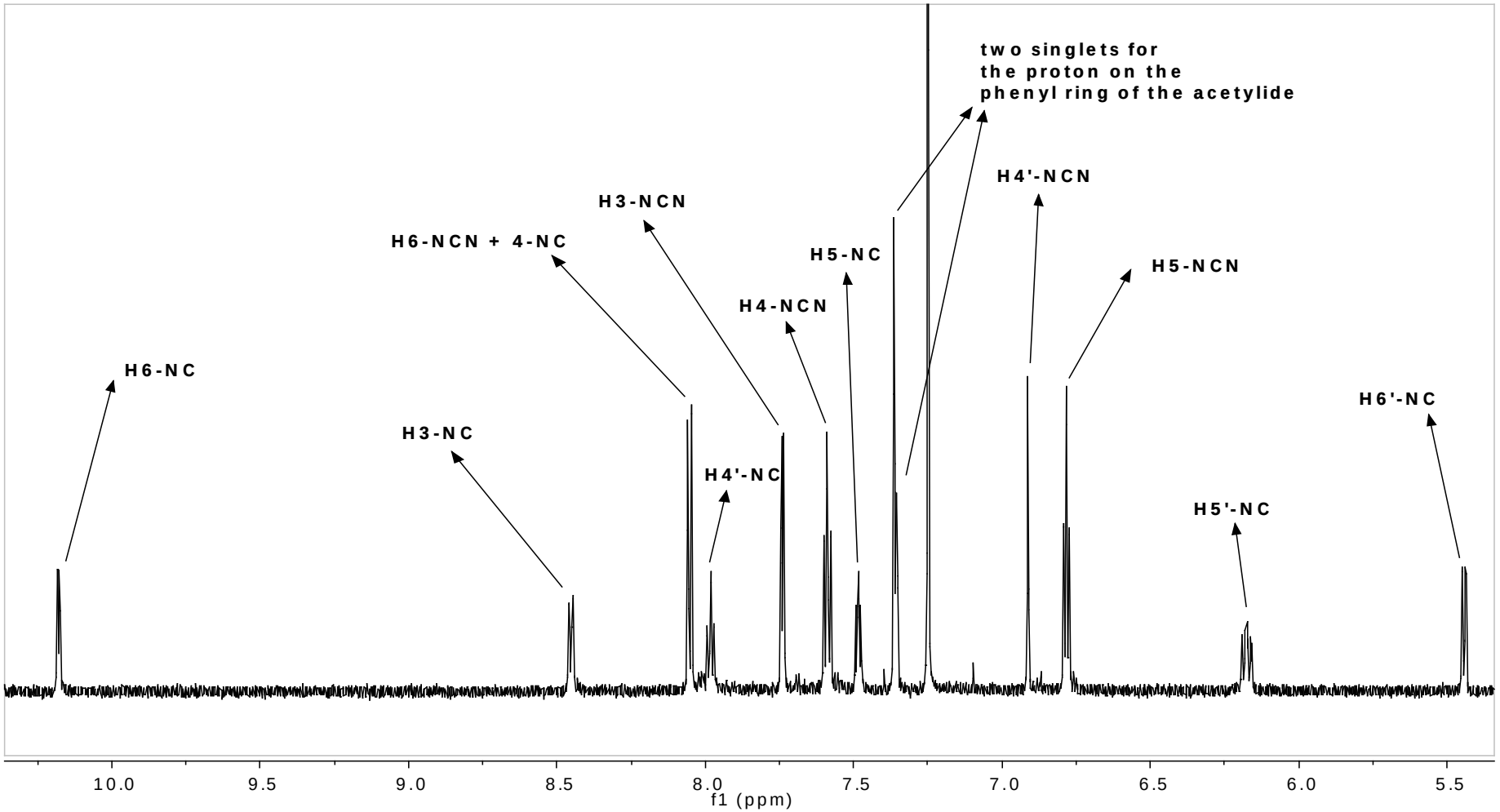

Figure 2.60: ^{1}H-NMR spectrum of Ir(**L1**)(dFppy)(**A1**) **(30)**.

Complex	Yield	Resonance of H^6-N^C ($CDCl_3$)/ppm	Resonance of $H^{6'}$-N^C ($CDCl_3$)/ppm	Mass Spectrometry (ES+) *m/z*
Ir(L1)(dFppy)Cl (1)	40%	10.15	5.15	642 $[M–Cl]^+$, 682 $[M–Cl+CH_3CN]^+$
Ir(L1)(dFppy)CN (22)	68%	9.99	5.41	668 $[M+H]^+$, 642 $[M-(CN)]^+$
Ir(L1)(dFppy)SCN (27)	95%	9.59	5.41	700 $[M+H]^+$, 642 $[M-(SCN)]^+$
Ir(L1)(dFppy)(A1) (30)	50%	10.18	5.44	879 $[M]^+$, 642 $[M-(dtfmbA)]^+$

Table 2.8: ^{1}H-NMR ($CDCl_3$) and mass spectrometry characterisation of the complexes with different ancillary ligands

In Table 2.8, the ^{1}H-NMR data of the complexes containing different ancillary ligands is summarised. Although the pattern relative to the signals assigned to the N^C^N and N^C ligand is similar for all complexes, the resonance of the proton H^6-NC is significantly influenced by the type of ancillary ligand incorporated in the coordination sphere of the complex. For example, considering the series of complexes containing **L1** as terdentate ligand, the H^6-NC signal is shifted to lower fields by the introduction of SCN and CN as ancillary ligand (respectively 9.59 ppm and 9.99 ppm) with respect to that of the halide complex (10.15 ppm). In the acetylide containing species the shift is observed in the other direction, with a H^6-NC resonating at 10.18 ppm. This trend is consistent with the data observed relative to the complexes bearing different cyclometalling ligands. The resonance of the H^6-NC is thus strongly influenced by the type of ancillary ligand coordinated to the iridium centre.

The same procedure was performed in order to coordinate different acetylides in place of chlorine in Ir(**L1**)(dFppy)Cl **(1)**. In particular **A2** (1-phenylacetylide), **A3** (1-(4-methoxy)phenylacetylide), **A5** (1-(4-benzonitrile)acetylide and **A4** (1-(4-dimethylamino)phenylacetylide) were used (Figure 2.59). However, even though

the eperiments performed are thought to have led to the target products, the very low solubility of the precipitates from the reaction mixtures made them difficult to characterise. Definitive evidence of purity and formation of the complexes was not achieved. To this aspect, Ir(**L3**)(ppy)Cl **(5)** represents a more suitable precursor for the synthesis of complexes containing acetylides as monodentate ancillary ligands, owing to the higher solubility of the complexes conferred by the $-CF_3$ groups on the N^C^N ligand. A range of acetylide derivatives were prepared from this precursor, using the same methodology, as indicated in Figure 2.61.

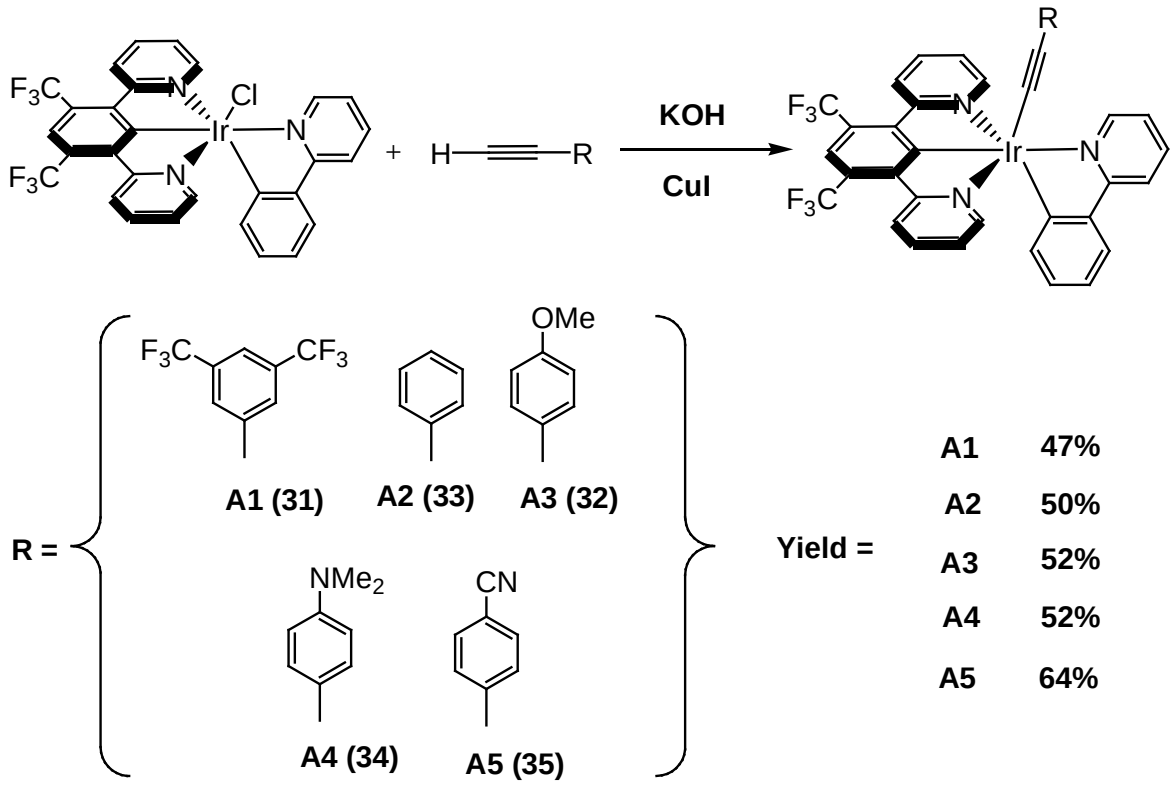

Figure 2.61: scheme for the synthesis of Ir(**L3**)(ppy)(acetylide) based complexes.

Formation of the complexes was confirmed by mass spectrometry by detection of the ions for $[Ir(\mathbf{L3})(ppy)(acetylide)]^+$ and proton NMR showing formation of a sole complex. Complexes containing the monoanionic ancillary btfmb and CNph manifested relatively high stability in solution, in which they also showed red

emission at room temperature. On the other hand the complexes containing OMe, NMe_2 and unsubstituted arylacetylides showed degradation upon storage under light and in solution. This is probably due to the fact that the electron-withdrawing $–CF_3$ and -CN substituents on the phenyl ring of the acetylide lower the electron density around the metal centre. So that the trans effect associated with the acetylide being trans to the cyclometallating carbon is less of a problem in terms of stability. In contrast, the electron donating effect of $-NMe_2$ and –OMe (and apparently even just ph itself) groups provokes the opposite effect, inflating the electronic density at the metal centre.

2.4. Rhodium complexes

2.4.1. Synthesis of rhodium di-chloro-bridged dimers

As for the iridium analogues, synthesis of the target Rh(III) complexes has to occur via formation of the intermediate di-chloro-bridged dimers (Figure 2.62), obtained by reacting $RhCl_3$ with the N^C^N ligands (**L1**), (**L2**) and (**L3**) in a mixture of ethoxy-ethanol/water at reflux temperature. The dimers were formed as precipitates and washed with water, ethanol and ether.[68] Similar observations were made about their characterisation and solubility to those for the iridium based dimers. Again, the $–CF_3$ substituted Rh dimer can be characterised in CD_3CN, due to its higher solubility, with respect to that of the $–CH_3$ and the –F containing counterparts, characterised in their mononuclear form in deuterated DMSO.

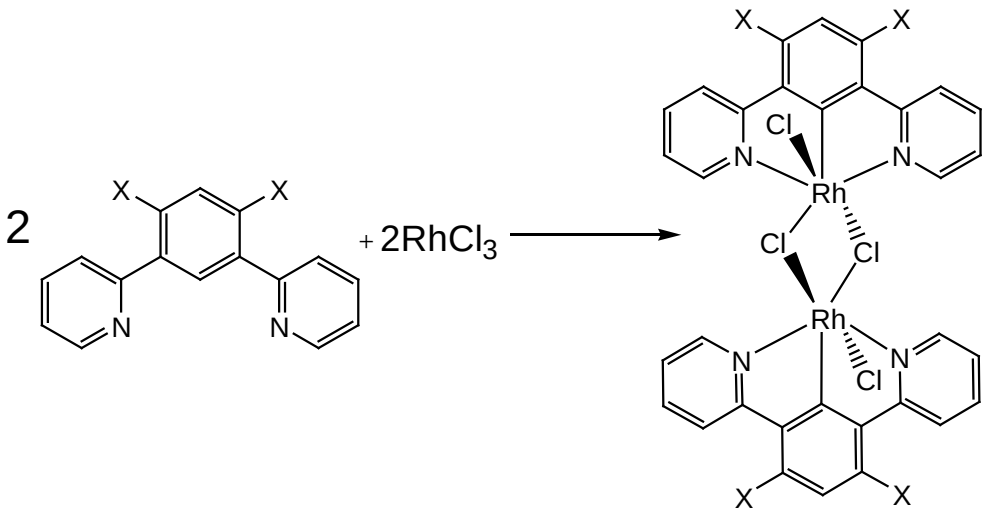

Figure 2.62: synthetic scheme for the di-chloro-brdged rhodium dimers, where X= -CH_3, -F, CF_3

2.4.2. Synthesis of Rh(N^C^N)(N^C)Cl complexes

Synthesis of Rh(N^C^N)(N^C)Cl is not new to the research interest of our group, as Whittle reported previously the synthesis of Ir(**L1**)(ppy)Cl. (Figure 2.63) Following reaction of [Rh(**L1**)Cl(μ-Cl)]$_2$ at 110°C in excess of ppyH and in the presence of AgOTf, formation of a side product, Rh(ppy)$_3$, alongside the desired complex, indicated some scrambling of ligands and suggested a weaker interaction between the Rh centre, a second row metal, and the N^C^N ligand unit, compared to that of complxes of iridium, a third row metal. Synthesis of the same complex in ethylene glycol at 196°C, revealed formation of the target Rh complex, which displayed loss of Cl over time by mass spectrometry.[24]

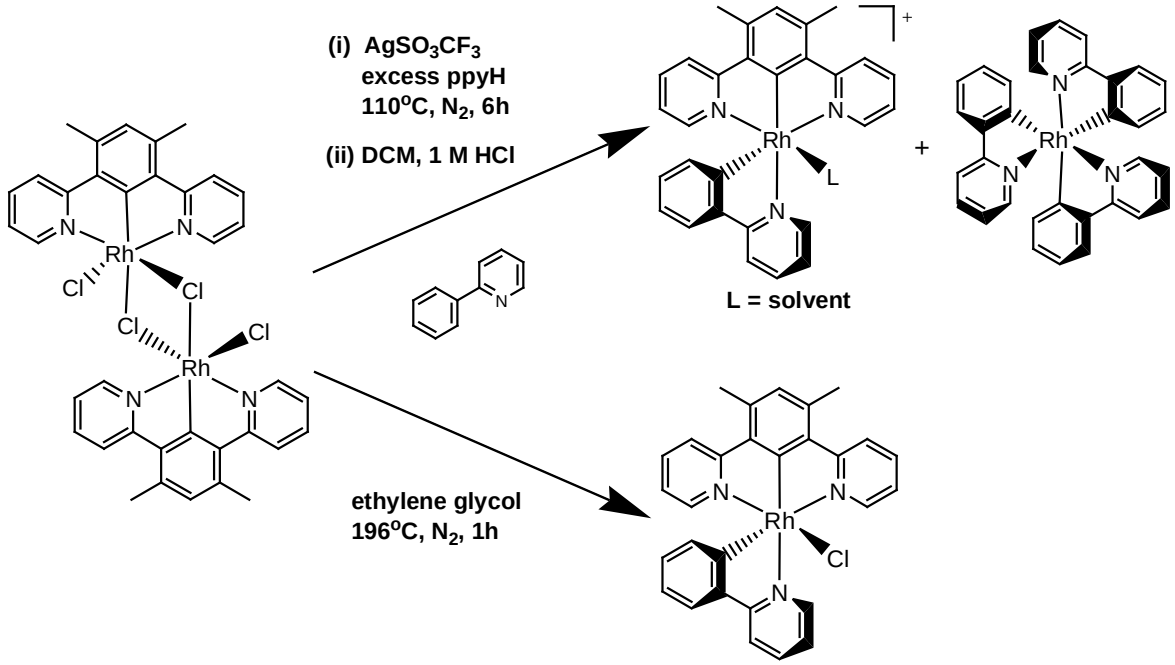

Figure 2.63[(24)]: synthesis of Rh(**L1**)(ppy)Cl

A similar synthetic method to that previously adopted by our research group for the synthesis of new Rh(N^C^N)(N^C)Cl was used in the present work, reacting dichloro bridged rhodium dimers with dFppyH in ethylene-glycol in the presence of AgOTf. The product was then washed several times in a 1M aqueous solution of HCl in order to remove any non-reacted dFppyH. Rh(**L1**)(dFppy)Cl **(38)** (Figure 2.64) was obtained as a pale brown solid with a yield of 41%. The formation of the complex as a sole product was confirmed by ^{1}H-NMR which showed a similar set of signals to those of Ir(**L1**)(dFppy)Cl **(1)**. A similar procedure was adopted for the synthesis of Rh(**L2**)(dFppy)Cl **(39)** and Rh(**L3**)(dFppy)Cl **(40)** (Figure 2.64). Although formation of the target complexes is not unequivocally confirmed by mass spectrometry for Rh(**L2**)(dFppy)Cl **(39)** and Rh(**L3**)(dFppy)Cl **(40)**, due to the presence of a sole peak related to the species of the form $[Rh(N^C^N)(N^C)]^{+}$, the formation of the chlorine containing species during the synthesis is suggested by the presence of this peak. Higher lability of the Rh-Cl compared to the Ir-Cl bond would be expected. Moreover, neutrality of the synthesised complexes is displayed by the relatively high solubility of all three desired complexes and by the pattern showed by the ^{1}H-NMR signals, typical of neutral complexes.

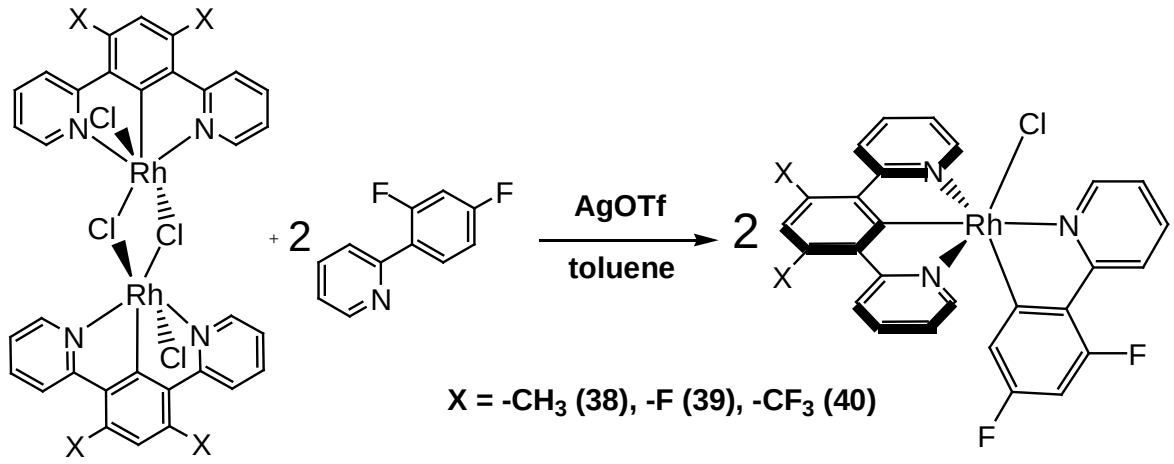

Figure 2.64: synthesis of Rh(N^C^N)(N^C)Cl, where X = $-CH_3$, -F or $-CF_3$

Complex	**Yield**	**Resonance of H^6-N^C ($CDCl_3$)/ppm**	**Resonance of $H^{6'}$-N^C ($CDCl_3$)/ppm**	**Mass Spectrometry (ES+) *m/z***
Ir(L1)(dFppy)Cl (1)	94%	10.15	5.51	642 $[M–Cl]^+$, 682 $[M–Cl+CH_3CN]^+$
Ir(L3)(dFppy)Cl (3)	35%	10.17	5.21	791 $[M–Cl+CH_3CN]^+$
Ir(L2)(dFppy)Cl (2)	39%	9.52	5.44	691 $[M–Cl+CH_3CN]^+$
Rh(L1)(dFppy)Cl (38)	41%	10.18	5.72	552 $[M\text{-}Cl]^+$, 586 [M]
Rh(L3)(dFppy)Cl (40)	56%	10.12	5.32	660 $[M–Cl]^+$]
Rh(L2)(dFppy)Cl (39)	16%	10.11	5.69	560 $[M\text{-}Cl]^+$

Table 2.9: ^{1}H-NMR and mass spectrometry characterisation of Rh(N^C^N)(N^C)Cl complexes

Comparing the NMR data of the Rh(N^C^N)(N^C)Cl complexes with their iridium analogues, as summarised in Table 2.9, the pattern of the signals relative to the cyclometallating ligands similar between rhodium and iridium complexes. Also the resonances relative to the proton H^6-NC and H^3-NC of the complexes of rhodium

containing the **L1** and **L3** are located at similar fields compared to those of the iridium analogues. The complex Ir(**L2**)(dFppy)Cl **(2)**, on the other hand, displays a resonance relative to the proton H^6-NC at 10.11 ppm, which is at higher fields compared to that of Ir(**L2**)(dFppy)Cl **(2)** (9.52 ppm).

2.5 Concluding remarks

In this chapter the synthesis of a series of N^C^N and N^C ligands *via* Stille cross-coupling and Miyaura cross-coupling is discussed. In particular synthetic ways to introduce substituents on the central phenyl ring (-CH_3, -F and –CF_3) and on the pyridyl rings (-OMe, -NMe_2, -CF_3) of the N^C^N ligands have been reported. Coordination of N^C^N ligands to an Ir(III) centre gave dimeric complexes of the structure [Ir(N^C^N)Cl(μ-Cl)]$_2$.

Reaction of [Ir(N^C^N)Cl(μ-Cl)]$_2$ with ppy and dFppy led to formation of neutral bis-cyclometallated complexes Ir(N^C^N)(N^C)Cl. The coordination of the second cyclometallating ligand selectively gave a sole isomer (C-*trans*-N) (see Section 2.3.2.). Formation of this isomer, due to the strong σ donor effect of the cyclometallating site of the N^C^N ligand, was suggested by spectroscopic data and X-ray crystallography (see Section 2.3.2.). A series of new Ir(N^C^N)(N^C)Cl complexes were thus synthesised in relatively mild conditions at 110° C, in the presence of AgOTf and using toluene as a solvent, whereas in previous works the synthesis of Ir(N^C^N)(N^C)Cl complexes was carried out at 196° C using ethylene glycol as a solvent.[66, 106] The Ir-Cl bond of the sixth coordination site displayed different stability depending on the type of substituents on the cyclometallating ring of the N^C^N ligand. In particular -CF_3 and –CH_3 substituted complexes are stable in both acetonitrile and chloroform whereas the -F substituted complexes could be characterised only in chloroform since the chloride ligand dissociated in acetonitrile.

Also other classes of iridium complexes have been presented in this work starting from the same iridium di-chloro bridged dimers used for the synthesis of Ir(N^C^N)(N^C)Cl complexes.

Reaction of $[Ir(N^C^N)Cl(\mu\text{-}Cl)]_2$ with bpy led to formation of positively charged mono-cyclometallated iridium complexes, $[Ir(N^C^N)(N^N)Cl]^+$, whereas reaction of $[Ir(N^C^N)Cl(\mu\text{-}Cl)]_2$ with a second N^C^N terdentate ligand led to formation, but only in some cases (see Section 2.3.4.), of positively charged bis-cyclometallated complexes $[Ir(N^C^N)(N^C^N)']^+$. In the $[Ir(N^C^N)(N^C^N)']^+$ complexes synthesised the two cyclometallating sites occupy a mutually trans position, due to the only coordination mode available with which the two cyclometallating sites can coordinate the metal centre as terdentate ligands.

Also the synthesis of new Ir(N^C^N)(pbi)Cl complexes has been carried out but unfortunately spectroscopic data and X-ray crystallography did not allow the identification of which isomer is selectively formed upon coordination of pbi as bidentate ligand (see Section 2.3.5.). However formation of Ir(N^C^N)(pbi)Cl complexes has beed confirmed by NMR spectroscopy and mass spectrometry. Further investigation might provide additional information on the structural properties of these systems.

Replacement of the Cl on Ir(N^C^N)(N^C)Cl has been carried out successfully in order to introduce –CN, -SCN and -≡-R as monodentate ancillary ligands, giving a series of complexes bearing one terdentate, one bidentate and one monodentate ligand and with three Ir-C bonds Ir(N^C^N)(N^C)(ancillary). These complexes containing three cyclometallating sites displayed relatively high stability in solution in contrast with previously investigated tris-cyclometallating complexes incorporating only terdentate ligands (e.g. Ir(N^C^N)(C^N^C), Ir(N^C^N)(C^N^O)), which low stability limited their performances in their application.[108, 109, 198]

CHAPTER 3

Photophysics, electrochemistry, DFT and OLEDs

3. Photophysics, electrochemistry, DFT and OLEDs

3.1. Ir(N^C^N)(N^C)Cl complexes

3.1.1. Theoretical studies based on DFT calculations

Prediction of the energy-minimised, gas-phase structures of the complexes and identification of the frontier orbitals has been carried out by density functional theory (DFT) calculations using B3LYP. The approach adopted is well-established for third-row transition metal complexes, using the LANL2DZ basis set for Ir(III), with the inner core electrons replaced by a relativistic core potential, and 6-31G for the ligands.[210] The frontier orbitals (HOMO–1 to LUMO+1) for Ir(**L1**)(ppy)Cl are represented in Figure 3.1, together with the percentage of the total electron density on the three ligands and the metal. Similarly in Figure 3.2 are represented those of the complexes Ir(**L3**)(ppy)Cl **(5)** and Ir(**L2**)(ppy)Cl **(4)**.

Complex	HOMO-1	HOMO	LUMO	LUMO+1
Ir(L1)(ppy)Cl	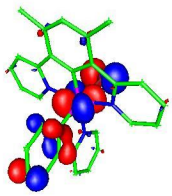	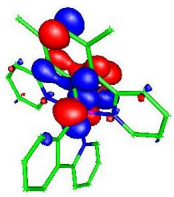	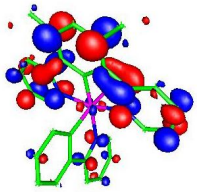	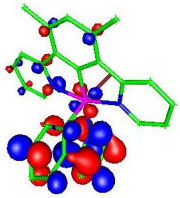
E(eV)	-0.18339	-0.18302	-0.05341	-0.04759
Ir	0.25	0.32	0.02	0.04
N^C^N	0.2	0.36	0.88	0.16
Cl	0.32	0.23	0	0
N^C	0.23	0.07	0.11	0.81

Figure 3.1: summary of DFT calculations for Ir(**L1**)(ppy)Cl, where E(eV) is the energy of the frontier orbital expressed in eV, and Ir, N^C^N, Cl, N^C represent the contribution of the respective parts of the molecule to the orbitals involved.

Complex	HOMO-1	HOMO	LUMO	LUMO+1
Ir(L2)(ppy)Cl (4)	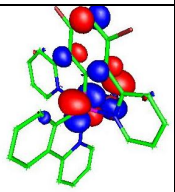	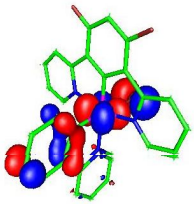	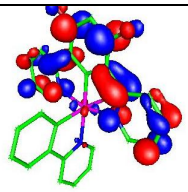	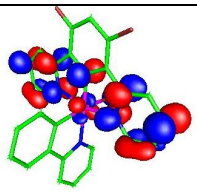
E(eV)	-0.19745	-0.19365	-0.0636	-0.05753
Ir	0.45	0.45	0.02	0.07
N^C^N	0.21	0.08	0.93	0.88
Cl	0.27	0.27	0	0.04
N^C	0.07	0.2	0.05	0.01
Ir(L3)(ppy)Cl (5)	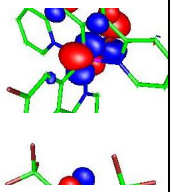	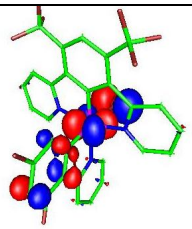	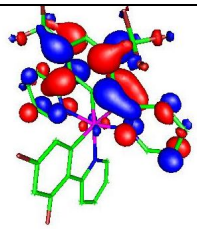	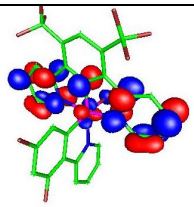
E(eV)	-0.20608	-0.20178	-0.09287	-0.06567
Ir	0.42	0.43	0.03	0.06
N^C^N	0.19	0.2	0.96	0.89
Cl	0.31	0.33	0	0.04
N^C	0.07	0.07	0.01	0.01

Figure 3.2: similarly to Figure 3.1, summary of DFT calculations for Ir(**L3**-NCN)(ppy)Cl and Ir(**L2**-NCN)(ppy)Cl

For the complex Ir(**L1**)(ppy)Cl (Figure 3.1), observing the contribution of the ligands, it is noticeble that the HOMO is delocalised across the metal, the ancillary ligand, and the cyclometallating ring of the N^C^N ligand. The calculations show also how the cyclometallating ring of the bidentate ligand makes only a minor contribution. Considering the HOMO-1 orbital, although the metal and halide have a similar contribution, in this case, it is the participation of the bidentate rather than the terdentate ligand that is more important. For the complexes Ir(**L2**)(ppy)Cl **(4)** and Ir(**L3**)(ppy)Cl **(5)** (Figure 3.2), the situation is similar to the methyl substituted complex, but an inversion in the order of the orbitals is observed; in fact, the HOMO is formed by the metal, ancillary ligand and the aryl ring of N^C, whilst HOMO–1 involves metal, halide and aryl ring of N^C^N. This inversion can be

explained by the fact that the energy of the orbitals with N^C^N contribution are influenced by the inductively electron-withdrawing nature of the fluorine and trifluoromethyl substituents, resulting in a lowering of the energy of N^C^N-based orbitals. The three complexes discussed above containing ppy as N^C will be here identified as series 1. Analogous considerations can be postulated for the three corresponding complexes with dFppy as bidentate N^C ligand Ir(**L1**)(dFppy)Cl **(1)**, Ir(**L3**)(dFppy)Cl **(3)** and Ir(**L2**)(dFppy)Cl **(2)** (series 2), DFT calculations of which are shown in Figure 3.5, a summary at the end of this chapter. The LUMOs of all six complexes have a very similar electron distribution to one another, being delocalised across the N^C^N ligands, but not significantly involving the other ligands or the metal ion. Identical considerations can be drawn for the LUMOs levels of the dFppy complexes.

3.1.2. Electrochemistry

Complex	E_{ox} / V vs SCE	E_{red} / V vs SCE
Ir(L1)(ppy)Cl	1.18 ($E^{1/2}$)	–2.12 (E^{p})
Ir(L1)(dFppy)Cl (1)	1.16 ($E^{1/2}$)	–2.14 (E^{p})
Ir(L2)(ppy)Cl (4)	0.99 ($E^{1/2}$)	< -2.20 (E^{p})
Ir(L2)(dFppy)Cl (2)	0.98 ($E^{1/2}$)	–1.90 (E^{p})
Ir(L3)(ppy)Cl (5)	1.02 ($E^{1/2}$)	–1.97 ($E^{1/2}$)
Ir(L3)(dFppy)Cl (3)	1.11 ($E^{1/2}$)	–1.65 (E^{p})

Table 3.1: cyclic volatammetry in solution of dichloromethane (~10^{-3} M) with Bu_4NBF_4 as supporting electrolyte at room temperature, data for the complexes bearing ppy and dFppy as N^C ligand.

Electrochemical study of the complexes, by cyclic voltammetry, in dichloromethane solution (~10^{-3} M) with Bu_4NBF_4 as supporting electrolyte at room temperature, was carried out using the ferrocene/ferrocenium couple as a reference ($E^{1/2}$ = 0.42 V vs SCE). All of the complexes display a reversible or pseudoreversible oxidation process between 0.9 and 1.2 V versus SCE (Figure

3.3), values that are comparable to those of bis-cyclometallated complexes with a monoanionic, bidentate ancillary ligand (e.g. for Ir(Meppy)$_2$(acac), E^{ox} = 0.92 V).[116] For the well studied tris-cyclometallated complexes, such as *fac*-Ir(ppy)$_3$ (E^{ox} = 0.77 V), oxidation occurs at lower potentials than those observed for the complexes of series 1 and 2.[95] Taking into consideration previous studies, the oxidation is thought to involve the metal and cyclometallating parts of the molecule, due to the high degree of covalency of the Ir–C bonds, which is also supported by the DFT calculations described above. Moreover, as illustrated in Figure 3.3 (also see data in Table 3.1), the substituents positioned on the N^C^N ligand cause a significant shifting effect on the oxidation potential of the complexes, resulting in oxidation of the –CF_3 substituted complex at lower potentials in comparison with the oxidation of the –F substituted complex.

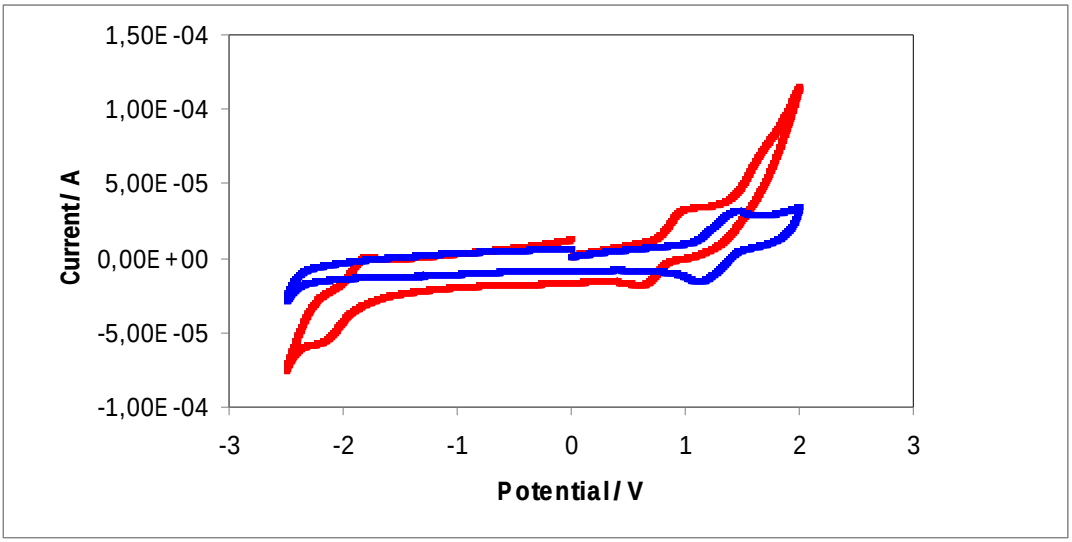

Figure 3.3: cyclic voltammetry of Ir(**L3**)(ppy)Cl **(5)** (red line) and Ir(**L2**)(ppy)Cl **(4)** (blue line), showing how the –CF_3 substituted complex is easier to oxidise than the –F substituted complex.

Amongst the set of six complexes, the reduction ranges from –1.65 V for Ir(**L3**)(dFppy)Cl **(3)** to –2.14 V for Ir(**L1**)(dFppy)Cl **(1)**, and to potentials lower than –2.20 V for Ir(**L2**)(ppy)Cl **(4)**. In this last case, the reduction could not be recorded

by the electrochemical analysis in dichloromethane, probably occuring at more negative potentials than that permitted by the solvent window. Nevertheless, due to the strongly electron-withdrawing influence of the trifluoromethyl group, reduction is clearly seen to be more accessible for the complexes containing these substituents. The reduction potentials observed are comparable to those of charge-neutral, bis- and tris-cyclometallated complexes (e.g. –2.17 V and –2.19 V for $Ir(Meppy)_2(acac)$ and $fac\text{-}Ir(ppy)_3$ respectively).[95, 116]

3.1.2. Ground state absorption

UV-visible spectral bands and relative exctinction coefficients of the six complexes in CH_2Cl_2 at room temperature are listed in Table 3.3. For all the complexes, intense bands in the region between 230 and 300 nm are observed, related to π-π* transitions of the aromatic ligands (Figure 3.4). Also, slightly weaker but still intense bands around 400 nm, with no counterpart in the free ligands, can be identified. Moreover less intense bands at lower energies are identified around or above 450 nm. Comparing the band at lower energies of the complexes within series 1 or series 2, the bands relative to the **L2** complexes are blue shifted with respect to those of the **L1**, whilst the bands of the **L3** complexes are shifted towards the red. Upon fluorination of the N^C ligand, in the dFppy coordinated complexes, a blue-shift is observed in series 2 compared to the corresponding complexes of series 1, although the N^C^N ligand clearly has a larger influence on the energies of corresponding bands (see Table 3.3).

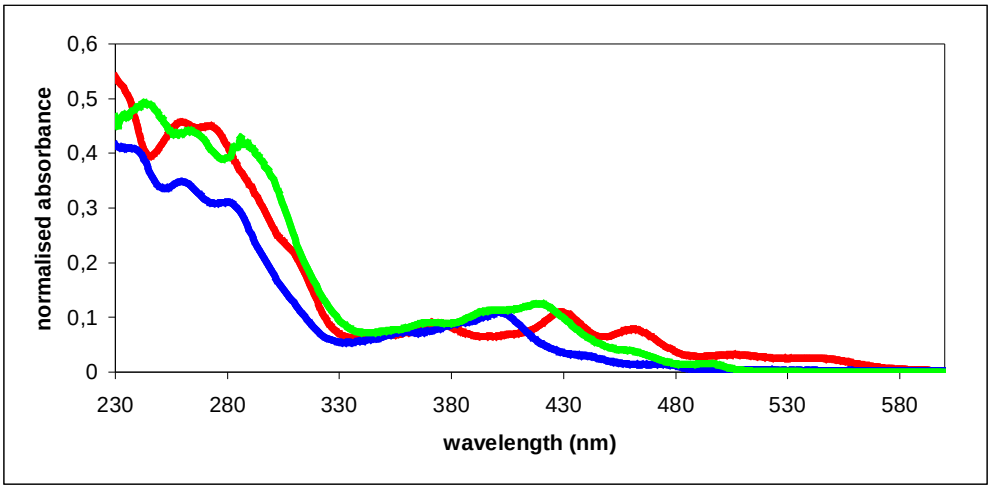

Figure 3.4: normalised absorption spectra to the most intense low-enegy band at room temperatue in dichloromethane of the complexes Ir(**L1**)(ppy)Cl (green line), Ir(**L3**)(ppy)Cl **(5)** (red line) and Ir(**L2**)(ppy)Cl **(4)** (blue line).

Quantitative comparison of experimental and theoretical data should be treated with caution, as the calculations apply to the gas-phase at 0 K, and do not take into account the spin-orbit coupling (SOC), whilst bands arising from transitions within the singlet and triplet manifolds may overlap. Nevertheless, in order to assist in the assignment of bands in this region, time-dependent DFT (TD-DFT) calculations have been carried out in order to provide useful information about the likely electronic origins of the observed bands, the results of which are summarised in Table 3.2 for the two lowest-energy triplet states and five lowest-energy singlet excited states. Looking at Ir(**L1**)(ppy)Cl, for example, the TD-DFT suggests that the lowest-energy band, which has a relatively low intensity (494 nm, ε = 1300 $M^{-1}cm^{-1}$), is probably due to the formally forbidden $S_0 \rightarrow T_1$ and $S_0 \rightarrow T_2$ transitions (calculated values 487 and 483 nm). These considerations are confirmed from further evidence observed from emission spectroscopy (see Section 3.1.4.). These transitions are found to be of HOMO–1→LUMO and HOMO→LUMO character respectively, and thus can be regarded as $d_{Ir}/\pi_{NC} \rightarrow \pi^*_{NCN}$ charge-transfer (mixed MLCT/LLCT) and $d_{Ir}/\pi_{NCN} \rightarrow \pi^*_{NCN}$ (mixed MLCT/IL) transitions respectively. Similar assignments are quite typical for iridium(III) complexes containing cyclometallating ligands, due to the high degree

of covalency in the C–Ir bond, leading to a mixed d/π character to the HOMO-1 and HOMO. Since the metal appears to have a high degree of partiipation, with a significant SOC, relaxation of the spin selection rule is observed. Meanwhile, the lowest-energy, spin-allowed singlet bands involve mostly the two highest-energy filled orbitals and the two lowest-energy unfilled orbitals, and they also have a high degree of $ML_{NCN}CT$ character. Analogous assignment can be postulated for all the other complexes (see Table 3.2 and the frontier orbitals illustrated in Figure 3.1 and 3.2) and the calculated HOMO-LUMO energy gaps agree with the trend observed in absorption energies amongst the complexes (Table 3.2). Upon introduction of electron-withdrawing trifluoromethyl groups into the N^C^N ligand, a decrease of the energy of all orbitals is caused but the effect is larger for the LUMO, being localised on the N^C^N ligand, than for the HOMO (see Figure 3.5). This provokes a shift of the transitions to lower energies, thus the absorption bands are red-shifted. Even though fluorine atoms are also expected to lower the energy of orbitals, due to their electron-withdrawing effect, a mesomeric electron-donating effect is revealed, which will tend to counteract the inductively withdrawing effect at positions *ortho* and *para* (but not *meta*) to the F atom. Since the metal is disposed *meta* to the F atoms, whereas the pyridyl rings of the N^C^N ligand are *ortho* to F, it is possible to predict that the HOMO will be lowered in energy more than the LUMO, leading to a blue-shift, as observed. These considerations agree with the work previously carried out by De Cola and co-workers on systems containing bidentate phenylpyridine-based ligand bearing –F and $–CF_3$ groups.[211] A corresponding effect is also manifested in the slightly higher energy of the spectra of the dfppy complexes compared to their ppy analogues, leading to the blue-shifted emission upon coordination of dFppy, as previously reported in the work of Tamayo *et al.*, in which tris-cyclometallated iridium complexes, containing three dFppy ligands, displayed blue-shifted MLCT absorption bands compared to those of the complexes containing unsubstituted ppy ligands.[96, 212, 213]

	Ir(L1)(ppy)Cl	Ir(L1)(dFppy)Cl (1)	Ir(L2)(ppy)Cl (4)	Ir(L2)(dFppy)Cl (2)	Ir(L3)(ppy)Cl (5)	Ir(L3)(dFppy)Cl (3)
T1	2.541 (487) H–1→L H–6→L H–5→L+1	2.598 (477) H–1→L H→L+2 H→L+5	2.604 (476) H→L H–5→L H–6→L	2.679 (463) H→L H–1→L+1 H–2→L H–6→L	2.109 (588) H–1→L	2.172 (571) H–1→L
T2	2.566 (483) H→L	2.627 (472) H→L	2.693 (460) H→L+1 H–1→L H–5→L+1	2.766 (448) H–1→L H→L+1 H–1→L+2	2.145 (578) H→L	2.261 (548) H→L
S1	2.805 (442), f = 0.015 H→L	2.885 (430), f = 0.027 H→L H–1→L+2	2.862 (433), f = 0.0003 H→L+1 H–1→L	2.957 (419), f = 0.004 H→L+1 H–1→L	2.322 (534), f = 0.018 H→L	2.438 (509), f = 0.017 H→L
S2	2.859 (433), f = 0.026 H–1→L	2.959 (419), f = 0.020 H–1→L H→L+3	2.873 (432), f = 0.019 H→L H–1→L+1	2.985 (415) f = 0.017 H→L H–1→L+1	2.416 (513), f = 0.040 H–1→L	2.479 (500), f = 0.042 H–1→L
S3	2.935 (422), f = 0.015 H→L+1 H→L H→L+2	2.979 (416), f = 0.0002 H→L+1 H→L	3.010 (412), f = 0.100 H–1→L	3.083 (402) f = 0.087 H–1→L	2.930 (423), f = 0.028 H→L+1	3.018 (411), f = 0.006 H–2→L H–7→L H–5→L H–4→L H→L
S4	2.954 (420), f = 0.011 H–1→L+1 H–2→L+2 H–1→L+2	3.024 (410), f = 0.012 H–1→L+1 H–1→L+2	3.034 (409), f = 0.015 H→L+2 H–1→L+1	3.112 (398) f = 0.014 H→L+2 H–1→L+3	2.942 (421), f = 0.005 H–2→L	3.026 (410), f = 0.021 H→L+1 H–2→L+1 H–3→L+1
S5	2.996 (414), f = 0.096 H–1→L+2 H→L	3.069 (404), f = 0.093 H–1→L+2 H+1→L-1	3.119 (397), f = 0.005 H–1→L+1 H→L+3	3.165 (392), f = 0.009 H–1→L+2	3.075 (403), f = 0.019 H→L+2	3.130 (396), f = 0.012 H–1→L+1 H→L+2

Table 3.2: TD-DFT B3LYP excitation energies for the two lowest-lying triplet states and five lowest-lying singlet states, in units of eV (with corresponding wavelength in parenthesis), and their oscillator strengths. The predominant nature of the excitation is also indicated (H = HOMO; L = LUMO).

	HOMO-1	HOMO	LUMO	LUMO+1
Ir(L1)(dFppy)Cl (1)	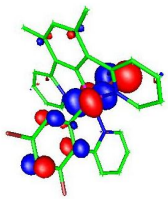	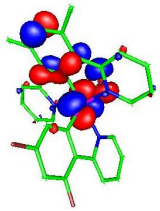	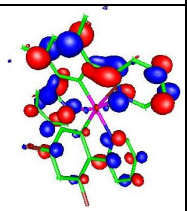	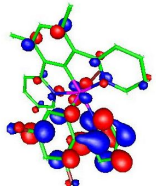
E(eV)	-0.19391	-0.19137	-0.05953	-0.05467
Ir	0.39	0.48	0.02	0.05
N^C^N	0	0.08	0.77	0.18
Cl	0.24	0.18	0	0
N^C	0.37	0.25	0.22	0.77
Ir(L2)(dFppy)Cl (2)	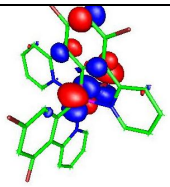	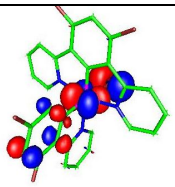	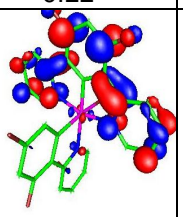	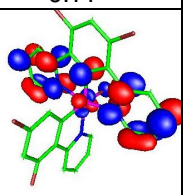
E(eV)	-0.20604	-0.20434	-0.06963	-0.06388
Ir	0.27	0.19	0	0.02
N^C^N	0.26	0.17	0.98	0.93
Cl	0.35	0.42	0	0.02
N^C	0.08	0.2	0.07	0.03
Ir(L3)(dFppy)Cl (3)	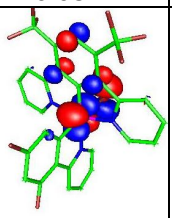	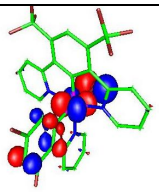	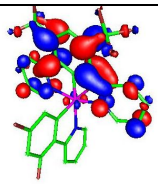	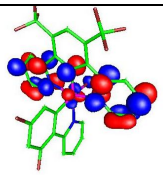
E(eV)	-0.21398	-0.21216	-0.09852	-0.07184
Ir	0.44	0.43	0.03	0.07
N^C^N	0.19	0.08	0.96	0.88
Cl	0.31	0.33	0	0.03
N^C	0.07	0.16	0.01	0.01

Figure 3.5: similarly to Figure 3.1, summary of DFT calculations for Ir(**L1**)(dFppy)Cl **(1)**, Ir(**L3**)(dFppy)Cl **(3)** and Ir(**L2**)(dFppy)Cl **(2)**.

Complex (series 1)	Absorption λ_{max} / nm (ε / mol^{-1} dm^3 cm^{-1})	Complex (series 2)	Absorption λ_{max} / nm (ε / mol^{-1} dm^3 cm^{-1})
Ir(L1)(ppy)Cl	264 (35 900), 288 (34 900), 369 (7 400), 397 (10 100), 418 (11 300), 457 (3 300), 494 (1 300)	**Ir(L1)(dFppy)Cl (1)**	286 (50 600), 363 (11 600), 390 (13 400), 412 (10 600), 451 (4 500), 488 (1 800)
Ir(L3)(ppy)Cl (5)	259 (45 600), 272 (45 300), 373 (8 900), 429 (11 100), 461 (8 000), 506 (3 100), 541 (2 400)	**Ir(L3)(dFppy)Cl (3)**	254 (43 800), 266 (42 900), 364 (7 900), 418 (9 900), 451 (6 900), 492 (3 000), 523 (2 200)
Ir(L2)(ppy)Cl (4)	260 (44 800), 280 (40 300), 358 (9 100), 381 (11 300), 402 (14 000), 438 (3 600), 473 (1 540)	**Ir(L2)(dFppy)Cl (2)**	278 (21 100), 351 (4 800), 375 (5 800), 393 (6 800), 433 (1 400), 467 (800)

Table 3.3: absorption bands of the series of complexes containing ppy (series 1) and dfppy (series 2) as N^C ligands

3.1.4. Emission from complexes in solution

The same six complexes manifest intense photoluminescence in degassed dichloromethane solution at ambient temperature. Data is compiled in Table 3.4

and the emission spectra at 298 K are shown in Figure 3.6, showing a broad range of emission colours, from blue to orange/red (λ_{max} from 476 to 593 nm). The order of emission energies is identical to that observed for the lowest-energy absorption bands. Also the complexes coordinated by dFppy are consistently blue-shifted by around 500 cm^{-1} compared to the corresponding ppy complexes. For the complexes bearing methyl and fluorine groups on the N^C^N unit, in particular, the difference in energy between the 0-0 vibrational component in emission and the lowest-energy absorption band is very small, of the order of 400 cm^{-1}, suggesting that the lowest-energy absorption band and the emission involve the same excited triplet state for these four complexes.

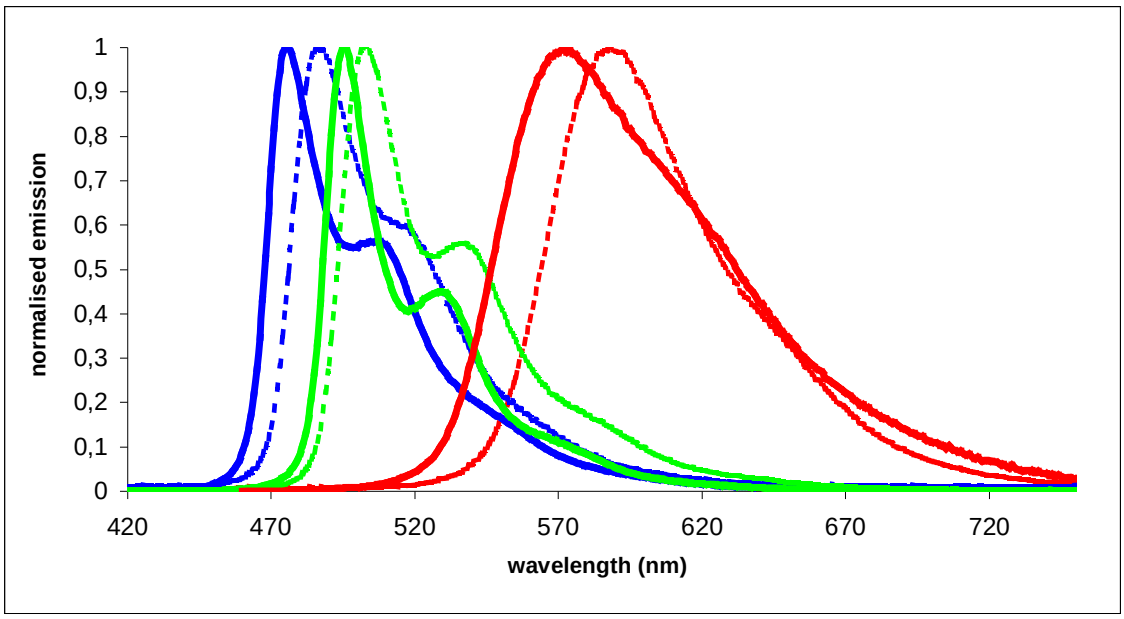

Figure 3.6: normalised emission spectra in degassed dichloromethane solution at room temperature of the complexes of series 1 (dotted lines) and series 2 (full lines), where $-CF_3$ substituted complexes are represented in red, $-CH_3$ substituted in green and –F substituted in blue.

The quantum yields of emission in degassed solution are high, ranging between 0.2 – 0.7. The green-emitting complexes of the **L1** ligand present the highest luminescence quantum yields, with values 0.71 and 0.66 for the ppy containing

species and for the dFppy containing species respectively, characterised by luminescence lifetimes of around 1.5 μs. Slightly smaller quantum yields have been measured for the orange/red-emitting complexes of **L3** (0.46 and 0.57 for the ppy coordinated complex and dFppy coordinated complex respectively), although their lifetimes are longer (3.3 and 4.0 μs respectively). On the other hand, the quantum yields and lifetimes are significantly reduced for the blue-emitting complexes of **L2** (0.20 in both cases).

The rate constants for radiative (k_r) and non-radiative (Σk_{nr}) decay can be estimated from the quantum yields and lifetimes: $k_r = \Phi_{lum}/\tau$ and $\Sigma k_{nr} = (1/\tau) - k_r$. The values thus obtained are summarised in Table 3.4. They indicate that the reduced quantum yields and shorter lifetimes of the blue-emitting **L2** based complexes are due to a greater non-radiative decay, Σk_{nr} compared to **L1** based systems. Blue-emitting transition metal complexes are subject to enhanced non-radiative decay pathways compared to those that emit in the green region, as encountered in numerous other studies with various metal ions including iridium(III) and platinum(II).[214, 215] This can be attributed to a decreased gap between the energy of the emissive excited state and higher-lying, deactivating d-d states, such that it becomes comparable to kT at ambient temperature[216], or to increased coupling with vibrational modes of the complex.[217] In the case of the complexes discussed here, the photoinduced cleavage of the Ir–Cl bond mentioned in the previous Chapter is thought to be the limiting factor. This process presumably proceeds via population of the d-d state and it is most significant for the two blue-emitting complexes, where the energy gap between the emissive state and the d-d state is necessary at its smallest. Despite this effect, however, the efficiencies remain quite competitive with some of the best blue phosphors reported to date. Upon cooling to 77 K, the lifetimes of the **L2** complexes become longer; and at this temperature the thermally-activated deactivating pathways are eliminated. The luminescence lifetimes of the red-emitting **L3** complexes are longer, compared to the other complexes. For these complexes, k_r is significantly decreased, whereas Σk_{nr} is slightly reduced. These observations suggest that the nature of the emissive state of the red emitting complexes is rather different from the others, and at 77 K, the luminescence lifetime increases by an order of magnitude to > 40 μs. This increase cannot

simply be due to reduced non-radiative decay, as the room temperature quantum yields were already around 0.5. The nature of the emissive state must be different under these conditions; the long lifetimes point to an excited state with a relatively poor SOC and thus perhaps with relatively little metal character.

Complex	λ_{max} / nm	τ degassed (aerated) /ns	Φ_{LUM} in degassed solution	k_r /10^4 s^{-1}	Σk_{nr} / 10^4 s^{-1}	k_Q /10^8 $M^{-1}s^{-1}$	λ_{max} / nm (77 K)	τ / µs (77 K)
Ir(L1)(ppy)Cl	503, 537	1400 (110)	0.71	51	20	38	489, 529, 564, 613	3.7
Ir(L3)(ppy)Cl (5)	590	3300 (1100)	0.46	14	16	28	576, 621	41
Ir(L2)(ppy)C	487, 516	390 (120)	0.20	51	210	26	471, 508, 537, 548, 593	2.5
Ir(L1)(dFppy)Cl (1)	495, 529	1500 (160)	0.66	44	23	25	481, 519, 553, 604	2.6
Ir(L3)(dFppy)Cl (3)	572	4000 (1700)	0.57	14	11	1.5	563, 607, 668(sh)	46
Ir(L2)(dFppy)Cl (2)	476, 508	410 (120)	0.20	49	190	27	464, 499, 528, 538, 578	2.0

Table 3.4: Luminescence data in solution in dichloromethane at 298±3 K and in EPA = diethyl ether / isopentane / ethanol (2:2:1 v/v) at 77 K for the complexes of series 1 and series 2, where; radiative (k_r) and non-radiative (Σk_{nr}) rate constants are calculated from τ and Φ_{lum} values; estimated uncertainty ±20%; k_Q, bimolecular rate constant for quenching by O_2, estimated from τ values in degassed and aerated solutions.

3.1.5. Ir(N^C^N)(N^C)Cl complexes of series 1 and 2 in OLEDs, and photochemistry in polymer matrices

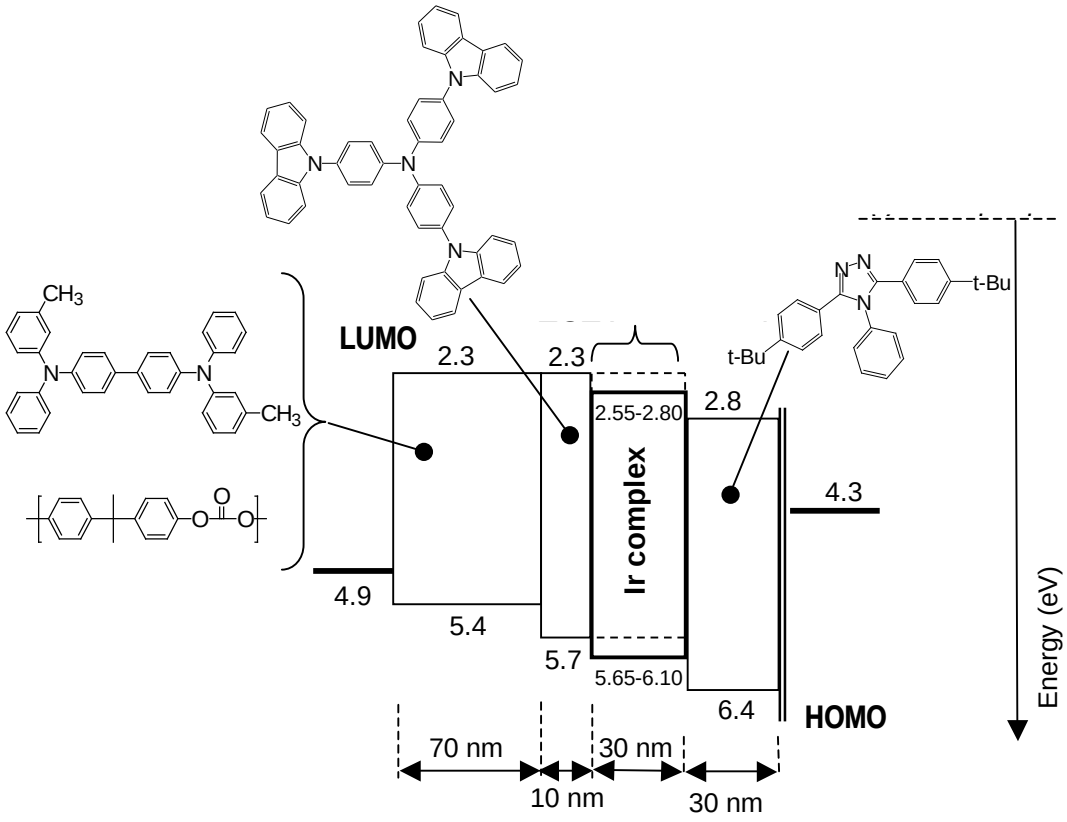

Figure 3.7[(219)]: composition of the devices doped with Ir(N^C^N)(N^C)Cl complexes

All complexes of series 1 and series 2 were investigated in electroluminescent devices, in collaboration with Dr. M. Cocchi and Dr. V. Fattori, of the ISOF institute in CNR, Bologna. The complexes were used as phosphorescent dopants in OLEDs. A schematic summary of the composition of the devices prepared for the investigation of Ir(N^C^N)(N^C)Cl dopants is illustrated in Figure 3.7. The preparation of the multilayer devices was carried out over glass substrates pre-coated with ITO (anode made of indium/tin oxide), by first spin-coating of a mixture of TPD/PC from dichloromethane solution. The following layer was composed of TCTA (see Figure 3.7) and was deposited by thermal evaporation under high vacuum. In succession, in the order as illustrated in Figure 3.7 from the left to the

right, the emitting layer (doped with the Ir(III) complex, 5% in TCTA) and the electron-transporting layer (TAZ) were deposited by combined sublimation under high vacuum. Finally, the cathode, consisting of LiF and Al, was similarly deposited over the previous layers.

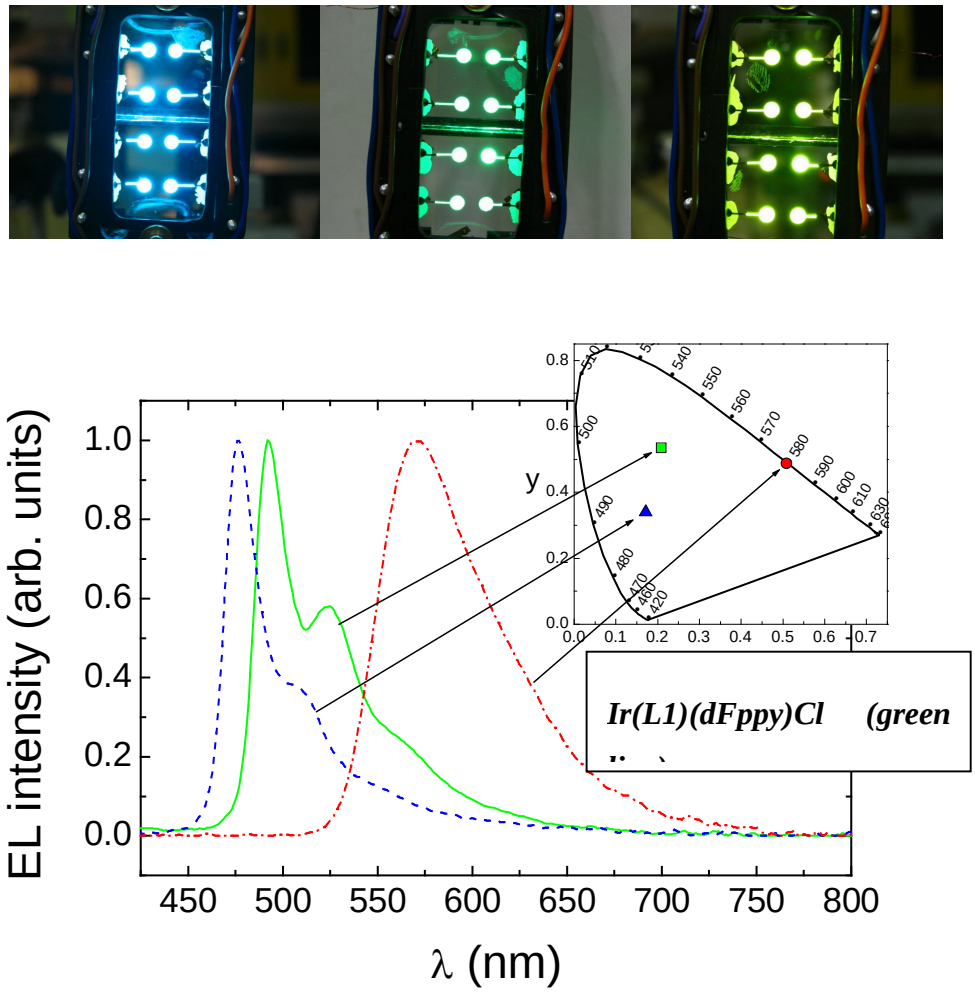

Figure 3.8: EL spectra and CIE diagram for the complexes of series 2, with photographs of the devices prepared emitting at different colours.

Figure 3.8 shows the EL (electroluminescence) spectra and the CIE coordinates diagram for the complexes of series 2, revealing a similar trend for the emitted colours to that observed in solution photochemistry, with maxima respectively at 476 nm, 496 nm and 593 nm for the –F, -CF_3 and –CH_3 substituted complexes of

series 2 (similar conclusions can be drawn for EL and CIE of the complexes of series 1, see Figure 3.9).

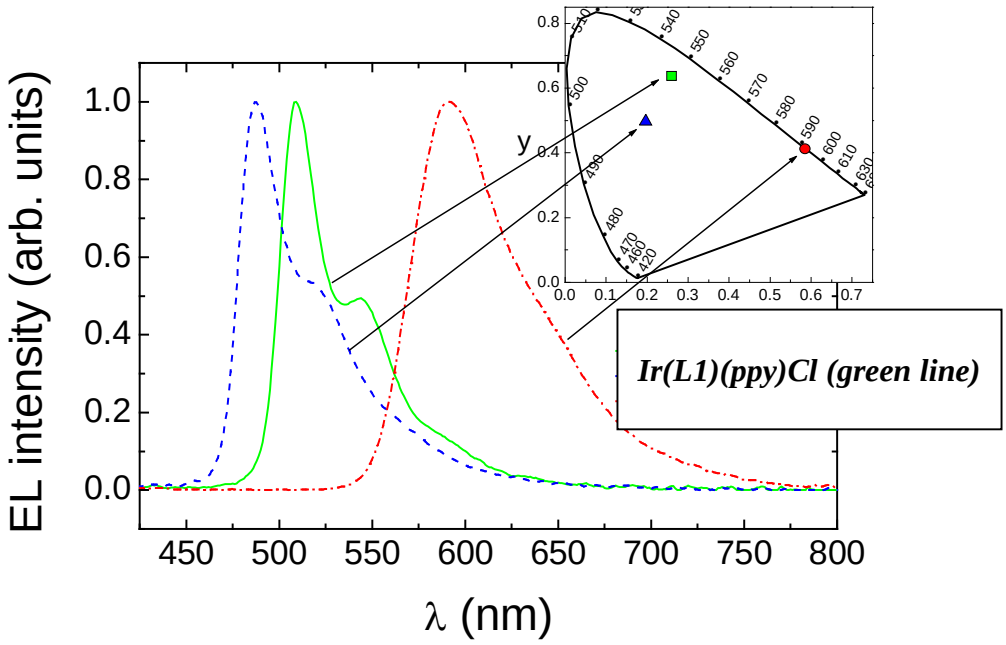

Figure 3.9: EL spectra and CIE diagram for the complexes of series 1.

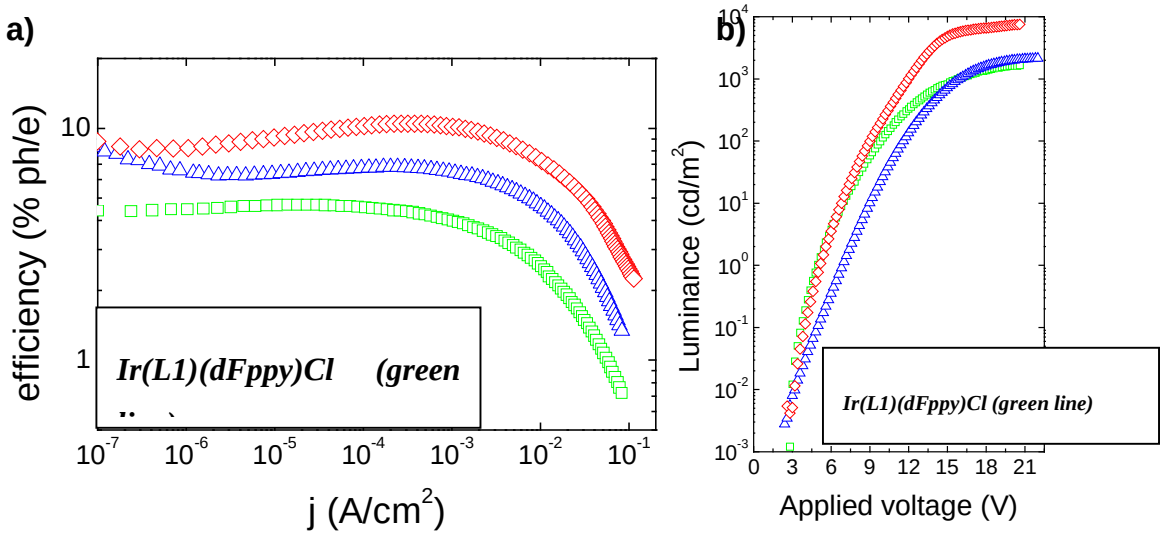

Figure 3.10: a) device efficiency (EL QE) vs potential (j); b) Luminance vs applied voltage for the complexes of series 2

Figure 3.10b) shows the dependence of the luminance *versus* the voltage applied, which increases up to 1000 cd/m^2 until high voltage roll-off for the complexes Ir(**L1**)(dFppy)Cl **(1)** and Ir(**L2**)(dfppy)Cl **(2)**, whereas for Ir(**L3**)(dFppy)Cl **(3)** saturation occurs at around 10000 cd/m^2. Figure 3.10a) shows the efficiency of the devices at different current densities. The efficiency is almost constant over a relatively wide range of current densities (between 10^{-5} and 10^{-2} A/cm^2). If the efficiencies of Ir(**L2**)(dFppy)Cl **(2)** and Ir(**L3**)(dFppy)Cl **(3)** are both within the order of satisfactory values, Ir(**L1**)(dFppy)Cl **(1)**, on the other hand, presents lower values of efficiency over this range of voltages. On the contrary, for the complexes of series 1, relatively high performances are registered for all three complexes (see Figure 3.11).

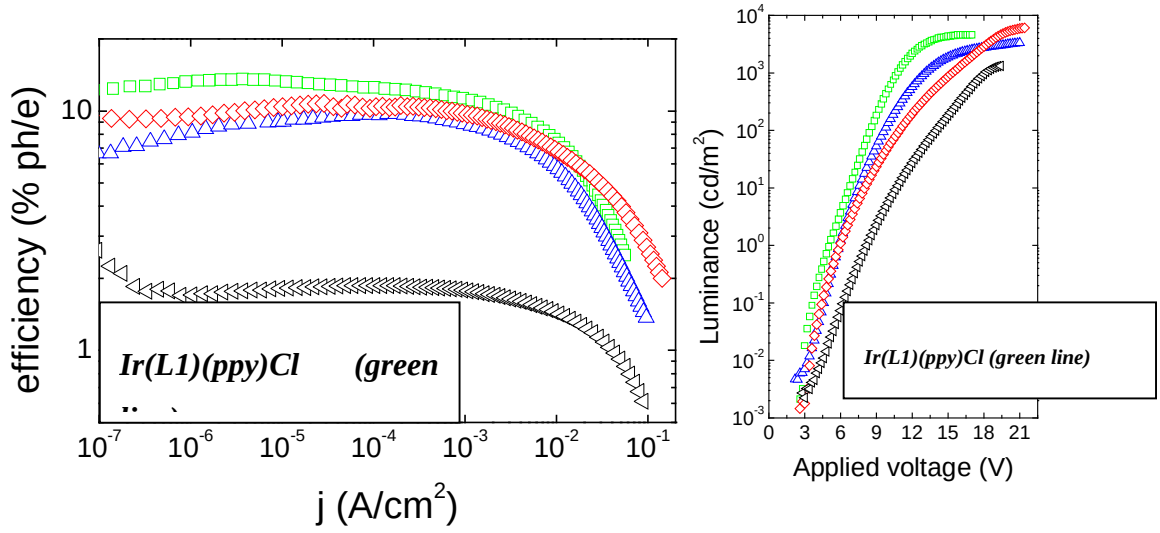

Figure 3.11: a) device efficiency (EL QE) vs potential (j); b) Luminance vs applied voltage for the complexes of series 1.

The lower performance of Ir(**L1**)(dFppy)Cl **(1)** can be explained by self-quenching phenomena occurring when the molecules of the complex come close together. The occurrence of self-quenching is confirmed by photoluminescence measurements in an inert polymer matrix. The photoluminescence of series 1 and 2 complexes at different concentrations in thin PMMA layers was measured. The

plots in Figure 3.12 show the dependence of the quantum yield and excited state lifetime in those samples on the estimated intermolecular distance. The intermolecular distance is inversely proportional to the concentration of the complexes in PMMA. Except for Ir(**L1**)(dFppy)Cl **(1)**, the complexes show only small variations in the quantum yields and the lifetimes over different intermolecular distances, suggesting that self-quenching is of little importance even when molecules are lying close to each other. On the other hand, for Ir(**L1**)(dFppy)Cl **(1)**, a significant decrease of both quantum yields and lifetimes is observed by decreasing the intermolecular distance, suggesting the occurance of significant self-quenching at higher concentration, accounting for the lower device efficiencies recorded for this complex at high currents.

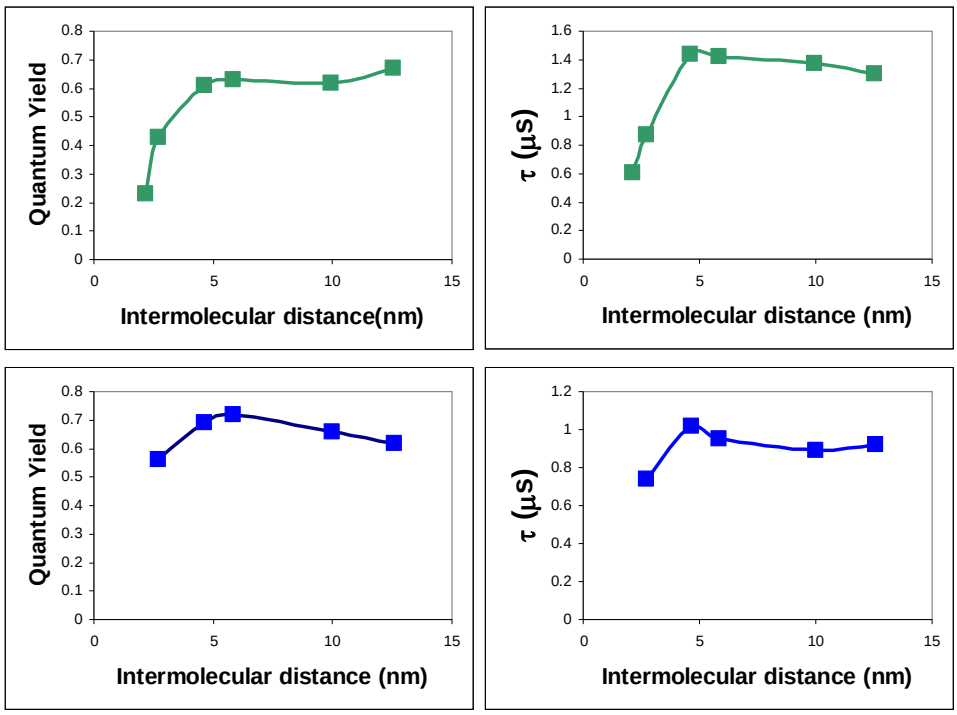

Figure 3.12: Quantum yields and lifetimes plotted against the estimated average intermolecular distance for Ir(**L1**)(dFppy)Cl **(1)** (green plot) and Ir(**L2**)(dFppy)Cl **(2)** (blue plot)

3.2. Strategies for further emission tuning of the Ir(N^C^N)(N^C)Cl complexes

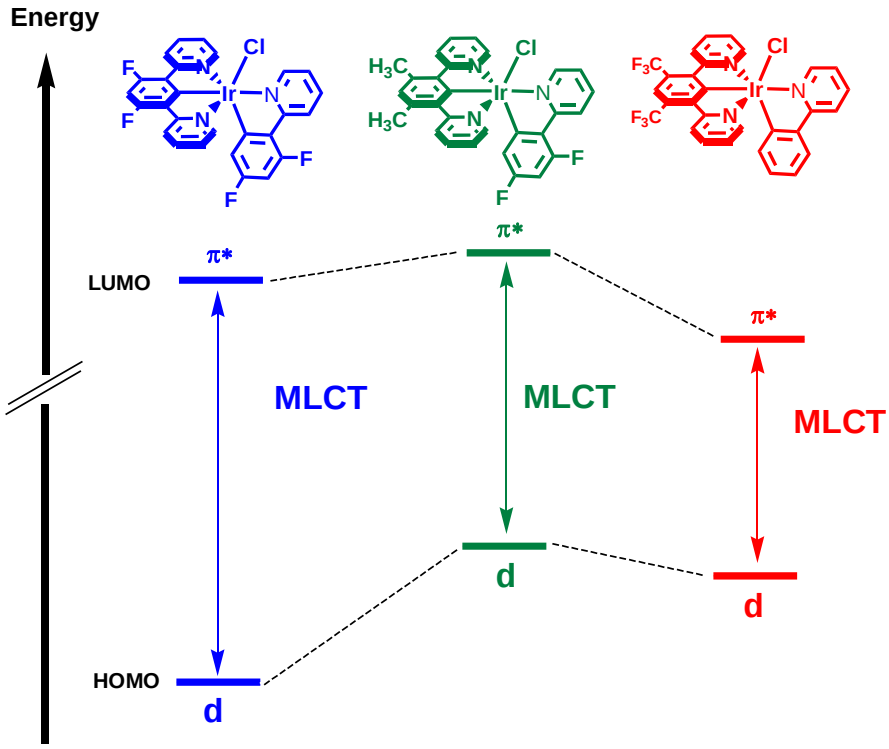

Figure 3.13: scheme of the substituent effect on the N^C^N ligand in tuning the colour of the emission in Ir(N^C^N)(N^C)Cl

Figure 3.13 summarises the likely origin of the emission tuning of the six complexes described this far, in which the substituent of the central aryl ring of the N^C^N ligand was varied. In order to further modulate the emission of the complexes, with the aim of achieving emission over a wider portion of the visible spectrum, other strategies can be deduced with the aid of DFT calculations. As a reminder, Figure 3.14 shows the frontier orbitals of the blue emitter Ir(**L2**)(dFppy)Cl **(2)**, which is essentially representative of all the complexes of this class.

HOMO-1	HOMO	LUMO	LUMO+1
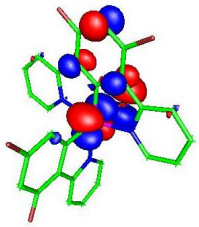	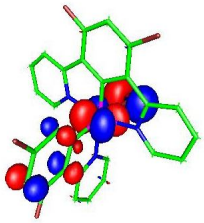	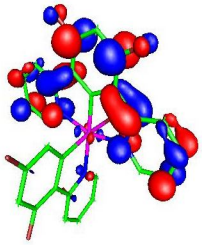	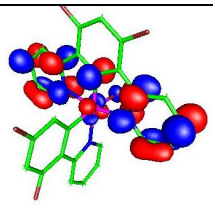

Figure 3.14: Frontier orbitals of Ir(**L2**)(dFppy)Cl **(2)** obtained by DFT.

For example, the significant contribution of the pyridyl 4-position to the LUMO and LUMO+1, but not in the occupied orbitals, suggests that substitution at this position might have a substantial effect on the HOMO-LUMO gap. On the other hand, since the monodentate ancillary ligand participates significantly in the HOMO and HOMO-1 levels, but not in the LUMO, the introduction of different types of monodentate ligands in the sixth position of the coordination sphere of the metal might also lead to changes of the HOMO-LUMO energy gap, thus tuning the colour of the emission by ancillary effect.

3.2.1. Effect of the substituents in the pyridyl ring of the N^C^N ligand

An important goal in OLED research is to obtain efficient deep blue emitters. Based on the DFT analysis presented above, the introduction of electron-donating substituents into the 4-position of the N^C^N pyridyl rings should raise the LUMO without significantly affecting the HOMO, leading to a blue-shift. Therefore, complexes of N^C^N ligands carrying methoxy (**L5**) or dimethylamino (**L6**) substituents in the pyridyl rings were prepared. DFppy was selected as the

bidentate ligand, as it has already been established from the work on series 2 vs. series 1 complexes that it leads to a further shift to the blue.

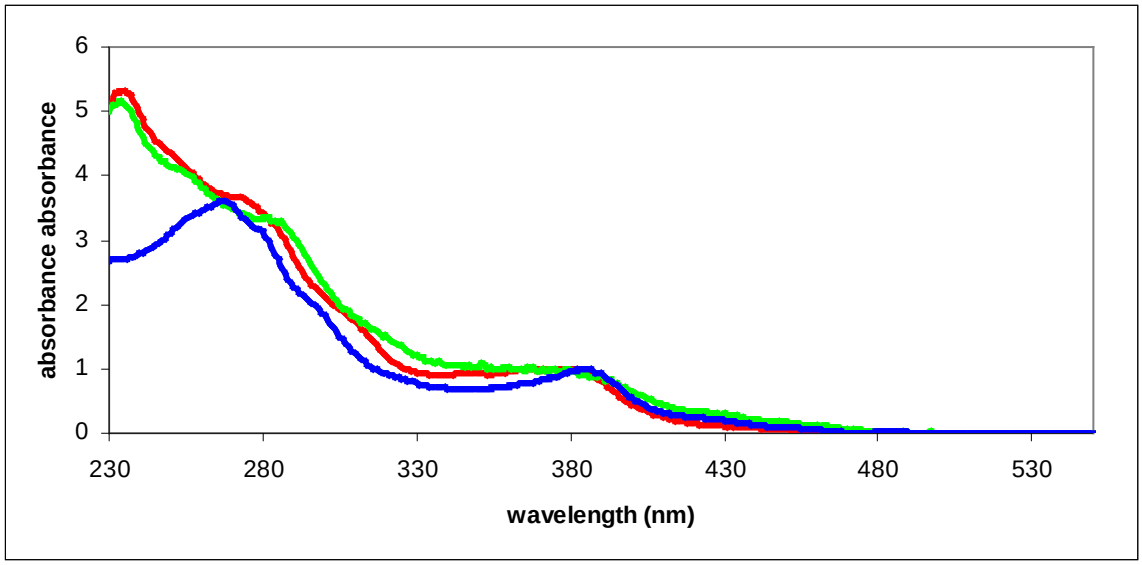

Figure 3.15: normalised absorption to the most intense low-enegy band in dichloromethane at room temperature of the complexes Ir(**L2**)(dFppy)Cl **(2)** (red line), Ir(**L5**)(dFppy)Cl **(6)** (green line), Ir(**L6**)(dFppy)Cl (blue line).

The absorption spectra of the two new complexes are shown in Figure 3.15, together with that of the "**L2**" of the previously discussed complexes, namely Ir(**L2**)(dFppy)Cl **(2)**. Data are compiled in Table 3.5. The complexes display the typical intense, high energy, $\pi-\pi^*$ bands at $\lambda < 330$ nm observed for all the bis-cyclometallated Ir(III) complexes of this type in Section 3.1. The lower-energy MLCT/LLCT bands at $\lambda > 330$ nm are slightly blue-shifted in the two new complexes carrying R substituents at position 4. For the lowest-energy intense band, $\lambda = 385$ nm for R = -OMe and R = $-NMe_2$, compared to 393 nm for R = -H, qualitatively as predicted by the DFT on the basis of the LUMO being destabilised by the electron-donating substituents. The same effect is also observed for the

lower-energy MLCT band at λ = 433 nm for R = -H, in fact, those of R = -OMe and R = -NMe_2 are both blue-shifted (respectively at λ = 426 nm and λ = 427 nm).

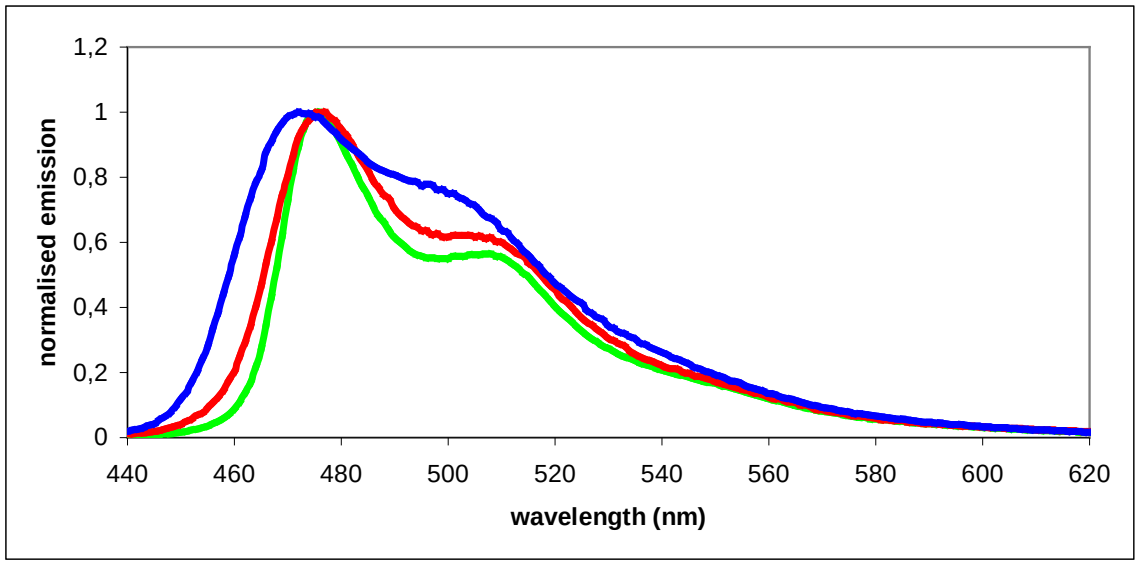

Figure 3.16: emission spectra in dichloromethane at room temperature of the complexes, Ir(**L2**)(dFppy)Cl **(2)** (green line), Ir(**L5**)(dFppy)Cl **(6)** (red line), Ir(**L6**)(dFppy)Cl (blue line).

The emission of the complex with R = -NMe_2 is also blue-shifted relative to R = -H. The emission maxima (0-0 bands) are at 472 nm and 476 nm respectively. Curiously, the emission of the complex with R = -OMe is essentially identical to that with R = -H (477 nm and 476 nm respectively). Appearently, either the composition of the orbitals in the triplet mainfold is somewhat different from the singlets, or the extent of relaxation/reorganisation in the excited state prior to emission may differ.

Although the effect of the R substituent is thus rather minimal, it is noticeable that the quantum yield of the R = -NMe_2 complex is substantially improved compared to that with R = -H (Φ = 0.41 and 0.20), this may be indicative of a less labile Ir-Cl bond or to less efficient population of the d-d state required for its cleavage.

Complex	λ_{max} / nm	τ degassed (aerated)	Φ_{LUM} in degassed solution	k_r /10^4 s^{-1}	Σk_{nr} / 10^4 s^{-1}	k_Q /10^8 $M^{-1}s^{-1}$	Absorption λ_{max} / nm (ε / mol^{-1} dm^3 cm^{-1})
Ir(L2)(dFppy)Cl (2) R = -H	476, 508	410 (120)	0.20	49	190	27	278 (21100), 351 (4830), 375 (5850), 393 (6800), 433 (1430), 467 (760)
Ir(L5)(dFppy)Cl (6) R = -OMe	477, 507	260(100)	0.15	58	94	27	233(13 300), 286(6 700), 385(2 300), 426(300)
Ir(L6)(dFppy)Cl R = -NMe_2	472, 497	550(80)	0.41	75	117	48	231 (24 600), 269 (31 000), 368 (6 700), 385 (8 300), 427 (2 000), 484 (300)

Table 3.5: Luminescence data in solution in dichloromethane at 298±3 K, where; radiative (k_r) and non-radiative (Σk_{nr}) rate constants are calculated from τ and Φ_{lum} values; estimated uncertainty ±20%; k_Q, bimolecular rate constant for quenching by O_2, estimated from τ values in degassed and aerated solutions.

Based on the previously discussed DFT calculations, the introduction of electron-withdrawing groups into the position 4 of the pyridyl rings of the N^C^N ligand should provoke an opposite effect to that observed in the complexes bearing electron-donating groups in the same position. Therefore $-CF_3$ groups may stabilise the LUMO with little effect on the HOMO level, leading to red-shifted emission. Ligands bearing $-CF_3$ groups on both the phenyl ring and the pyridyl rings of the N^C^N coordinating unit were selected for this purpose, combined with ppy bidentate ligand in the coordination sphere of the metal centre.

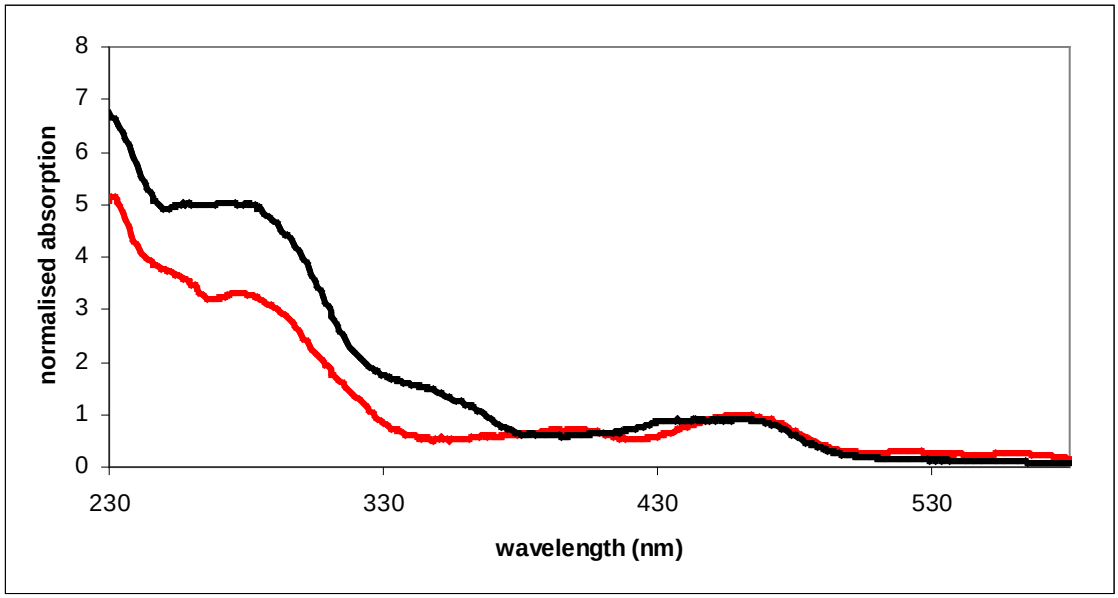

Figure 3.17: normalised absorption to the most intense low-enegy band in dichloromethane at room temperature of the complexes Ir(**L4**)(ppy)Cl **(9)** (red line), Ir(**L3**)(ppy)Cl **(5)** (black line)

Figure 3.17 shows the absorption spectra of the complex Ir(**L4**)(ppy)Cl **(9)** in comparison with that of Ir(**L3**)(ppy)Cl **(5)** and their data are compiled in Table 3.6. Although it is not possible to conclude that the spectrum of the **L4** complex is unequivocally red-shifted, especially since the profiles are different in the key 400-500 nm region, it can be seen that the new complex has more prominent lower energy band at $\lambda > 500$ nm.

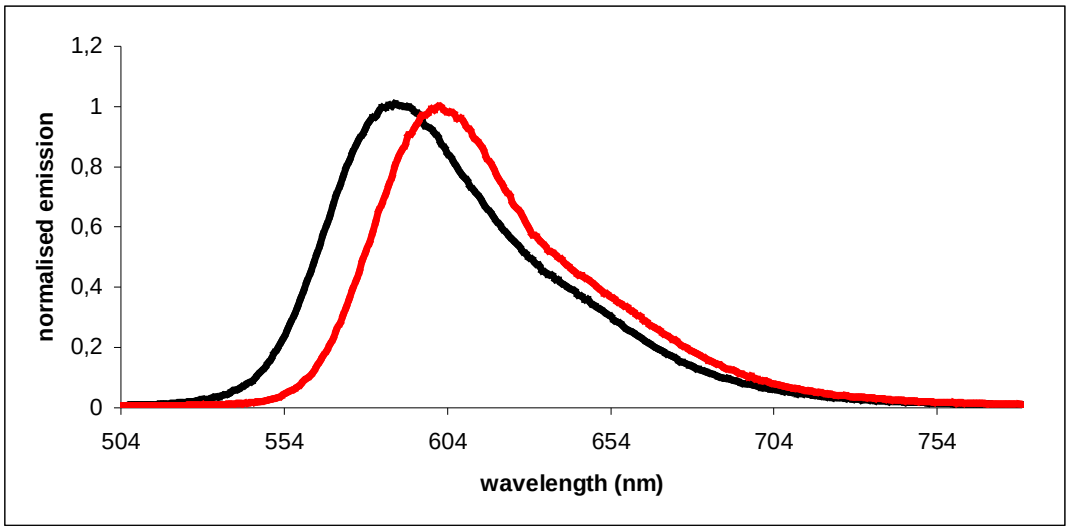

Figure 3.18: emission spectra in dichloromethane at room temperature of the complexes Ir(**L3**)(ppy)Cl **(5)** (black line), Ir(**L4**)(ppy)Cl **(9)** (red line).

The emission band of Ir(**L4**)(ppy)Cl **(9)** (λ_{MAX} = 601 nm) is more clearly red-shifted compared to that of Ir(**L3**)(ppy)Cl **(5)** (λ_{MAX} = 590 nm) (Figure 3.18), suggesting that the trifluoro-methyl groups on the position 4 of the pyridyl rings of the N^C^N have the effect of stabilising the LUMO level with respect to the HOMO level.

Complex	λ_{max} / nm	τ degassed (aerated)	Φ_{LUM} in degassed solution	k_r /10^4 s^{-1}	Σk_{nr} / 10^4 s^{-1}	k_Q /10^8 $M^{-1}s^{-1}$	Absorption λ_{max} / nm (ε / mol^{-1} dm^3 cm^{-1})
Ir(L3)(ppy)Cl (5) R = -H	590	3300 (1100)	0.46	14	16	28	260 (44 800), 280 (40 300), 358 (9 100), 381 (11 300), 402 (14 000), 438 (3 600), 473 (1 540)
Ir(L4)(ppy)Cl (9) R = -CF_3	601	2800 (1200)	0.36	13	23	21	233 (19 500), 276 (12 500), 399 (2 600), 461 (3 800), 523 (1 100), 562 (900)

Table 3.6: Luminescence data in solution in dichloromethane at 298±3 K, where; radiative (k_r) and non-radiative (Σ k_{nr}) rate constants are calculated from τ and Φ_{lum} values; estimated uncertainty ±20%; k_Q, bimolecular rate constant for quenching by O_2, estimated from τ values in degassed and aerated solutions.

3.2.2. Effect of substituents in bidentate ligands

The DFT analysis suggests that the N^C bidentate ligand in Ir(N^C^N)(N^C)Cl complex contributes significantly to the HOMO orbital, whereas it contributes only marginally to the other frontier orbitals. Changing the nature of the bidentate ligand or introducing substituents into the position 4 of the N^C unit may influence the energy of the HOMO-LUMO energy gap. In particular, with the intent of blue-shifting the emission of the previously discussed blue-emitting complexes, electron-donating groups are introduced into the pyridyl ring of the bidentate. Moreover, phenyl pirazole as an N^C-oordinating ligand is here investigated to observe the effect of changing the nature of the N^C.

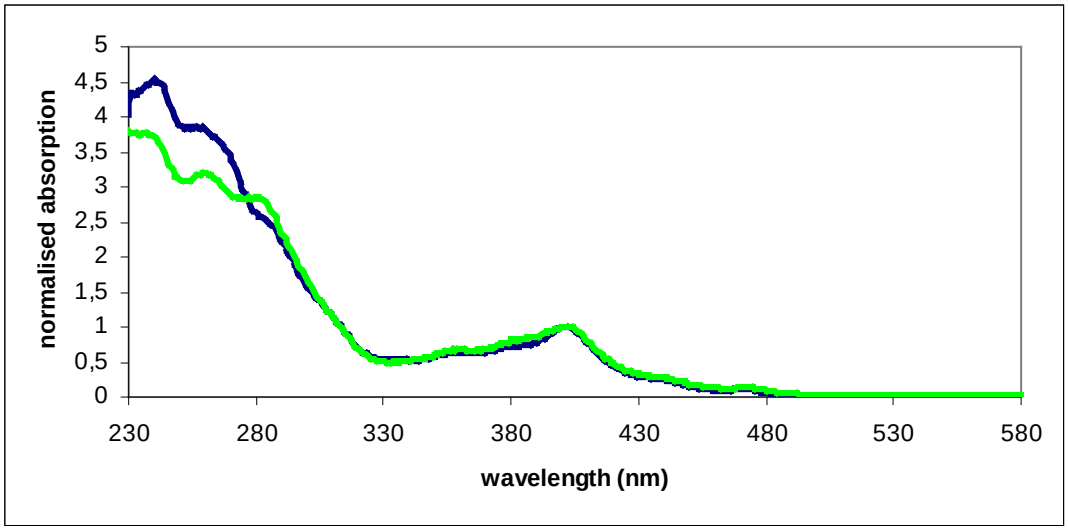

Figure 3.19: normalised absorption to the most intense low-enegy band in dichloromethane at room temperature of the complexes Ir(**L2**)(ppy)Cl (4) (green line), Ir(**L2**)(ppyz)Cl **(12)** (blue line)

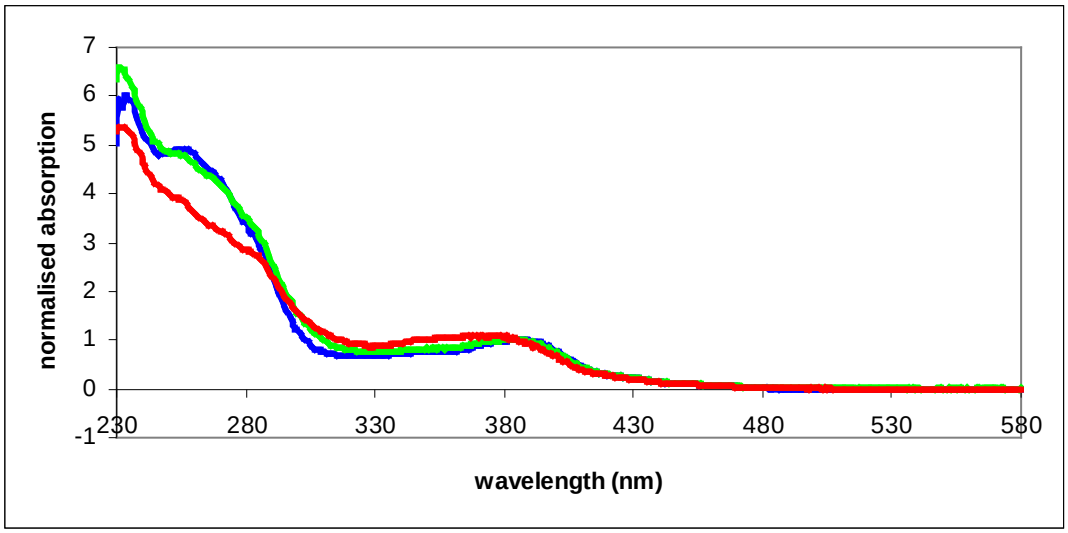

Figure 3.20: normalised absorption to the most intense low-enegy band in dichloromethane at room temperature of the complexes Ir(**L2**)(dFppic)Cl **(10)** (green line), Ir(**L2**)(dFpOMepy)Cl **(11)** (blue line), Ir(**L2**)(dFppy)Cl **(2)** (red line).

In Figure 3.19 the absorption spectrum of Ir(**L2**)(ppyz)Cl **(12)** is shown in relation to that of Ir(**L2**)(ppy)Cl **(4)** and the data compiled in Table 3.7. In both complexes, the maximum of the MLCT/LLCT low-energy band is at 402 nm. This suggests that the N^C ligand has little influence in affecting the HOMO-LUMO energy gap, confirming the indications provided by DFT calculations, in which the pyridyl ring of the N^C ligand has little contribution in the frontier orbitals. As compiled in Table 3.7, the emission of these two complexes is esseitially identical results only marginally shifted (respectively 486 and 487 nm), confirming the observations deduced in absorption.

In Figure 3.20 the aborption speactra of the complexes Ir(**L2**)(dFppic)Cl **(10)** (R_{NC} = $-CH_3$), Ir(**L2**)(dFpOMepy)Cl **(11)** (R_{NC} = -OMe) and Ir(**L2**)(dFppy)Cl **(2)** (R_{NC} = -H) are compared to each other. In the three complexes, the maximum of the MLCT/LLCT low-energy band is between 384 nm and 386 and, for identical reasons as for the phenylpyrazole containing complex, the absorption is not affected upon introduction of substituents into the pyridyl ring of the bidentate ligand. Also in this case, by analysing the data compiled in Table 3.8, the emission reflects the behaviour observed in absorption for this series of three complexes (the maxima being within the range 477-478 nm).

In Table 3.7 the data for a complex bearing a benzothiopheneisoquinoline-based unit as bidentate ligand, namely Ir(**L3**)(btiq)Cl **(11)**, are also compiled in comparison with Ir(**L3**)(ppy)Cl **(5)**. Figure 3.21 shows the absorption spectra for these complexes, in which the relatively intense low-energy MLCT state of the complex bearing the bidentate btiq (435 nm) is red-shifted in relation to that of the ppy coordinated species (429 nm). Figure 3.22 shows the emission spectra in degassed solution of the same two complexes. Here too, the red-shift, due to the introduction of the bidentate ligand btiq (λ_{MAX} = 667 nm) is observed with respect to the complex incorporating ppy (λ_{MAX} = 590 nm). The significant red-shift observed can be attributed, according to the DFT on the Ir(N^C^N)(N^C)Cl, to the role of a more extended π system in destabilising the HOMO level, leading to a narrower HOMO-LUMO energy gap compared to that of systems bearing ppy bidentate ligands. The relatively low, in relation to the previously studied red-emitting complexes, measured quantum yields and the relatively long lifetimes suggest a weak participation of the metal centre to the excited states, which probably have significant LC character.

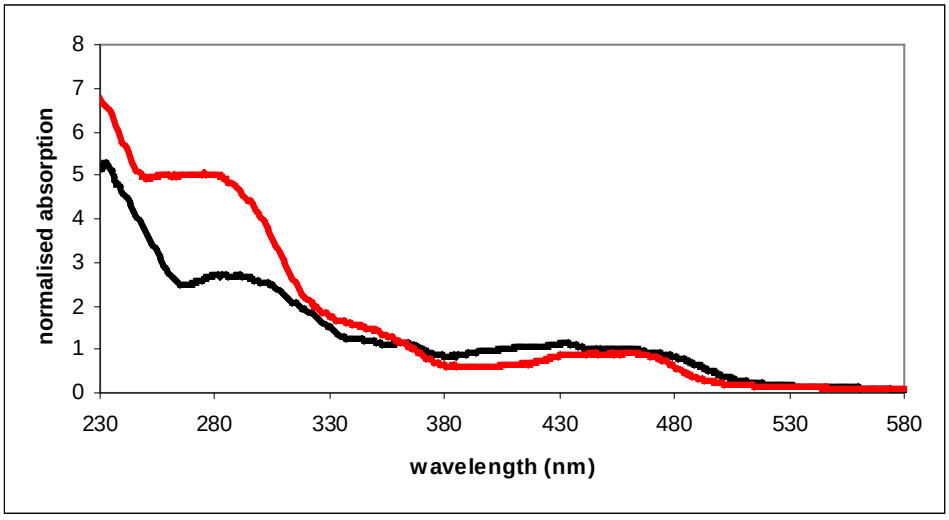

Figure 3.21: normalised absorption to the most intense low-enegy band in dichloromethane at room temperature of the complexes Ir(**L3**)(ppy)Cl **(5)** (red line) and Ir(**L3**)(btiq)Cl **(11)** (black line)

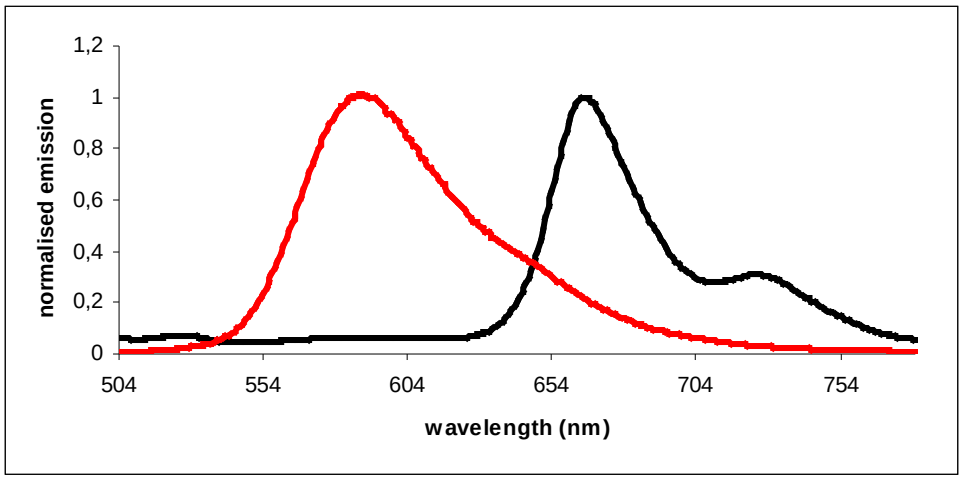

Figure 3.22: emission spectra in dichloromethane at room temperature of the complexes Ir(**L3**)(ppy)Cl **(5)** (red line) and Ir(**L3**)(btiq)Cl **(11)** (black line).

Complex	λ_{max} / nm	τ degassed (aerated)	Φ_{LUM} in degassed solution	k_r /10^4 s^{-1}	Σk_{nr} / 10^4 s^{-1}	k_Q /10^8 $M^{-1}s^{-1}$	Absorption λ_{max} / nm (ε / mol^{-1} dm^3 cm^{-1})
Ir(L2)(ppy)Cl (4)	487, 516	390 (120)	0.20	51	210	26	260 (44 800), 280 (40 300), 358 (9 100), 381 (11 300), 402 (14 000), 438 (3 600), 473 (1 540
Ir(L2)(ppyz)Cl (12)	486, 515	210(90)	0.16	76	103	27	239(24 600), 261(21 800), 361 (3 700), 384 (4 200), 402 (5 900), 438 (1 500), 475 (1 000)
Ir(L5)(dFppy)Cl (6) R_{NC} = -H	477, 507	260(100)	0.15	58	94	27	233(13 300), 286(6 700), 385(2 300), 426(300)
Ir(L5)(dfpOMepy)Cl (8) R_{NC} = -OMe	477, 511	260 (90)	0.18	69	104	32	234 (40 700), 254 (29 000), 325 (4 800), 357 (5 200), 386 (6 900), 460 (400)
Ir(L5)(dfppic)Cl (7) R_{NC} = -CH_3	478, 509	290 (100)	0.25	86	91	32	233 (33 500), 257 (24 600), 352 (4 200), 384 (5 100), 450 (600)
Ir(L3)(btiq)Cl (11)	667	3300 (700)	0.04	1.2	29	5	233 (57 000), 290 (29 200), 347 (13 000), 366 (11 900), 435 (11 200), 463 (10 800), 546 (1 400)
Ir(L3)(ppy)Cl (5)	590	3300 (1100)	0.46	14	16	28	259 (45 600), 272 (45 300), 373 (8 900), 429 (11 100), 461 (8 000), 506 (3 100), 541 (2 400)

Table 3.7: Luminescence data in solution in dichloromethane at 298±3 K, where; radiative (k_r) and non-radiative (Σk_{nr}) rate constants are calculated from τ and Φ_{lum} values; estimated uncertainty ±20%; k_Q, bimolecular rate constant for quenching by O_2, estimated from τ values in degassed and aerated solutions.

3.2.3. Emission tuning through the ancillary ligand

3.2.3.1. Complexes Ir(N^C^N)(N^C)CN and Ir(N^C^N)(N^C)SCN

3.2.3.1.1. DFT calculations

Complex	HOMO-1	HOMO	LUMO	LUMO+1
Ir(L1)(dFppy)CN (22)	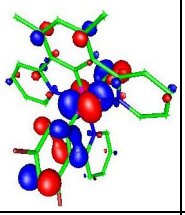	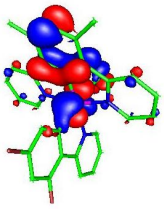	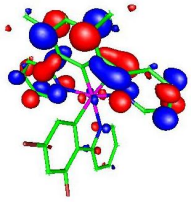	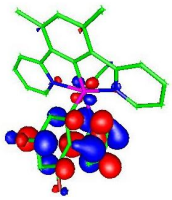
E(eV)	-0.20444	-0.19742	-0.06234	-0.05712
Ir	0.53	0.46	0.02	0.04
N^C^N	0.18	0.41	0.90	0.10
CN	0.09	0.07	0	0
N^C	0.20	0.06	0.08	0.86
Ir(L1)(dFppy)SCN (27)	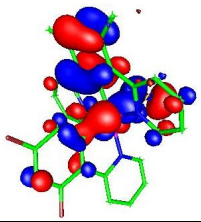	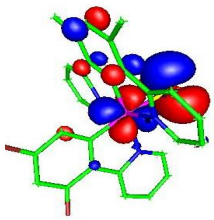	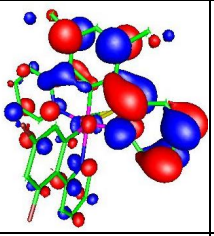	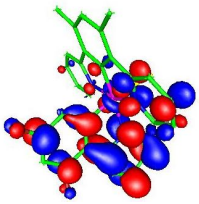
E(eV)	-0.2074	-0.19202	-0.06575	-0.06072
Ir	0.34	0.32	0.03	0.05
N^C^N	0.35	0.10	0.86	0.19
SCN	0.19	0.52	0.01	0.01
N^C	0.11	0.05	0.10	0.75

Figure 3.23: DFT calculations for the complexes Ir(**L1**)(dFppy)Cl **(1)**, Ir(**L1**)(dFppy)CN and Ir(**L1**)(dFppy)SCN.

DFT calculations on halide containing complexes, see Section 3.1.1., displayed the importance of the monodentate ancillary ligand in participating to the HOMO and HOMO-1 orbitals. Thus, displacement of the Cl by different ligands would be anticipated to lead to a change in the energies of the MOs involved in the emission of the complexes. Figure 3.23 shows the frontier orbitals of the complexes Ir(**L1**)(dFppy)CN **(22)** and Ir(**L1**)(dFppy)SCN **(27)** obtained by DFT. The HOMO and HOMO-1 are comparable with those observed for the halide analogue,

although the cyano containing system presents a higher degree of participation of the metal to the HOMO-1 level than that of the complexes previously studied. This effect is not observed for the -SCN containing complex, -SCN being a weaker-field ligand than -CN and its calculated frontier orbitals are identical to those of the –Cl based parent complex. Comparing the LUMO and LUMO+1 levels, no significant differences are reported from those of Ir(**L1**)(dFppy)Cl **(1)**.

3.2.3.1.2. Photophysical studies

Ground state absorption spectroscopy was carried out on the complexes, Ir(**L1**)(dFppy)CN **(22)**, Ir(**L1**)(dFppy)SCN **(27)**, Ir(**L2**)(dFppy)CN **(23)** and Ir(**L5**)(dFppy)CN in dichloromethane at room temperature. All complexes show the typical band pattern at high energies described for the previously discussed iridium complexes. The low-energy MLCT transitions of the complexes containing cyano and thiocyano ancillary ligands are all blue shifted in relation to those of the parent halide complexes, by 6-20 nm, the biggest shift being that of Ir(**L5**)(dFppy)CN (λ_{MLCT} = 364 nm) in respect to Ir(**L5**)(dFppy)Cl **(6)** (λ_{MLCT} = 384 nm), suggesting a stabilisation of the HOMO and HOMO-1 energy levels due to the introduction of the cyano and thiocyano ancillary ligands. Ir(**L1**)(dFppy)CN **(22)** and Ir(**L1**)(dFppy)SCN **(27)** display their highest-energy, even though not the most intensive, MLCT transitions at energies respectively 371 nm and 386 nm, both blue-shifted compared to that of Ir(**L1**)(dFppy)Cl **(1)** (λ_{MLCT} = 393 nm).

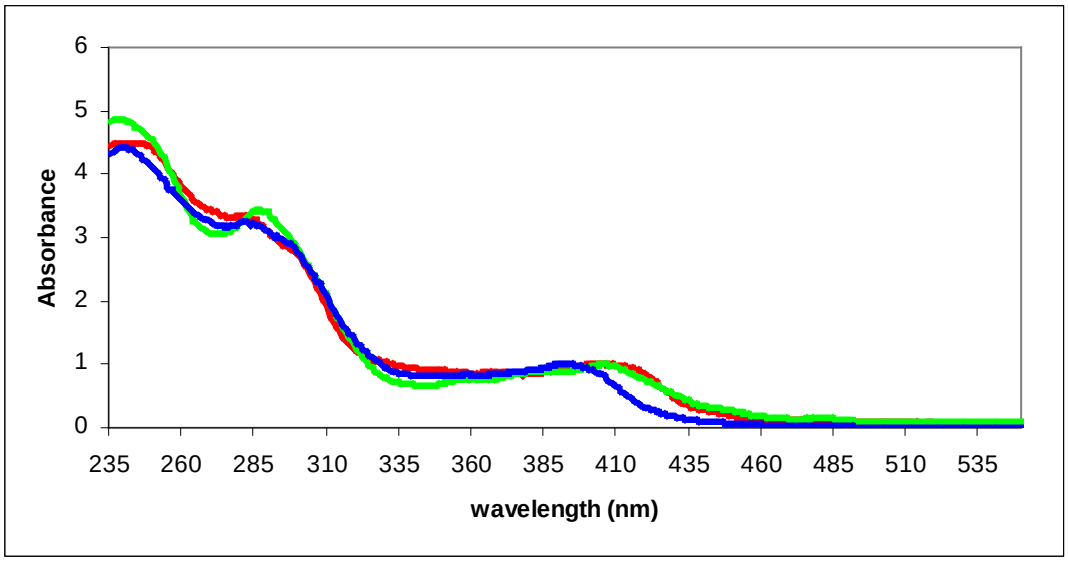

Figure 3.24: normalised absorption to the most intense low-enegy band in dichloromethane at room temperature of the complexes Ir(**L1**)(dFppy)CN **(22)** (green line), Ir(**L1**)(dFppy)SCN **(27)** (red line), Ir(**L1**)(dFppy)Cl **(1)** (bue line).

The photoluminescence studies, data for which are compiled in Table 3.8, of the same complexes display structured MLCT character bands. The order of the emission maxima reflect that observed in absorption spectroscopy, in fact all the complexes containing –CN or –SCN ancillary ligands are blue-shifted with respect to the –Cl analogues (Figure 3.26). The shift caused by the introduction of the –SCN ligand is, however, smaller than that caused by –CN, the shifts being respectively of 8 nm and 15 nm (relative to the corresponding chloro complex in the case of Ir(**L1**)(dFppy)X) (Figure 3.26). The diplacement of the chlorine ancillary by –CN in the **L2** -based species provokes a shift 14 nm, whereas a shift of 21 nm is observed for that related to the **L5**-based system. Appearently, the introduction of the –CN ancillary somehow activated the effect of the methoxy substituents on the position 4 of the pyridyl-N^C^N, destabilising the LUMO level, this effect being only marginal in the chlorine coordinated complexes. This led to an emission maximum at 456 nm for the complex Ir(**L5**)(dFppy)CN, which is the bluest-emitting complex discussed in this work (Figure 3.25). Measured quantum yields of the **L2**-based complexes are similar to those reported in Section 3.1.4. for the previously reported blue emitters and similar considerations are valid here

relative to the radiative and non-radiative rate constants. For the **L1** -based systems, however, upon the introduction of the cyano and thiocyano groups, the increased stability of the Ir-ancillary bond leads to improved and very high quantum yields, as confirmed by the very low non-radiative rate constants calculated for these two complexes (see Table 3.8).

The improved performances of the complexes Ir(**L1**)(dFppy)CN **(22)** and Ir(**L1**)(dFppy)SCN **(27)** are also observed in their application in OLED devices, which were prapered following a method identical to that described in Section 3.1.5. Figures 3.27 and 3.28, show the increased efficiency of the devices doped with –CN and –SCN containing complexes over those of the –Cl analogues.

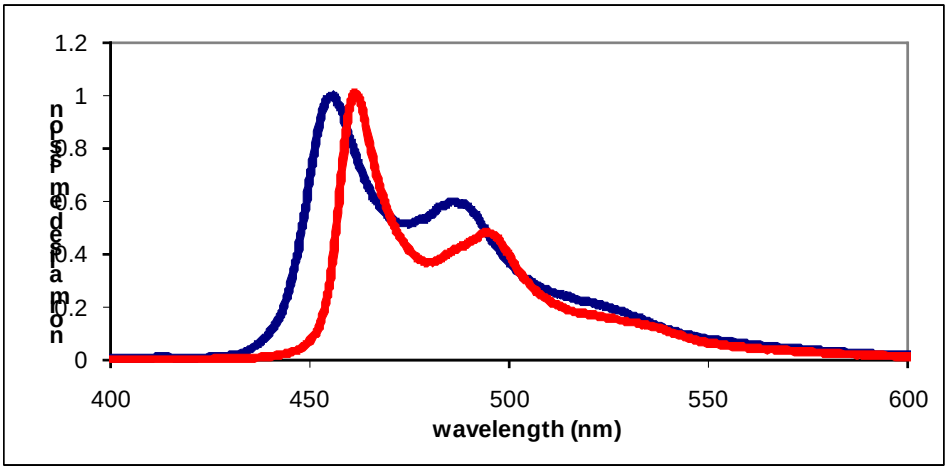

Figure 3.25: emission spectra in dichloromethane at room temperature of the complexes Ir(**L2**)(dFppy)CN **(23)** (red line), Ir(**L5**)(dFppy)CN (blue line)

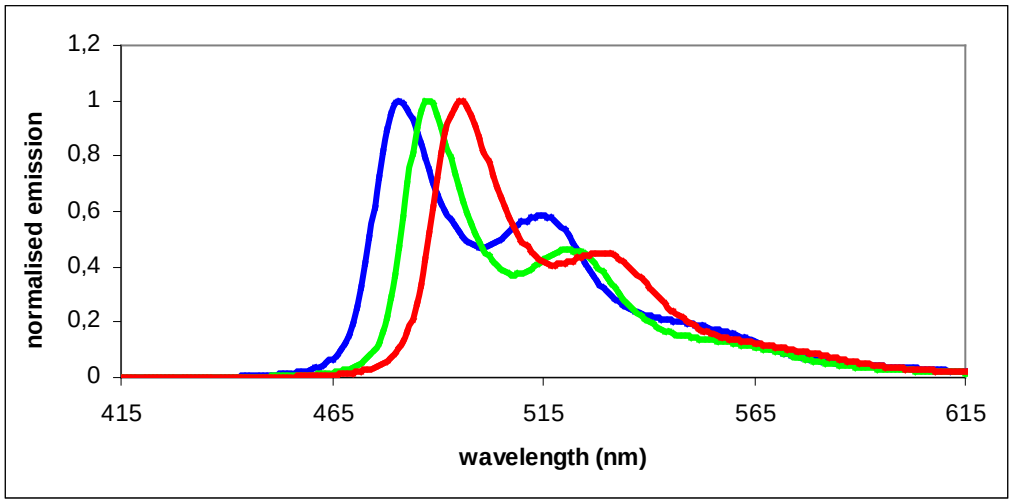

Figure 3.26: emission spectra in dichloromethane at room temperature of the complexes Ir(**L1**)(dFppy)CN **(22)** (blue line), Ir(**L1**)(dFppy)SCN **(27)** (gree line), Ir(**L1**)(dFppy)Cl **(1)** (red line).

Complex	λ_{max} / nm	τ degassed (aerated)	Φ_{LUM} in degassed solution	k_r /10^4 s^{-1}	Σk_{nr} / 10^4 s^{-1}	k_Q /10^8 $M^{-1}s^{-1}$	Absorption λ_{max} / nm (ε / mol^{-1} dm^3 cm^{-1})
Ir(L1)(dFppy)Cl (1)	495, 529	1500 (160)	0.66	44	23	25	286 (50 600), 363 (11 600), 393 (13 400), 412 (10 600), 451 (4 500), 488 (1 800)
Ir(L1)(dFppy)CN (22)	480, 515	300(30)	0.93	310	23	120	247(22 700), 281(16 900), 371 (4 300), 406(4 900), 479 (700)
Ir(L1)(dFppy)SCN (27)	487, 521	1900(190)	0.97	51	2	210	241(33 600), 287(23 100), 352 (4 800), 386 (5 700), 406(6 700), 485 (700)
Ir(L2)(dfppy)Cl (2)	476, 508	410 (120)	0.20	49	190	27	278 (21 100), 351 (4 800), 375 (5 800), 393 (6 800), 433 (1 400), 467 (800)
Ir(L2)(dFppy)CN (23)	462, 497	780 (200)	0.26	33	95	13	232 (16 300), 274 (14 600), 340 (2 500), 364 (2 700), 382 (4 400), 458 (400)
Ir(L5)(dFppy)Cl (6)	477, 507	260(100)	0.15	58	94	27	233(13 300), 286(6 700), 385(2 300), 426(300)
Ir(L5)(dFppy)CN	456, 486	460 (190)	0.14	30	187	15	232 (13 400), 270 (8 500), 307 (2 600), 364 (2 500), 390 (1 800), 447 (100)

Table 3.8: Luminescence data in solution in dichloromethane at 298±3 K, where; radiative (k_r) and non-radiative (Σk_{nr}) rate constants are calculated from τ and Φ_{lum} values; estimated uncertainty ±20%; k_Q, bimolecular rate constant for quenching by O_2, estimated from τ values in degassed and aerated solutions.

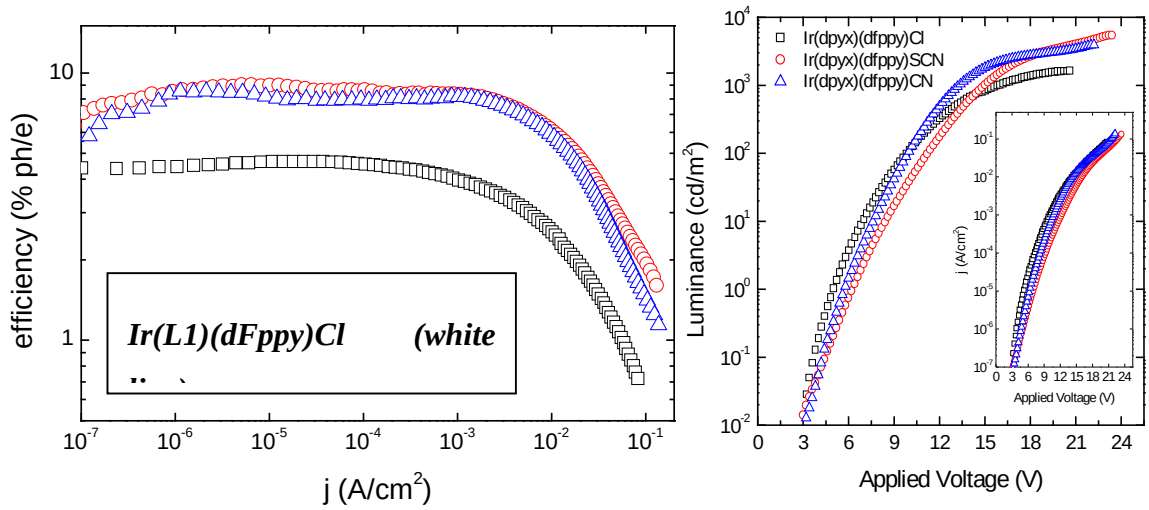

Figure 3.27: a) device efficiency (EL QE) vs potential (j); b) Luminance vs applied voltage for the complexes Ir(**L1**)(dFppy)CN **(22)** and Ir(**L1**-NCN)(dFppy)SCN **(27)** compared to that of Ir(**L1**)(dFppy)Cl **(1)**.

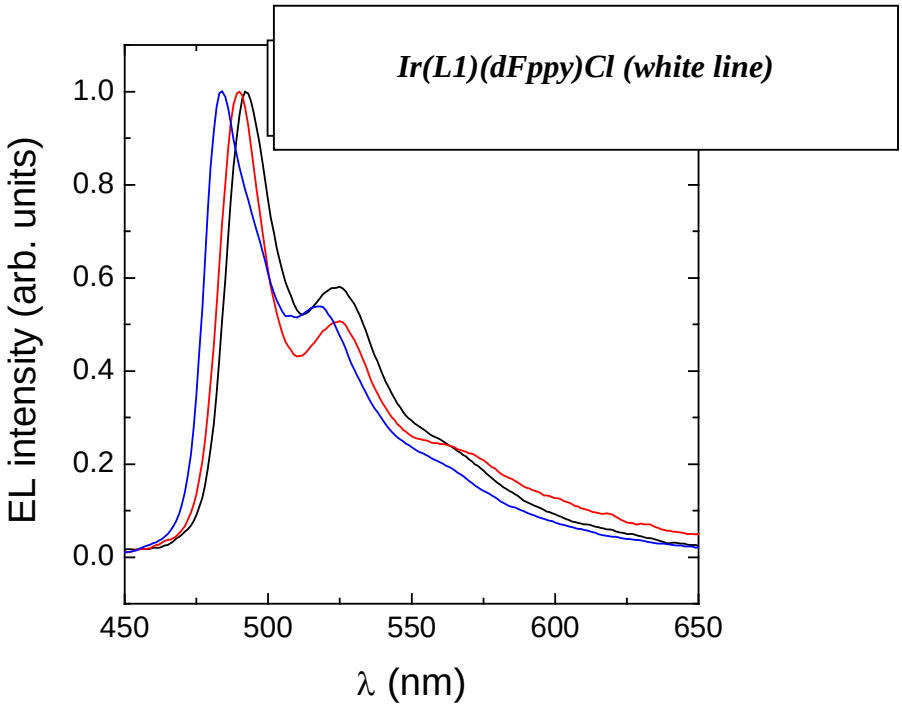

Figure 3.28: EL spectra and CIE diagram for the complexes Ir(**L1**)(dFppy)CN **(22)** and Ir(**L1**)(dFppy)SCN **(27)** compared to that of Ir(**L1**)(dFppy)Cl **(1)**.

3.2.3.2. Ir(N^C^N)(N^C)(acetylide) complexes

Photophysical studies on complexes containing acetylides as the ancillary monodentate ligand are here discussed. The data for Ir(**L1**)(dFppy)(**A1**) **(30)** (**A1** = 1,3-trifluoromethyl-phenylacetylide), Ir(**L3**)(ppy)(**A5**) **(35)** (**A5** = 1-(4-benzonitrile)acetylide) and Ir(**L3**)(ppy)(**A1**) **(31)** are summarised in Table 3.10. Absorption spectroscopy of all complexes is characterised by similar bands to those encountered in the previously studied complexes of the class Ir(N^C^N)(N^C)Cl, although only small shifts involving the energy of the MLCT transitions are observed upon introduction of the different acetylide ligands (see Table 3.9). On the other hand emission spectroscopy displays more interesting points of discussion. In fact, as shown in Figure 3.29, the emission maxima can be tuned by the introduction of different acetylide ligands. Comparing, see Table 3.9, the chloride and the differently substituted acetylide systems, all the species containing acetylide ligands display red-shifted emission in the order Cl < **A5** < **A1** (respectively 590 nm, 598 nm and 606 nm). The order observed can be explaned with the electron-withdrawing effect of the substituents on the phenyl ring of the acetylide, effect that presumably, in contrast to what was observed in the –CN coordinated complexes, leads to a destabilasation of the HOMO level or stabilasation of the LUMO level.

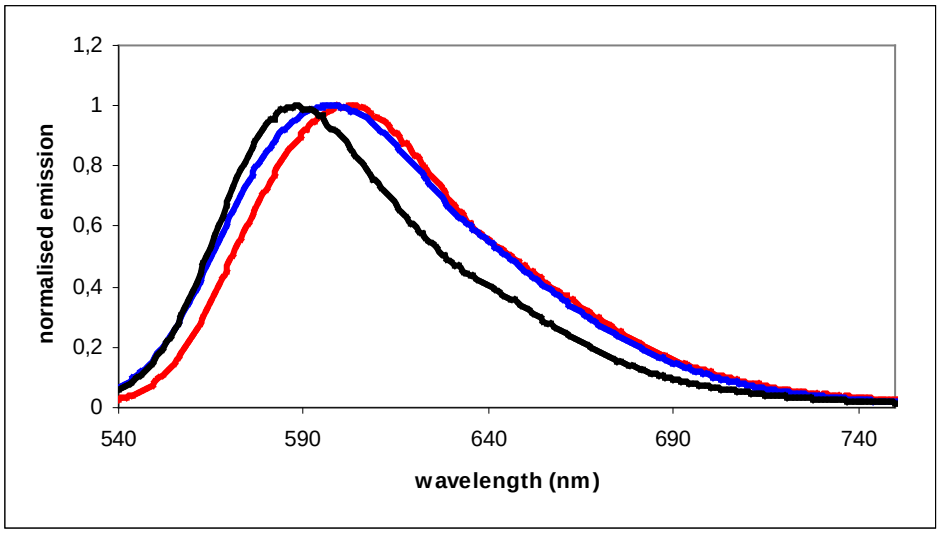

Figure 3.29: emission spectra in dichloromethane at room temperature of the complexes, Ir(**L3**)(ppy)(**A5**) **(35)** (blue line), Ir(**L3**)(ppy)(**A1**) **(31)** (red line), Ir(**L3**)(ppy)Cl **(5)** (black line).

Complex	λ_{max} / nm	τ degassed (aerated)	Φ_{LUM} in degassed solution	k_r /10^4 s^{-1}	Σk_{nr} / 10^4 s^{-1}	k_Q /10^8 $M^{-1}s^{-1}$	Absorption λ_{max} / nm (ε / mol^{-1} dm^3 cm^{-1})
Ir(L1)(ppy)(A1) (30)	495, 527	1400 (90)	0.77	55	16	500	251(37 100), 295(36 100), 413(7 900), 453(4 600), 489(1 600)
Ir(L3)(ppy)(A1) (31)	606	4100 (960)	0.34	9	15	36	230(26 200), 270(24 700), 344(3 300), 372(2 600), 421(2 100), 474(2 000), 515(1 200), 548(1 100)
Ir(L3)(ppy)(A5) (35)	598	5 300 (1 900)	0.25	5	47	21	234(39 800), 266(35 700), 321(24 000), 370(8 700), 422(5 100), 473(4 800), 556(2 000)
Ir(L3)(ppy)Cl (5)	590	3300 (1100)	0.46	14	16	28	259 (45 600), 272 (45 300), 373 (8 900), 429 (11 100), 461 (8 000), 506 (3 100), 541 (2 400)

Table 3.9: Luminescence data in solution in dichloromethane at 298±3 K, where; radiative (k_r) and non-radiative (Σk_{nr}) rate constants are calculated from τ and Φ_{lum} values; estimated uncertainty ±20%; k_Q, bimolecular rate constant for quenching by O_2, estimated from τ values in degassed and aerated solutions.

3.3. [Ir(N^C^N)(N^N)Cl]$^+$ complexes

3.3.1. DFT calculations and electrochemical studies of [Ir(N^C^N)(N^N)Cl]$^+$ complexes

The synthesis of [Ir(N^C^N)(bpy)Cl]$^+$ complexes has been described in the previous Chapter, for [Ir(**L3**)(bpy)Cl]$^+$ **(13)** and [Ir(**L2**)(bpy)Cl]$^+$ **(14)**. Electrochemical data for these two mono-cyclometallated complexes containing bpy as bidentate ligand are listed in Table 3.10. together with data for [Ir(**L1**)(bpy)Cl]$^+$, for comparison.

Complex	E_{ox} / V vs SCE	E_{red} / V vs SCE
[Ir(L1)(bpy)Cl]$^+$	1.28 $E^{1/2}$	-1.52 $E^{1/2}$
[Ir(L2)(bpy)Cl]$^+$ (14)	1.92 $E^{1/2}$	-1.96 $E^{1/2}$
[Ir(L3)(bpy)Cl]$^+$ (13)	1.24 E^{p}	-1.85 $E^{1/2}$

Table 3.10: electrochemical data vs SCE for the mono-cyclometallated complexes with bpy as bidentate ligand

[Ir(**L1**)(bpy)Cl]$^+$ and [Ir(**L2**)(bpy)Cl]$^+$ **(14)** exhibit reversible oxidations at similar potentials, respectively 1.28 V and 1.24 V, values comparable to that of [Ir(ppy)$_2$(bpy)]$^+$, which was reported at 1.28 V.[112] Comparing these positively charged bpy containing mono-cyclometallated complexes with the neutral complexes Ir(N^C^N)(N^C)Cl, reported in the previous section, oxidation is located at higher potentials, reflecting their cationic nature. The oxidation of [Ir(**L3**)(bpy)Cl]$^+$ **(13)** occurs at even higher potentials, which would be consistent with an electron-withdrawing effect of the –CF_3 groups, although care should be taken here in making a quantitative comparison, since the oxidation wave in this complex is not electrochemically reversible and the quoted value is the peak potential.

Based on the results of DFT calculations, the oxidation can again be attributed to the removal of an electron from an orbital spanning the iridium centre and the cyclometalating site of the N^C^N unit (Figure 3.30), as for the neutral bis-cyclometallated complexes discussed earlier. On the other hand, the LUMO levels of the two complexes (Figure 3.30) are located on the bpy ligand, in contrast to the previous set of complexes, where the LUMO was likely based on the N^C^N pyridyl rings. The LUMO+1 is located on the N^C^N ligand in the –F substituted complex and on the bpy in the $–CF_3$ substituted complex.

Complex	HOMO-1	HOMO	LUMO	LUMO+1
[Ir(L3)(bpy)Cl]$^+$ (13)	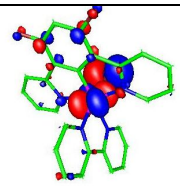	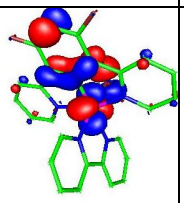	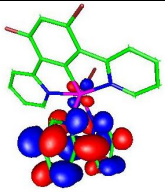	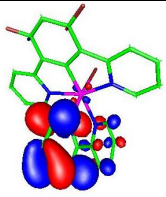
E(eV)	-0.32201	-0.31928	-0.20253	-0.16794
Ir	0.41	0.42	0.05	0.03
N^C^N	0.17	0.3	0.02	0.07
Cl	0.38	0.22	0	0
N^N	0.04	0	0	0
[Ir(L2)(bpy)Cl]$^+$ (14)	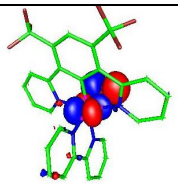	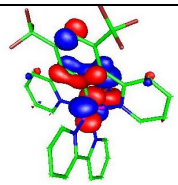	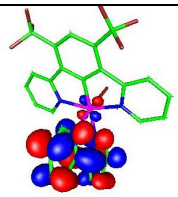	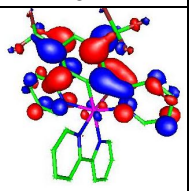
E(eV)	-0.32977	-0.32671	-0.20743	-0.19788
Ir	0.43	0.42	0.04	0.03
N^C^N	0.09	0.25	0.04	0.95
Cl	0.04	0.06	0.91	0.02
N^N	0.44	0.27	0	0

Figure 3.32: DFT calculations for [Ir(**L3**)(bpy)Cl]$^+$ **(13)** and [Ir(**L2**)(bpy)Cl]$^+$ **(14)**.

3.3.2. Photophysical properties of [Ir(N^C^N)(N^N)Cl]$^+$ complexes

The absorption spectra of [Ir(**L3**)(bpy)Cl]$^+$ **(13)** and [Ir(**L2**)(bpy)Cl]$^+$ **(14)** (Figure 3.31) display LC transitions below 300 nm and charge-transfer bands at lower energies. With the support of the computational studies (Figure 3.30), the bands

at 387 nm and 370 nm, respectively for the two complexes, are assigned as MLCT character, whereas those at lower in energy are assigned as being mixed MLCT/LLCT origin, according to the trend previously observed for [Ir(**L1**)(bpy)]$^{+}$.[24] The higher energy that characterises the MLCT transitions of the bpy containing complexes, compared to those of Ir(N^C^N)(N^C)Cl, can be attributed to the lower energy of the metal d orbitals, reflecting the presence of only two rather than three anionic ligands in the coordination sphere ot the Ir(III). Moreover, substituent effect on the terdentate ligand of [Ir(N^C^N)(N^C)Cl]$^{+}$ systems has a similar outcome, to what was observed previously in Section 3.1.2. for bis-cyclometallated neutral complexes, in fact in the –F substituted complex the MLCT related band is blue shifted which respect to the analogous band of the –CF_3 substituted parent complex.

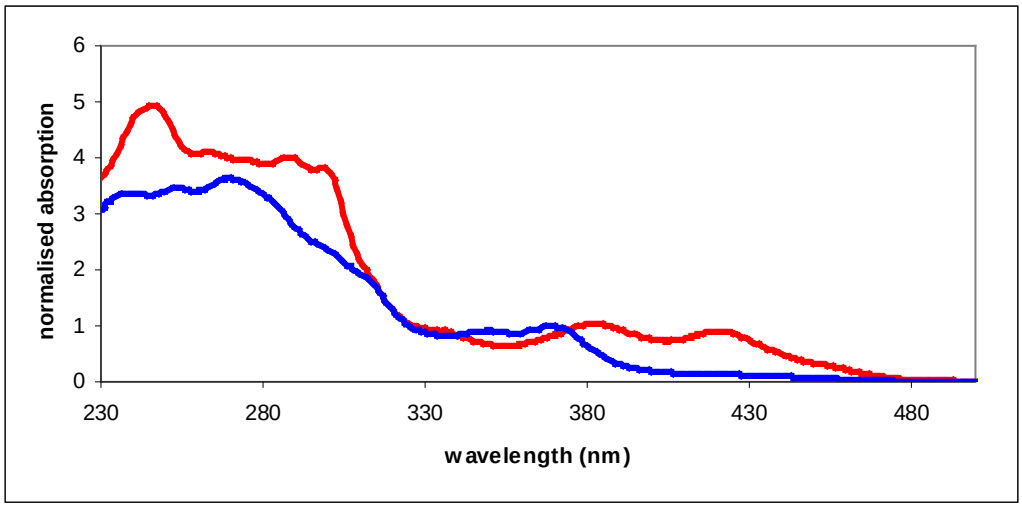

Figure 3.31: normalised absorption spectra to the most intense low-enegy band in dichloromethane at room temperature for [Ir(**L3**)(bpy)Cl]$^{+}$ **(13)** (red line) and [Ir(**L2**)(bpy)Cl]$^{+}$ **(14)** (blue line).

The emission spectra of [Ir(**L3**)(bpy)Cl]$^{+}$ **(13)** and [Ir(**L2**)(bpy)Cl]$^{+}$ **(14)** (Figure 3.32) in dichloromethane at room temperature are characterised by rather unusually shaped profiles, which appear to consist of a set of structured vibronically-resolved

bands to high energy, superimposed on a broader low-energy band. Based on the DFT results presented above it is possible that this profile arises from dual emission from MLCT and LLCT states. The emission maxima follow the sequence [Ir(**L2**)(bpy)Cl]$^+$ **(14)** (484 nm) < [Ir(**L1**)(bpy)Cl]$^+$ (502 nm) < [Ir(**L3**)(bpy)Cl]$^+$ **(13)** (506 nm). The excited state lifetimes of the cationic complexes are longer (in both degassed and aeretad solutions) than for the analogous containing ppy. Indeed, the calculated k_r values are an order of magnitude smaller than for the Ir(N^C^N)(N^C)Cl complexes, which is fully consistent with a lower degree of metal character in the excited state. This observation reveals the importance of the effect of introducing a second cyclometallating unit in increasing metal participation in the excited states of the complex. The quantum yields of the complexes bearing bpy bidentate ligands are an order of magnitude lower then those of Ir(N^C^N)(N^C)Cl (see Tables 3.11 and 3.4).

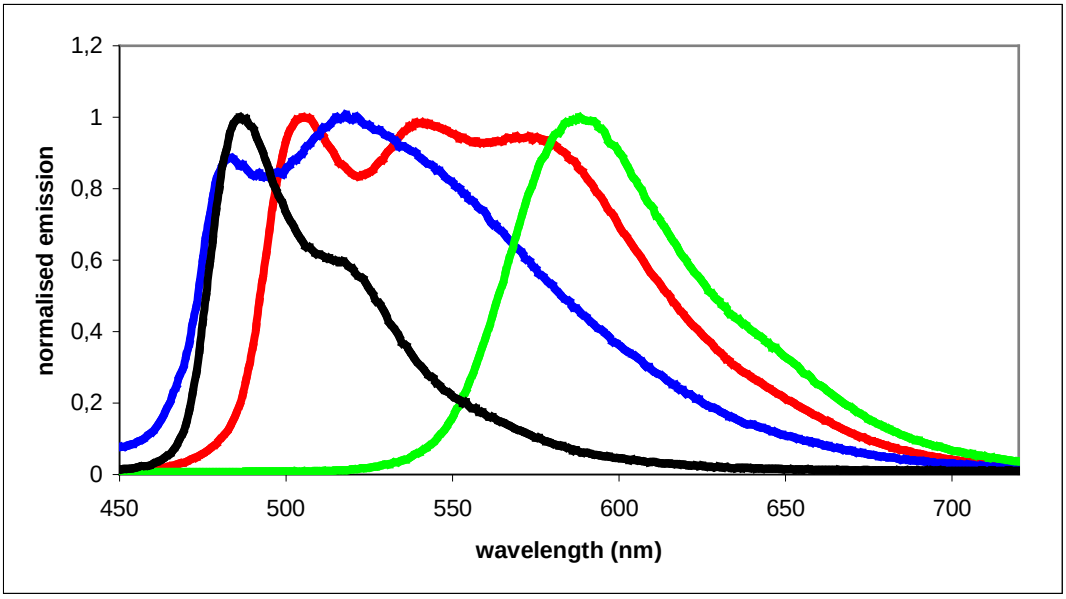

Figure 3.32: normalised emission spectra of [Ir(**L3**)(bpy)Cl]$^+$ **(13)** (red line) and [Ir(**L2**)(bpy)Cl]$^+$ **(14)** (blue line) in dichloromethane at room temperature, each compared with Ir(**L3**)(ppy)Cl **(5)** (green line) and Ir(**L2**)(ppy)Cl **(4)** (black line).

Complex	λ_{max} / nm	τ degassed (aerated)	Φ_{LUM} in degassed solution	k_r /10^4 s^{-1}	Σk_{nr} / 10^4 s^{-1}	k_Q /10^8 $M^{-1}s^{-1}$	Absorption λ_{max} / nm (ε / mol^{-1} dm^3 cm^{-1})
$[Ir(L3)(bpy)Cl]^+$ (13)	506, 540, 580	4090 (1280)	0.06	1.4	23	24	248(97 600), 289(77 400), 336(24 300), 387(11 400), 426(3 700)
$[Ir(L2)(bpy)Cl]^+$ (14)	484, 518	2260 (1320)	0.03	1.3	43	14	254(15 100), 270(15 800), 352(3 800), 370(4 200)

Table 3.11: Luminescence data in solution in dichloromethane at 298±3 K, where; radiative (k_r) and non-radiative (Σk_{nr}) rate constants are calculated from τ and Φ_{lum} values; estimated uncertainty ±20%; k_Q, bimolecular rate constant for quenching by O_2, estimated from τ values in degassed and aerated solutions.

3.4. Ir(N^C^N)(pbi)Cl and [Ir(N^C^N)(Mepbi)Cl]$^+$ complexes

3.4.2. Photophysical studies

Ground state absorption spectroscopy of both series of complexes, containing pbi and Me-pbi is summarised in Table 3.12. The charge-neutral charged complexes (pbi coordinated) display the usual intense LC high-energy bands and the weaker, typical for cyclometallated complexes, bands at lower energies (Figure 3.33). Between 320 nm and 340 nm the Me-pbi coordinated complexes display relatively intense CT bands, whereas for the pbi coordinated systems the bands in the same regions are weaker. At lower energies (between 350 nm and 400 nm) all four complexes show bands of mixed MLCT/LLCT character, with the Me-pbi incorporating systems displaying red-shifted bands compared to those of the pbi incorporating systems, suggesting, for the Me-pbi-based complexes, that the LUMO level may be on the Me-pbi instead of the N^C^N ligand. At energies above 400 nm MLCT bands are shown by the complexes Ir(**L3**)(pbi)Cl **(19)** and [Ir(**L3**)(Me-pbi)Cl]$^+$ **(21)**.

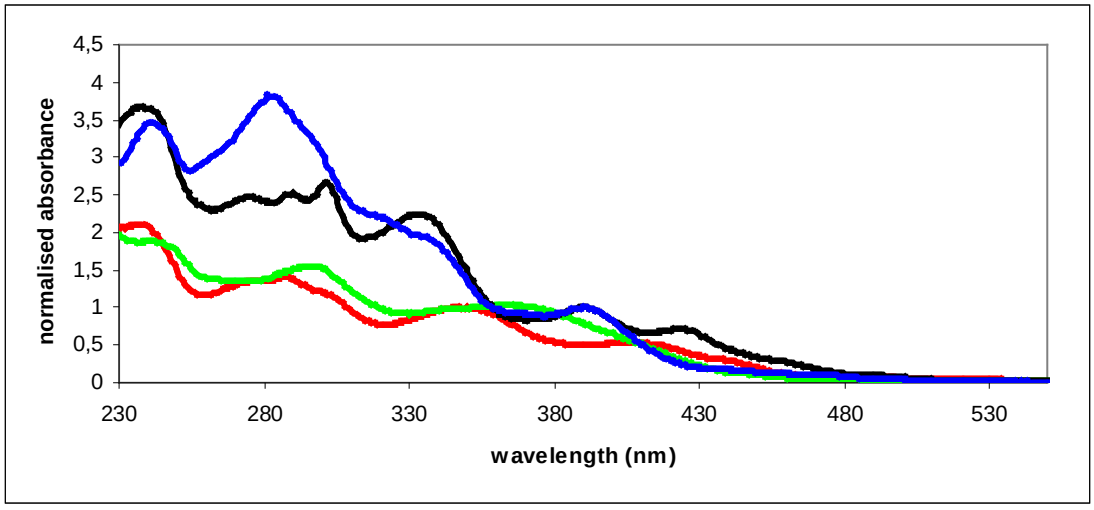

Figure 3.33: normalised absorption spectra to the most intense low-enegy band in dichloromethane at room temperature for Ir(**L1**)(pbi)Cl **(17)** (green line), Ir(**L3**)(pbi)Cl **(19)** (red line), [Ir(**L3**)(Me-pbi)Cl]$^+$ **(21)** (black line) and [Ir(**L1**)(Me-pbi)Cl]$^+$ **(20)** (blue line).

Emission of the two Ir(N^C^N)(pbi)Cl complexes in degassed dichloromethane solution show emission of an MLCT character with Ir(**L3**)(pbi)Cl **(19)** (λ_{MAX}= 577) being red-shifted compared to Ir(**L1**)(pbi)Cl **(17)** (λ_{MAX}= 493) (Figure 3.34). The two $[Ir(N^C^N)(Me\text{-}pbi)Cl]^+$ complexes show structured bands of dual emission from MLCT and LLCT states, as previously observed for $[Ir(N^C^N)(bpy)Cl]^+$ complexes.

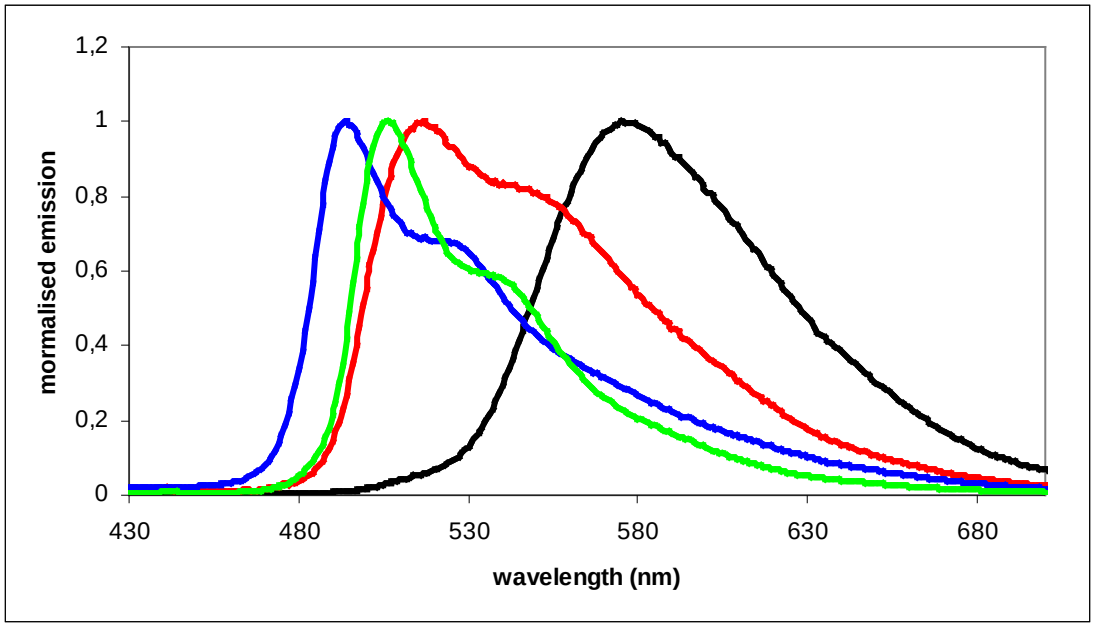

Figure 3.34: normalised emission spectra in dichloromethane at room temperature for Ir(**L1**)(pbi)Cl **(17)** (blue line), Ir(**L3**)(pbi)Cl **(19)** (black line), $[Ir(\mathbf{L3})(Me\text{-}pbi)Cl]^+$ **(21)** (red line) and $[Ir(\mathbf{L1})(Me\text{-}pbi)Cl]^+$ **(20)** (green line).

Complex	λ_{max} / nm	τ degassed (aerated)	Φ_{LUM} in degassed solution	k_r /10^4 s^{-1}	Σk_{nr} / 10^4 s^{-1}	k_Q /10^8 $M^{-1}s^{-1}$	Absorption λ_{max} / nm (ε / mol^{-1} dm^3 cm^{-1})
Ir(L1)(pbi)Cl (17)	493, 522	170 (90)	0.06	3.5	108	27	242(800), 298(600), 373(400), 482 (100)
Ir(L3)(pbi)Cl (19)	577	1 500 (950)	0.14	9	57	18	238(4 800), 290(2 300), 350(1 300), 411(600), 441(300), 502(100)
[Ir(L1)(Mepbi)Cl]$^+$ (20)	506, 534	1300 (170)	0.04	3	74	25	243(3 800), 288(3 600), 320(1 000), 390(1 000), 467(100)
[Ir(L3)(Me-pbi)Cl]$^+$ (21)	516	220 (200)	0.21	95	360	23	242(4 900), 302(2 500), 338(1 200), 390(900), 423(600), 491(100)

Table 3.12: Luminescence data in solution in dichloromethane at 298±3 K, where; radiative (k_r) and non-radiative (Σk_{nr}) rate constants are calculated from τ and Φ_{lum} values; estimated uncertainty ±20%; k_Q, bimolecular rate constant for quenching by O_2, estimated from τ values in degassed and aerated solutions.

3.5. Concluding remarks

In this chapter photophysical and electrochemical properties of the complexes synthesised have been investigated. Particular attention was given to strategies to tune the emission of Ir(N^C^N)(N^C)X complexes (X = -Cl or monodentate ancillary ligand) via modifications on the N^C^N, N^C and X ligands.

Emission tuning by introduction of different substituents on the N^C^N ligand was achieved, in particular with substituents on the central phenyl ring (Y = -F, $-CH_3$, $-CF_3$) and on the position 4 of the pyridyl rings (R = -H, -OMe, $-NMe_2$, $-CF_3$). The effect of the substituents Y on complexes with R = -H, X = -Cl and ppy as a bidentate ligand led to a trend in the emission maxima of the complexes as follows: –F (λ_{MAX} = 487 nm) < $-CH_3$ (λ_{MAX} = 503 nm) < $-CF_3$ (λ_{MAX} = 590 nm). This trend can be explained by mesomeric effect of the –F groups resulting in a stabilisation of the HOMO level in respect to the LUMO level, thus the HOMO-LUMO energy gap is increased. A different effect is provoked by the uniquely electron-withdrawing effect of the $-CF_3$ groups which stabilise the energy of the LUMO with little effect on the HOMO level leading to a smaller HOMO-LUMO energy gap. The effect of the groups R of the N^C^N ligand is investigated in complexes with Y = -F, X = Cl and dFppy as a bidentate ligand. Blue-shifted emission is obtained when R = $-NMe_2$ (λ_{MAX} = 472 nm) in respect to R = -H (λ_{MAX} = 476 nm) and –OMe (λ_{MAX} = 477 nm). The electron-donor effect of the $-NMe_2$ is thought to destabilise the LUMO level with respect to the HOMO level.

Blue-shifted emission was observed in complexes incorporating dFppy as N^C unit instead of ppy, the magnitude of which is around 500 cm^{-1} due to the mesomeric effect of the fluorine atoms on dFppy. The complex bearing btiq as bidentate ligand and with X = -Cl, Y = $-CF_3$ and R = -H displayed red-shifted emission (λ_{MAX} = 667 nm) compared to that of the ppy containing analogue (λ_{MAX} = 590 nm) due to a destabilisation of the HOMO level introduced by a more extended π system with btiq.

Displacement of the chlorine atom in the sixth coordination site of Ir(N^C^N)(N^C)Cl complexes led to a blue-shift of the emission maxima in

complexes with –CN (λ_{MAX} = 480 nm) and –SCN (λ_{MAX} = 487 nm) as ancillary ligand compared to that of the complex with Y = -CH_3, R = -H and dFppy as bidentate ligand (λ_{MAX} = 495 nm). Coordination of **A1** (1,3-trifluoromethyl-phenylacetylide) as monodentate ancillary ligand on the complex Ir(**L3**)(ppy)Cl **(5)** (Y = -CF_3, R = -H, λ_{MAX} = 590 nm) led to red-shifted emission with λ_{MAX} = 606 nm.

It is possible to conclude that, following the emission tuning strategies adopted, the series of complexes investigated displays emission over a wide range of colours with the blue emission of Ir(**L5**)(dFppy)CN (Y = -F, R = -OMe, λ_{MAX} = 462 nm) and the red emission of Ir(**L3**)(btiq)Cl **(11)** (Y = -CF_3, R = -H, λ_{MAX} = 667 nm) as extremes.

The measured quantum yields of the complexes Ir(N^C^N)(N^C)Cl synthesised range between 0.2 and 0.7, an order of magnitude higher compared to those of $[Ir(N^C^N)(N^N)Cl]^+$ (Φ_{LUM} = 0.03-0.06), due to the increased metal participation in the excited in complexes with a second cyclometallating ligand. The complexes synthesised exhibit quantum yields comparable or, in some cases, higher compared to those of systems containing only bidentate ligands used for OLED applications such as $Ir(ppy)_3$ (Φ_{LUM} = 0.4).[87] Ir(N^C^N)(dFppy)Cl and Ir(N^C^N)(ppy)Cl have been used as phosphorescent dopants in multi-layer OLEDs. The devices manifested relatively high efficiencies (EL QE = 0.03-0.11) and stability over a wide range of current densities. Among the most efficient iridium-based OLEDs are those with the green emitters $Ir(ppy)_3$ and $Ir(ppy)_2(acac)$, with EL QE = 0.19.[149, 151] In this work the most efficient device was the one incorporating Ir(**L1)**(ppy)Cl **(1)** (EL QE = 0.11). It is worth highlighting the higher measured quantum yields of the complexes containing -CN and –SCN as monodentate ancillary ligand, in particular those of Ir(**L1**)(dFppy)CN **(22)** and Ir(**L1**)(dFppy)SCN **(27)**. These complexes in fact displayed, in both solution (Φ_{LUM} = 0.9) and devices (EL QE = 0.08) improved emission properties compared to those of Ir(**L1**)(dFppy)Cl (Φ_{LUM} = 0.7 and EL QE = 0.03).

CHAPTER 4

Multimetallic complexes with cyclometallated Ir(III) units containing terdentate ligands

4. Multimetallic complexes with cyclometallated Ir(III) units containing terdentate ligands

4.1. Background and previous work

Ir(III) complexes are potentially interesting components for the construction of supramolecular systems which can be used for collection and conversion of light energy.[87] Multimetallic systems can manifest, in some cases, properties typical of the single units composing the assembly, or, in other cases, completely new properties, depending upon the degree of communication between the metal centres. One of the most commonly adopted strategies for the synthesis of multimetallic complexes is to react metallic fragments, in which one of the ligands is easily replaceble, with a ditopic bridging ligand in a 2:1 stoichiometric quantity. Such strategies work well for homo-multimetallic systems, but the preparation of hetero-metallic systems requires a two step method, in which the bridging ligand is in excess, in order to favour coordination at one end of one metallic fragment and, in a second step, coordination of a different metal fragment through the other end (see Figure 4.1).

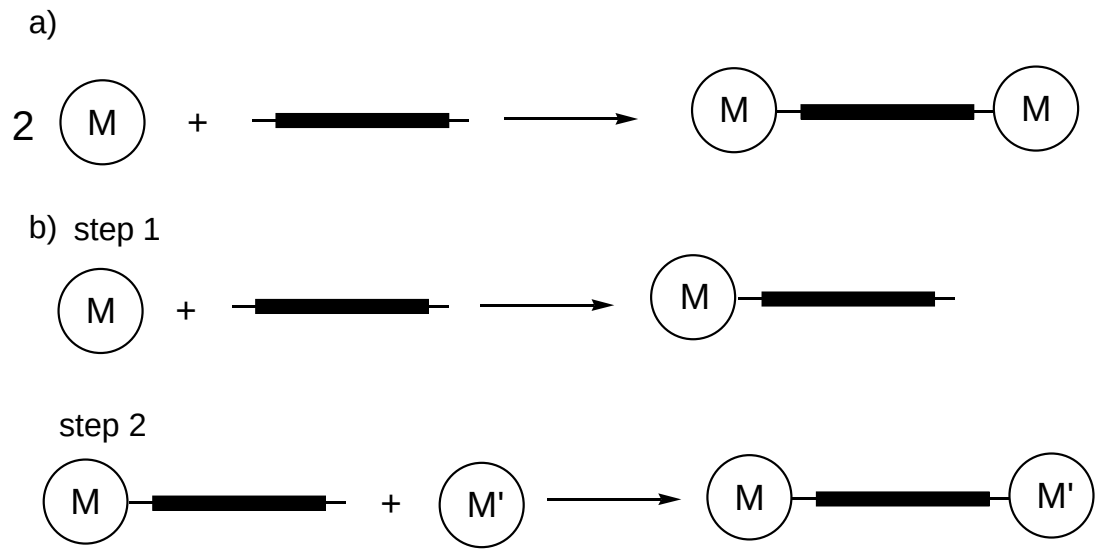

Figure 4.1: a) strategy for the synthesis of homometallic dinuclear systems; b) two-step strategy for the synthesis of heterometallic dinuclear systems using a preformed bridging ligand.

Many examples of binuclear homometallic Ir(III) systems are reported in literature. For example di-chloride-bridged dimers containing bidentate cyclometallating ligands, are obtained as intermediates in the synthesis of tris-chelate complexes. They have been found to be only poorly emissive at room temperature due to a rapid non-radiative decay that cleaves the dimer in the excited state. However some improvements in emission are observed when strongly electron-withdrawing groups (such as $–NO_2$) are attached to the cyclometallating ligands. An increase of luminescence quantum yields is also observed in dimers containing isocyanate bridging ligands.[219] Some examples of binuclear Ir(III) complexes with cyclometallating ligands of the ppy type and containing *p*-phenylene spacing units have also been reported.[220, 221] In this case the photophysical properties of the complex are influenced by the length of the spacer and the presence of substituents on the cyclometallating ligands. In general luminescence quantum yields for this class of complexes are found to be improved with respect to those of the chloride-bridged analogues.[87] For this type of complex, luminescence originating from a ^{3}MLCT excited state involving the bridging ligand is reported.

Blue-shifted emission is observed, compared to that of $Ir(ppy)_3$, when significant electronic comunication is present between the metal centres as in the case of $[(ppy)_2Ir(\mu\text{-bpt})Ir(ppy)_2]^+$ (bpt shown in figure 4.2), where efficient mixing occurs between the *d* orbitals of the metal and the π of the bridging ligand.

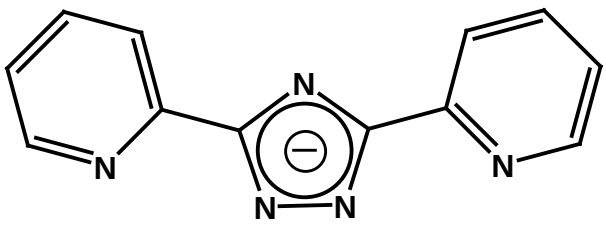

Figure 4.2: bpt bridging ligand

Polynuclear complexes containing Ir(III) centres and, in addition, other types of metals such as Os(II), Ru(II), Re(I) or Cu(I) linked by bridging ligands of different types show photoinduced processes, such as energy transfer between different metal centres.

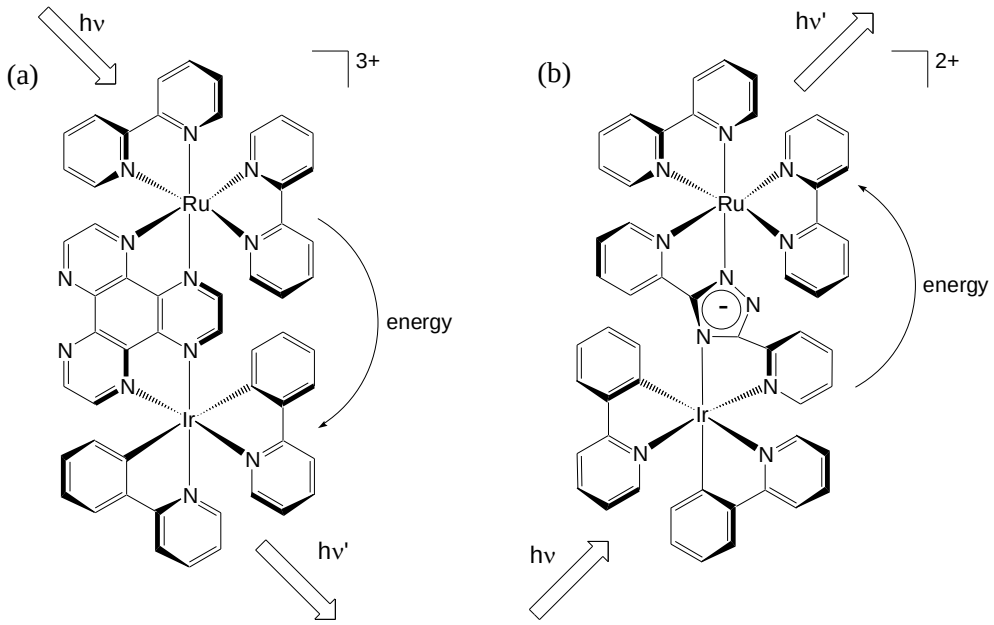

Figure 4.3[122]: examples of multicentered complexes that show energy transfer processes containing Ir(III) and Ru(II) units; a) $[(bpy)_2Ru\text{-}\mu\text{-}(HAT)Ir(ppy)_2]^{3+}$ and (b) $[(bpy)_2Ru(bpt)Ir(ppy)_2]^{2+}$

For example the complex shown in Figure 4.3a), reported by Kirsch-De Mesmaeker and co-workers, emission was assigned to an iridium-centred state of SBLCT character. In such complexes, absorption by a metal centre is observed and emission by another metal centre of the molecule occurs subsequently to an energy transfer process. In the complex shown in Figure 4.3a) emission is identified on the Ir centre, following Ru→Ir energy transfer. In Figure 4.3b) is shown an example reported by Reedijk and co-workers, in which the lowest-energy MLCT state is localised on the iridium centre and the bridging ligand, the emission observed is instead characteristic of the ruthenium unit, due to energy transfer Ir→Ru.[222]

The research group of De Cola investigated some examples of heterometallic cyclometallated complexes containing Ir(III) and Ru(II) units in the presence of *p*-phenylene spacers of various length in which the MLCT state is localised on one of the two metals and on the bridging ligand. Energy transfer Ir→Ru occurs. (figure 4.4)

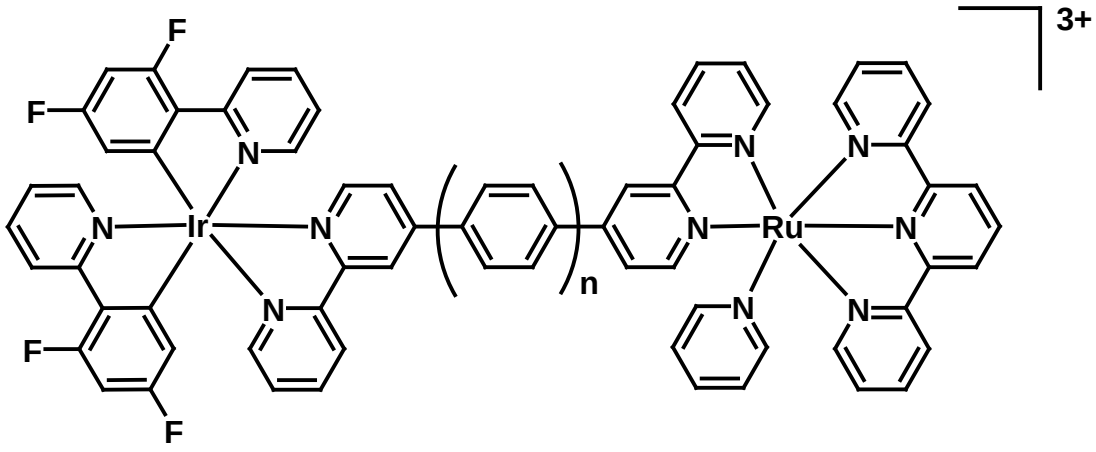

Figure 4.4[21]**:** example of an heterometallic cyclometallated complex containing Ir(III) and Ru(II) units where energy transfer process occurs

Another example of an energy transfer process is represented by the complex containing Ir(III) and Eu(III) units in Figure 4.5, from the Ir-based MLCT state to the $^5D_0$ of the Eu (III) ion, such that the emission spectrum contains contribution from both moieties (λ_{MAX} = 400, 491 for nm Ir and 615 nm for Eu). The net effect is white light.[223]

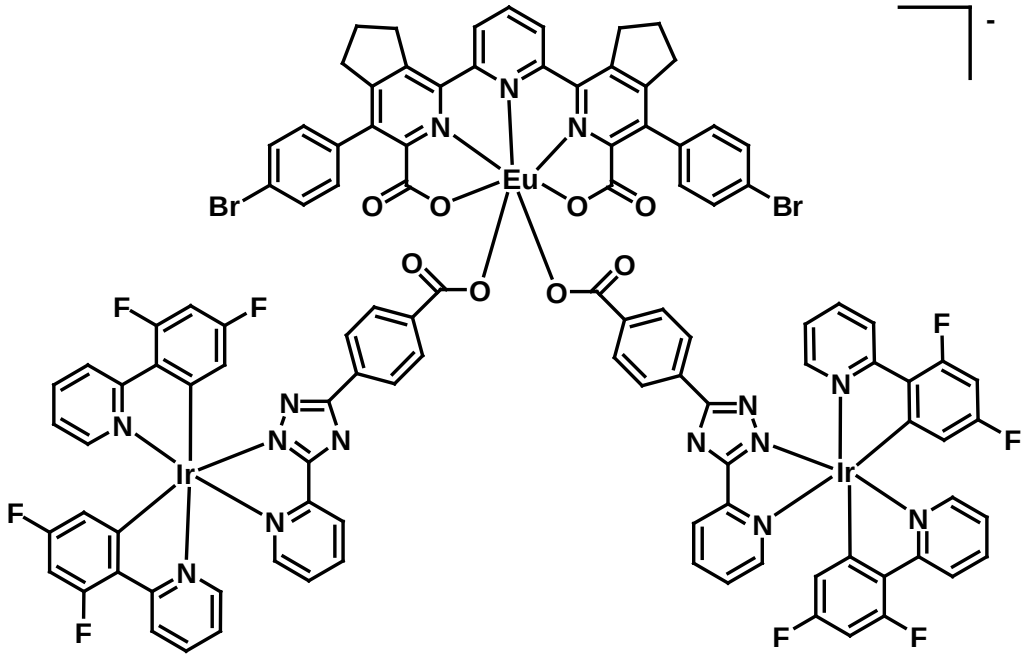

Figure 4.5[87]: partial energy transfer in a complex containing Ir(III) and Eu(III) units

A different synthetic strategy was adopted by Constable and co-workers, in which the synthesis of multimetallic complexes is achieved by preparing complexes which can act as ligands. In the presence of active functionalities on the complex, through appropriate reactions, fragments capable of coordinating other metal centres can be introduced *in situ* (Figure 4.6).[223] For example, the ruthenium complex $[Ru(Cltpy)_2]^{2+}$, containing 4'-chloro-2,2':6',2''-terpyridine, was reacted with 2,6-bis(2-pyridyl)-4-pyridone, leading to formation of species containing two vacant terpyridine coordination sites which were then in turn reacted with $[Ru(tpy)Cl_3]$ in order to obtain the tris-metallic species showed in Figure 4.6.

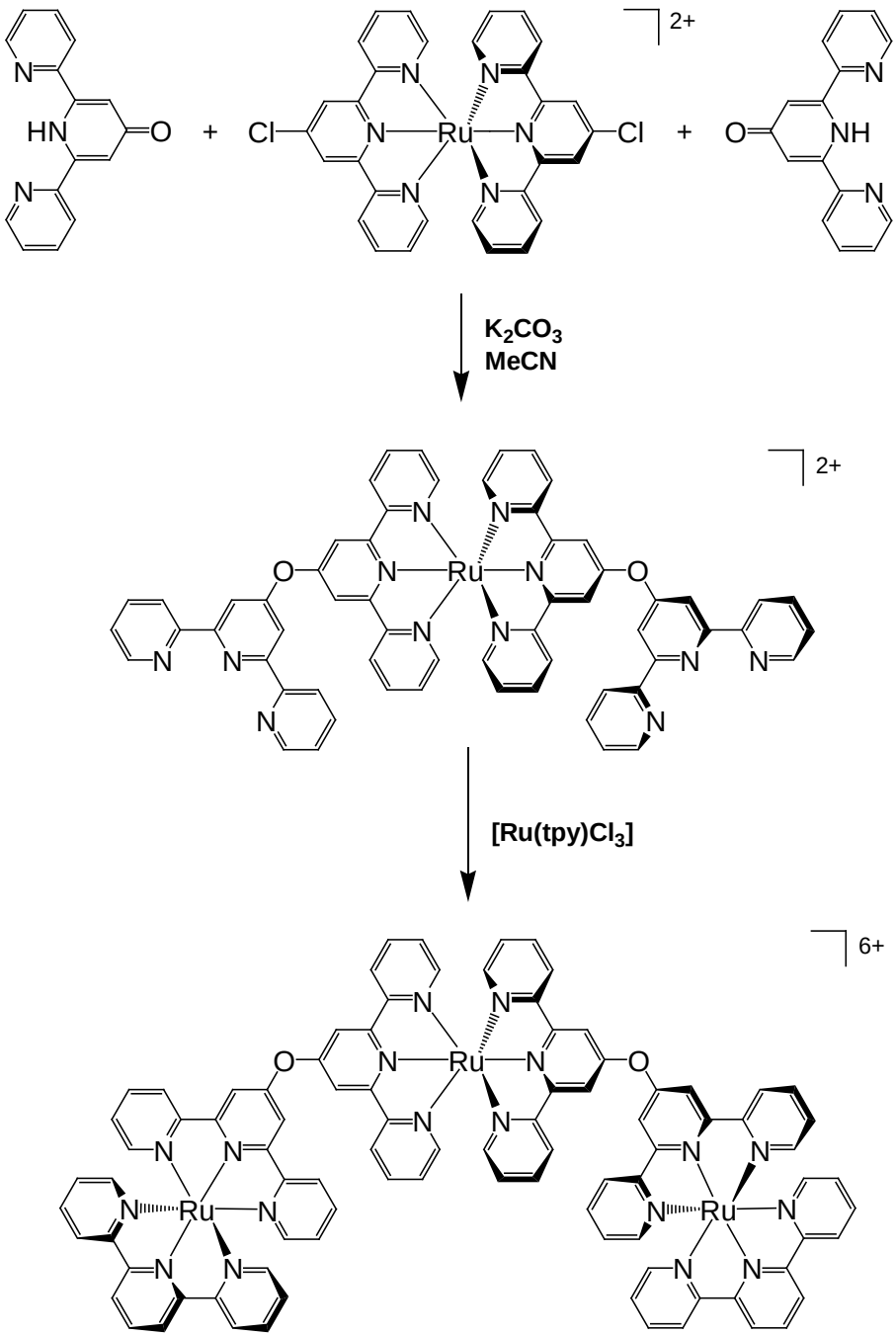

Figure 4.6[24]: *In situ* elaboration of complexes

Within our research group, synthetic pathways via *in situ* chemical reactions onto previously prepared building blocks have been carried out in order to synthesise both homo- and hetero- metallic multinuclear species. In particular, as building blocks, bis-terdentate complexes were chosen due to their achiral nature, yielding multimetallic species avoiding laborious separation processes between

stereoisomers that are obtained when chiral bidentate complexes are linked. In the present work, particular attention is focused on homo-metallic dinuclear species. In the work carried out by Whittle, a series of homo-metallic dinuclear complexes prepared via cross-coupling reactions was reported.[24] Among them, as examples, the complexes $[\{Ir(dpydmb)\}_2\mu\text{-}(mtbpy\text{-}\phi_3\text{-}mtbpy)][PF_6]_2$ and $[\{Ir(dpydmb)\}_2\mu\text{-}(mtbpy\text{-}\phi_4\text{-}mtbpy)][PF_6]_2$ were afforded via Suzuki coupling of $[Ir(dpydmb)(mtbpy\text{-}\phi\text{-}Br)]^+$, with aryl-diboronic acids in degassed DMSO and in presence of the catalyst $Pd(PPh_3)_4$, (Figure 4.7).

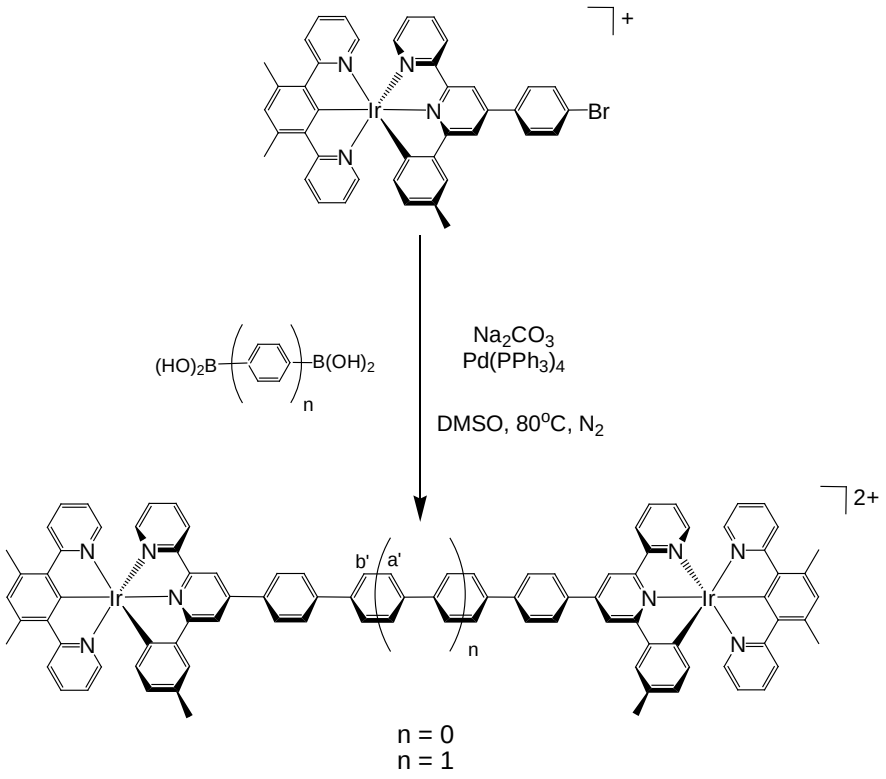

Figure 4.7[24]: scheme for the synthesis of homo-metallic dinuclear complexes previously reported by our research group

The photophysical properties of the homo-metallic dinuclear complexes were studied, displaying, in ground state absorption spectroscopy, intense transitions between 220 nm and 400 nm and weaker bands at lower energies, similar

behaviour to that observed for the mononuclear iridium complexes. Within the region between 330 nm and 400 nm, the dinuclear species differ, from the mononuclear ones, by displaying CT transitions associated with the $^1\pi-\pi^*$ transitions involving the aromatic bridge. Emission spectroscopy on the same systems was characterised by single structureless bands with lifetimes of the order of 140 ns, leading to the assignment of a charge transfer character of the excited states, although an additional very long component was observed at 77 K, possibly associated with a transition localised on the polyphenylene bridge.

4.2. Synthesis of multimetallic complexes using acetylide and tetrazolate-based bridging ligands

This section reports on the utility of the Ir(N^C^N)(N^C)Cl unit in the preparation of homo-metallic dinuclear complexes. The strategy envisaged exploits the ease with which the monodentate chloride ligand can be displaced, allowing one end of a ditopic bridging ligand to be coordinated to the $[Ir(N^C^N)(N^C)]^+$ fragment. Two classes of such bridging ligands are investigated. One involves linear aryl bis-acetylides H-C≡C-Ar-C≡C-H, exploiting the methodology discussed earlier for the preparation of mononuclear Ir(N^C^N)(N^C)(-C≡C-R) complexes. The second involves bis-tetrazoles, in which tetrazolate anion will act as a monodentate ligand to each metal ion. The synthetic strategy adopted, leading to formation of the multimetallic complexes, is to react a chosen metal fragment with a 2:1 stoichiometric amount of the dianionic bridging ligand, giving formation of the desired symmetric species, similar to the scheme drawn in Figure 4.1a). The reacting fragment selected for exploiting the build-up of such species is Ir(**L3**)(ppy)Cl **(5)**, due to its ease of synthesis, the high solubility during the work-up, facile purification method and the proven availability of the sixth coordination site under appropriate reaction conditions. Preliminary studies of electrochemical and photophysical properties have been made in order to compare them with previously studied systems and observe the synergy of the two metal centres combined together and the role of the extended π system bridging the metal centres.

4.2.1. Synthesis of the bridging ligands

For the first method, the synthesis of the requisite bis-acetylide proligand was performed using Sonogashira coupling conditions.[225] The general mechanism of the Sonogashira coupling is illustrated in Figure 4.8. The mechanism involves two cycles, one involving palladium and the other copper. In the palladium cycle, oxidative addition of Pd(0) species occurs with the aryl halide to give Pd(II), which then reacts with a copper-acetylide species, produced in the copper cycle, producing an acetylide-coordinated palladium species and expelling copper iodide. The palladium-coordinated species, containing the organic substrates in mutually trans position to each other, undergoes trans-cis isomerisation. Reductive elimination, during the final step of the palladium cycle, regenerates Pd(0) expelling the aryl-acetylide coupled compound. The copper cycle involves formation of the organo-copper compound combined with deprotonation of the acetylide functionality to give the copper acetylide involved in the palladium cycle, which, by expelling CuI, regenerates the copper catalyst.

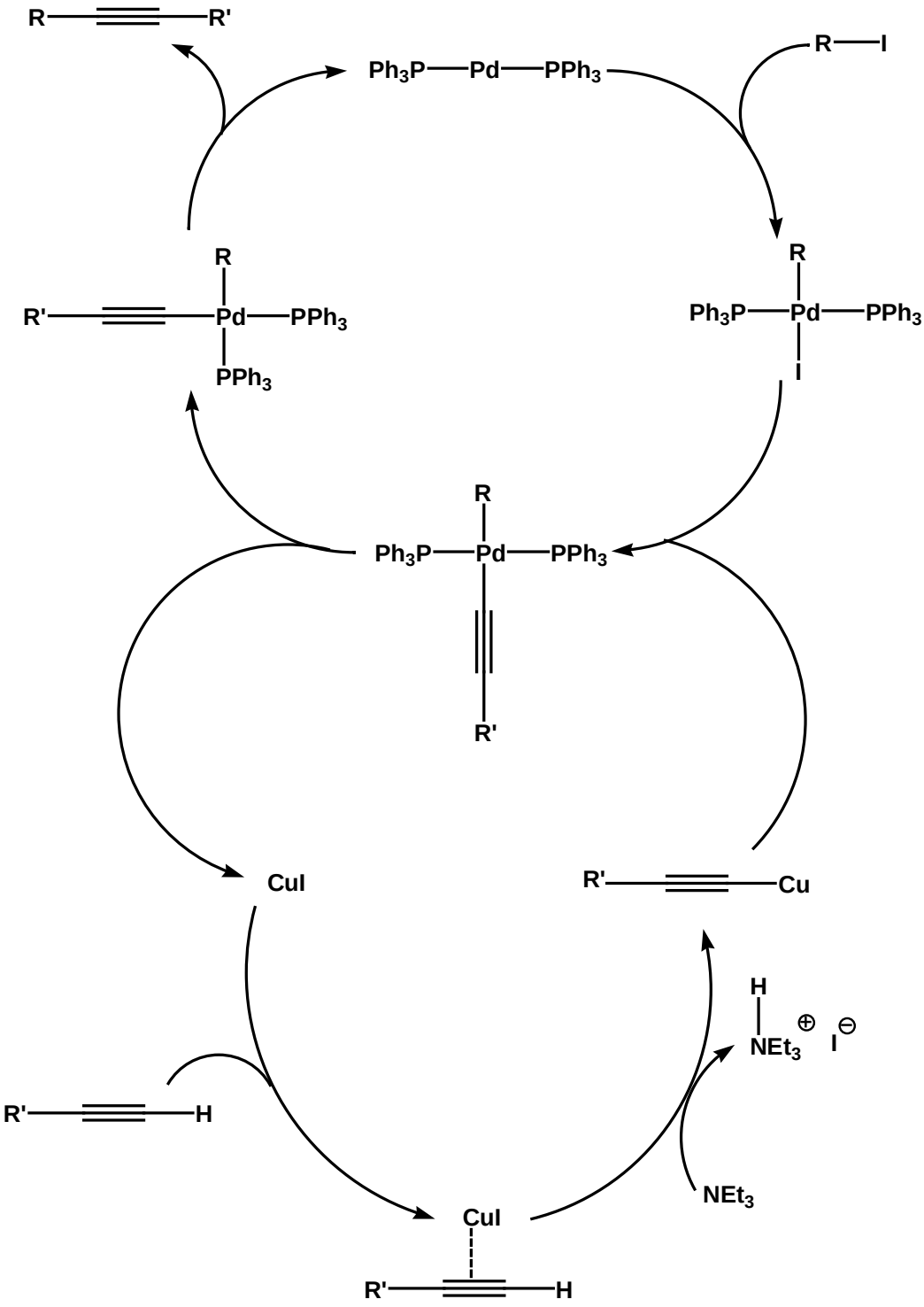

Figure 4.8: general scheme for the Sonogashira coupling of acetylides

The synthesis of 4,4'-diethynyl-biphenyl (Figure 4.9) was performed by reaction of 4,4'-diodo-1,1-biphenyl with trimethylsilyl acetylide (TMSA) using dry degassed Et_3N in the presence of $Pd(PPh_3)_2Cl_2$ and CuI. A catalytic amount of the

intermediate compound bearing terminal ethynyl-tri-methylsilyl groups was purified by silica gel chromatography and, hydrolysed to the bis-acetylide in a solution of MeOH/NaOH, after which further purification by silica gel chromatography was required. Formation of the desired bis-acetylide species, with an overall yield of 33%, was confirmed by proton NMR and mass spectrometry with reference to literature data for the same molecule.

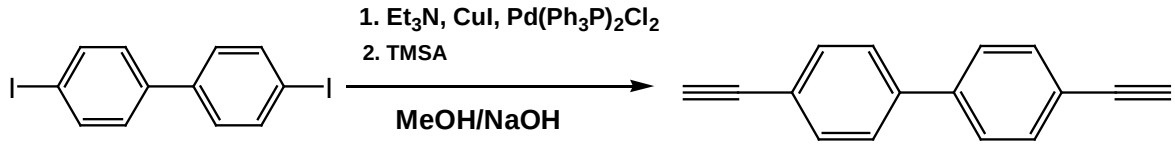

Figure 4.9: scheme for the synthesis of 4,4'-diethynyl-biphenyl

The synthesis of an analogous biphenyl bearing tetrazolyl rings at the two extremes of the molecule was also carried out (Figure 4.10). The synthesis of this molecule required two successive steps. The first step comprised homo-coupling between two molecules of 4-bromo-benzonitrile, under conditions similar to those adopted for the Suzuki cross-coupling. The reaction was carried out in DMF, using $Pd(CH_3CN)_2Cl_2$ as a catalyst and in the presence of Et_3N, giving the target compound in 22% yield, after silica gel purification.

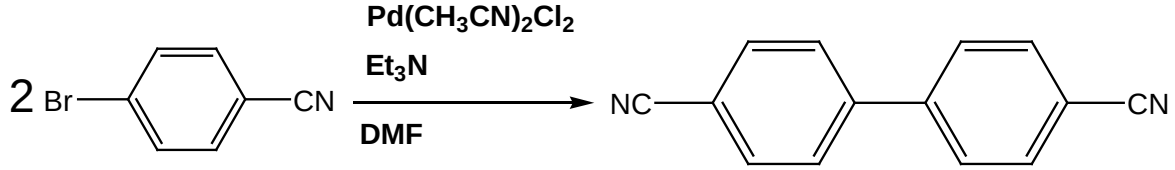

Figure 4.10: scheme for the synthesis of 4,4'-bis-cyanobiphenyl

The 4,4-bis-cyano-biphenyl was then converted into a bis-tetrazolyl system (Figure 4.11) by means of a 1,3-cycloaddition, with azide anion, performed by treatment of the nitrile with NaN_3 in the presence of $[Et_3NH]^+[Cl]^-$ in toluene at 0°C. The desired product was obtained as a precipitate from the reaction mixture upon protonation of the sodium tetrazolyl species, with a yield of 48% from the nitrile species.

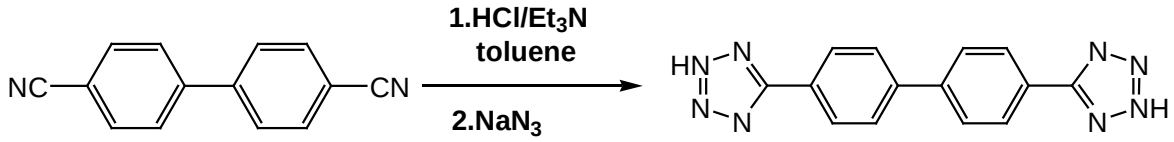

Figure 4.11:scheme for the synthesis of 4,4'-tetrazolyl-biphenyl

4.2.2. Synthesis of homo-metallic dinuclear complexes

As discussed in Chapter 2, the chlorine atom in the sixth coordination site, in the Ir(N^C^N)(N^C)Cl class of complexes, can be easily displaced allowing introduction of monodentate ancillary ligands. There, we discussed the synthesis of cyano, thiocyano and acetylide complexes in this way.

The synthesis of an aryl bis-acetylide bridged dinuclear complex was accomplished using the methodology described earlier for mononuclear acetylide adducts. Thus, Ir(**L3**)(ppy)Cl **(5)** was treated with 4,4'-diethynyl-biphenyl (2:1 ratio) in the presence of KOH and CuI, to give the target complex in 53% yield (Figure 4.12). Its identity was confirmed by proton NMR, which showed a peak pattern characteristic of the previously studied iridium mononuclear complexes and two doublets for the protons located on the phenyl rings of the bridge. Mass spectrometry revealed a peak corresponding to the desired dinuclear system with an isotopic pattern characteristic of dinuclear iridium complexes.

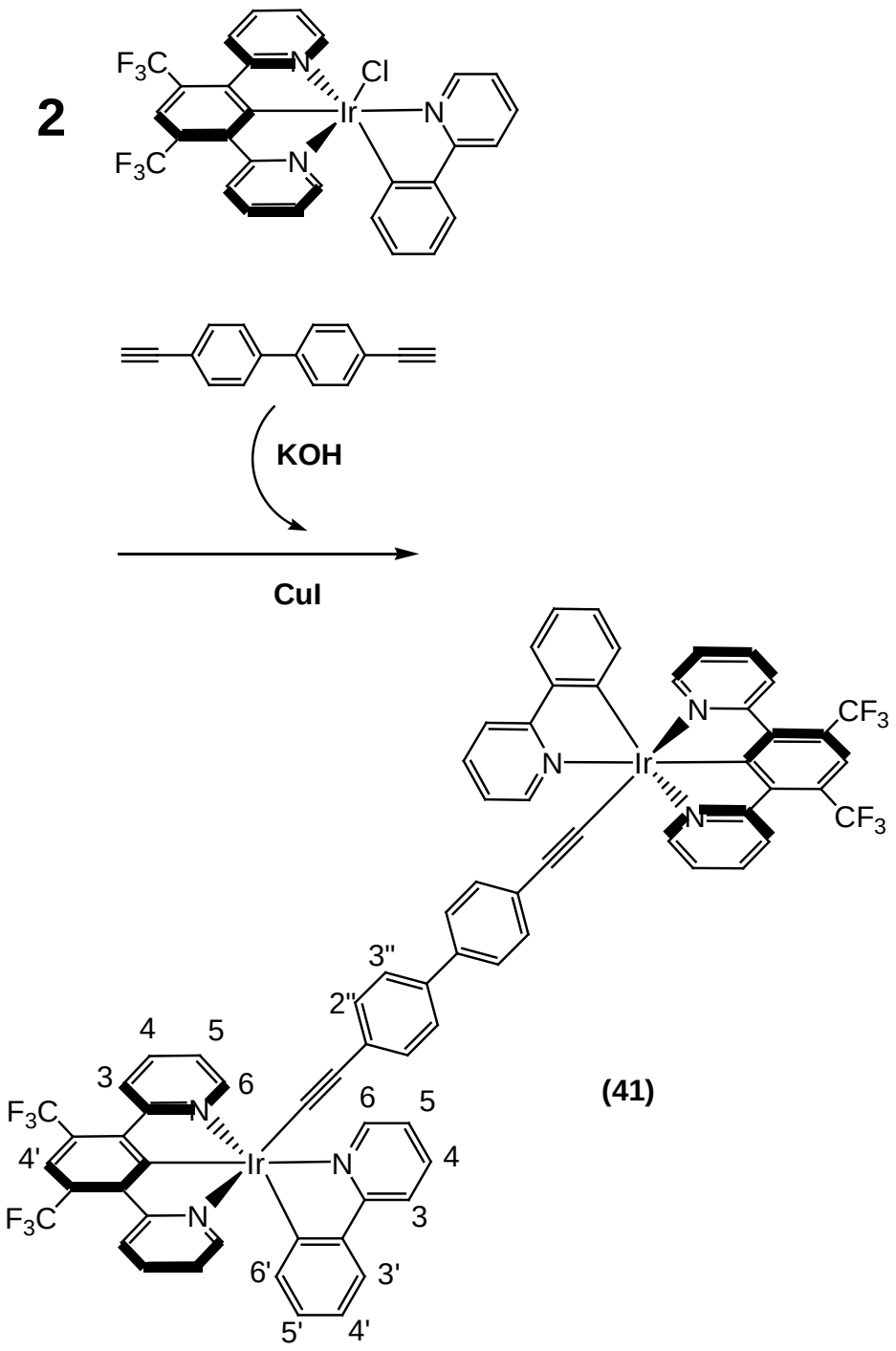

Figure 4.12: synthetic scheme for the synthesis of [{Ir(**L3**)(ppy)}$_2$(μ-bpha)] **(41)**.

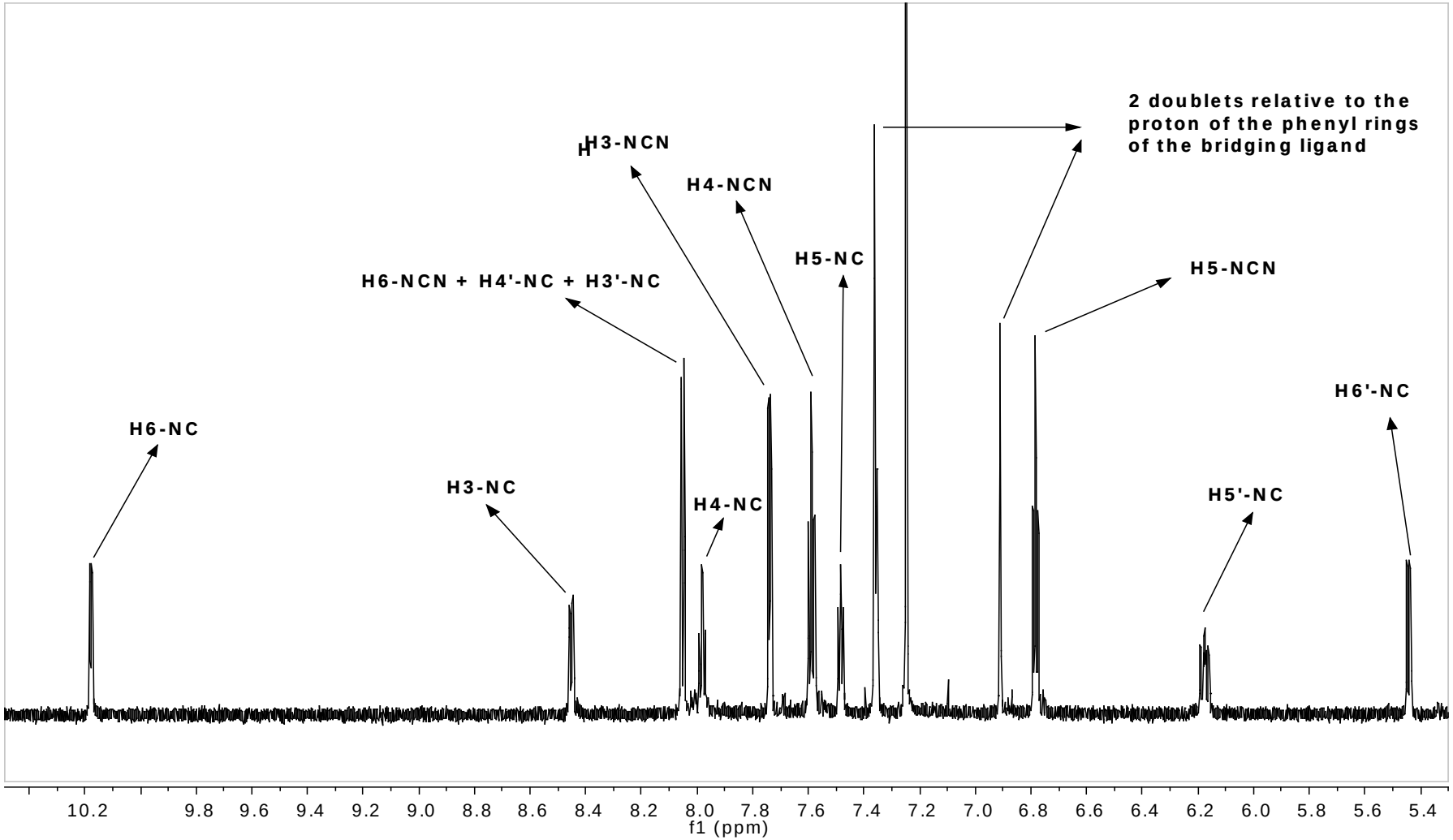

Figure 4-13: ^{1}H-NMR in $CDCl_3$ of [{Ir(**L3**)(ppy)}$_2$(μ-bpha)] **(41)**.

In order to investigate the possibility of introducing tetrazolyl type of monoanionic ancillary ligands onto the [Ir(**L3**)(ppy)]$^{+}$ fragment, prior to working with the bistetrazole, the synthesis of Ir(**L3**)(ppy)(phtr) **(36)** (phtr = 5-phenyl-tetrazole) (Figure 4.15) and Ir(**L3**)(ppy)(Brphtr) **(37)** (Brphtr = 1-(4-bromo-phenyl-tetrazole)) was attempted. Tetrazole-based monoanionic ancillary ligands have already been used in Ru(II) complexes by Stagni and co-workers.[226] The tetrazole was first deprotonated, by treatment with Et_3N, and reacted with a solvato-complex ([Ru(tpy)(bpy)(acetone)]$^{3+}$, prepared by pretreatment of the corresponding chloro complex with $AgPF_6$ (Figure 4.14). The same method was thus adopted to introduce monodentate phenyl tetrazole-based ancillary ligands onto the iridium coordination sphere.

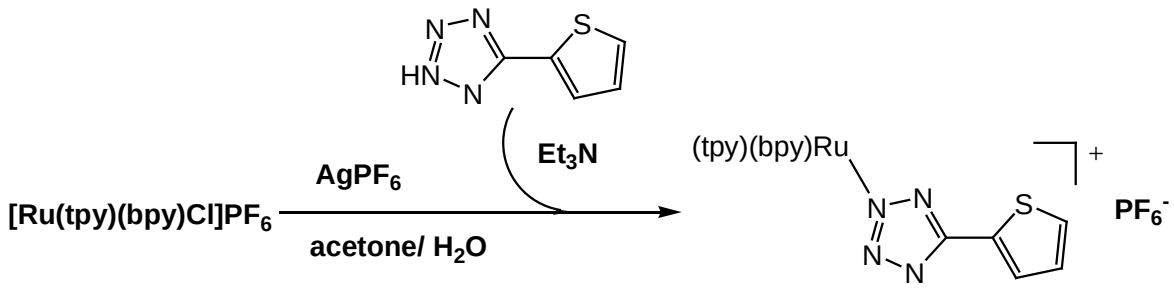

Figure 4.14: synthesis of [Ru(tpy)(bpy)(thtr)]$^{+}$ carried out by Stagni *et al.*

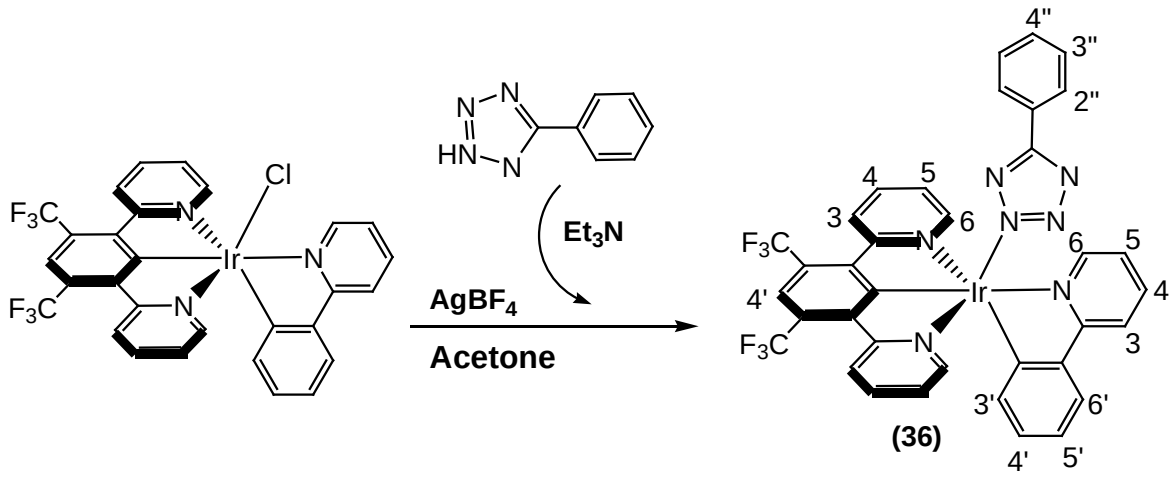

Figure 4.15: scheme for the synthesis of Ir(**L3**)(ppy)(phtr) **(36)**.

The synthetic route summarised in Figure 4.15 involves two steps. In the first, the mononuclear species Ir(**L3**)(ppy)Cl **(5)** is treated with $AgBF_4$ in a solution of acetone/water 2:1 (v/v) to remove the ancillary chlorine atom from the iridium coordination sphere. During the second step, the so-formed solvato-complex is reacted with the anion of 5-phenyl tetrazole pre-formed by deprotonation with Et_3N, giving the complex in 28% yield. An identical method was adopted for the synthesis of Ir(**L3**)(ppy)(Brphtr) **(37)**, obtained with a yield of 97%.

Having established a reliable method for the introduction of the tetrazolate anion, the same approach was then applied to coordination of the bis-tetrazolate to two iridium fragments (1:2 stoichiometric ratio) to form homo-metallic dinuclear complex (Figure 4.16). The target complex was purified by silica gel chromatography, with a yield of 10%.

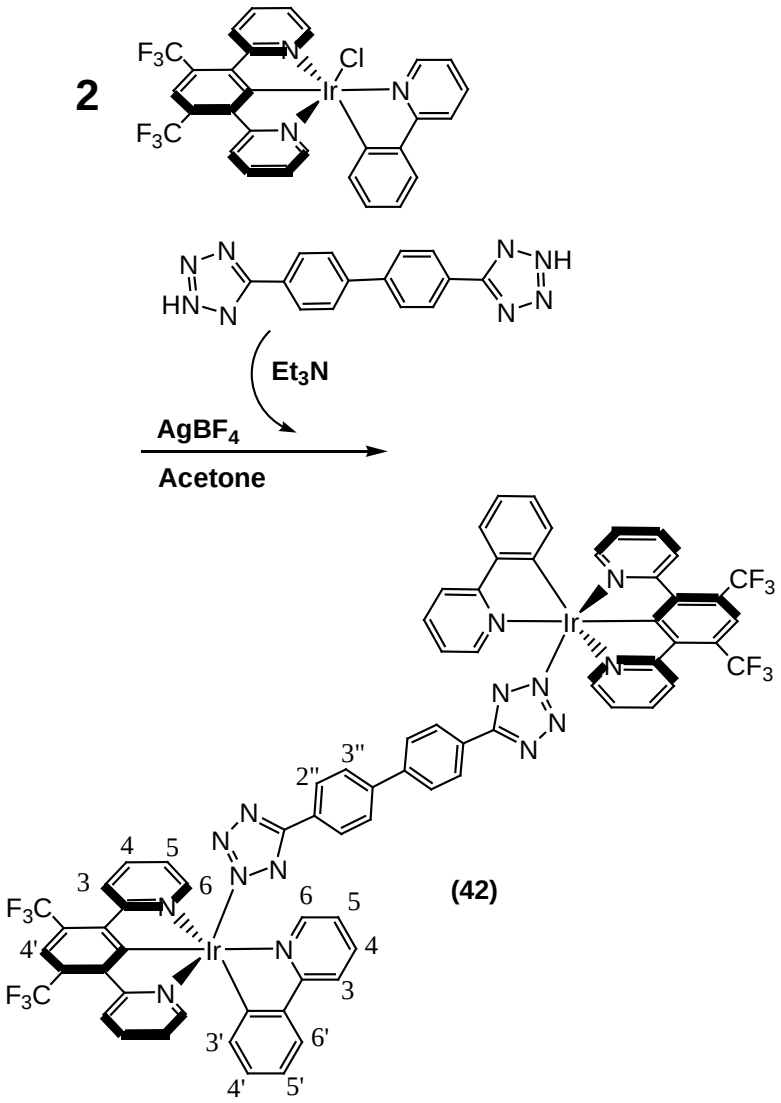

Figure 4.16: scheme for the synthesis of [{Ir(**L3**)(ppy)}$_2$(μ-bphtr)] **(42)**.

4.3. Electrochemistry and preliminary assessment of photophysical properties

4.3.1. Electrochemical studies

Electrochemical studies (Table 4.1), carried out in degassed dichloromethane solution, of the homo-metallic complexes synthesised in this work, revealed pseudoreversible oxidation at 1.11 V (vs SCE) for [{Ir(**L3**)(ppy)}$_2$(μ-bpha)] **(41)** and an irreversible oxidation at 0.70 V for [{Ir(**L3**)(ppy)}$_2$(μ-bphtr)] **(42)**. These values

are similar to those previously reported for homo-metallic iridium complexes (e.g. [{Ir(**L1**)}$_2$μ-(mtbpy-ϕ_n-mtbpy)]$^{2+}$ E^{ox} = 0.84 V and [{Ir(**L1**)}$_2$μ-(mtbpy-ϕ_4-mtbpy)][PF_6]$_2$ E^{ox} = 1.01 V (vs SCE)).[24] As for the homo-metallic complexes studied previously by the research group, the weak electronic communication between the two iridium centres and the symmetry of the dinuclear complex lead to oxidations, for both complexes, at the same potential for each metallic unit of the complex. Comparing the oxidation of the tetrazolyl bridged species with the analogue monometallic complex Ir(**L3**)(ppy)(Brphtr) **(37)**, due to the presence of the bridging ligand which probably allows a major delocalisation of the positive charge over the dinuclear complex, oxidation occurs at lower potentials.

The presence of the bridging ligand influences also the reduction, which is located at more accessible potentials, compared with the processes relative to the mononuclear species reported in Table 4.1 and with Ir(**L3**)(ppy)Cl **(5)**, which displayed a reduction process at –1.97 V vs SCE.

Complex	E_{ox} / V vs SCE	E_{red} / V vs SCE
Ir(L3)(ppy)Cl (5)	1.02 $E^{1/2}$	–1.97 $E^{1/2}$
Ir(L3)(ppy)(Brphtr) (37)	1.35 E^{p}	-1.76 $E^{1/2}$
[{Ir(L3)(ppy)}$_2$(μ-bpha)] (41)	1.11 $E^{1/2}$	-0.51 E^{p}
[{Ir(L3)(ppy)}$_2$(μ-bphtr)] (42)	0.70 E^{p}	-1.45 $E^{1/2}$

Table 4.1: electrochemical data cyclic voltammetry in degassed solution of dichloromethane

4.3.2. Ground state absorption

Ground state absorption data are summarised in Table 4.2 with the spectra portrayed in Figure 4.17. The dinuclear complexes here discussed display intense bands between 225 nm and 360 nm, similar behaviour to that observed for previously studied homo-metallic dinuclear iridium complexes. The bands between 225 nm and 300 nm are assigned as π-π* transitions, whereas the transitions between 300 nm and 360 nm are assigned as CT transitions related to the bridging ligand, which are significantly more intense for the dinuclear species

than those of the analogous mononuclear complexes Ir(**L3**)(ppy)(phtr) **(36)** and Ir(**L3**)(ppy)Cl **(5)** (Figure 4.17). At lower energies, the dinuclear complexes display MLCT/LLCT bands. Comparing the MLCT/LLCT bands of [{Ir(**L3**)(ppy)}$_2$(μ-bphtr)] **(42)** and Ir(**L3**)(ppy)(phtr) **(36)**, the bands relative to the dinuclear complex are slightly blue-shifted compared to those of the mononuclear by around 5-10 nm. Both [{Ir(**L3**)(ppy)}$_2$(μ-bphtr)] **(42)** and [{Ir(**L3**)(ppy)}$_2$(μ-bpha)] **(41)** display MLCT/LLCT bands blue-shifted to those of Ir(**L3**)(ppy)Cl **(5)** of around 10-20 nm. The dinuclear species also display weaker MLCT bands above 500 nm, as observed in the mononuclear species.

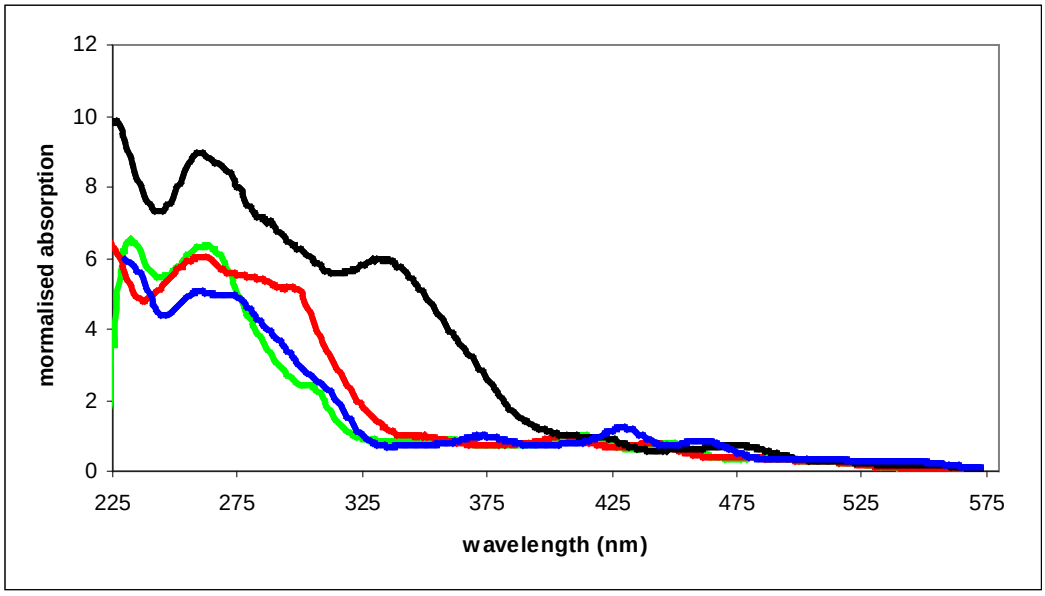

Figure 4.17: normalised absorption spectra to the most intense low-enegy band in dichloromethane at room temperature for Ir(**L3**)(ppy)(phtr) **(36)** (green line), Ir(**L3**)(ppy)Cl **(5)** (blue line), [{Ir(**L3**)(ppy)}$_2$(μ-bphtr)] **(42)** (red line) and [{Ir(**L3**)(ppy)}$_2$(μ-bpha)] **(41)** (black line).

4.3.3. Emission and excited states

Emission of the dinuclear complexes in degassed dichloromethane solution at ambient temperature (Figure 4.18) displays broad structureless bands for both complexes, with emission maxima respectively at 602 nm and 556 nm for the diethynyl bridged and the tetrazolyl bridged species. The emission is assigned as

mixed CT and LC character and each of the dinuclear complexes has an emission maximum at similar energies in relation to that of the mononuclear complexes containing the corresponding homotopic ancillary ligand. In fact, [{Ir(**L3**)(ppy)}$_2$(μ-bpha)] **(41)** displays a maximum at 602 nm, similar to that of Ir(**L3**)(ppy)(**A1**) **(31)** (λ_{max} = 606 nm) and [{Ir(**L3**)(ppy)}$_2$(μ-bphtr)] **(42)** with emission maximum at 556 nm, similar to that of Ir(**L3**)(ppy)(Brphtr) **(37)** (λ_{max} = 553 nm). Comparing the two dinuclear species with Ir(**L3**)(ppy)Cl **(5)** (λ_{max} = 590 nm), [{Ir(**L3**)(ppy)}$_2$(μ-bpha)] **(41)** is red-shifted and [{Ir(**L3**)(ppy)}$_2$(μ-bphtr)] **(42)** blue-shifted. These values suggest only weak participation of the bridging ligand in the excited states of the complexes. This is supported by the similarity in the lifetimes of the dinuclear and mononuclear species. The calculated luminescence quantum yields of the dinuclear complexes are respectively 0.15 for [{Ir(**L3**)(ppy)}$_2$(μ-bpha)] **(41)** and 0.40 for [{Ir(**L3**)(ppy)}$_2$(μ-bphtr)] **(42)**, values similar to those measured for the mononuclear anologues.

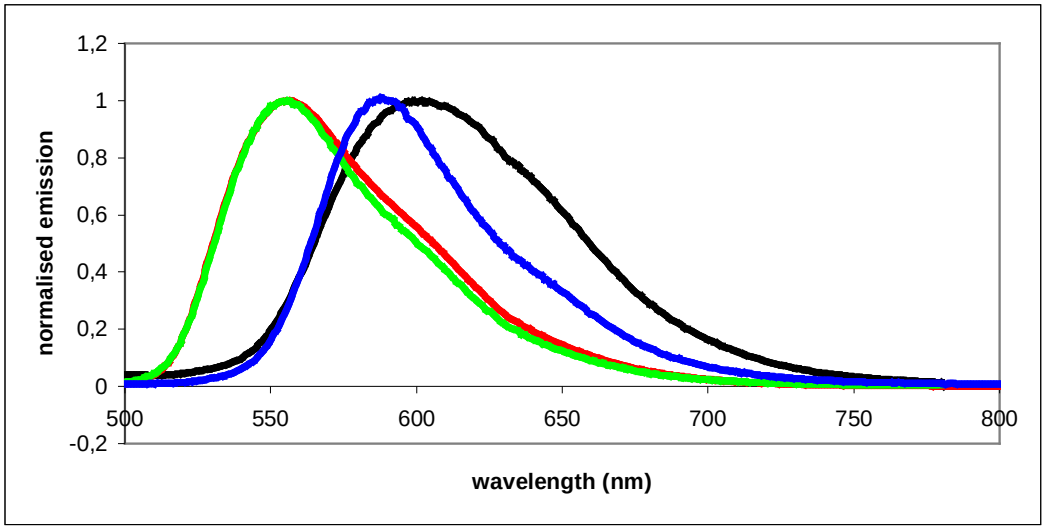

Figure 4.18: normalised emission spectra in dichloromethane at room temperature of [{Ir(**L3**)(ppy)}$_2$(μ-bphtr)] **(42)** (red line) and [{Ir(**L3**)(ppy)}$_2$(μ-bpha)] **(41)** (black line), Ir(**L3**)(ppy)Cl **(5)** (blue line) and Ir(**L3**)(ppy)(phtr) **(36)** (green line).

Complex	λ_{max} / nm	τ degassed (aerated)	Φ_{LUM} in degassed solution	k_r /10^4 s^{-1}	Σk_{nr} / 10^4 s^{-1}	k_Q /10^8 $M^{-1}s^{-1}$	Absorption λ_{max} / nm (ε / mol^{-1} dm^3 cm^{-1})
Ir(L3)(ppy)Cl (5)	590	3300 (1100)	0.46	14	16	28	259 (45 600), 272 (45 300), 373 (8 900), 429 (11 100), 461 (8 000), 506 (3 100), 541 (2 400)
Ir(L3)(ppy)(phtr) (36)	556	5 300 (1 800)	0.34	6.4	13	16	233(48 400), 262(46 500), 306(18 600), 362(6 800), 413(7 600), 452(6 100), 491(3 000), 527(1 600)
Ir(L3)(ppy)(Brphtr) (37)	553	5 300 (1 900)	0.32	6	13	15	235(38 400), 264(42 900), 304(15 100), 360(4 900), 412(5 500), 450(4 400), 493(1 900), 515(1 400)
[{Ir(L3)(ppy)}$_2$(μ-bpha)] (41)	602	1 500 (600)	0.15	10	56	45	232(52 900), 265(45 600), 342(25 400), 424 (6 500), 482(3 600), 529(2 100), 570(1 600)
[{Ir(L3)(ppy)}$_2$(μ-bphtr)] (42)	556	5 200 (1 900)	0.40	8	11	14	231(52 300), 268(44 000), 299(37 200), 351(15 300), 405 (7 100), 441(5 800), 480(3 200), 513(2 000)

Table 4.2: Luminescence data in solution in dichloromethane at 298±3 K, where; radiative (k_r) and non-radiative (Σk_{nr}) rate constants are calculated from τ and Φ_{lum} values; estimated uncertainty ±20%; k_Q, bimolecular rate constant for quenching by O_2, estimated from τ values in degassed and aerated solutions.

4.4 Concluding remarks

In Chapter 2 the availability of the sixth coordination site of Ir(**L3**)(ppy)Cl **(5)** has been confirmed by the introduction, of acetylide-type monodentate ancillary ligands into this position displacing the Cl atom. In this Chapter, the synthesis of a dinuclear homo-metallic complex ([{Ir(**L3**)(ppy)}$_2$(μ-bpha)]) **(41)** is reported, which was obtained from Ir(**L3**)(ppy)Cl **(5)** as "building block" and a linear bis-acetylide as a bridging ligand with a yield of 53%.

Also the reactivity of Ir(**L3**)(ppy)Cl **(5)** towards tetrazoles was investigated. The synthesis of [{Ir(**L3**)(ppy)}$_2$(μ-bphtr)] **(42)** (Y = 10%) is also reported by using Ir(**L3**)(ppy)Cl **(5)** as a "building block" and a bis-tetrazole bridging ligand.

The complexes synthesised in Chapter 2, whose photophysical properties are discussed in Chapter 3, can thus also be used as "building blocks" for the preparation of multimetallic systems.

CHAPTER 5

Experimental

5. Experimental

5.1. Synthetic procedures and characterisation

The solvents used throughout were of Analar® quality and used as supplied, except for acetonitrile which was HPLC grade. Water was purified using the $Purite_{STILL}$ Plus™ system having conductivity of ≤ 0.04 μS cm^{-1}. All reagents were used as supplied.

Thin layer chromatography was carried out using silica plates (Merck Art 5554) or neutral aluminium oxide plates (Merck Art 5550), both types being fluorescent upon irradiation at 254 nm. Preparative column chromatography was carried out using silica (Merck Silica Gel 60, 230-400 mesh), or neutral alumina (Merck Aluminium Oxide 90, Brockman activity 2-3).

NMR spectra were recorded on a Varian Mercury-200 spectrometer (200 MHz for ^{1}H, 50 MHz for ^{13}C and 188 MHz for ^{19}F), Varian Unity-300 spectrometer (300 MHz for ^{1}H), Varian Mercury-400 spectrometer (400 MHz for ^{1}H and 101 MHz for ^{13}C), Bruker Advance-400 spectrometer (400 MHz for ^{1}H), Varian Inova-500 spectrometer (500 MHz for ^{1}H, 126 MHz for ^{13}C and 470 MHz for ^{19}F) or Varian DD-700 spectrometer (700 MHz for ^{1}H, 176 MHz for ^{13}C and 658 MHz for ^{19}F), and were referenced to residual protiosolvent resonances. All NMR data is reported with chemical shifts (δ) quoted in ppm and coupling constants (J) in Hz. ^{1}H-NMR spectra were assigned with assistance from ^{1}H-^{1}H COSY (correlation spectroscopy, through-bond interactions) and ^{1}H-^{1}H NOESY (nuclear Overhauser effect spectroscopy, through-space interactions) spectra. ^{13}C-NMR spectra were recorded with proton decoupling and were assigned with assistance from ^{1}H-^{13}C HSQC (heteronuclear single quantum correlation) and ^{1}H-^{13}C HMBC (heteronuclear multiple bond correlation) spectra.

Electrospray ionisation mass spectra (ES^{+} MS and ES^{-} MS) were recorded with a Micromass LCT spectrometer or Thermo-Finnigan LTQ FT spectrometer with methanol or acetonitrile as the carrier solvent. MALDI mass spectra were recorded with a Voyager-DE STR BioSpectrometry Workstation or a Thermo-

Finnigan LTQ FT spectrometer. High resolution mass spectra were recorded with a Micromass LCT spectrometer at 5000 resolution using sodium iodide as the reference, or a Thermo Finnigan LTQ FT spectrometer at 100000 resolutions with external calibration. Electron ionisation, EI, mass spectra and the corresponding high resolution mass spectra were recorded by the EPSRC National Mass Spectrometry Service at the University of Wales, Swansea. Gas chromatography-mass spectra (GC-MS) were recorded using a Thermoquest Trace mass spectrometer. Accurate ASAP spectra were recordered with Xevo QtoF mass spectrometer (Waters, Ltd, UK).

C, H and N analysis was performed using an Exeter Analytical E-440 elemental analyser. Melting points were determined on a Gallenkamp 889339 capillary melting point apparatus and are quoted to the nearest 1^{o}C.

5.2. Photochemical and photophysical measurements

UV-visible absorption spectra were measured using a Biotek Instruments XS spectrometer operating with LabPower software. All samples were contained in quartz cuvettes of 1 cm pathlength, and run against a reference of pure solvent contained within a matched cuvette. Extinction coefficients were determined by dilution technique and graphical application of the Beer-Lambert law.

$$A(\lambda) = \varepsilon(\lambda)cl$$

$A(\lambda)$ is the absorbance at a specified wavelength, $\varepsilon(\lambda)$ is the extinction coefficient at that wavelength ($dm^3\ mol^{-1}\ cm^{-1}$), c is the concentration of the species that is absorbing ($mol\ dm^{-3}$) and l is the pathlength (cm).

Steady-state luminescence spectra were recorded using a Jobin Yvon FluoroMax-2 spectrofluorimeter, equipped with a red-sensitive Hamamatsu R928 photomultiplier tube (PMT), and operated with DataMax software. Samples for emission measurements were contained within quartz fluorescence cuvettes of 1 cm pathlength and the absorbance of each solution at the excitation wavelength was kept below 0.1 to minimise inner filter effects. Emission was detected at right

angles to the emission source, with appropriate filters used where required to remove second order peaks. All emission spectra were corrected after data acquisition for the dark count and for the wavelength dependent spectral response of the detector. All quoted emission maxima refer to the values after correction. Excitation spectra were automatically corrected for lamp output, through use of a beam splitter, which directs 8% of the excitation light to a reference photodiode.

Luminescence quantum yields were recorded with respect to a standard of ruthenium(II) tris(2,2'-bipyridine) chloride in aqueous solution, where $\Phi_{st} = 0.028$ and solution containing 2,6-di(2-pyridyl)benzene-1-platinum(II) chloride in degassed CH_2Cl_2 ($\Phi = 0.60$ [ref]) as standards; estimated uncertainty in Φ is ± 20% or better .[226] The luminescence quantum yield of the sample (Φ) is calculated relative to the standard using the following equation.[227]

$$\Phi = \Phi_{st}\left[\frac{I}{I_{st}}\right]\left[\frac{A_{st}}{A}\right]\left[\frac{n^2}{n_{st}^2}\right]$$

Where *I* is the integrated emission intensity at a given excitation wavelength, *A* is the absorbance at that wavelength and *n* is the refractive index of the solvent. The symbols with the subscript ‘st’ are the respective values for the standard.

The quartz cuvettes of 1 cm pathlength used for emission measurements were modified with appropriate glassware to allow connection to a high-vacuum line. The degassing of samples was achieved by a minimum of three freeze-pump-thaw cycles, whilst connected to the high-vacuum line. A final vapour pressure of < 5 x 10^{-2} mbar at 77 K was achieved, monitored using a Pirani gauge.

Low temperature (77 K) measurements of the samples were obtained as EPA glasses (EPA = diethyl ether-isopentane-ethanol, 2:2:1 by volume). The sample as a solution in EPA was placed in a 4 mm diameter glass tube; then lowered inside a glass Dewar of liquid nitrogen where it remained whilst the measurements were taken.

The excited state lifetime measurements were measured using time-correlated single-photon counting (TCSPC). The samples were excited in 1 cm pathlength quartz fluorescence cuvettes at 374.0 nm with an EPL-375 pulsed-diode laser. The emitted light passed through a monochromator and was detected at 90^{o} using a Peltier-cooled R928 photomultiplier tube. The estimated uncertainty in these lifetimes is < 10%. Longer lifetimes, > ~ 10 μs, were measured using multi-channel scaling following excitation by a pulsed xenon lamp.

5.3. Electrochemical measurements

Cyclic voltammetry was carried out in a background electrolyte of tetrabutylammonium tetrafluoroborate (0.1 or 0.02 M) in acetonitrile. A μAutolab type III potentiostat was used with computer control and data storage *via* GPES Manager. A three electrode assembly was employed, consisting of a platinum wire counter electrode, platinum flag reference electrode and a platinum working electrode. The measurements were carried out in a glass cell charged with 2 mg of complex in 2 mL of electrolyte and purged with nitrogen.

5.4. Density functional theory calculations

B3LYP density functional theory, DFT, calculations were performed using the Gaussian98[(228)] and Gaussian03[(229)] software packages. "Double-ζ" quality basis sets were employed for the ligands (6-31G) and the iridium and rhodium metal centres (LANL2DZ).[(230)] The inner core electrons of iridium were replaced with a relativistic effective core potential (ECP), leaving the outer core [$(5s)^2(5p)^6$] electrons and the $(5d)^6$ valence electrons of iridium(III). Likewise for rhodium(III) the inner core electrons were replaced leaving the outer core [$(4s)^2(4p)^6$] electrons and the $(4d)^6$ valence electrons. The geometries were fully optimised without symmetry constraints.

5.5. X-ray crystallography

The single crystal X-ray diffraction experiments were carried out at 120 K, using graphite monochromated Mo Kα radiation (λ = 4.855 Å) on a Bruker SMART 1K area detector diffractometer, equipped with a Oxford Cryosystems N_2 open-flow cooling device. Series of narrow ω-scans (0.3˚) were performed at several φ-settings in such a way as to cover a sphere of data to a maximum resolution between 0.70 and 0.77 Å. Cell parameters were determined and refined using the Bruker SMART software, and raw frame data were integrated using the Bruker SAINT program. The structure was solved by direct methods and refined by full-matrix least squares on F^2 using SHELX. Reflection intensities were corrected by numerical integration using SADABS. All non-hydrogen atoms were refined with anisotropic displacement parameters and the hydrogen atoms were positioned geometrically and refined using a riding model. Crystal data and structure refinement parameters: Ir(**L1**)(dFppy)Cl **(1)**: $C_{62}H_{50}N_6Ir_2Cl_{10}F_4$; M_r = 1693.98.55; triclinic, space group P-1, *a* = 9.0957(7), *b* = 11.7420(10), *c* = 15.0721(12) Å, *a* = 102.7213(14), *β* = 93.4583(14), *g* = 102.1817(14)˚; V = 1525.2(3) $Å^3$; D_c = 1.844 mg mm^{-3}; Z = 1; *μ* = 4.855 mm^{-1}; reflections collected/unique 19537 / 7357 [R_{int} = 0.0665]; final *R* indices [$I > 2\sigma(I)$]: R_1 = 0.0450 and *w*R_2 = 0.0949; *R* indices (all data): R_1 = 0.0673 and *w*R_2 = 0.1029. Ir(**L3**)(ppy)Cl **(5)**: $C_{33}H_{27}ON_3IrClF_6$; M_r = 823.23; *T* = 120 K; triclinic, space group P-1, *a* = 8.8709(15), *b* = 11.996(2), *c* = 14.940(3) Å, *a* = 85.119(6), *β* = 89.961(6), *g* = 75.957(6)˚; V = 1536.4(4) $Å^3$; D_c = 2.007 mg mm^{-3}; Z = 2; *μ* = 4.501 mm^{-1}; reflections collected/unique 21764 / 8106 [R_{int} = 0.0368]; final *R* indices [$I > 2\sigma(I)$]: R_1 = 0.0299 and *w*R_2 = 0.0648; *R* indices (all data): R_1 = 0.0406 and *w*R_2 = 0.0682.

5.6. Synthesis of bidentate ligands (N^C)

Synthesis of 2-(4,6-difluorophenyl)-pyridine[208] [dFppyH]

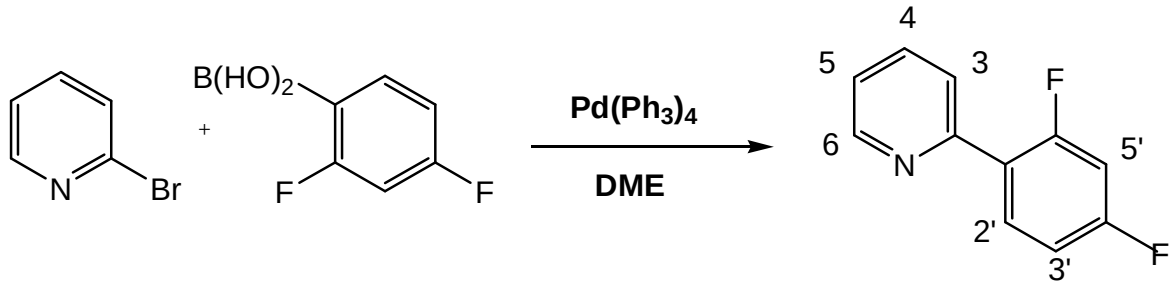

A mixture (2.9 ml, 3.0 mmol) of 2-bromo-pyridine, 525 mg (3.3 mmol) of 2,4-difluoro-phenyl boronic acid, K_2CO_3 (1.24 g, 9.0 mmol) in 0.2 mL of water was dissolved in 10 mL of DME, was degassed via three freeze-pump-thaw cycles and $Pd(PPh_3)_4$ (173 mg, 0.15 mmol) was added under nitrogen. The reaction mixture was then refluxed under nitrogen atmosphere for 22 hours and cooled to room temperature. The DME was removed under reduced pressure and DCM was added to the residue and the solution was washed with 3*100 mL of aqueous solution of NaOH 1M. The organic layer was collected and dried over $MgSO_4$. Purification was achieved by silica gel chromatograohy (from 100% hexane up to 98% hexane, 2% ether). The product was a white solid 280 mg (1.47 mmol, 49%). ^{1}H-NMR ($CDCl_3$, 400 MHz): δ 8.72 (d, 1H, ^3J = 4.5, H^6), 8.00 (td, 1H, ^3J = 8.8, 6.7, $H^{2'}$), 7.77-7.40 (m, 2H, H^4 and H^3), 7.27 (ddd, 1H, ^3J = 8.7, 4.8, 0.9, H^5), 7.07 (dddt, 1H, ^3J = 8.8, 8.0, 2.4, 1.2, $H^{3'}$), 6.92 (dddd, 1H, ^3J = 11.2, 8.8, 2.4, 0.8, $H^{1'}$). ^{13}C-NMR ($CDCl_3$, 400 MHz): δ 164.6-159.4 ($C^{4'}$, $C^{6'}$), 152.6 (C^1), 149.9 (CH^6), 136.6 (CH^4), 124.3 (CH^3), 123.8 ($C^{1'}$), 122.6 ($CH^{2'}$), 112.0 ($CH^{3'}$), 104.5 ($CH^{5'}$). ^{19}F-NMR ($CDCl_3$, 400 MHz): δ -109.7 (1F, m), -113.4 (1F, m). Mass Spectrometry (ES^+) : *m/z* 192 $[M+H]^+$.

Synthesis of 2-(2-pyridyl-N-methyl)benzimidazole[231] [Mepbi]

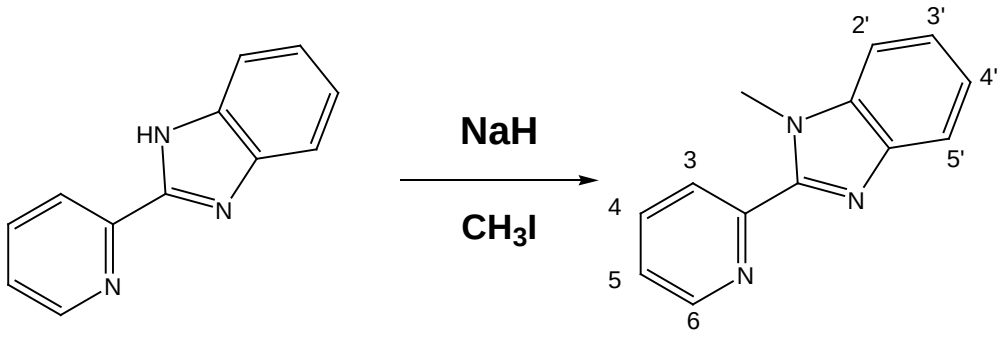

To a suspension of dried THF (~10 ml) and NaH (34 mg, 0.85 mmol) was added a solution of 2-(2-pyridyl)benzimidazole (150 mg, 0.77 mmol). The mixture was strirred for 20 minutes then a solution of MeI (119 mg, 0.85) in THF (~5 ml) was added and stirred overnight. The resulting mixture was then washed with 1M NaOH aqueous solution. The combined organic layer was dried under vacuum evaporation and the product obtained as a yellow/brown solid (77 mg, 48%). H^1-NMR ($CDCl_3$, 400 MHz): δ 8.69 (d, 1H, ^3J = 3.6, H^6), 8.38 (d, 1H, ^3J = 7.6, H^3), 7.85-7.80 (d+t, 2H, $H^{2'}$+$H^{3'}$), 7.43 (d, 1H, ^3J = 8.0, $H^{5'}$), 7.34-7.28 (t+t+t, 3H, H^5+H^4+$H^{4'}$). Mass spectrometry (ES+): *m/z*: 210 $[M]^+$.

Synthesis of 2-Bromo-pyridine-N-oxide[202]

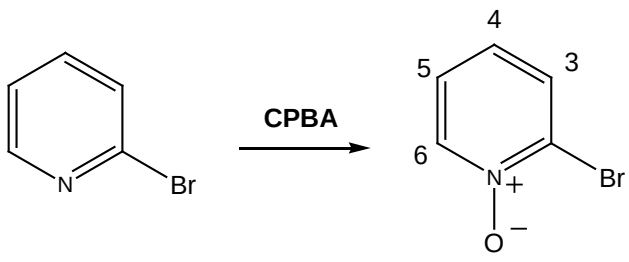

3-Chloroperoxybenzoic acid (4.25 g, 70% pure, 19 mmol) was dissolved in chloroform (50 ml). Then 2-bromopyridine was added (2.5 g, 15.8 mmol) and the mixture stirred at room temperature for 3 days. The resulting mixture was extracted with H_2SO_4 (15%, 3 x 50ml). Sodium thiosulphate was added to the aqueous phase and a yellow precipitate was observed. The solution was neutralised by using Na_2CO_3 and extractions with chloroform were carried out, at this point the solution turned pink. After drying over $MgSO_4$ the solvent was eliminated by vacuum evaporation. The crude product was a purple oil (1.75g, 64%) and was used without purification in the next step. ^{1}H-NMR (CD_3Cl, 400 MHz): δ 8.37 (1H, dd, ^{3}J = 6.7, H^6), 7.65 (1H, dd, ^{3}J = 8.0, H^3), 7.26 (1M, m, H^4), 7.11(1H, td, J=8, H^5).

Synthesis of 2-Bromo-4-nitropyridine-N-oxide[202]

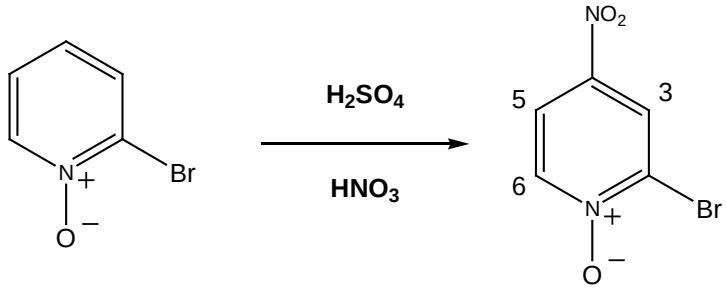

2-Bromopyridine-N-oxide (1.75 g, 8 mmol) was added to aqueous H_2SO_4 (96%, 15 ml) at 0°C. Fuming nitric acid (98%, 5ml) was added to the solution still at 0°C. The resulting mixture was heated at 130°C for 3 hours. After cooling to room temperature the mixture was poured into ice (the solution turned from yellow to green at this stage) and neutralised with Na_2CO_3 and a precipitate was formed,

wich was washed with water. The solid was then dissolved in dichloromethane, dried over $MgSO_4$ and the solvent removed under reduced pressure after filtration. The product was a yellow solid (0.6 g, 2.7 mmol, 27%) and was used without further purification. ^{1}H-NMR ($CDCl_3$, 400 MHz): δ 8.08 (1H, dd, ^3J = 7.2, ^4J = 3.3, H^6), 8.41 (1H, dd, ^3J = 7.2, ^4J = 0.4, H^3), 8.52 (1H, d, ^3J = 3.1, H^5).

Synthesis of 2-Bromo-4-nitropyridine[(202)]

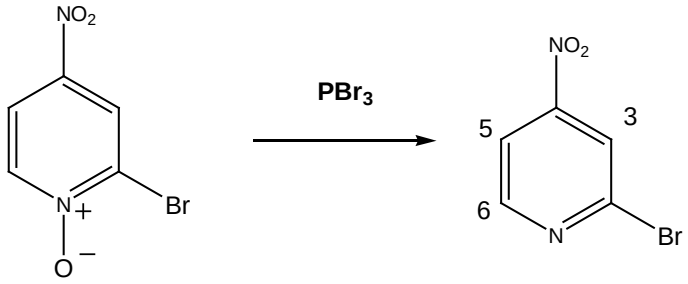

2-Bromo-4-nitropyridine-N-oxide (0.6 g, 2.7 mmol) and PBr_3 (1.1 g, 4.1 mmol) were dissolved in 25 ml of chloroform and refluxed for 2 hours. The resulting mixture then poured into ice and neutralised with Na_2CO_3. Extractions with chloroform were then performed and the organic layer dried over $MgSO_4$. After vacuum evaporation the product was obtained (444 mg, 2.2 mmol, 81%). ^{1}H-NMR ($CDCl_3$, 400 MHz): δ 8.00 (1H, dd, ^3J = 5.4, 2.0, H^6), 8.22 (1H, d, ^3J = 1.9, H^3), 8.68 (1H, d, ^3J = 5.4, H^5).

Synthesis of 2-Bromo-4-methoxypyridine[202] [Br-OMepy]

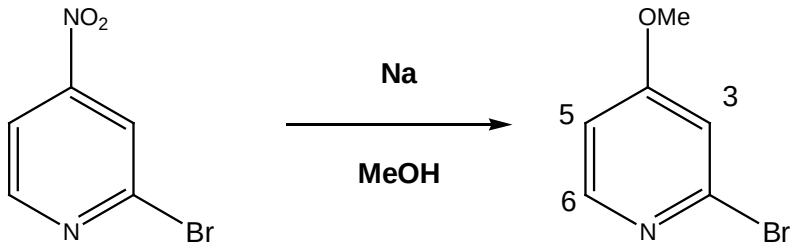

2-Bromo-4-nitropyridine (444 mg, 2.2 mmol) was added to a solution of sodium (0.97 g, 4.4 mmol) in methanol (25 ml). The mixture was stirred at room temperature overnight, then 10ml of water were added and the solvent removed under reduced pressure to give the product as a yellow oil (307 mg, 1.7 mmol, 75%). ^{1}H-NMR ($CDCl_3$, 400 MHz): б 6.78 (1H, dd, ^{3}J = 5.9, H^6), 7.00 (1H, d, 2.3, H^3), 8.17 (1H, d, ^{3}J = 5.8, H^5).

Synthesis of 2-tri-n-butyl-stannyl-4-methylpyridine[232]

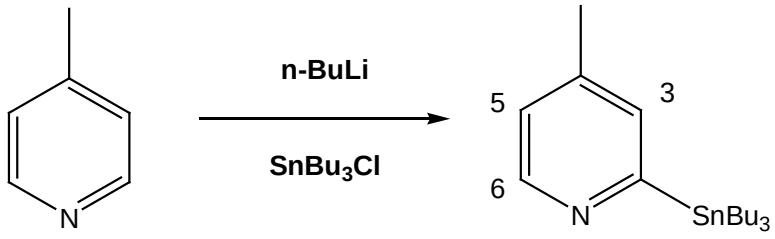

2-(Dimethylamino)ethanol (0.8 ml, 8mmol) and 4-methyl-pyridine (0.39 ml, 4 mmol) were placed in a 100 ml two necked round bottom flask fitted with

condenser and suba seal. Dry hexane was added (25 ml) under nitrogen atmosphere. The solution was cooled to –78°C and a 2.5 M solution of n-BuLi in hexane (10 ml, 16 mmol) was added dropwise over 30 minutes. A solution of Bu_3SnCl (2.8 ml, 4mmol) in 6 ml of THF was then added dropwise over 20 minutes. The mixture was then stirred at –78°C for 90 minutes and allowed to warm to room temperature. To this, 30 ml of water were added and the reaction mixture was stirred at room temperature for 10 minutes. The crude product was extracted in diethyl ether and dried over $MgSO_4$ and the solvent evaporated under vacuum. The product was a brown oil (0.5 g, 1.8 mmol, 45%). ^1H NMR ($CDCl_3$, 400 MHz) δ 8.57 (d, 1H, H^6), 7.20 (s, 1H, H^3), 6.93 (d, ^3J = 2.9, H^5), 2.28 (s, 3H, H^{Me}).

Synthesis of 2-(2,4-difluorophenyl)-4-methyl-pyridine[208] [dFp-Mepy]

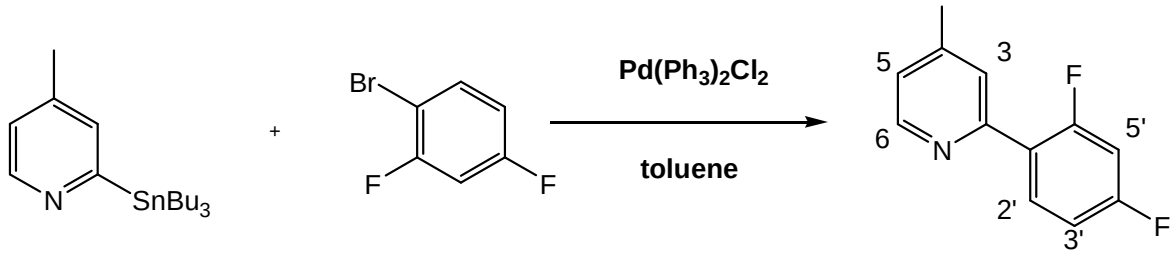

In a Schlenk were added of 2-tri-n-butyl-stannyl-4-methylpyridine 112 mg (0.29 mmol), 2,6-di-Bromo-m-xylene (58 mg, 0.29 mmol), bis(triphenylphosphine)Palladium Chloride (25 mg, 0.1 mmol), triphenyl phosphine (8 mg, 0.028 mmol) dissolved in 5 mL of xylene. The reaction mixture was degassed via five freeze-pump-thaw cycles and heated until reflux temperature was reached for 48 hours. After cooling to room temperature the mixture was added to 20 mL of saturated aqueous solution of KF and stirred for 30 minutes, the solution was then filtered and the solid washed several times with water and

toluene. The filtrate was added to a solution of $NaHCO_3$ (100 mL, 10% w/w) and extracted with DCM (2x100 mL). The combined organic layer was dried over $MgSO_4$ and purified by silica gel separation chromatography (from 100% hexane to 50% ether, 50% hexane). The product was a pale yellow solid 44 mg (0.21mmol, 74%). ^{1}H NMR ($CDCl_3$, 400 MHz): δ 8.58 (d, ^{3}J = 5.3, 1H, H^6), 7.98 (m, 1H, H^3), 7.58 (s, 1H, $H^{5'}$), 7.17 – 6.78 (m, 3H, H^5+$H^{2'}$+$H^{3'}$), 2.46 (s, 3H, H^{Me}). ^{19}F-NMR: -110.04 (1F, s), -113.38 (1F, s). Mass spectroscopy (ES+): *m/z* 206 $[M+H]^+$.

Synthesis of 2-(2,4-difluoro-phenyl)-4-methoxy-pyridine[(208)] [dFp-OMepy]

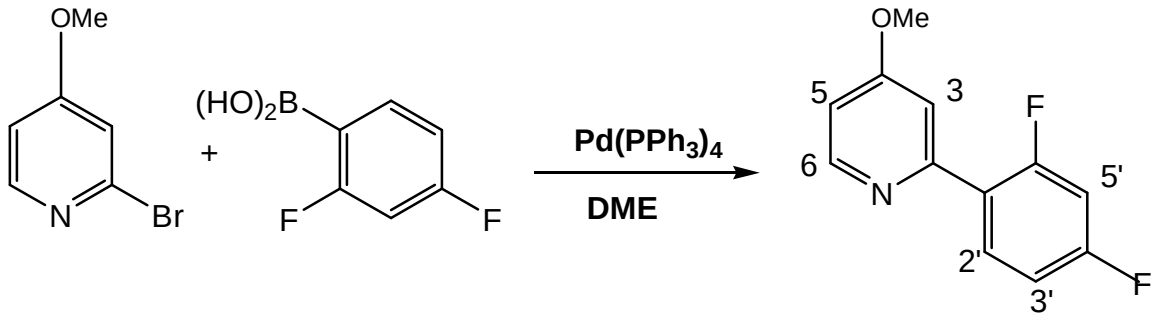

A mixture of 2-bromo-4-methoxypyridine (150 mg, 0.8 mmol), 2,4-difluoro-phenyl boronic acid (126 mg, 0.8 mmol), aqueous K_2CO_3 (300 mg, 2.2 mmol) in 0.2 mL of water, all dissolved in 10 mL of DME was degassed via three freeze-pump-thaw cycles and $Pd(PPh_3)_4$ (58 mg, 0.05 mmol) was added under nitrogen. The reaction mixture was then refluxed under nitrogen atmosphere for 22 hours and cooled to room temperature. The DME was removed under reduced pressure and DCM was added. The solution was washed with 3*100 mL of aqueous solution of NaOH 1M, the organic layer was collected and dried over $MgSO_4$. Purification was achieved by silica gel chromatograohy (from 100% hexane up to 80% hexane, 20% ether). The product was a white solid 150 mg (0.64mmol, 80%). ^{1}H NMR

($CDCl_3$, 400 MHz) δ 8.50 (d, ^3J = 5.7, 1H, H^6), 8.08–7.87 (m, 1H, $H^{5'}$), 7.34–7.18 (m, 1H, H^3), 7.02–6.93 (m, 1H, H^5), 6.88 (d, ^3J = 2.5, 1H, $H^{3'}$), 6.81–6.72 (m, 1H, $H^{2'}$), 3.87 (s, H^{Me}). ^{19}F-NMR: -109.8 (1F, m), -113.1 (1F, m). Mass spectrometry (ES+): *m/z* 220 $[M+H]^+$.

Synthesis of 1-benzo[b]thiophene1-isoquinoline[(208)] [btiq]

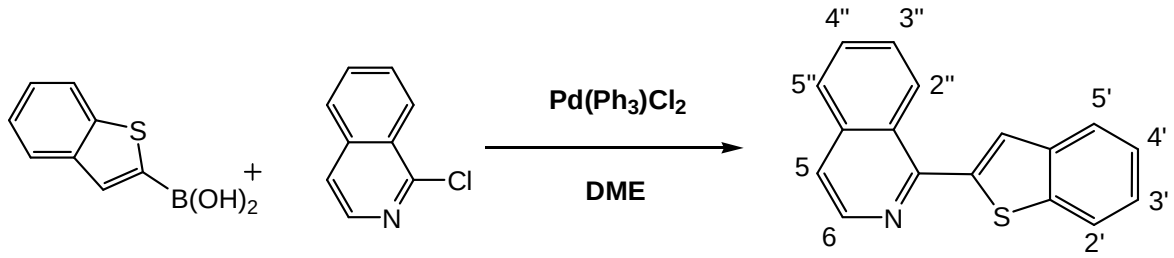

4-Benzo[b]thiophene boronic acid (177 mg, 1 mmol) and 1-chloroisoquinoline (68 mg, 0.42 mmol) were dissolved in a mixture of toluene (3ml), ethanol (3ml) and aqueous solution of Na_2CO_3 (2M, 1.5 ml). The mixture was degassed through four freeze-pump-thaw cycles. $Pd(Ph_3P)_4$ (20 mg, 0.017 mmol) was then added under nitrogen and the solution was heated at reflux temperature for 42 hours. After cooling to room temperature, 5 ml of water was added and the product extracted in dichloromethane, then dried over $MgSO_4$ and filtered. Purification of the target compound was achieved via silica gel chromatography (hexane/ diethyl ether 90/10). The product is a pale yellow solid (78 mg, 0.30 mmol, 30%). ^{1}H NMR ($CDCl_3$, 400 MHz): δ 8.53 (s, H^{th}) 8.52 (d, ^3J = 5.7, 1H, H^6), 8.13 (d, ^3J = 8.5, 1H, $H^{2''}$), 7.91 (d, ^3J = 8.2, 1H, $H^{5''}$), 7.78 – 7.64 (d+d+t, 3H, H^5+$H^{5'}$+$H^{3''}$), 7.61 – 7.45 (t+d+t+t, 4H, $H^{4''}$+$H^{4'}$+$H^{3'}$+$H^{2'}$). Mass Spectrometry (ES^+): *m/z* 262 $[M+H]^+$

5.7. Synthesis of terdentate ligands (N^C^N)

Synthesis of 2,4-di-bromo-m-xylene[199]

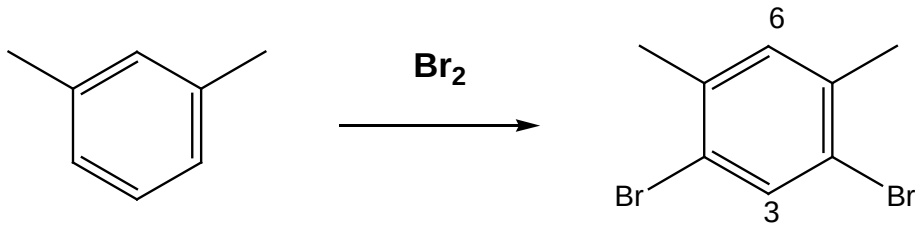

In a 250 ml flask, bromine (21.9 g, 137 mmol) was added to m-xylene (7.5 g, 111 mmol) over 5 minutes. Then iodine (0.25 g, 1 mmol) was added over 30 minutes, the resulting mixture was stirred for 3 hours. An aqueous solution of NaOH (4M, 50 ml), was added and the precipitate formed was filtered and dried under vacuum. The product was purified by recrystallization from ethanol (6.39 g, 24mmol, 22%). ^{1}H-NMR ($CDCl_3$, 300 MHz): δ 7.67 (s 1H, H^3), 7.10 (s, 2H, H^6). ^{13}C-NMR($CDCl_3$, 300 MHz): δ 136.9 (C^2), 134.9 (CH^3), 132.6 (C^1), 122.0 (CH^6), 22.2 (C^{Me}). Mass spectrometry (ES+): *m/z* 264 $[M]^+$.

Synthesis of 2-tri-n-butyl-stannyl-pyridine[232]

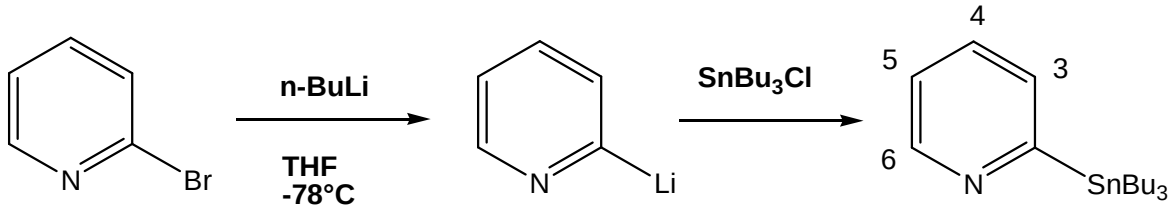

2-Bromopyridine (3ml, 31.6 mmol) was placed in a 100 ml two necked round bottom flask fitted with condenser and suba seal. Dry THF was added (25 ml) under nitrogen atmosphere. The solution was cooled to –78°C and n-Buli (21ml of a 2.5 M solution in hexane, 34.8 mmol) was added dropwise over 30 minutes. A solution of Bu_3SnCl (10.29 ml, 34mmol) in 6 ml of THF was then added dropwise over 20 minutes. The mixture was then stirred at –78°C for 90 minutes and allowed to warm to room temperature. To this 30 ml of water was added and the reaction mixture was stirred at room temperature for 10 minutes. The product was extracted in diethyl ether and dried over $MgSO_4$ and the solvent evaporated under vacuum. The product was a brown oil (6.5 g, 17.8 mmol, 56%). ^{1}H NMR (400 MHz, $CDCl_3$) δ 8.81 – 8.67 (m, 1H, H^6), 7.49 (td, ^3J = 7.5, 1.8 Hz, 1H, H^4), 7.40 (ddd, ^3J = 7.4, 1.5, 1.0 Hz, 1H, H^3), 7.11 (ddd, ^3J = 7.6, 4.9, 1.5 Hz, 1H, H^5).

Synthesis of 1,3-di-(2-pyridyl)-4,6-dimethylbenzene [L1][197]

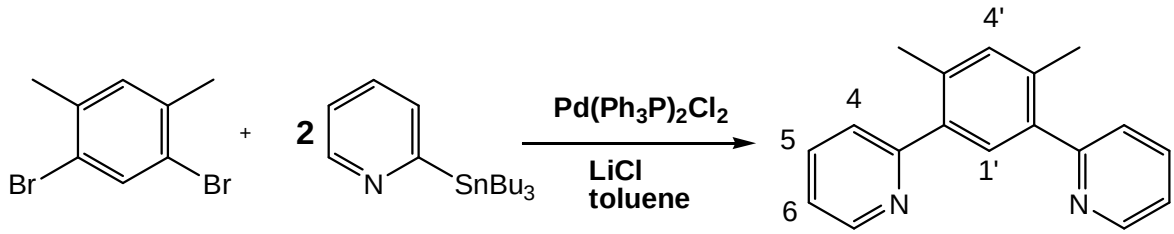

In a Schlenk were added 2-tri-n-butyl-stannyl-pyridine (4.09 g, 9.00 mmol), 2,6-di-bromo-m-xylene (1.00 g, 3.79 mmol), bis(triphenylphosphine)Palladium chloride (106 mg, 0.40 mmol), lithium chloride (1.34 g, 31.6 mmol) of dissolved in 25 mL of toluene. The reaction mixture was degassed via five freeze-pump-thaw cycles and heated until reflux temperature was reached for 24 hours. After cooling to room temperature the mixture was added to a saturated aqueous solution of KF (20 ml) and stirred for 30 minutes. The solution was then filtered and the solid

washed several times with water and toluene, the filtrate was added to a solution of $NaHCO_3$ (100 mL, 10% w/w) and extracted with DCM (2x100 mL). The combined organic layer was dried over $MgSO_4$ and purified by silica gel separation chromatography (from 100% hexane to 90% ether, 10% hexane). The product was a pale yellow solid 214 mg (0.08mmol, 26%). ^{1}H-NMR ($CDCl_3$, 200 MHz): δ 8.61 (d, 2H, ^{3}J = 4.9, H^{6}), 7.63 (td, ^{3}J = 7.7, 2H, H^{5}), 7.44 (s, 1H, $H^{4'}$), 7.36 (d, 2H, ^{3}J = 7.7, H^{3}), 7.15 (s, 1H, $H^{1'}$), 6.91 (t, 2H, ^{3}J = 7.5, H^{4}), 2.40 (s, 6H, H^{Me}). ^{13}C-NMR ($CDCl_3$, 400 MHz): δ 159.7 (C^{2}), 149.1 (CH^{6}), 138.1 ($C^{2'}$), 136.1 (C^{4}), 135.8 ($C^{3'}$), 133.3 ($CH^{4'}$), 131.1 ($CH^{1'}$), 124.2 (CH^{3}), 121.6 (CH^{5}), 20.0 (C^{Me}). Mass spectrometry (ES+): *m/z* 261 $[M]^{+}$.

Synthesis of 2,6-di-bromo-3,5-(bis-trifluoromethyl)aniline[(201)]

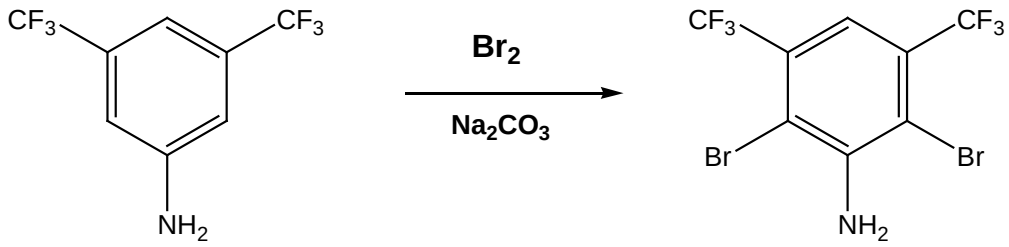

Dichloromethane (100 mL) was added to a mixture of bis(trifluoromethyl)aniline (1.0 g, 4.4 mmol), Na_2CO_3 (467 mg, 5.6 mmol) and iron filings (0.128 g, 2.18 mmol) in a 250 mL round-bottom flask. A solution of bromine (1 mL) in dichloromethane (30 ml) was added with stirring, and the mixture then heated at reflux temperature for 3 d with stirring. Upon cooling, saturated $Na_2CO_{3(aq)}$ (150 mL) was added, the mixture was extracted with diethyl ether (3 x 100 mL), the combined organic phase dried over anhydrous $MgSO_4$, and the solvent removed under reduced pressure. The crude product was purified by chromatography on silica (100% hexane to 80% hexane / 20% ether), to give a yellow solid (1.30 g,

3.4 mmol, 77%). ^{1}H-NMR ($CDCl_3$, 400 MHz): δ 7.37 (1H, s, H^4), 5.24 (2H, s, H^{NH2}).

Synthesis of 1,3-di-bromo-3,5-bis-(trifluoromethyl)benzene[201]

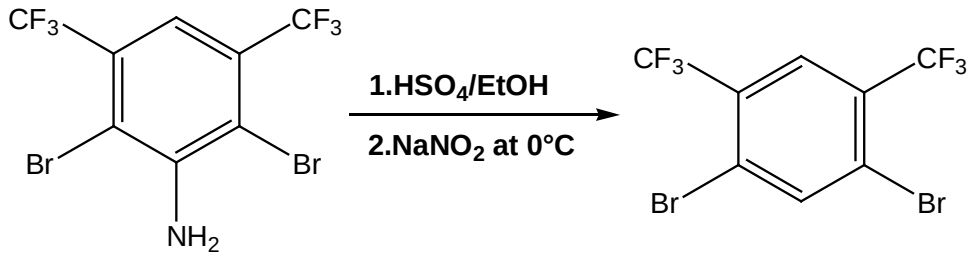

2,6-Dibromo-3,5-bis(trifluoromethyl)aniline (1.30 g, 3.4 mmol) from step (i) was dissolved in hot ethanol (20 mL) and concentrated sulfuric acid (2.55 mL, 95%) was added to the boiling solution. The mixture was then cooled to 0°C, and sodium nitrite (2.56 g, 0.037 mol) was added. The mixture was allowed to warm to room temperature and stirring continued for 15 min. It was then refluxed until gas evolution ceased. The solvent was removed under reduced pressure, and the crude product was purified by chromatography on silica (hexane) to give the product as a colourless solid (460 mg, 1.24 mmol, 37%). ^{1}H-NMR (400 MHz, $CDCl_3$): δ 8.11 (1H, s, H^4), 7.95 (1H, s, H^1).

Synthesis of 1,3-di-(2-pyridyl)-4,6-di-(trifluoromethyl)benzene [L3]

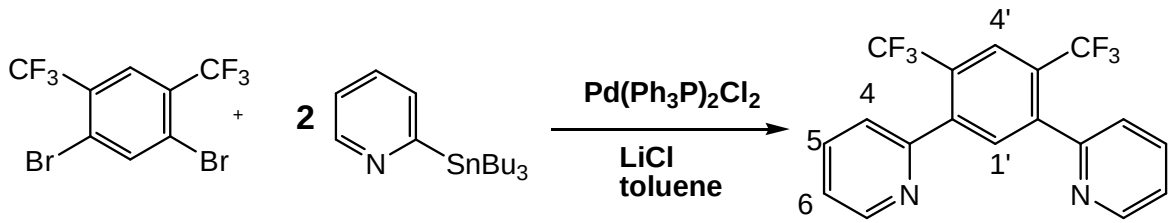

Toluene (25 mL) was added to a mixture of 2-tri-n-butyl-stannyl-pyridine (2.2 g, 6.0 mmol),1,3dibromo-4,6-bis(trifluoromethyl)benzene (840 mg, 2.3 mmol), $Pd(PPh_3)_2Cl_2$ (200 mg, 0.29 mmol), and lithium chloride (1.2 g, 28 mmol). The mixture was degassed via five freeze-pump-thaw cycles and then heated at reflux under an atmosphere of nitrogen for 24 h. After cooling to room temperature, the mixture was added to a saturated aqueous solution of KF (20 mL) and stirred for 30 min. The solution was filtered and the solid residue washed with water and toluene. The combined filtrate and washings was added to a solution of $NaHCO_3$ (100 mL, 10% w/w) and extracted into dichloromethane (2 × 100 mL). The organic phase was dried over $MgSO_4$ and the solvent then removed to yield a brown residue, which was purified by silica gel separation chromatography (gradient elution from 100% hexane to 20% hexane / 80% diethyl ether), leading to the product as a pale yellow solid (210 mg, 0.56 mmol, 25%). ^{1}H NMR ($CDCl_3$, 700 MHz): δ 8.70 (2H, dd, ^{3}J = 5.0, ^{4}J = 1.5, H^{6}), 8.17 (1H, s, 8.17, $H^{4'}$), 7.78 (2H, ddd, ^{3}J = 7.0, 7.0, 1.5, H^{3}), 7.71 (1H. s, $H^{1'}$), 7.49 (2H, t, ^{3}J = 7.5, H^{4}), 7.35 (2H, td, ^{3}J = 7.5, 5.0, ^{4}J = 1.5, H^{5}). ^{13}C NMR ($CDCl_3$, 175.9 MHz): δ 156.0 (C^{2}), 149.5 (CH^{6}), 143.2 (CH^{3}), 136.2 (CH^{4}), 135.3 ($CH^{4'}$), 128.4 (q, $^{2}J_{C-F}$ = 31, $CH^{1'}$), 125.0 (septet, $^{3}J_{C-F}$ = 5, $C^{3'}$), 124.0 (s, CH^{5}), 123.3 (q, $^{1}J_{C-F}$ = 274, CF_3), 123.2 (s, C^{2}). ^{19}F NMR ($CDCl_3$, 282.2 MHz): δ –57.5. MS (ES^{+}): m/z 369 $[M+H]^{+}$. HRMS (ES+): m/z 369.0818. Calcd for $C_{18}H_{11}N_2F_6$: m/z 369.0826. Elemental analysis: C, 57.7; H, 3.9; N, 6.2 %. Calcd for $C_{18}H_{10}N_2F_6$: C, 58.7; H, 2.7; N, 7.6 %. Melting Point: 106°C.

Synthesis of 1,3-di-bromo-4,6-difluorobenzene

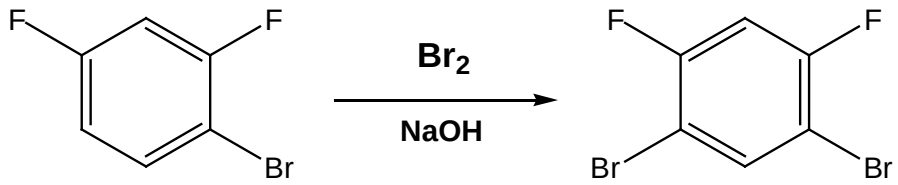

2,4-Difluorobromobenzene (7.53 g, 39 mmol) and iron filings (100 mg) were placed in a two-necked round-bottomed flask equipped with an addition funnel and a condenser holding a drying tube filled with KOH pellets. The flask was heated to 60°C. Bromine (9.33 g, 59 mmol) was added dropwise via the funnel over 1 h, and the mixture then allowed to stir for an additional 1.5 h. The solution was poured into aqueous NaOH (10%, 30 mL) with stirring. The organic layer was collected and the aqueous layer was extracted twice with toluene. The combined organic layers were combined and dried with anhydrous Na_2SO_4. The solvent was removed under reduced pressure to give the product as a light cream solid (7.24 g, 26.8 mmol, 68%). ^{1}H NMR ($CDCl_3$, 300 MHz): δ 7.75 (1H, td, ^3J = 7.0, ^5J = 2.0, H^1), 6.97 (1H, td, ^4J = 8.0, ^5J = 2.0, H^4). ^{19}F NMR ($CDCl_3$, 400 MHz): δ –103.8 (dd, $^3J_{F–H}$ = 7.5, $^4J_{F–H}$ = 7.5).

Synthesis of 1,3-di-(2-pyridyl)-4,6-difluorobenzene[L2]

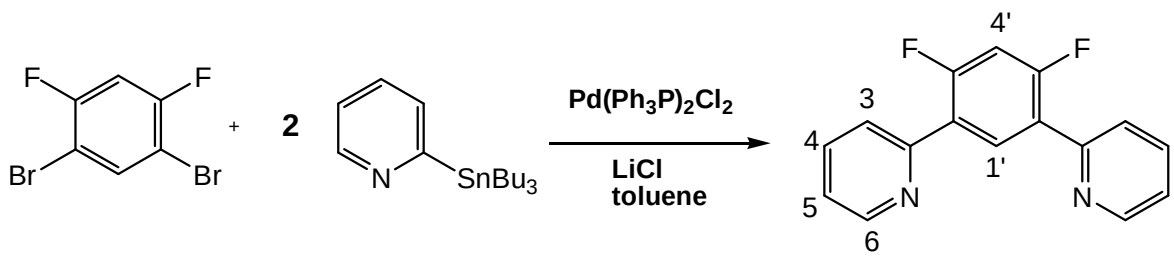

2-(Tributyltin)pyridine (4.17 g, 85% purity by ^{1}H NMR, 9.62 mmol), 1,3-dibromo-4,6-difluorobenzene (1.09 g, 4.01 mmol), $Pd(PPh_3)_2Cl_2$ (0.104 g, 0.15 mmol), LiCl (1.24 g, 29.3 mmol) and toluene (6 mL) were placed in a Schlenk tube. The mixture was degassed by four freeze-pump-thaw cycles, then heated under a nitrogen atmosphere to 120°C for 48 h. After cooling to room temperature, saturated aqueous KF (10 mL) was added and the mixture stirred for 30 min. The precipitated solid was removed by filtration and washed with water (25 mL) and toluene (30 mL). The filtrate was added to $NaHCO_3$ solution (10%, 50 mL) and the resulting mixture extracted with dichloromethane (2 x 100 mL). The organic phase was dried over $MgSO_4$, and the solvent was removed under reduced pressure to leave a pale brown residue. Purification by column chromatography (silica, hexane/ether gradient elution from 100/0 to 25/75) led to the desired product, 1,3-di(2-pyridyl)-4,6-difluorobenzene, as a pale yellow solid (570 mg, 2.13 mmol, 53%). R_f = 0.55 (silica, hexane/ether 25/75). M.p. = 156–158°C. ^{1}H NMR ($CDCl_3$, 500 MHz): δ 8.72 (2H, dd, ^{3}J = 5.0, ^{4}J = 1.0, H^{6}), 8.62 (1H, t, $^{4}J_{H-F}$ = 9.0, $H^{4'}$), 7.76 (4H, m, H^{4} and H^{3}), 7.26 (2H, m, H^{5}), 7.03 (1H, t, $^{3}J_{H-F}$ = 10.5, $H^{1'}$). ^{13}C NMR ($CDCl_3$, 125.7 MHz): δ 160.7 (dd, $^{1}J_{C-F}$ = 255, $^{3}J_{C-F}$ = 12, CH^{3}), 152.8 ($C^{2'}$), 150.1 ($CH^{1'}$), 136.7 ($C^{3'}$), 133.9 (t, $^{3}J_{C-F}$ = 4.5, CH^{5}), 124.7 (dd, $^{2}J_{C-F}$ = 10, $^{4}J_{C-F}$ = 5.5, CH^{6}), 124.5 (t, $^{4}J_{C-F}$ = 9.0, $C^{4'}$), 122.8 (C^{2}), 105.2 (t, $^{2}J_{C-F}$ = 27, $C^{2'}$). ^{19}F-NMR ($CDCl_3$, 188 MHz): δ -113.3 (t, 2F, J_{F-H} = 10). HRMS (ES+) m/z = 269.0886 $[M+H]^{+}$; calcd for $C_{16}H_{11}F_2N_2$ = 269.0890. Anal. calcd for $C_{16}H_{10}F_2N_2$ = C, 71.63; H, 3.76; N, 10.44%. Found C, 71.52; H, 3.81; N, 10.43%.

Synthesis of 1,3-di-(4-pinacolatoboron)-4,6-difluorobenzene

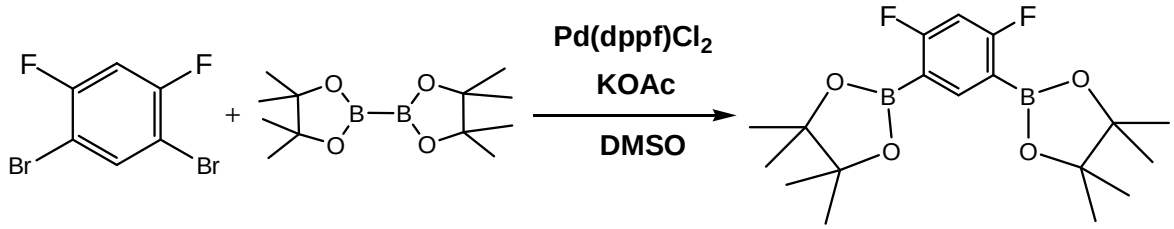

A Schlenk tube was charged with Pd(dppf)Cl_2 (32mg, 0.039mmol), KOAc (379mg, 3.86mmol) and bis(pinacolato)diboron (344mg, 1.35mmol) dissolved in 5ml of dried DMSO. The mixture was degassed through several vacuum-nitrogen cycles before adding 1,3-di-bromo-4,6-di-fluoro–benzene (400mg, 0.65mmol), after which the mixture was strirred overnight at 80°C under nitrogen. After coling to room temperature 50ml of toluene were added and the solution was washed with water in order to remove the DMSO from the organic layer. The latter was dried over $MgSO_4$. Separation chromatography on silica gel (hexane/diethyl ether 60/40) yielded the desired product (125mg, 0.34mmol, 53%). ^{1}H-NMR ($CDCl_3$, 400 MHz): δ 8.07 (1H, t, J = 8.0, H^4), 6.61 (1H, t, J = 10.0, H^1) 1.33 (24H, s, H^{Me}).

Synthesis of 1,3-di-(4-methoxy-2-pyridyl)-4,6-difluorobenzene[L5]

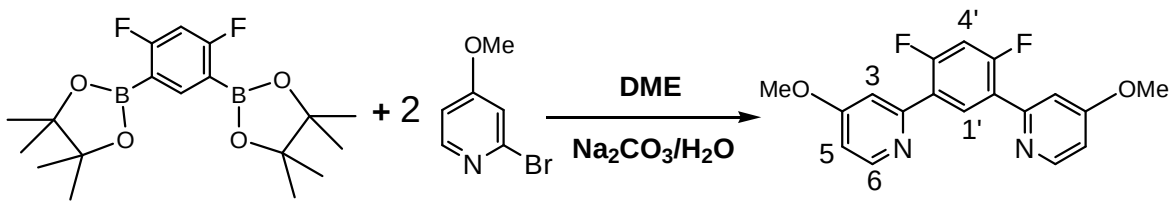

A schlenk was charged with 1,3-di-(4-methoxy-2-pyridyl)-4,6-di-fluoro-benzene (154 mg, 0.42 mmol), 2-bromo-4-methoxypyridine (150 mg, 0.84 mmol), dimethoxyethane (4mL) and $Na_2CO_3.H_2O$ (1 M, 4 mL) and was degassed by three freeze-pump-thaw cycles. $[Pd(PPh_3)_4]$ (0.0389 g, 0.034 mmol) was added under a positive flow of N_2 and the reaction was left stirring at 80ºC for 48 hours. DCM (70 mL) was added to the solution which then was washed with 3 x 100 mL NaOH solution (1 M). The DCM layer was separated and dried ($MgSO_4$) and the solvent removed under reduced pressure. The resulting black oily solid was purified by flash column chromatography (alumina, hexane/ethyl actetate, gradient elution from 100/0 to 60/40) giving the desired product as a white solid (43 mg, 33%). ^{1}H-NMR ($CDCl_3$, 400 MHz): δ 8.60 (2H, t, J = 8.4, H^6), 8.57 (1H, d, J = 5.2, $H^{1'}$), 7.95 (2H, d, J = 1.6, H^4), 7.08 (1H, t, J = 10.0, $H^{4'}$), 6.86 (2H, dd, ^{3}J = 5.2, ^{4}J = 2.6, H^5), 4.01 (6H, s, H^{OMe}).

Synthesis of 2-tri-n-butyl-stannyl-4-(trifluoromethyl)pyridine[232]

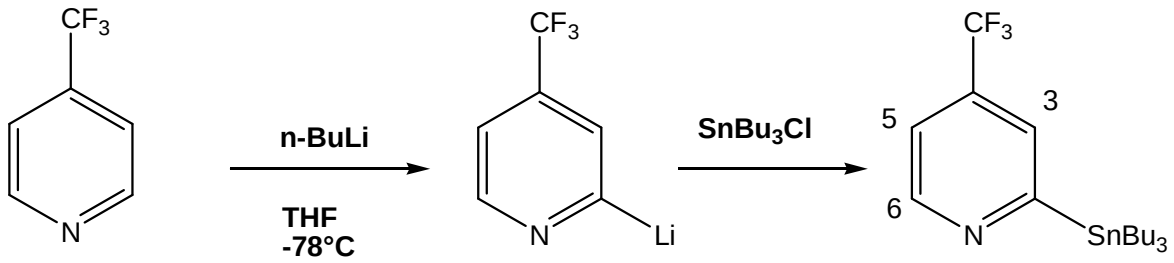

2-(dimethyl amino)ethanol (0.8 ml, 8mmol) and 4-trifluoromethyl-pyridine (0.4 ml, 3.2 mmol) were placed in a 100 ml two necked round bottom flask fitted with condenser and suba seal. Dry hexane was added (25 ml) under nitrogen athmosphere. The solution was cooled to –78°C and a solution of n-BuLi 2.5 M in hexane (10 ml, 16 mmol) was added dropwise over 30 minutes. A solution of

Bu_3SnCl (2.8 ml, 4mmol) in 6 ml of THF was then added dropwise over 20 minutes. The mixture was then stirred at –78°C for 90 minutes and allowed to ward to room temperature. To this, 30 ml of water was added and the reaction mixture was stirred at room temperature for 10 minutes. The product was extracted in diethyl ether and dried over $MgSO_4$ and the solvent evaporated under vacuum. The product was a brown oil (0.5 g, 1.6 mmol, 50%). ^{1}H NMR (400 MHz, $CDCl_3$) δ 8.88 (d, 1H, J=5.2, H^6), 7.88 (s, 1H, H^3), 7.27 (d, 1H, *J* = 4.8, H^5).

Synthesis of 1,3-bis-(4-(trifluoromethyl)-2-pyridyl)-4,6-bis-(trifluoromethyl)benzene [L4]

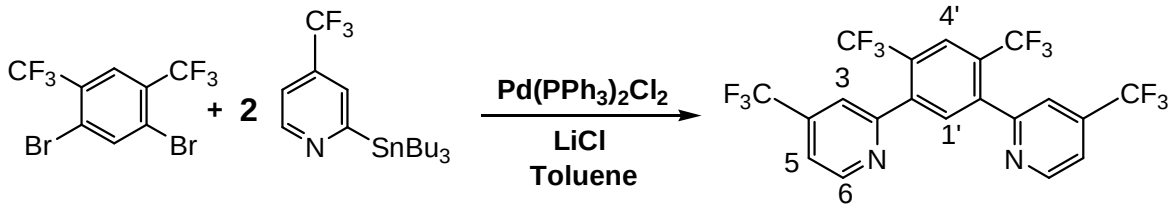

Toluene (25 mL) was added to a mixture of 2-tri-n-butyl-stannyl-4-tri-fluoro-methyl-pyridine (1.0 g, 3.2 mmol), 2,6-dibromo-3,5-bis(trifluoromethyl)benzene (300 mg, 0.8 mmol), $Pd(PPh_3)_2Cl_2$ (100 mg, 0.15 mmol), and lithium chloride (0.4 g, 7 mmol). The mixture was degassed via five freeze-pump-thaw cycles and then heated at reflux under an atmosphere of nitrogen for 24 h. After cooling to room temperature, the mixture was added to a saturated aqueous solution of KF (20 mL) and stirred for 30 min. The solution was filtered and the solid residue washed with water and toluene. The combined filtrate and washings was added to a solution of $NaHCO_3$ (100 mL, 10% w/w) and extracted into dichloromethane (2 × 100 mL). The organic phase was dried over $MgSO_4$ and the solvent then removed to yield a brown residue, which was purified by silica gel separation chromatography (gradient elution from 100% hexane to 20% hexane / 80% diethyl

ether), leading to the product as a pale yellow solid (35 mg, 0.07 mmol, 25%). ^{1}H NMR ($CDCl_3$, 400 MHz): δ 8.84 (2H, d, ^{3}J = 5.2, H^{6}), 8.17 (1H, s, $H^{4'}$), 7.66 (3H, s+s, H^{3}+$H^{1'}$), 7.54 (2H. dd, J=4.0, 1.2, H^{5}). ^{13}C NMR ($CDCl_3$, 400 MHz): δ 157.2, 150.9, 150.8, 135.3, 126.3, 122.8, 119.9, 119.3, 119.2. ^{19}F NMR ($CDCl_3$, 282.2 MHz): δ –57.5 (3F), -65.2 (3F). MS (ES^{+}): *m/z* 504 $[M+H]^{+}$.

5.8. Synthesis of bridging ligands

Synthesis of 4,4'-diethynylbiphenyl[233] [bpha]

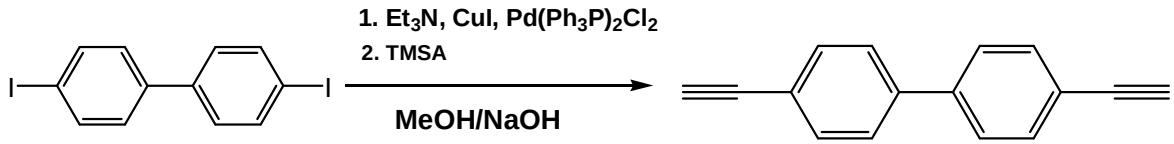

In a schlenk under nitrogen, 4,4'-diodobiphenyl (362 mg, 0.90 mmol) was dissolved in triethylamine (15 ml). To the mixture, CuI (5 mg), $Pd(Ph_3P)_2Cl_2$ (50 mg) and TMSA (0.4 g, 4 mmol) were added. After heating to 50° C overnight, the mixture was cooled to room temperature and the formed precipitate was filtered and washed with ether (100 ml). Purification was perfomed via silica gel separation chromatography (hexane) to give the intermediate compound 4,4'-bis[(trimethylsilyl)ethynyl] biphenyl. The latter was deprotected by stirring at room temperature with a solution of MeOH/NaOH (100 ml, 1:1). Extraction of the resulting solution was carried out in ether (3x100 ml) and the organic layer was dried over $MgSO_4$ then filtered. After removal of the solvent by vacuum evaporation the product was purified by silica gel chromatography (petroleum ether). The product was a white solid (60 mg, 0.3 mmol, 33%). ^{1}H-NMR ($CDCl_3$, 400 MHz): δ 7.48 (d, 4H, J= 3.2, H^{phen}), 7.46 (d, 4H, J= 3.2 H^{phen}), 3.07 (s, 2H, $H^{acetylide}$).

Synthesis of 4,4'-bis-cyano phenyl[234]

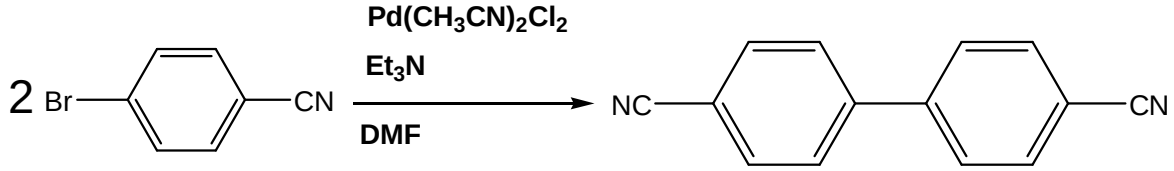

In a 100 ml round bottom flask was added 4-bromo-1-cyano-phenyl (367 mg, 2.17 mmol), $Pd(CH_3CN)_2Cl_2$ (115 mg, 0.30 mmol), Et_3N (1.5 ml) and 10 ml of DMF. The mixture was refluxed at 110° C for 48 hours. After cooling to room temperature the mixture was diluted with 20 ml of water and extracted with ether (3x100 ml). The organic layer was dried over $MgSO_4$ and filtered. Silica gel separation chromatography (hexane, ethyl acetate 3:1) gave the pure product as a white solid (98 mg, 0.48 mmol, 22%). ^{1}H-NMR ($CDCl_3$, 400 MHz): δ 7.69 (d, 2H, J=8.0, H^{phen}), 7.78 (d, 2H, J=8.0, H^{phen}).

Synthesis of 4-4' tetrazolyl-bis-phenyl [btrph][235]

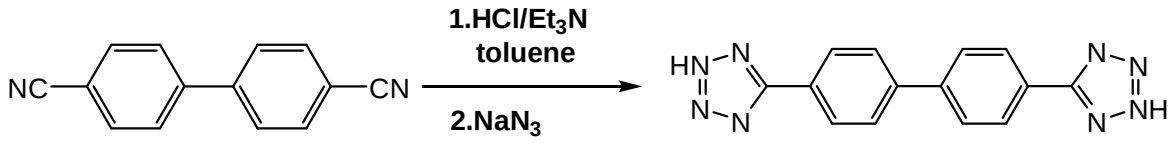

In a 100 ml round bottom flask with 30 ml of toluene stirring at 0°C were added $HCl_{(aq)}$ 1.3 ml (14.1 mmol) and Et_3N 2.1 ml (14.1 mmol). The solution was allowed to warm up to room temperature then addition of 202 mg (1.12 mmol) of 4-4'-bis

cyano-phenyl and 385 mg (4.48 mmol) of sodium azide was carried out. The solution was heated for 20 hours at 110°C. After cooling to room temperarue the solvent was removed by vacuum evaporation and the residue dissolved in water (20 ml). HCl (3M) was added dropwise to the solution causing precipitation of a white solid at pH=4. The solid was then filtered and washed with 1M solution of HCl. The product was obtained as a white solid (156 mg, 0.54 mmol, 48%). ^{1}H-NMR (d_6-DMSO, 400 MHz): δ 8.29 (2H, d, J=8.4, H^{phen}), 8.11 (2H, d, J=8.4, H^{phen}).

5.9. Synthesis of Iridium di-chloro bridged dimers

Synthesis of 1,3-di-(2-pyridyl)-4,6-dimethylbenzene di-chloro bridged Iridium dimmer[24] $[Ir(L1)Cl(\mu\text{-}Cl)]_2$

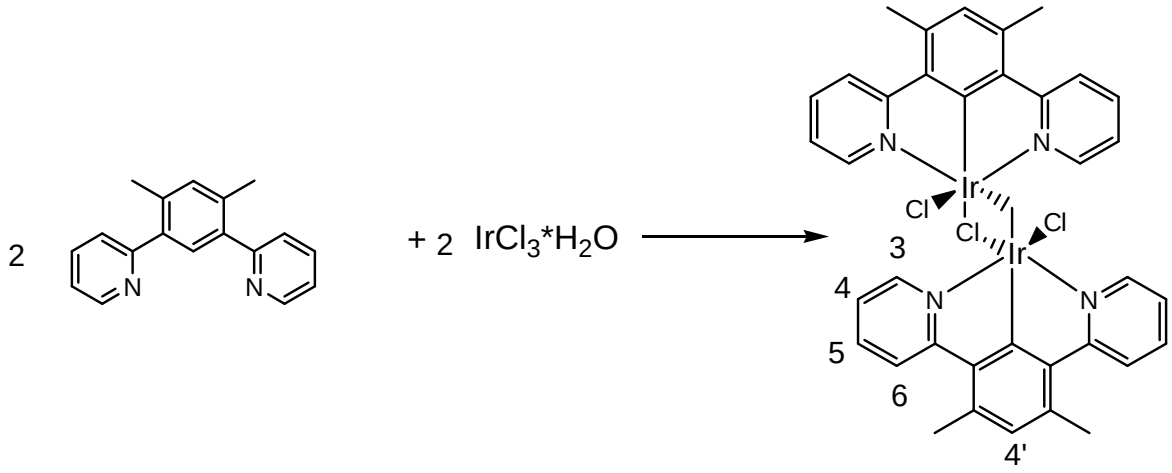

A suspension of 1,3-di-(2-pyridyl)-4,6-dimethyl-benzene (214 mg, 0.82 mmol) and iridium chloride monohydrate (258 mg, 0.82mmol) in a mixture of 2-ethoxyethanol (21 ml) and water (9ml) was refluxed for 24 hours under nitrogen atmosphere. A yellow solid formed in the solution, which after cooling to room temperature, was collected by centrifuge, washed with water (3*5ml), ethanol (3*5 ml) and ether (3*5 ml), and finally dried under vacuum. The product was a yellow solid 240 mg (0.23mmol, 56%). ^{1}H-NMR (DMSO-d_6): δ 9.20 (2H, d, J=5.6, H^6), 8.16 (2H, d, J=8.4, H^3), 8.05 (2H, td, J=8.4, J=1.6, H^4), 7.53 (2H, d, J=6.0, H^5), 6.97 (1H, s, $H^{4'}$), 2.75 (6H, s, H^{Me}).

Synthesis of 1,3-di-(2-pyridyl)-4,6-bis-(trifluoromethyl)benzene di-chloro bridged Iridium dimer $[Ir(L3)Cl(\mu\text{-}Cl)]_2$

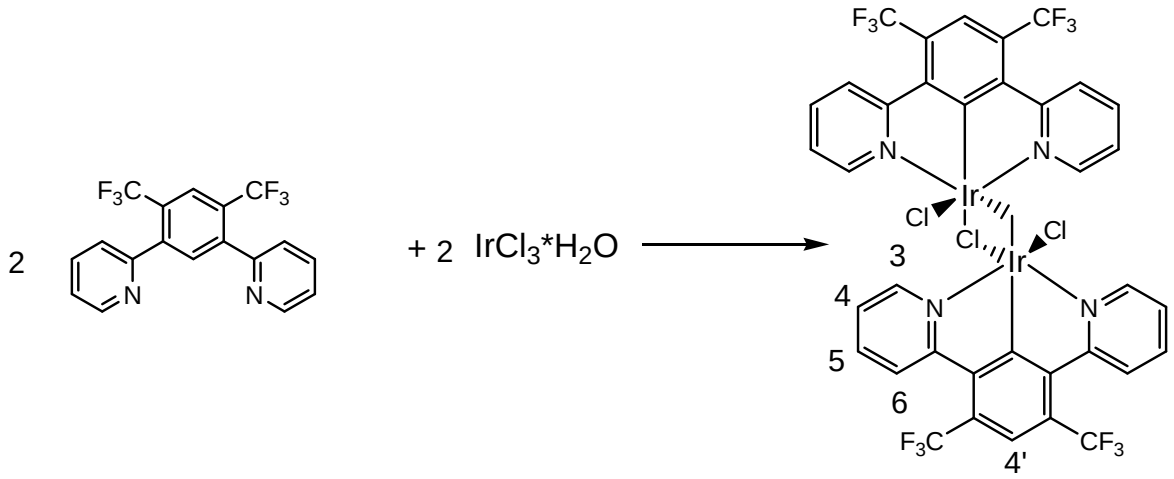

A suspension of H**L3** (155 mg, 0.42 mmol) and $IrCl_3.3H_2O$ (145 mg, 0.42 mmol) in a mixture of 2-ethoxyethanol (14 mL) and water (6 mL) was refluxed for 24 h under a nitrogen atmosphere. The solvent was removed under reduced pressure, to yield the product as an orange solid which was used in subsequent reactions without further purification (173 mg, 77%). ^{1}H NMR (200 MHz, CD_3CN): δ 9.25 (2H, d, J=5.1, H^{1py}), 8.48 (2H, d, J=9.7, H^{6}), 8.09 - 7.97 (3H, t+s, H^{4}+$H^{4'}$), 7.65 (2H, d, J= 5.7, H^{5}). ^{19}F NMR (200 MHz, CD_3CN): δ –60.1 (s, 6F, CF_3).

Synthesis of 1,3-di-(2-pyridyl)-4,6-difluorobenzene di-chloro bridged Iridium dimer[Ir(L2)Cl(μ-Cl)]$_2$

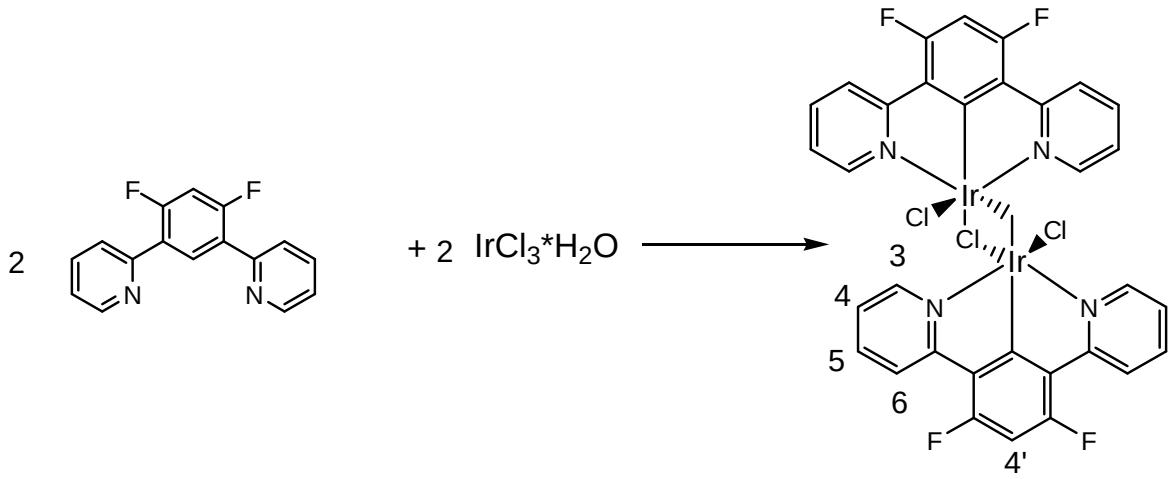

A suspension of H**L2** (250 mg, 0.93 mmol) and $IrCl_3.3H_2O$ (327 mg, 0.93 mmol) in a mixture of 2-ethoxyethanol (14 mL) and water (6 mL) was refluxed for 24 h under a nitrogen atmosphere. After cooling to room temperature, the yellow solid that formed was separated by centrifugation, washed successively with water, ethanol and diethyl ether (3 × 5 mL of each), and finally dried under vacuum. This solid (383 mg, 78%) has low solubility in all common solvents, and was used in subsequent reactions without further purification.

Synthesis of 1,3-di-(4-methoxy-2-pyridyl)-4,6-difluorobenzene di-chloro bridged Iridium dimer[Ir(L5)Cl(μ-Cl)]$_2$

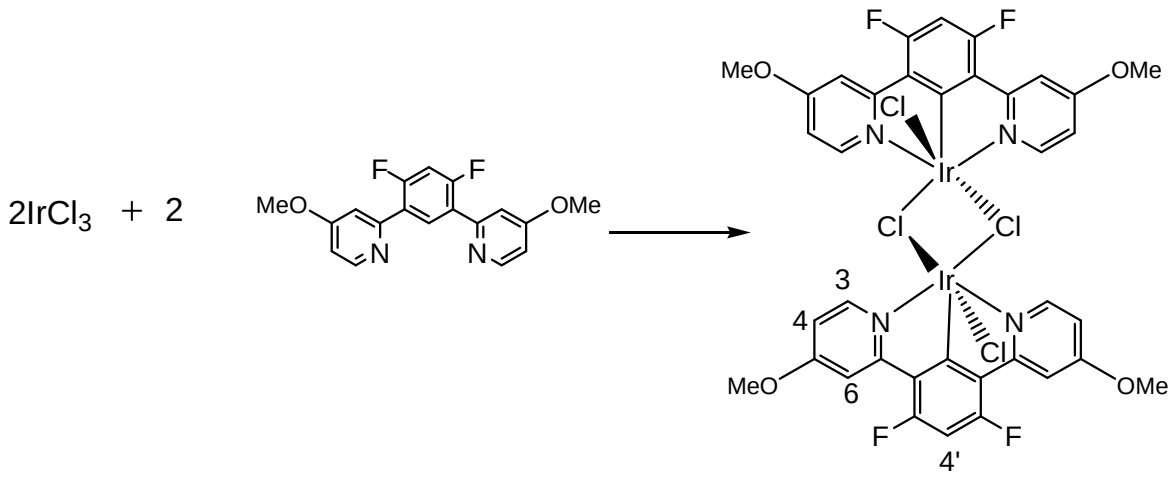

A suspension of 1,3-di-(4-methoxy-2-pyridyl)-4,6-difluorobenzene (50 mg, 0.15 mmol) and iridium chloride monohydrate (53 mg, 0.15mmol) in a mixture of 2-ethoxyethanol (7 ml) and water (3ml) was refluxed for 24 hours under nitrogen atmosphere. A yellow solid formed in the solution, which after cooling to room temperature, was collected by centrifuge, washed with water (3*5ml), ethanol (3*5 ml) and ether (3*5 ml), and finally dried under vacuum. The product obtained was 55 mg (0.047, 62%). ^{1}H-NMR (DMSO-d_6): δ 8.93(2H, d, H^6), 7.55-7.60 (3H, s+s, H^3+$H^{4'}$), 7.10 (2H, d, H^5), 3.34 (6H, s, H^{OMe}).

Synthesis of 1,3-di-(4-(trifluoromethyl)2-pyridyl)-4,6-bis-(trifluoromethyl)benzene di-chloro bridged Iridium dimer $[Ir(L4)Cl(\mu\text{-}Cl)]_2$

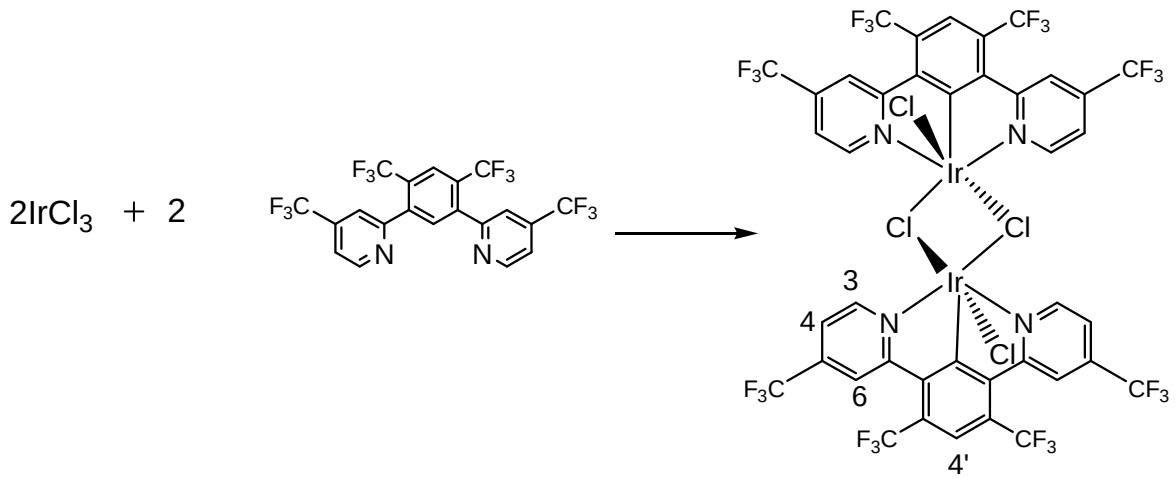

A suspension of H**L4** (35 mg, 0.07 mmol) and $IrCl_3.3H_2O$ (28 mg, 0.08 mmol) in a mixture of 2-ethoxyethanol (7 mL) and water (3 mL) was refluxed for 24 h under a nitrogen atmosphere. The solvent was removed under reduced pressure, to yield the product as an orange solid which was used in subsequent reactions without further purification (45 mg, 0.03 mmol, 42%). ^{1}H NMR (400 MHz, $CDCl_3$): δ 8.64 (2H, d, appears as a broad singlet, H^6), 8.06 (1H, s, $H^{4'}$), 7.70 (3H, d+s, H^5+H^3). ^{19}F NMR (376 MHz, $CDCl_3$): δ –57.5 (s, 12 F), -59.8 (s, 12 F).

5.10. Synthesis of rhodium di-chloro bridged dimers

Synthesis of 1,3-di-(2-pyridyl)-4,6-dimethylbenzene di-chloro bridged rhodium dimer $[Rh(L1)Cl(\mu\text{-}Cl)]_2$

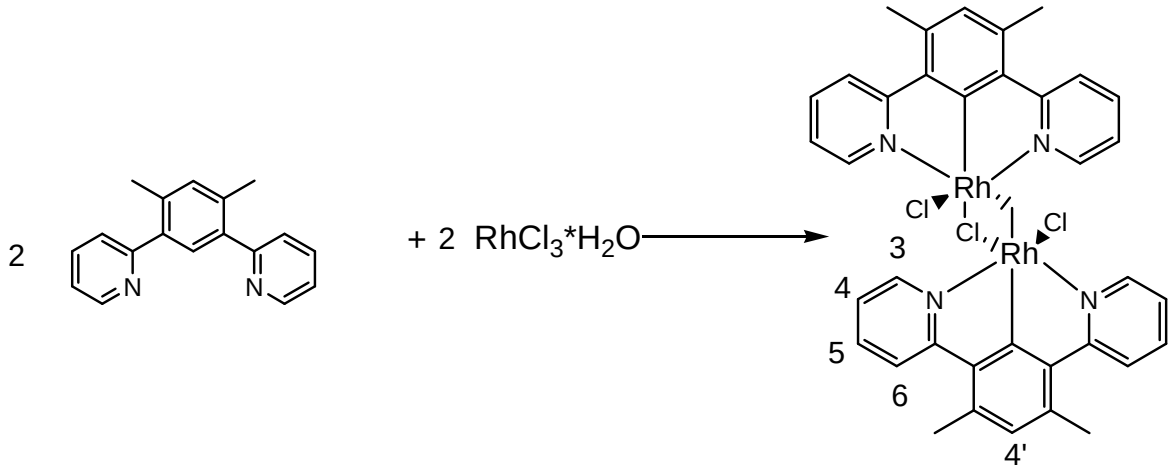

A suspension of 1,3-di-(2-pyridyl)-4,6-dimethylbenzene (256 mg, 0.98 mmol) and rhodium chloride monohydrate (191 mg, 1mmol) in a mixture of 2-ethoxyethanol (21 ml) and water (9ml) was refluxed for 24 hours under nitrogen atmosphere. A pale brown solid formed in the solution, which after cooling to room temperature, was collected by centrifuge, washed with water (3*5ml), ethanol (3*5 ml) and ether (3*5 ml), and finally dried under vacuum. The product was a yellow solid 240 mg (0.28 mmol, 56%).

Synthesis of 1,3-di-(2-pyridyl)-4,6-difluorobenzene di-chloro bridged rhodium dimer $[Ir(L2)Cl(\mu\text{-}Cl)]_2$

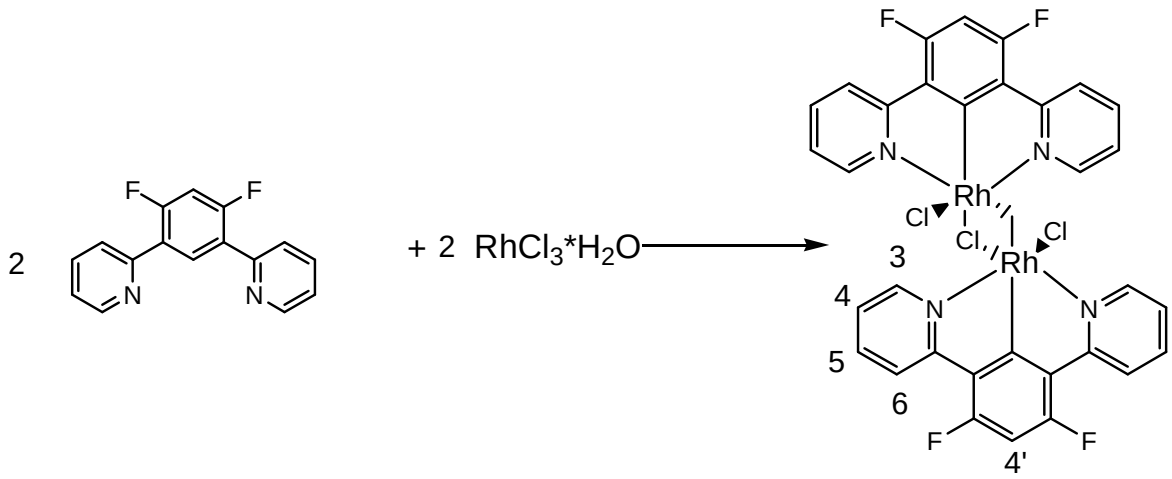

A suspension of 1,3-di-(2-pyridyl)-4,6-difluorobenzene (60 mg, 0.22 mmol) and rhodium chloride monohydrate (43 mg, 0.22) in a mixture of 2-ethoxyethanol (14 ml) and water (6ml) was refluxed for 24 hours under nitrogen atmosphere. A pale brown solid formed in the solution, which after cooling to room temperature, was collected by centrifuge, washed with water (3*5ml), ethanol (3*5 ml) and ether (3*5 ml), and finally dried under vacuum. The product obtained was 58 mg (0.067 mmol, 60%).

Synthesis of 1,3-di-(2-pyridyl)-4,6-bis-(trifluoromethyl)benzene di-chloro bridged rhodium dimer $[Ir(L3)Cl(\mu\text{-}Cl)]_2$

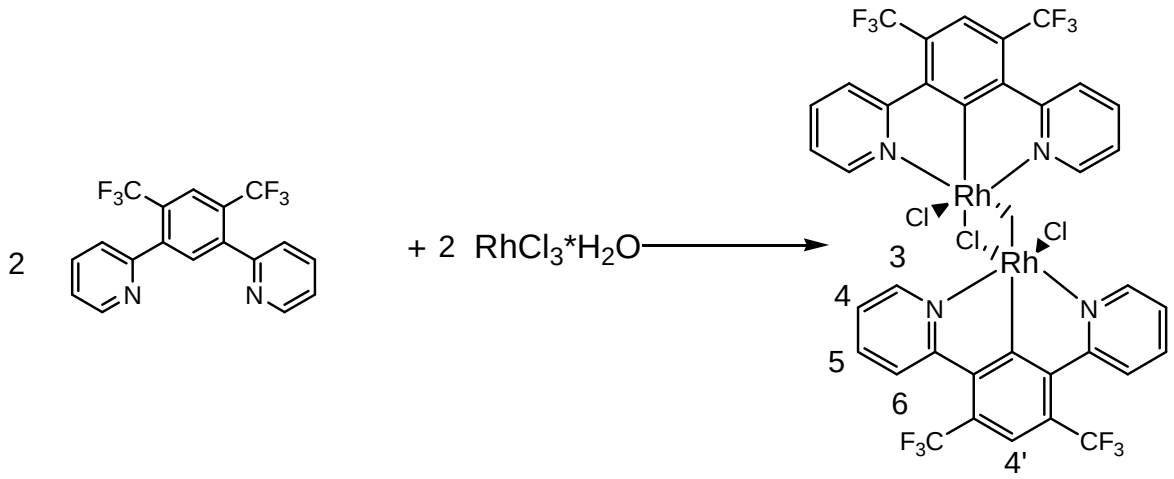

A suspension of 1,3-di-bromo-4,6-bis-(trifluoromethyl)benzene (280 mg, 0.76 mmol) and rhodium chloride monohydrate (193 mg, 0.76) in a mixture of 2-ethoxyethanol (21 ml) and water (9ml) was refluxed for 24 hours under nitrogen atmosphere. After cooling down to room temperature an orange solid formed in the solution. The solid was collected by centrifuge, washed with water (3*5ml), ethanol (3*5 ml) and ether (3*5 ml), and finally dried under vacuum. 61 mg (0.057 mmol, 14%). ^{19}F-NMR ($CDCl_3$): -67.8.

5.11. Synthesis of iridium complexes

Synthesis of Ir(1,3-di(2-pyridyl)-4,6-dimethylbenzene-N,$C^{2'}$,N)(2,4-(difluorophenyl)pyridine-N,$C^{2'}$) chloride [Ir(L1)(dFppy)Cl] (1)

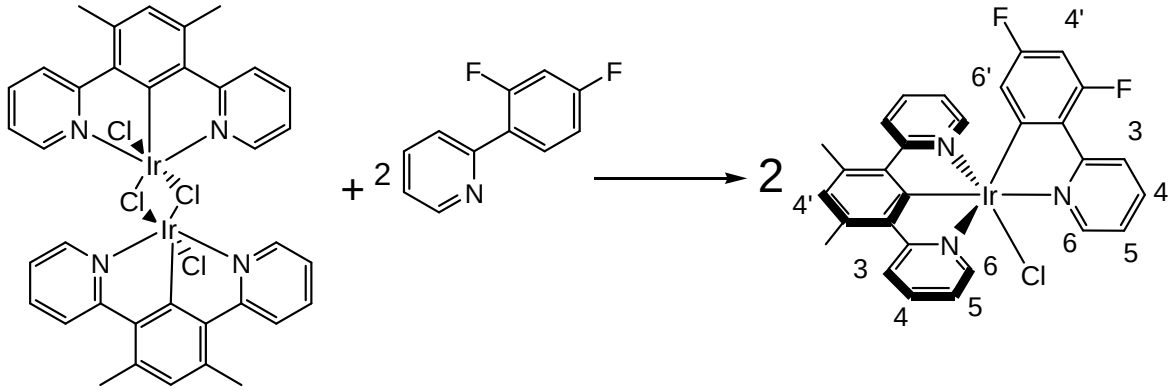

A mixture of [Ir(**L1**)Cl(μ-Cl)$_2$] (50 mg, 0.048 mmol), dFppyH (19 mg, 0.096 mmol) and silver triflate (57 mg, 0.22 mmol) in toluene (4 mL) was refluxed for 24 h under a nitrogen atmosphere. The precipitated AgCl was removed by centrifuge and washed with acetonitrile. The filtrate and washings were combined, the solvent removed under reduced pressure, and the residue purified by chromatography (silica gel, CH_2Cl_2/MeOH, gradient elution from 100/0 to 98/2), leading to the product as a yellow solid (61 mg, 0.090 mmol, 94%). ^{1}H-NMR (700 MHz, $CDCl_3$): δ 10.15 (1H, dd, ^{3}J = 4.9, ^{4}J = 0.7, H^6-NC), 8.42 (d, 1H, ^{3}J = 8.4, H^3-NC), 8.01 (d, 2H, ^{3}J = 8.4, H^6-NCN), 7.97 (td, 1H, ^{3}J = 7.0, ^{4}J = 1.4, H^4-NC), 7.58-7.52 (5H, H^4-NCN+H^3-NCN+H^5-NC), 6.88 (s, 1H, H$^{4'}$-NCN), 6.78 (td, 2H, ^{3}J = 7.7, ^{4}J = 1.4, H^5-NCN), 6.18 (m, 1H, ^{3}J = 11.9, ^{4}J = 2.8, H$^{4'}$-NC), 5.51 (dd, 1H, ^{3}J = 9.1, ^{4}J = 2.1, H$^{6'}$-NC), 2.82 (s, 6H, H^{Me}). ^{1}H-NMR (700 MHz, CD_3CN): δ 9.44 (1H, d, ^{3}J = 5.4, H^6-NC), 8.55 (d, 1H, ^{3}J = 8.3, H^3-NC), 8.26 (t, 1H, ^{3}J = 7.9, H^4-NC), 8.22 (d, 2H, ^{3}J = 8.3, H^6-NCN), 7.86 (t, 2H, ^{3}J = 7.4, H^4-NCN), 7.79 (t, 1H, ^{3}J = 7.7, H^5-NC), 7.70 (d, 2H, ^{3}J = 6.2, H^3-NCN), 7.14 (s, 1H, H$^{4'}$-NCN), 7.05 (t, 2H, ^{3}J = 7.4, H^5-NCN), 6.42 (m, 1H, ^{3}J = 11.9, ^{4}J = 2.5, H$^{4'}$-NC), 5.43 (dd, 1H, ^{3}J = 12.0, ^{4}J = 2.6, H$^{6'}$-NC), 2.87 (s, 6H, H^{Me}). ^{13}C-NMR ($CDCl_3$, 176 MHz) δ 187.2 (C$^{1'}$-NC or C$^{1'}$-NCN), 182.5

($C^{1'}$-NC or $C^{1'}$-NCN), 170.0 (C^{2}-NCN), 153.3 (CH^{4}-NCN), 151.2 (C^{6}-NC), 149.7 (C^{1}-NC), 138.1 (CH^{5}-NC), 137.5 ($C^{2'}$-NCN), 137.3 (CH^{6}-NC or $CH^{5'}$-NC), 136.5 (CH^{3}-NCN), 129.9 ($C^{3'}$-NCN and $CH^{4'}$-NCN), 123.2 ($C^{4'}$-NC), 123.0 (CH^{3}-NC), 122.9 (CH^{6}-NCN), 122.9 (CH^{5}-NCN), 121.6 ($C^{6'}$-NC or $C^{4'}$-NC), 121.5 (C^{2}-NC), 118.4 ($CH^{5'}$-NC), 97.5 ($CH^{3'}$-NC), 22.3 (C^{Me}). ^{19}F NMR ($CDCl_3$, 376 MHz): δ –108.7, (1F, NC), -109.4 (1F, NC). MS (ES+): *m/z* 642, $[M–Cl]^+$, 682 $[M–Cl+CH_3CN]^+$. HRMS (ES+): m/z 642.1314 $[M+H]^+$. Calcd for $C_{29}H_{22}N_3F_2{}^{191}Ir$: *m/z* 641.1411. Elemental analysis. found: 46.57% C, 2.91% H, 6.39% N, calculated: 51.48% C, 3.11 H%, 6.21%.

Synthesis of Ir(1,3-di-(2-pyridyl)-4,6-difluorobenzene-N,$C^{2'}$,N)(2,4-(difluorophenyl)pyridine-N,$C^{2'}$) chloride [Ir(L2)(dFppy)Cl] (2)

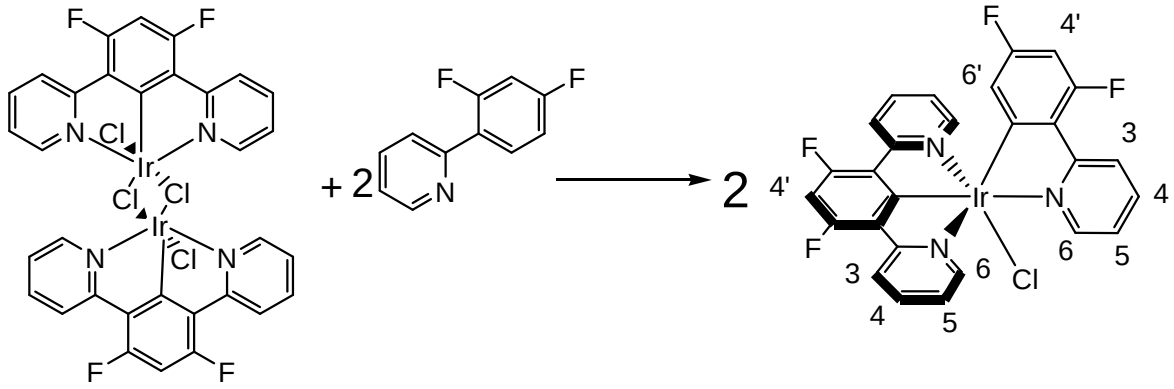

Prepared from [Ir(**L2**)Cl(μ-Cl)]$_2$ (50 mg, 0.047 mmol) and dFppyH (19 mg, 0.095 mmol) in the presence of AgOTf (50 mg, 0.18 mmol) in toluene (4 mL), using the procedure described above for Ir(**L1**)(dFppy)Cl **(1)**. The product was purified by chromatography (silica, CH_2Cl_2/MeOH, gradient elution from 100/0 to 96/4), leading to the product as a yellow solid (25 mg, 0.034 mmol, 39%). ^{1}H NMR ($CDCl_3$): δ ($CDCl_3$, 700 MHz): δ 9.52 (1H, d, ^{3}J = 5.0, H^6-NC), 8.49 (1H, d, ^{3}J = 7.5, H^3-NC), 8.12 (2H, d, ^{3}J = 7.5, H^6-NCN), 8.08 (1H, d, ^{3}J = 7.5, H^4-NC), 7.72 (2H,

dd, ^{3}J = 7.5, ^{4}J = 1.5, H^{4}-NCN), 7.68 (1H, m, $H^{4'}$-NC), 7.50 (2H, d, ^{3}J = 5.0, H^{3}-NCN), 6.94 (2H, ddd, ^{3}J = 7.5, ^{4}J = 1.5, H^{5}-NCN), 6.84 (1H, m, ^{3}J = 12, H^{5}-NC), 6.27 (1H, dd, ^{3}J = 13, ^{4}J = 2.5, $H^{5'}$-NC), 5.44 (1H, dd, ^{3}J = 9.0, ^{4}J = 2.5, $H^{3'}$-NC). ^{13}C-NMR ($CDCl_3$, 176 MHz) δ 165.8, 164.3, 161.5 ($C^{1'}$-NC or C^{2}-NCN or $C^{1'}$-NCN), 159.5 ($C^{2'}$-NC), 151.3 ($C^{2'}$-NCN and $C^{3'}$-NCN), 149.5 (CH^{6}-NC), 145.7 ($C^{4'}$-NC), 143.4 ($C^{6'}$-NC), 137.7 (C^{2}-NC), 137.6 (CH^{4}-NC), 136.9 (CH^{3}-NCN), 133.9 ($C^{5'}$-NC), 131.9 (CH^{4}-NCN), 127.0 ($CH^{3'}$-NC), 123.9 (CH^{5}-NC), 122.8 (CH^{6}-NCN), 122.2 (CH^{5}-NCN), 121.7 ($CH^{4'}$-NCN), 188.9 (CH^{3}-NC). ^{19}F NMR ($CDCl_3$, 376.3 MHz): δ –107.7 (2F, d, $^{3}J_{F–H}$ = 12, NCN), –107.9 (1F, ddd appears as q, $^{3}J_{F–H}$ = $^{4}J_{F–F}$ = 9, $F^{5'}$-NC), –109.4 (1F, dd, J = 11, $F^{3'}$-NC). MS (ES+): *m/z* 683 $[M]^+$, 648 $[M–Cl]^+$. HRMS (ES+): *m/z* 689.1073 $[M–Cl+CH_3CN]^+$. Calcd for $C_{29}H_{18}N_4F_4{}^{191}Ir$: *m/z* 689.1077. Elemental analysis: found C 43.06%, N 5.77%, H 2.31%, calculated for $ClC_{27}H_{15}N_3F_4{}^{191}Ir$: C 47.37%, N 6.14% , H 2.19%.

Synthesis of Ir(1,3-di-(2-pyridyl)-4,6-di-(trifluoromethyl)benzene-N,$C^{2'}$,N)(2,4-(difluorophenyl)pyridine-N,$C^{2'}$) chloride [Ir(L3)(dFppy)Cl] (3)

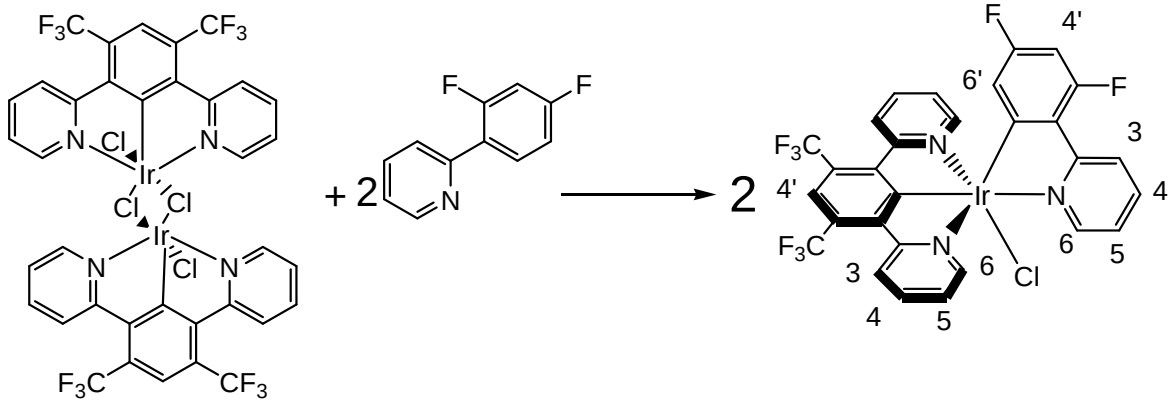

This complex was prepared from [Ir(**L3**)Cl(μ-Cl)]$_2$ (42 mg, 0.033 mmol) and dFppyH (13 mg, 0.066 mmol) in the presence of silver triflate (35 mg, 0.14 mmol) in toluene (4 mL), as described above for Ir(**L1**)(dFppy)Cl **(1)**. The crude product

was purified by chromatography (silica gel, CH_2Cl_2/MeOH, gradient elution from 100/0 to 99/1), giving an orange solid (18 mg, 0.023 mmol, 35%). ^{1}H NMR ($CDCl_3$, 700 MHz): δ 10.17 (1H, d, ^{3}J = 5.5, H^6-NC), 8.49 (1H, d, ^{3}J = 8.5, H^3-NC), 8.42 (2H, d, ^{3}J = 8.0, H^6-NCN), 8.09 (1H, s, H$^{4'}$-NCN), 8.07 (1H, td, ^{3}J = 8.0, ^{4}J = 1.2, H^4-NC), 7.76 (4H, m, H^4-NCN and H^5-NCN), 7.62 (1H, dd, ^{3}J = 7.0, ^{4}J = 1.2, H^5-NC), 6.25 (1H, m, ^{3}J = 12, ^{4}J = 2.5, H$^{5'}$-NC), 5.21 (1H, dd, $^{3'}$J = 9.0, ^{4}J = 2.5, H$^{3'}$-NC). ^{19}F NMR ($CDCl_3$, 376.4 MHz): δ –59.2 (6F, s, CF_3), –108.0 (1F, m, ^{4}J = 9.0, F$^{5'}$-NC), –109.4 (1F, dd, ^{3}J = 11, ^{4}J = 2.4, F$^{3'}$-NC). ^{13}C-NMR ($CDCl_3$, 176 MHz) δ 183.9 (C$^{4'}$-NC or C$^{1'}$-NC), 175.0 (CH$^{3'}$-NC or C$^{1'}$-NC), 165.1 (C^2-NCN), 160.1 (C$^{2'}$-NC), 153.5 (C$^{1'}$-NCN or C$^{3'}$-NCN), 151.3 (CH^3-NCN), 149.6 (CH^6-NC), 141.9 (C$^{2'}$-NC), 138.9 (CH^4-NC), 137.3 (CH^4-NCN), 125.1 (CH^6-NCN), 124.6 (CH^5-NCN), 123.7 (C^2-NC), 123.3 (CH^3-NC), 122.9 (CH^5-NC), 122.9 (C$^{1'}$-NCN or C$^{3'}$-NCN), 118.7 (CH$^{4'}$-NCN), 117.6 (C$^{6'}$-NC), 98.5 (C$^{4'}$-NC), 15.7 (C^{CF3}). ^{1}H NMR (CD_3CN, 500 MHz): δ 10.02 (1H, d, ^{3}J = 5.5, H^6-NC), 8.49 (1H, d, ^{3}J = 8.5, H^3-NC), 8.43 (2H, d, ^{3}J = 9.0, H^6-NCN), 8.18 (1H, dd, ^{3}J = 7.5, ^{3}J = 7.5, H^4-NC), 8.11 (1H, s, H$^{4'}$-NCN), 7.91 (2H, ddd, ^{3}J = 9.0, ^{3}J = 9.0, ^{4}J = 1.5, H^3-NCN), 7.87 (2H, t, ^{3}J = 5.5, H^4-NCN), 7.75 (1H, dd appears as t, ^{3}J = 6.5, H^5-NC), 7.16 (2H, dd, ^{3}J = 6.5, H^5-NCN), 6.35 (1H, dd, ^{3}J = 13, ^{4}J = 2.5, H$^{5'}$-NC), 5.20 (1H, dd, ^{3}J = 9.0, ^{4}J = 2.5, H$^{3'}$-NC). MS (ES+): *m/z* 791 $[M–Cl+CH_3CN]^+$. HRMS (ES+): *m/z* 789.1042 $[M–Cl+CH_3CN]^+$. Calcd for $C_{31}H_{18}N_4F_8Ir$: *m/z* 789.1013. Elemental analysis: Found C, 43.3%; H, 2.5%; N, 4.61 %. Calcd for $C_{29}H_{15}N_3F_8IrCl·H_2O$: C, 43.4%; H, 2.1%; N, 5.2 %.

Synthesis of Ir(1,3-di(2-pyridyl)-4,6-dimethylbenzene-N,C$^{2'}$,N)(2-phenylpyridine-N,C$^{2'}$) chloride [Ir(L1)(ppy)Cl]

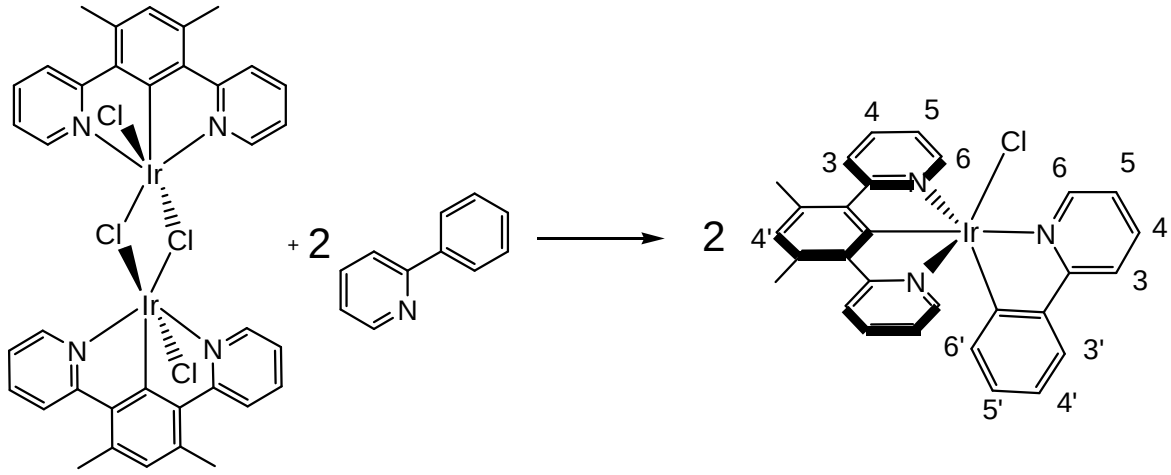

[Ir(**L1**)Cl(μ-Cl)]$_2$ (35 mg, 0.033 mmol) and silver(I) trifluoromethanesulfonate (44 mg, 0.17 mmol) in 2-phenylpyridine (ppyH) (250 μl, 1.75 mmol) were heated to 110°C under a nitrogen atmosphere for 24 h. After cooling to room temperature, dichloromethane (25 ml) was added and the remaining solid removed by filtration. Washing of the filtrate with HCl (1 M, 3 × 25 ml), drying over MgSO4, and removal of solvent under reduced pressure gave a yellow residue. This was purified by column chromatography (silica, dichloromethane/methanol, gradient elution from 100/0 to 99.75/0.25) to give the desired product as a yellow solid (25 mg, 0.036 mmol, 59%). 1H-NMR (CDCl3, 500 MHz) δ = 10.12 (1H, d, ^{3}J = 5.3, H^{6}-NC), 8.07 (1H, d, ^{3}J = 8.0, H^{3}-NC), 8.00 (2H, d, ^{3}J = 8.4, H^{6}-NCN), 7.96 (1H, td, ^{3}J = 8.0, 1.4, H^{4}-NC), 7.65 (2H, d, ^{3}J = 5.6, H^{3}-NCN), 7.59 (1H, t, ^{3}J = 7.7, H^{5}-NC), 7.51-7.55 (3H, m, H$^{3'}$-NC+H^{4}-NCN), 6.88 (1H, s, H$^{4'}$-NCN), 6.75 (2H, ddd, ^{3}J = 7.2, ^{4}J = 5.9, ^{5}J = 1.0, H^{5}-NCN), 6.71 (1H, td, ^{3}J = 7.4, ^{4}J = 1.2, H$^{5'}$-NC), 6.54 (1H, td, ^{3}J = 7.5, ^{4}J = 1.0, H$^{4'}$-NC), 6.00 (1H, d, J = 7.7, H$^{6'}$-NC), 2.83 (6H, s, H^{Me}). Mass Spectrometry MS (ES^{+}) *m/z* 606 ([M – Cl]+), 638 ([M –Cl + MeOH]+).

Synthesis of Ir(1,3-di-(2-pyridyl)-4,6-difluoromethylbenzene-N,C$^{2'}$,N)(2-phenylpyridine-N,C$^{2'}$) chloride [Ir(L2)(ppy)Cl] (4)

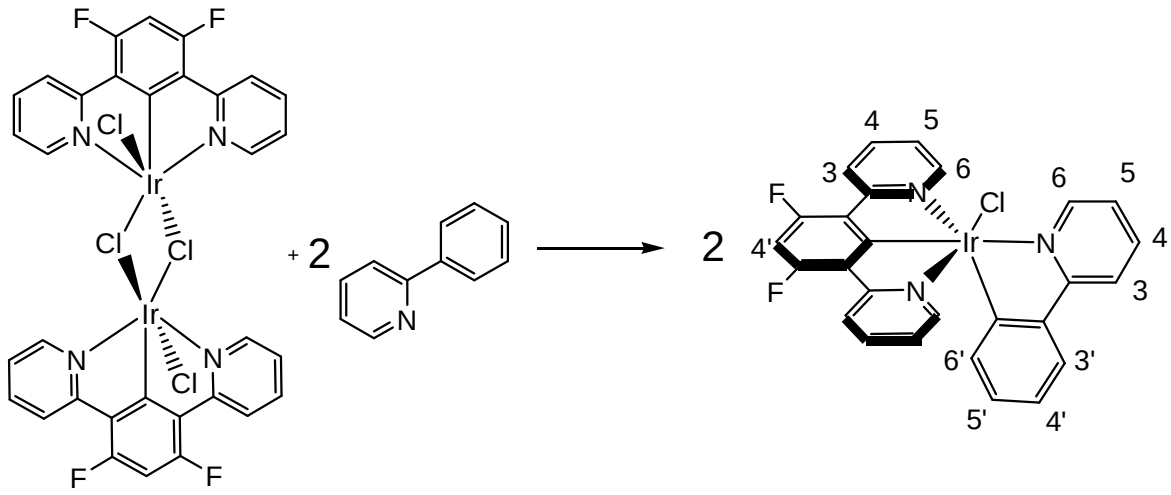

This complex was prepared from [Ir(**L2**)Cl(μ-Cl)]$_2$ (50 mg, 0.047 mmol) and ppyH (15 mg, 0.095 mmol) in the presence of AgOTf (50 mg, 0.18 mmol) in toluene (4 mL), using the procedure described above for Ir(**L1**)(dFppy)Cl **(1)**. The product was purified by chromatography (silica, CH_2Cl_2/MeOH, gradient elution from 100/0 to 96/4), leading to the product as a yellow solid (54 mg, 0.083 mmol, 88%). ^{1}H NMR ($CDCl_3$, 500 MHz): δ 10.12 (1H, dd, ^{3}J = 5.5, ^{4}J = 1.0, H^6-NC), 8.10 (3H, ^{3}J = 5.0, H^3-NC+^{6}-NCN), 8.01 (1H, td, ^{3}J = 8.0, ^{4}J = 1.5, H^4-NC), 7.64 – 7.56 (6H, m, H^3-NCN+H^4-NCN+H^5-NC+H$^{3'}$-NC), 6.84 (2H, ddd, ^{3}J = 7.0, ^{4}J = 1.5, H^5-NCN), 6.79 (1H, t, ^{3}J = 11, H$^{5'}$-NCN), 6.78 (1H, m, H$^{4'}$-NC), 6.63 (1H, ddd, ^{3}J =7.5, ^{4}J = 1.0, H$^{4'}$-NC), 6.07 (1H, dd, ^{3}J = 7.5, ^{4}J = 1.0, H$^{6'}$-NC). ^{13}C-NMR ($CDCl_3$, 176 MHz) δ 184.8 (C$^{1'}$-NCN), 177.2 (C$^{2'}$-NC), 166.4 (C^2-NCN), 164.7 (C$^{3'}$-NCN+C$^{2'}$-NCN), 150.9 (CH$^{6'}$-NC, C^4-NCN CH^4-NC or CH^3-NCN), 149.2 (CH^6-NC), 137.8 (CH$^{4'}$-NCN), 136.7 (CH$^{6'}$-NC, CH^4-NC, CH^4-NCN or CH^3-NCN), 135.6 (CH$^{3'}$-NC), 129.4 (CH$^{4'}$-NC), 123.8 (CH$^{6'}$-NC, CH^4-NCN CH^4-NC or CH^3-NCN), 122.9 (C^6-NCN), 122.8 (C$^{1'}$-NCN), 122.8 (C$^{1'}$-NC), 122.6 (C^2-NC), 122.4 (CH^5-NCN, C^5-NC or CH$^{5'}$-NC), 121.7 (CH^5-NCN, CH^5-NC or CH$^{5'}$-NC), 118.8 (CH^3-NC), 96.9 (CH^5-NCN, C^5-NC or CH$^{5'}$-NC). ^{19}F NMR ($CDCl_3$, 376 MHz): δ –109.0 (2F, d, ^{3}J = 12, NCN). MS

(ES+): *m/z* 655 $[M–Cl+CH_3CN]^+$. HRMS (ES+): *m/z* 653.1267 $[M–Cl+CH_3CN]^+$. Calcd for $C_{29}H_{20}N_4F_2{}^{191}Ir$: *m/z* 653.1265. Elemental analysis. found: 50.09% C, 3.58% H, 4.29% N, calculated: 50.00% C, 2.62 H%, 6.48%.

Synthesis of Ir(1,3-di-(2-pyridyl)-4,6-di-(trifluoromethyl)benzene-N,C$^{2'}$,N)(2-phenylpyridine-N,C$^{2'}$) chloride [Ir(L3)(ppy)Cl] (5)

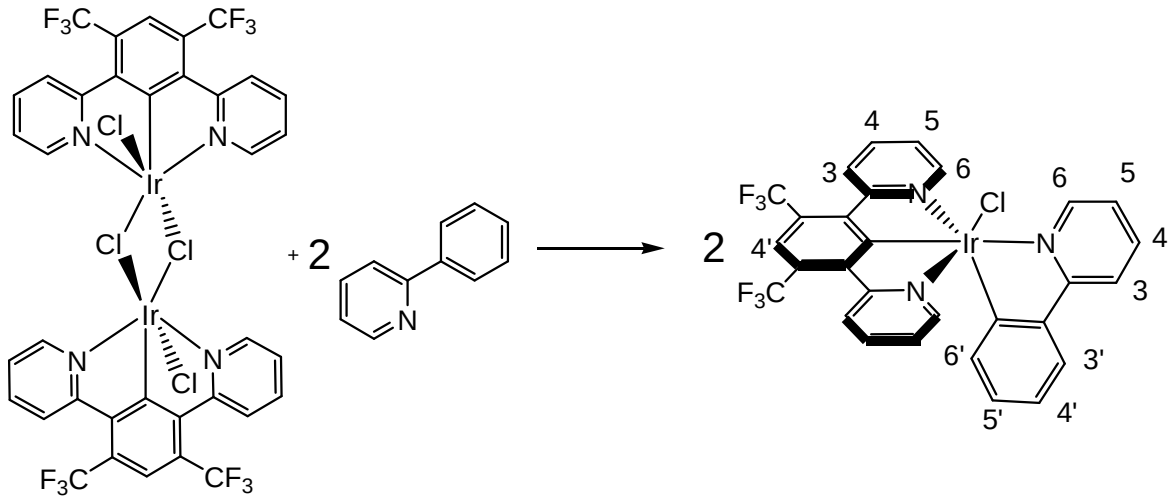

A mixture of [Ir(**L3**)Cl(μ-Cl)]$_2$ (30 mg, 0.028 mmol), ppyH (0.25 mL, 270 mg, 1.74 mmol) and AgOTf (30 mg, 0.12 mmol) in toluene (4 mL) was heated at reflux under an atmosphere of nitrogen for 24 h. After cooling to room temperature, the precipitated AgCl was removed by centrifuge and washed with acetonitrile. The filtrate and washings were combined, and the solvent removed under reduced pressure. The residue was taken up into CH_2Cl_2 (15 mL) and the solution washed with $HCl_{(aq)}$ (1M, 3 × 10 mL), followed by water (10 mL). After drying over $MgSO_4$, the solvent was removed under reduced pressure, and the residue purified by chromatography (silica, CH_2Cl_2/MeOH, gradient elution from 100/0 to 95/5), to give the product as an orange-red solid (19 mg, 0.051 mmol, 91%). ^{1}H NMR ($CDCl_3$, 500 MHz): δ 10.12 (1H, dd, ^3J = 5.5, ^4J = 1.0, H^6-NC), 8.39 (2H, d, ^3J = 8.0, H^6-

NCN), 8.11 (1H, d, H^3-NC), 8.06 (1H, s, $H^{4'}$-NCN), 8.04 (1H, td, ^3J = 8.0, ^4J = 1.0, H^4-NC), 7.83 (2H, dd, ^3J = 6.0, ^4J = 1.0, H^3-NCN), 7.71 (2H, ddd, ^3J = 8.0, 8.0, ^4J = 1.0, H^4-NCN), 7.61 (2H, m, H^4-NC+H^5-NC), 6.99 (2H, ddd, ^3J = 8.0, ^4J = 1.0, $H^{3'}$-NCN), 6.76 (1H, ddd, ^3J = 7.5, ^4J = 1.0, $H^{5'}$-NC), 6.62 (1H, ddd, ^3J = 7.5, ^4J = 1.0, $H^{4'}$-NC), 6.07 (1H, dd, ^3J = 5.5, ^4J = 1.0, $H^{6'}$-NC). ^{13}C-NMR ($CDCl_3$, 125 MHz) δ 184.9 ($CH^{6'}$-NCN), 165.2 (C^2-NC), 164.9 (C^2-NCN), 164.7 ($C^{2'}$-NCN), 151.2 ($C^{2'}$-NC), 143.2 ($C^{1'}$-NC), 136.9 (CH^3-NCN), 136.7 ($C^{3'}$-NC), 136.4 ($CH^{6'}$-NC), 130.1 ($CH^{5'}$-NC), 125.8 (C^6-NCN), 124.6 (CH^5-NC), 124.5 (CH^5-NCN), 123.5 (CH^4-NCN), 123.3 ($CH^{4'}$-NC), 122.7 ($CH^{3'}$-NCN), 122.4 ($CH^{5'}$-NC), 119.6 (CH^3-NC), 119.3 ($CH^{4'}$-NCN), 118.4 (CH^4-NC), 31.2 (C^{CF3}). ^{19}F NMR ($CDCl_3$, 376.4 MHz): δ –59.1 (6F, s, NCN). Mass Spectrometry (ES+): *m/z* 755 [M-CH_3CN]. HRMS (ES+): *m/z* 753.1198 [M–Cl+CH_3CN]$^+$. Calcd for $C_{31}H_{20}N_4ClF_6{}^{191}Ir$: *m/z* 753.1201. Elemental analysis: found: 46.54% C, 2.46% H, 6.15% N, calculated: C 46.52%, N=5.61%, H=2.27%.

Synthesis of Ir(1,3-di-(4-methoxy-2-pyridyl)-4,6-difluorobenzene-N,$C^{2'}$,N)(2,4-difluorophenylpyridine-N,$C^{2'}$) chloride [Ir(L5)(dFppy)Cl] (6)

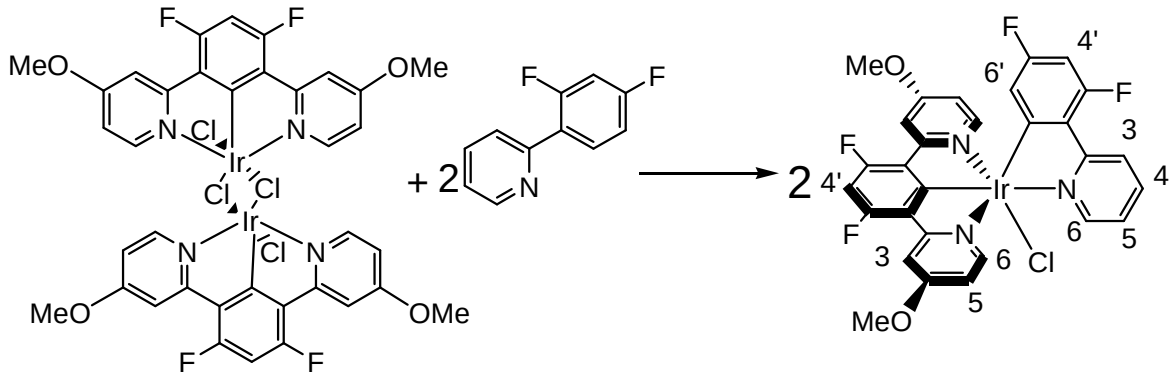

This complex was prepared from [Ir(**L5**)Cl(μ-Cl)]$_2$ (20 mg, 0.017 mmol), dFppyH (7 mg, 0.038 mmol) and Silver triflate (9 mg, 0.034 mmol) in 3 ml of toluene, using

the procedure described above for Ir(**L1**)(dFppy)Cl **(1)**, purification was achieved via silica gel separation chromatography (from DCM 100% to DCM 98%, MeOH 2%). The product was a yellow solid (17 mg, 0.022, 65%). ^{1}H NMR (400 MHz, $CDCl_3$) δ 10.11 (dd, ^{3}J = 5.5, ^{4}J = 1.0, 1H, H^{6}-NC), 8.4 (dd, ^{3}J = 8.4, ^{4}J = 1.2, 2H, H^{6}-NCN), 7.96 (td, ^{3}J = 7.8, ^{4}J = 1.6, 1H, H^{3}-NC), 7.65 – 7.38 (m, 4H, H^{3}-NCN+H^{5}-NC+H^{3}-NC), 6.72 (t, ^{3}J = 11.6 Hz, 1H, $H^{4'}$-NCN), 6.41 (ddd, ^{3}J = 14.2, ^{4}J = 6.6, ^{5}J = 2.8, 2H, H^{5}-NCN), 6.22 (ddd, ^{3}J = 13.0, ^{4}J = 9.0, ^{5}J = 2.4 Hz, 1H, $H^{3'}$-NC), 5.56 (dd, ^{3}J = 9.0, ^{4}J = 2.5 Hz, 1H, $H^{6'}$-NC), 3.84 (s, 7H, H^{OMe}). ^{19}F-NMR (400 MHz, $CDCl_3$) δ:-108.8 (2F, J=11.8, NCN), -109.2 (1F, NC), 110.5 (1F, NC). Mass Spectrometry (MALDI+): *m/z* 751 $[M\text{-}CH_3CN]^+$. HRMS (ASAP+): *m/z* 744.0790 $[M+H]^+$. Calculated for $C_{29}H_{20}N_3O_2F_4Cl^{191}Ir$: *m/z* 744.0786.

Synthesis of Ir(1,3-di-(4-methoxy-2-pyridyl)-4,6-difluorobenzene-N,C$^{2'}$,N)(2,4-(difluorophenyl)-4-methylpyridine-N,C$^{2'}$) chloride [Ir(L5)(dFppic)Cl] (7)

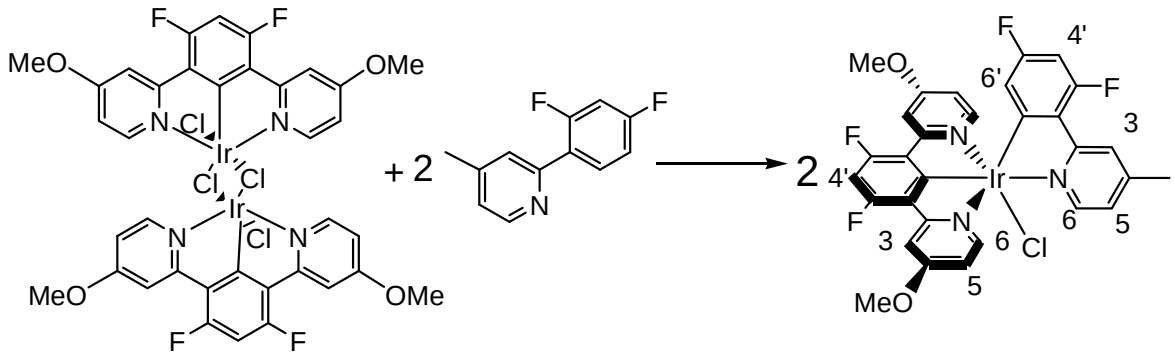

This complex was prepared from [Ir(**L5**)Cl(*μ*-Cl)]$_2$ (20 mg, 0.017 mmol), dFppyH (8 mg, 0.039 mmol) and Silver triflate (9 mg, 0.034 mmol) in 3 ml of toluene, using the procedure described above for Ir(**L1**)(dFppy)Cl **(1)**, purification was achieved via silica gel separation chromatography (from DCM 100% to DCM 98%, MeOH 2%). The product was a yellow solid (17 mg, 0.022, 65%). ^{1}H NMR ($CDCl_3$, 400 MHz) δ 9.96 (d, ^{3}J = 5.7, 1H, H^{6}-NC), 8.26 (s, 1H, H^{3}-NC), 7.62 (d, ^{3}J = 8.8, 2H,

H^6-NCN), 7.39–7.12 (m, 5H, H^3-NCN+H^3-NCN+H^5-NC), 6.76 (t, ^3J = 11.6, 1H, $H^{4'}$-NCN), 6.44 (dd, ^3J = 6.6, ^4J = 2.9 Hz, 2H, H^5-NCN), 6.25 (ddd, ^3J = 13.0, ^4J = 9.0, ^5J = 2.4, 1H, $H^{4'}$-NC), 5.58 (dd, ^3J = 8.9, ^4J = 2.5, 1H, $H^{6'}$-NC), 3.88 (s, 6H, H^{OMe}). Mass Spectrometry (MALDI+): *m/z* 759 $[M]^+$, *m/z* 724 $[M\text{-}Cl]^+$. HRMS (ASAP+): *m/z* 757.0865 $[M]^+$. Calculated for $C_{30}H_{21}N_3O_2F_4Cl^{191}Ir$: 757.0864 m/q.

Synthesis of Ir(1,3-di-(4-methoxy-2-pyridyl)-4,6-difluorobenzene-N,C$^{2'}$,N)(2,4-(difluorophenyl)-4-methoxypyridine-N,C$^{2'}$) chloride [Ir(L5)(dFpOMepy)Cl] (8)

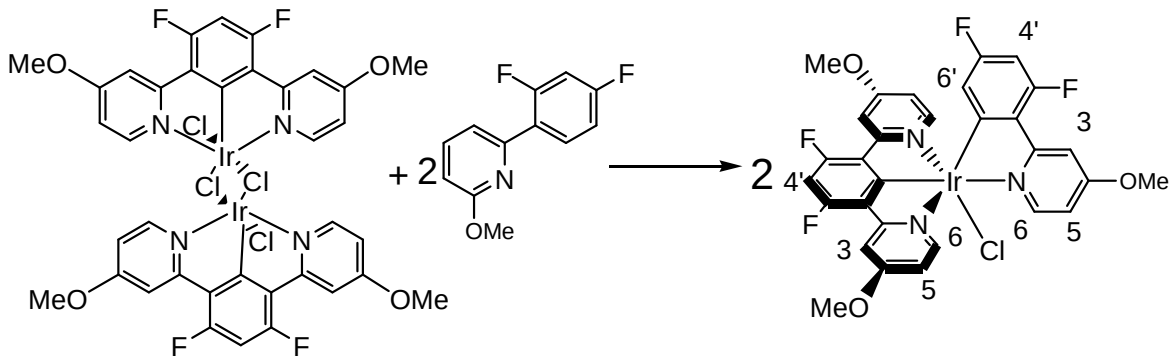

This complex was prepared from [Ir(**L5**)Cl(μ-Cl)]$_2$ (50 mg, 0.047 mmol), dFppyH (21 mg, 0.095 mmol) and Silver triflate (58 mg, 0.219 mmol) in 3 ml of toluene, using the procedure described above for Ir(**L1**)(dFppy)Cl **(1)**, purification was achieved via silica gel separation chromatography (from DCM 100% to DCM 98%, MeOH 2%). The product was a yellow solid (19 mg, 0.024, 26%). ^{1}H NMR (400 MHz, $CDCl_3$) δ 9.89 (d, ^3J = 6.4, 1H, H^6-NC), 7.93 (s, 1H, H^3-NC), 7.59 (d, ^3J = 2.7, 2H, H^6-NCN), 7.45 – 6.97 (m, 3H, H^3-NCN+H^5-NC), 6.73 (t, ^3J = 11.6, 1H, $H^{4'}$-NCN), 6.43 (dd, J = 6.6, ^4J = 2.9, 2H, H^5-NCN), 6.22 (m, 1H, $H^{4'}$-NC), 5.55 (dd, ^3J = 9.0, ^4J = 2.4, 1H, $H^{6'}$-NC), 4.07 (s, 3H, H^{OMe}-NC), 3.86 (s, 6H, H^{OMe}-NCN). ^{19}F-NMR ($CDCl_3$, 376 MHz): δ -108.9 (2F, ^3J=11.2, NCN), -109.48, 110.5 (2F, s, NC).

Mass Spectrometry (ASAP+): 740 *m/z* $[M\text{-}Cl]^+$, *m/z* 775 $[M]^+$. HRMS (ASAP+): *m/z* 773.0820 $[M]^+$. Calculated for $C_{30}H_{21}N_3O_3F_4Cl^{191}Ir$: *m/z* 773.0814.

Synthesis of Ir(1,3-di-(4-(trifluoromethyl)-2-pyridyl)-4,6-bis-(trifluoromethyl)benzene-N,C$^{2'}$,N)(2-phenylpyridine-N,C$^{2'}$) chloride [Ir(L4)(ppy)Cl] (9)

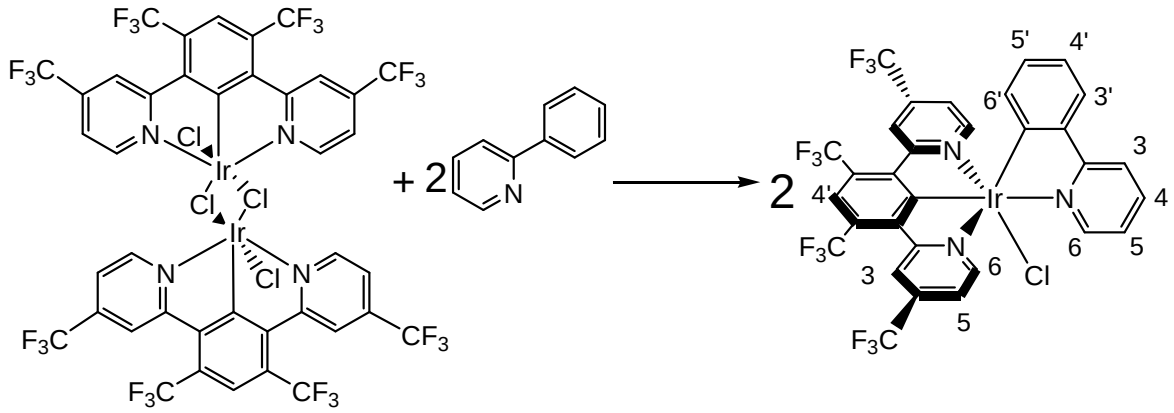

A mixture of [Ir(**L4**)Cl(μ-Cl)]$_2$ (15 mg, 0.010 mmol), ppyH (0.25 mL, 270 mg, 1.74 mmol) and AgOTf (10 mg, 0.04 mmol) was heated at reflux under an atmosphere of nitrogen for 24 h. After cooling to room temperature, the solution was diluted in DCM (5 ml) and the precipitated AgCl was removed by centrifuge and washed with DCM. The filtrate and washings were combined, and the solvent removed under reduced pressure. The residue was taken up into CH_2Cl_2 (15 mL) and the solution washed with $HCl_{(aq)}$ (1M, 3 $\times$ 10 mL), followed by water (10 mL). After drying over $MgSO_4$, the solvent was removed under reduced pressure, and the residue purified by chromatography (silica, CH_2Cl_2/MeOH, gradient elution from 100/0 to 95/5), to a give the product as an orange-red solid (7 mg, 0.008 mmol, 40%). ^{1}H NMR ($CDCl_3$, 400 MHz): δ 10.01 (d, 1H, ^3J = 5.6, H^6-NC), 8.63 (d, 2H, appears as a singlet, H^6-NCN), 8.17-8.09 (d+s, 3H, H^3-NC+H^4-NCN), 8.02 (d, 2H, ^3J = 5.6, H^5-

NCN), 7.99 (d, 1H, ^{3}J = 8.0, $H^{3'}$-NC), 7.76-7.59 (t+s, 2H, $H^{4'}$-NCN+H^{4}-NC), 7.44 (t, 1H, ^{3}J = 6.8, H^{5}-NC), 6.82 (t, 1H, ^{3}J = 7.6, $H^{5'}$-NC), 6.61 (t, 1H, ^{3}J = 7.6, $H^{4'}$-NC), 5.58 (d, 1H, ^{3}J = 7.6, $H^{6'}$). ^{19}F-NMR ($CDCl_3$, 376 MHz): δ -59.5 (6F, NCN), 65.4 (6F, NCN). Mass Spectrometry (MALDI+): *m/z* 891 $[M+CH_3CN]^+$. HRMS (ASAP+): *m/z* 883.0328 $[M]^+$. Calculated for $C_{31}H_{15}N_3F_{12}Cl^{191}Ir$: *m/z* 883.0369.

Synthesis of Ir(1,3-di-(4-(trifluoromethyl)-2-pyridyl)-4,6-bis-(trifluoromethyl)-benzene-N,$C^{2'}$,N)(2-(1-benzo[b]thiophene)iso-1-quinoline-N,$C^{2'}$)chloride [Ir(L4)(btiq)Cl] (10)

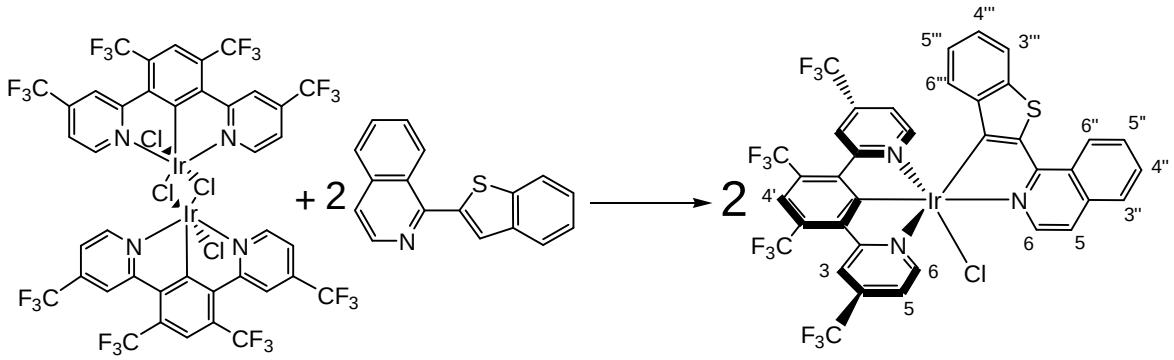

A mixture of [Ir(**L4**)Cl(*μ*-Cl)]$_2$ (15 mg, 0.010 mmol), btiqH (7 mg, 0.027 mmol) and AgOTf (10 mg, 0.04 mmol) in 3 ml of toluene was heated at reflux under an atmosphere of nitrogen for 24 h. After cooling to room temperature, the precipitated AgCl was removed by centrifuge and washed with DCM. The residue was taken up into CH_2Cl_2 (15 mL) and the solution washed with $HCl_{(aq)}$ (1M, 3 × 10 mL), followed by water (10 mL). After drying over $MgSO_4$, the solvent was removed under reduced pressure, and the residue purified by chromatography (silica, CH_2Cl_2/MeOH, gradient elution from 100/0 to 95/5), to a give the product as an orange-red solid (3 mg, 0.003 mmol, 15%). ^{1}H NMR ($CDCl_3$, 400 MHz): δ 10.04 (d, 1H, ^{3}J = 6.0, H^{6}-NC), 9.19 (d, 1H, ^{3}J = 8.8, $H^{3''}$-NC), 8.62-8.61 (d+.d, 3H,

$H^{6"}$-NC+H^{6}-NCN), 8.28 (s, 1H, $H^{4'}$-NCN), 8.11 (d, 1H, ^{3}J = 10.0, $H^{6'''}$-NC), 7.95 – 7.60 (m, 7H, $H^{4"}$-NC+$H^{5"}$-NC+H^{5}-NC+$H^{5"}$-NC+H^{5}-NCN), 7.10 (dd, ^{3}J = 11.0, ^{4}J = 4.1, 1H, $H^{6'''}$-NC), 6.96 (dd, ^{3}J = 9.5, ^{4}J = 3.7, 2H, H^{3}-NCN), 6.80 (dd, 1H, ^{3}J = 11.3, ^{4}J = 4.1, $H^{4"}$-NC), 5.99 (d, ^{3}J = 8.3, 1H $H^{3"}$-NC). ^{19}F-NMR ($CDCl_3$, 376 MHz): δ -59.5 (s, 6F), -65.4 (s, 6F).

Synthesis of Ir(1,3-di-(2-pyridyl)-4,6-di-(trifluoromethyl)benzene-N,$C^{2'}$,N)(2-(1-benzo[b]thiophene)iso-1-quinoline-N,$C^{2'}$) chloride [Ir(L3)(btiq)Cl] (11)

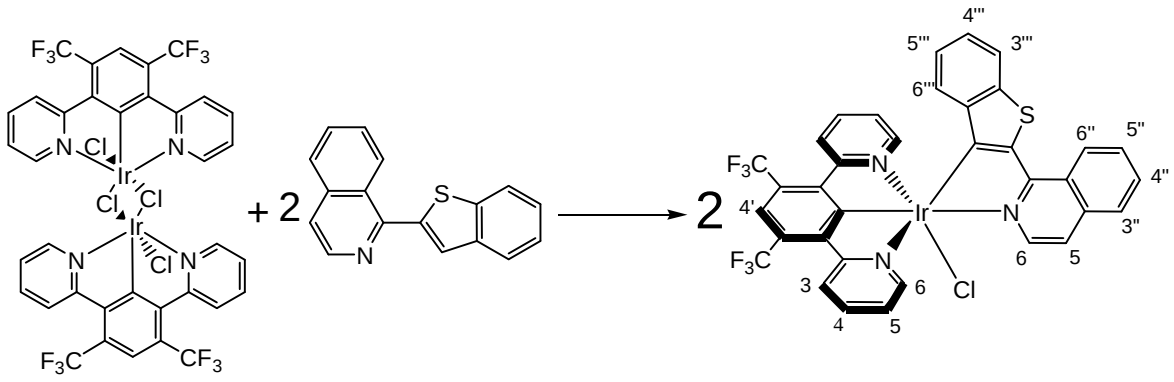

A mixture of [Ir(**L3**)Cl(μ-Cl)]$_2$ (33 mg, 0.030mol), btiqH (7 mg, 0.28 mmol), and silver triflate (33mg, 0.14mmol) in 4 ml of toluene was heated at reflux temperature, using the procedure described above for Ir(**L1**)(dFppy)Cl **(1)**, purification was achieved via silica gel separation chromatography (from 100% DCM to 95% DCM; 5% MeOH). The product was a reddish solid (44 mg, 0.051 mmol, 86%). ^{1}H NMR (400 MHz, $CDCl_3$) δ 10.12 (d, ^{3}J = 6.3,H^{6}-NC), 9.22 (d, ^{3}J = 8.1, 1H, $H^{3"}$-NC), 8.39 (d, J = 8.6, 2H, H^{6}-NCN), 8.22 (s, 1H, $H^{4'}$-NCN), 8.10 (d, J = 7.8, 1H, $H^{6"}$-NC), 7.95 – 7.60 (m, 8H, $H^{4"}$-NC+$H^{5"}$-NC+$H^{3'''}$-NC+H^{3}-NCN+H^{4}-NCN+H^{5}-NC), 7.10 (dd, ^{3}J = 11.0, ^{4}J = 4.1, 1H, $H^{5'''}$-NC), 6.96 (dd, ^{3}J = 9.5, ^{4}J = 3.7, 2H, H^{25}-NCN), 6.80 (dd, ^{3}J = 11.3, ^{4}J = 4.1, 1H, $H^{4'''}$-NC), 5.99 (d, ^{3}J = 8.3, 1H $H^{6'''}$-NC). ^{19}F-NMR (CD_3Cl, 660 MHz): δ –108.6 (6F, d, ^{3}J = 11.2, NCN). Mass

Spectrometry (ASAP+): = *m/z* 855 $[M]^+$. HRMS (ASAP+): *m/z* 853.0515 $[M]^+$. Calculated for $C_{35}H_{19}N_3F_6SCl^{191}Ir$: *m/z* 853.0498.

Synthesis of Ir(1,3-di-(2-pyridyl)-4,6-difluorobenzene-N,C$^{2'}$,N)(1-phenylpyrrazole-N,C$^{2'}$) chloride [Ir(L2)(ppyz)Cl] (12)

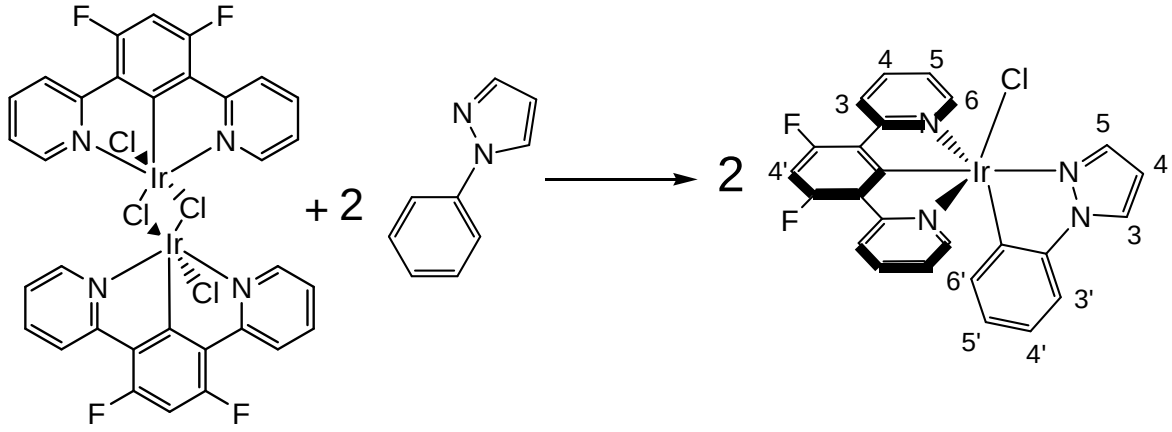

A mixture of [Ir(**L2**)Cl(μ-Cl)]$_2$ (40 mg, 0.038 mmol), 1-phenylpyrrazole (11 mg, 0.071 mmol) and silver triflate (39 mg, 0.15 mmol) in 4 ml of toluene was refluxed for 24 hours under nitrogen atmosphere. The solution was cooled to room temperature and the precipitated AgCl was removed by centrifuge and washed with acetonitrile. The combined organic layer was dried under reduced pressure. The product was purified via silica gel chromatography (from 100% DCM to 96% DCM; 4% MeOH), and obtained as a yellow solid (29 mg, 0.045mmol, 62%). ^{1}H-NMR ($CDCl_3$, 400 MHz): δ 8.56 (dd, 1H, ^3J = 2.0, ^4J = 0.8, H^5-NC), 8.17 (dd, 1H, ^3J = 2.8, ^4J = 0.8, H^3-NC), 8.01 (d, 2H, ^3J = 8.8, H^6-NCN), 7.68 (ddd, 2H, ^3J = 5.6, ^4J = 1.6, ^5J = 0.8, H^3-NCN), 7.54 (td, 2H, ^3J = 8.0, ^4J = 1.6, H^4-NCN), 7.01 (dd, 1H, ^3J = 8.4, ^4J = 1.6, H$^{3'}$-NC), 6.85-6.80 (t+t, 3H, H^5-NC+H^5-NCN), 6.73-6.66 (t+t, 2H, H$^{4'}$-NC+H$^{4'}$-NCN), 6.45 (td, 1H, ^3J = 8.8, ^4J = 1.6, H$^{5'}$-NC), 5.88 (dd, 1H, ^3J = 4.0, ^4J = 1.6, H$^{6'}$-NC). ^{19}F-NMR ($CDCl_3$, 660 MHz): δ -108.6 (2F, J=11.9, NCN). Mass

Spectrometry (MALDI+): *m/z* 603 $[M\text{-}Cl]^+$, *m/z* 638 $[M]^+$. HRMS (ASAP+): *m/z* 637.0726 $[M+H]^+$. Calculated for $C_{25}H_{17}N_4F_2Cl^{191}Ir$: *m/z* 637.0716.

Synthesis of [Ir(1,3-di-(2-pyridyl)-4,6-di-(trifluoromethyl)benzene-N,C$^{2'}$,N)(2,2'-bipyridine-N,N) chloride]$^+$[PF_6]$^-$ [Ir(L3)(bpy)Cl]$^+$ (13)

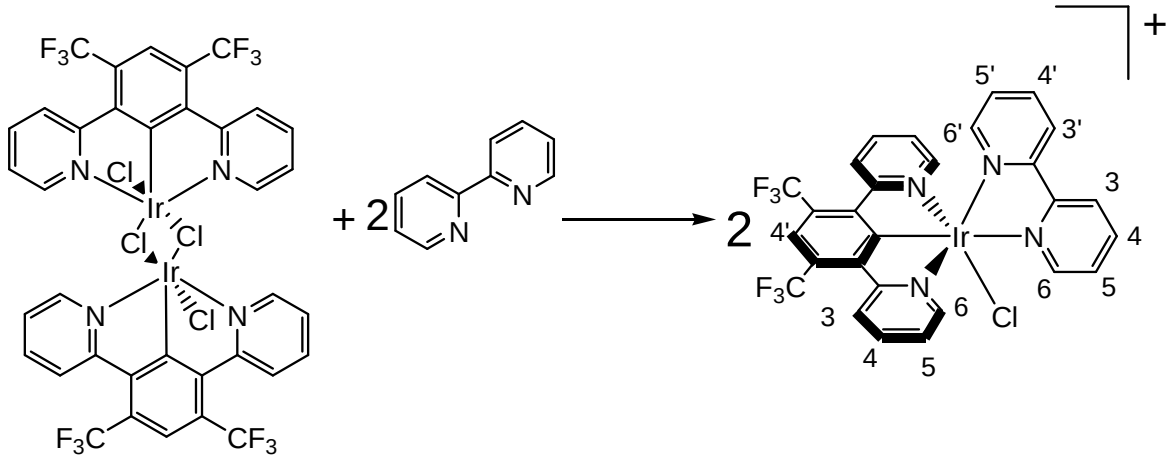

A mixture of [Ir(**L3**)Cl(μ-Cl)]$_2$ (30 mg, 0.029 mmol), bipyridine (10 mg, 0.060 mmol) and silver triflate (45 mg, 0.18 mmol) in 3 ml of ethylene glycol was refluxed for 24 hours and then cooled down to room temperature, 20 mL of saturated aqueous solution of KPF_6 was added and the precipitate collected by centrifuge. The solid was dissolved in acetonitrile and dried under reduced pressure. Purification was achieved by silica gel chromatography (100 % DCM to 99.5% DCM/ 0.5% MeOH). The product is an orange solid 26 mg (0.036 mmol, 76%). ^{1}H-NMR (CD_3CN, 700 MHz): δ 9.88 (ddd, 1H, ^3J = 5.3, ^4J = 1.7, ^5J = 0.8, H^6-NN), 8.67 (d, 1H, ^3J = 8.3, H^3-NN), 8.54-8.48 (s+d, 3H, H^6-NCN+H$^{4'}$-NCN), 8.40 (d, 1H, ^3J = 8.5, H$^{3'}$-NN), 8.23-8.15 (d+t, 3H, H^3-NCN+H^5-NN), 7.87 (td, 2H, ^3J = 8.0, ^4J = 1.6, H^4-NCN), 7.57 (td, 2H, ^3J = 7.9, ^4J = 1.4, H^5-NCN), 7.20-7.00 (d+t+t, 4H, H$^{4'}$+H$^{5'}$+H$^{6'}$-NN). ^{13}C-NMR (CD_3CN, 176 MHz) δ 175.3, 164.0, 157.7, 155.5, 153.9, 153.0, 149.3, 142.7, 141.0, 140.5, 139.9, 129.5, 128.4, 126.4, 126.3, 126.2, 126.1, 125.1, 124.3,

54.6 (C^{CF3}). ^{19}F-NMR (CD_3CN, 188 MHz): δ –60.1 (6F, s, NCN), -71.5 and -75.2 (6F, s, PF_6). Mass Spectrometry (ES+): *m/z* 751 $[M\text{-}Cl]^+$. HRMS (ES+): *m/z* 751.0670 $[M\text{-}Cl]^+$. Calculated for $C_{28}H_{17}N_4F_6Cl^{191}Ir$: *m/z* 751.1332. Elemental analysis: 38.54% C, 2.13% H, 6.68% N, calculated: 44.80% C, 2.27% H, 7.47% N.

Synthesis of Ir[(1,3-di-(2-pyridyl)-4,6-difluorobenzene-N,C$^{2'}$,N)(2,2'-bipyridine-N,N) chloride]$^+$[PF_6]$^-$ [Ir(L2)(bpy)Cl]$^+$ (14)

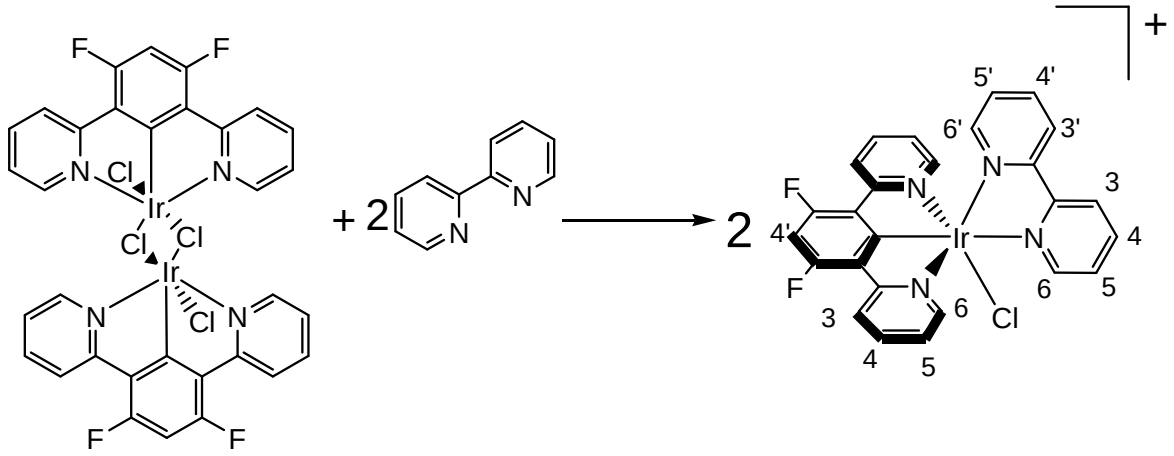

A mixture of [Ir(**L2**)Cl(μ-Cl)]$_2$ (30 mg, 0.029 mmol), bipyridine (10 mg, 0.060 mmol) and silver triflate (45 mg, 0.18 mmol) in 3 ml of ehtylene glycol, using identical synthetic procedure as for [Ir(**L3**)(bpy)Cl]$^+$ **(13)**, purification was achieved by silica gel chromatography (100 % DCM to 99.5% DCM/ 0.5% MeOH). The product is an orange solid 26 mg (0.074 mmol, 62%). ^{1}H-NMR (CD_3CN, 400 MHz): δ 9.79 (d, 1H, ^{3}J = 5.2, H^6-NN), 8.61 (d, 1H, ^{3}J = 8.0, H^3-NN), 8.35 (d, 2H, ^{3}J = 8.4, H^6-NCN), 8.19-8.15 (s+t, 2H, H$^{4'}$-NCN+H^4-NN), 7.74-7.64 (t+t+d, 5H, H^3-NCN+H^5-NCN+H^5-NN), 7.45 (d, 1H, ^{3}J = 8.0, H$^{3'}$-NN), 7.01 (t, 2H, ^{3}J = 7.6, H^3-NCN), 6.85 (t, 1H, ^{3}J = 7.6, H$^{4'}$-NN), 6.56 (t, 1H, ^{3}J = 7.6, H$^{5'}$-NN), 5.30 (d, 1H, ^{3}J = 8.4, H$^{6'}$-NN). ^{19}F-NMR(CD_3CN): -59.39 (2F, ^{3}J = 11.6, NCN), -71.5 and -75.2 (6F, s, PF_6). Mass

Spectrometry (ES+): *m/z* 651 $[M\text{-}Cl]^+$. HRMS (ES+): *m/z* 651.0732 $[M\text{-}Cl]^+$. Calculated for $C_{26}H_{17}N_4F_2Cl^{191}Ir$: *m/z* 651.1176. Elemental analysis: 39.44% C, 2.19% H, 6.89% N, calculated: 45.48% C, 2.48% H, 8.16% N.

5.12. $[Ir(N\hat{}C\hat{}N)(N\hat{}C\hat{}N)]^+$ and $[Ir(N\hat{}C\hat{}N)_2]^+$ complexes

Synthesis of [Ir(1,3-di-(2-pyridyl)-4,6-dimethylbenzene-N,C$^{2'}$,N)(1,3-di-(2-pyridyl)-4,6-difluorobenzene-N,C$^{2'}$,N)]$^+$[PF_6]$^-$ [Ir(L1)(L2)]$^+$ (15)

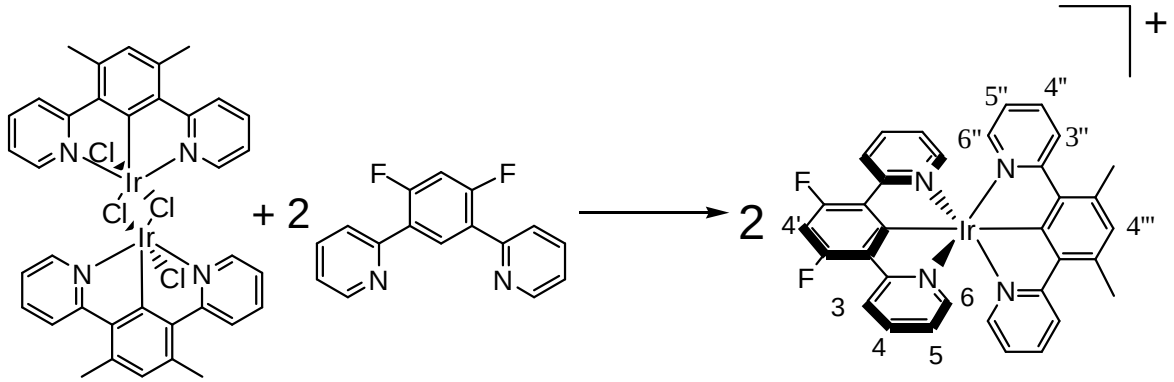

A mixture of [Ir(**L1**)Cl(μ-Cl)]$_2$ (20 mg, 0.019 mmol), H**L2** (13 mg, 0.038 mmol) and silver triflate (30 mg, 0.11 mmol) in 4 ml of toluene was refluxed for 24 hours under nitrogen atmosphere. The solution was cooled to room temperature and the precipitated AgCl was removed by centrifuge and washed with acetonitrile. The combined organic layer was dried under vacuum and dissolved in DCM and 20 mL of saturated aqueous solution of KPF_6 was added and the precipitate collected by centrifuge. The combined organic layer was dried under reduced pressure and purification was achieved via silica gel separation chromatography (from DCM 100% to DCM 97%, MeOH 3%). The product was a yellow solid (28 mg, 0.032 mmol, 84%). ^{1}H-NMR (CD_3CN, 400 MHz): δ 8.12-8.18 (d+d, 4H, H^6+$H^{6''}$), 7.40-7.69 (t+t, 4H, H^4+$H^{4''}$), 7.40 (d, 2H, ^3J = 5.6, $H^{3''}$), 7.32 (d, 2H, ^3J = 5.2, H^3), 7.23 (s,

1H, $H^{4'''}$), 7.15 (t, 1H, ^3J = 6.0, $H^{4'}$), 6.85-6.76 (t+t, 4H, H^5+$H^{5''}$), 2.91 (s, 6H, H^{Me}). ^{19}F-NMR (CD_3CN, 400 MHz) : δ -108.5 (d, 2F, ^3J = 12.4, NCN), -71.5 and -75.2 (6F, s, PF_6). Mass Spectrometry (ES+): *m/z* 719 $[M]^+$. HRMS (ASAP+): *m/z* 717.1590 $[M]^+$. Calculated for $C_{34}H_{24}N_4F_2{}^{191}Ir$: *m/z* 717.1517.

Synthesis of [Ir-di-(1,3-di(2-pyridyl)-4,6-di-fluoro-benzene-N,$C^{2'}$,N)]$^+$[PF_6]$^-$ [Ir(L2)$_2$]$^+$ (16)

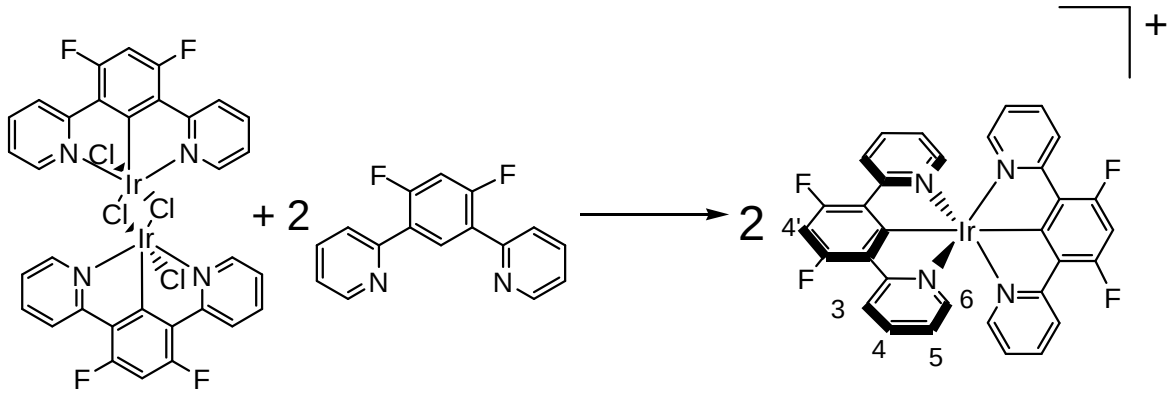

A mixture of [Ir(**L2**)Cl(μ-Cl)]$_2$ (30 mg, 0.029 mmol), H**L2** (16 mg, 0.058 mmol) and Silver triflate (45 mg, 0.18 mmol) in 4 ml of toluene was heated at reflux temperature, using the same method adopted for the synthesis of [Ir(**L1**)(**L2**)]$^+$ **(15)**, purification was achieved via silica gel chromatography (from DCM 100% to DCM 94%, MeOH 6%). The product was a yellow solid (14 mg, 0.017 mmol, 27%). ^{1}H-NMR (CD_3CN, 400 MHz): δ 8.19 (dd, 4H, ^3J = 8.4, H^6), 7.69 (td, 4H, ^3J = 8.0, H^4), 7.41 (dd, 2H, ^3J = 4.8, H^3), 7.15 (s, 2H, H^{4b}), 6.87 (td, 4H, ^3J = 8.0, H^5). ^{19}F-NMR (CD_3CN, 400 MHz): δ -108.3 (d, 4F, J=12.0, NCN), -71.5 and -75.2 (6F, s, PF_6). Mass Spectrometry (ES+): *m/z* 727 $[M]^+$.

5.13. Complexes with pyridylbenzimidazole as bidentate ligand

Synthesis of Ir(1,3-di-(2-pyridyl)-4,6-dimethylbenzene-N,C$^{2'}$,N)(2-(2-pyridyl)benzimidazole) chloride [Ir(L1)(pbi)Cl] (17)

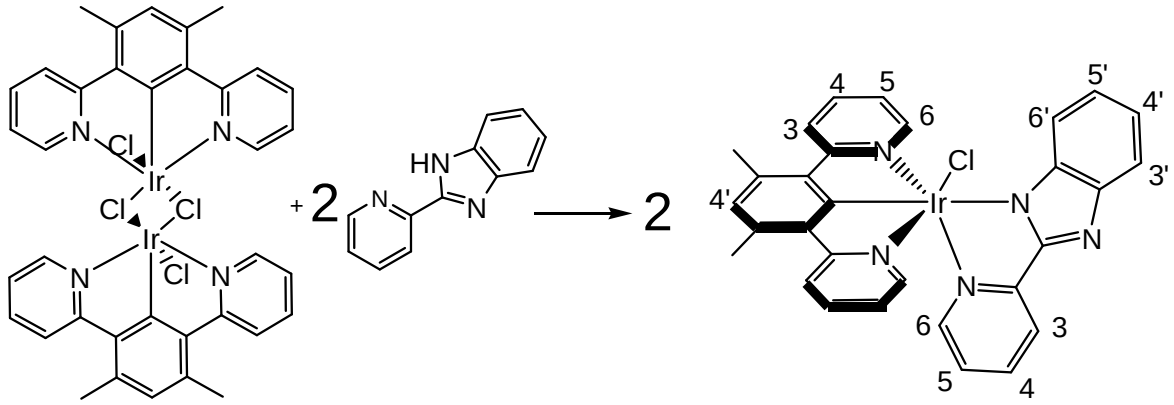

A mixture of [Ir(**L1**)Cl(μ-Cl)]$_2$ (50 mg, 0.047 mmol), pbiH (20 mg, 0.1 mmol) and silver triflate (50 mg, 0.18 mmol) in 4 ml of toluene was refluxed for 24 hours under nitrogen atmosphere. The solution was cooled to room temperature and the precipitated AgCl was removed by centrifuge and washed with acetonitrile. The combined organic layer was dried under reduced pressure, dissolved in dichloromethane and washed with 1M aqueous solution of HCl and dried over $MgSO_4$. The product was purified via silica gel separation chromatography (from 100% DCM to 98.5% DCM; 1.5% MeOH). The product was a yellow solid (18 mg, 0.026 mmol, 28%). ^{1}H-NMR ($CDCl_3$, 500 MHz): δ 8.73 (d, 1H, ^{3}J = 8.5, H^6-pbi), 8.39 (d, 1H, ^{3}J = 7.5, H$^{3'}$-pbi), 8.07 (d, 2H, ^{3}J = 8.5, H^6-NCN), 8.01 (d, 1H, ^{3}J = 8.5, H$^{5'}$-pbi), 7.94 (d, 2H, ^{3}J = 8.6, H^3-NCN), 7.64 (td, 2H, ^{3}J = 9.5, ^{4}J = 2.0, H^4-NCN), 7.51 (t, 1H, ^{3}J = 9.5, ^{4}J = 1.7, H$^{4'}$-pbi), 7.41 (t, 1H, ^{3}J = 8.0, H^4-pbi), 7.32 (t, 1H, ^{3}J = 7.0, H^5-pbi), 7.09 (d, 1H, ^{3}J = 5.5, H^3-pbi), 6.97 (s, 1H, H$^{4'}$-NCN), 6.90 (td, 2H, ^{3}J = 7.0, ^{4}J = 1.0, H^5-NCN), 6.71 (t, 1H, ^{3}J = 8.0, ^{4}J = 1.7, H$^{6'}$-pbi), 2.86 (s, 6H, H^{Me}). Mass Spectrometry (ES+): *m/z* 682 [M+H]$^+$. HRMS (ES+): *m/z* 680.1339 [M+H]$^+$. Calcd for $C_{30}H_{24}N_5Cl^{191}Ir$: *m/z* 680.1349. Elemental analysis: 48.19% C, 3.17% H, 9.03% N, calculated: 52.78% C, 3.37% H, 10.26% N

Synthesis of Ir(1,3-di-(2-pyridyl)-4,6-difluorobenzene)(2-(2-pyridyl)benzimidazole-N,C$^{2'}$,N) chloride [Ir(L2)(pbi)(Cl] (18)

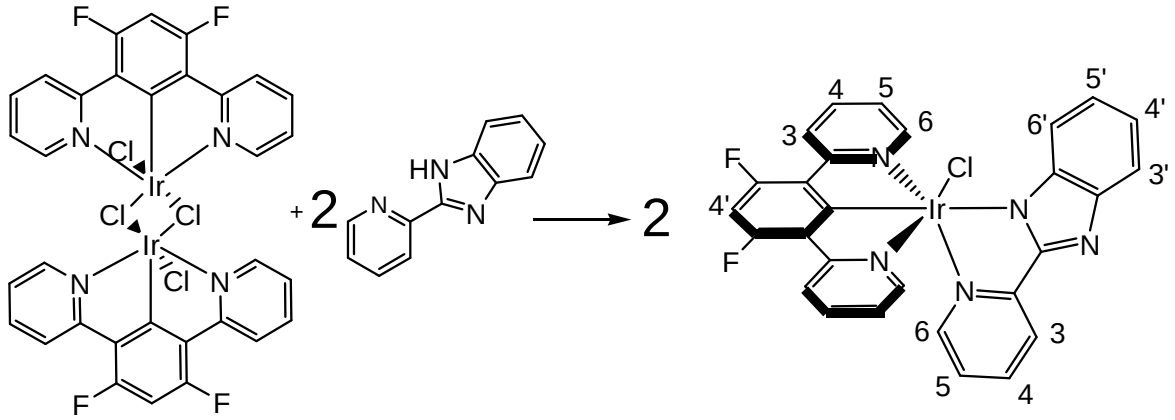

A mixture of [Ir(**L2**)Cl(μ-Cl)]$_2$ (50 mg, 0.047 mmol), pbiH (20 mg, 0.1 mmol) and silver triflate (50 mg, 0.15 mmol) in 4 ml of toluene was heated at reflux temperature, using the same synthetic method as for Ir(**L1**)(pbi)Cl **(17)**. The product was purified via silica gel separation chromatography (from 100% DCM to 97% DCM; 3% MeOH), and obtained as a yellow solid (27 mg, 0.040 mmol, 42%). ^{1}H-NMR ($CDCl_3$, 500 MHz): δ 9.88 (d, 1H, ^{3}J = 4.5, H^{6}-pbi), 8.65 (d, 1H, ^{3}J = 8.5, H^{3}-pbi), 8.20 (t, 1H, ^{3}J = 6.5, H^{4}-pbi), 8.12 (d, 2H, ^{3}J = 8.0, H^{6}-NCN), 7.62 (td, 1H, ^{3}J = 6.0, ^{4}J = 1.0, H^{5}-pbi), 7.61 (td, 2H, ^{3}J = 7.5, ^{4}J = 1.0, H^{4}-NCN), 7.50-7.32 (t+d, 3H, H^{3}-NCN+H$^{3'}$-pbi), 6.98-6.91 (t+d+t, 4H, H$^{4'}$-pbi+H^{5}-NCN+H$^{4'}$-NCN), 6.71 (t, 1H, ^{3}J = 7.5, H$^{5'}$-pbi), 5.82 (d, 1H, ^{3}J = 8.5, H$^{6'}$-pbi). ^{19}F-NMR($CDCl_3$, 376 MHz): δ -107.6 (2F, d, ^{3}J = 11.3, NCN). Mass Spectrometry (ES+): *m/z* 690 [M+H]$^{+}$. HRMS (ES+): *m/z* 688.0824 [M+H]$^{+}$. Calcd for $C_{28}H_{18}N_5ClF_2{}^{191}Ir$: *m/z* 688.0848. Elemental analysis: 46.67% C, 2.64% H, 9.03% N, calculated: 48.76% C, 2.61% H, 10.16% N

Synthesis of Ir(1,3-di-(2-pyridyl)-4,6-di-(trifluoromethyl)benzene-N,C$^{2'}$,N)(2-(2-pyridyl)bezimidazol) chloride [Ir(L3)(pbi)Cl] (19)

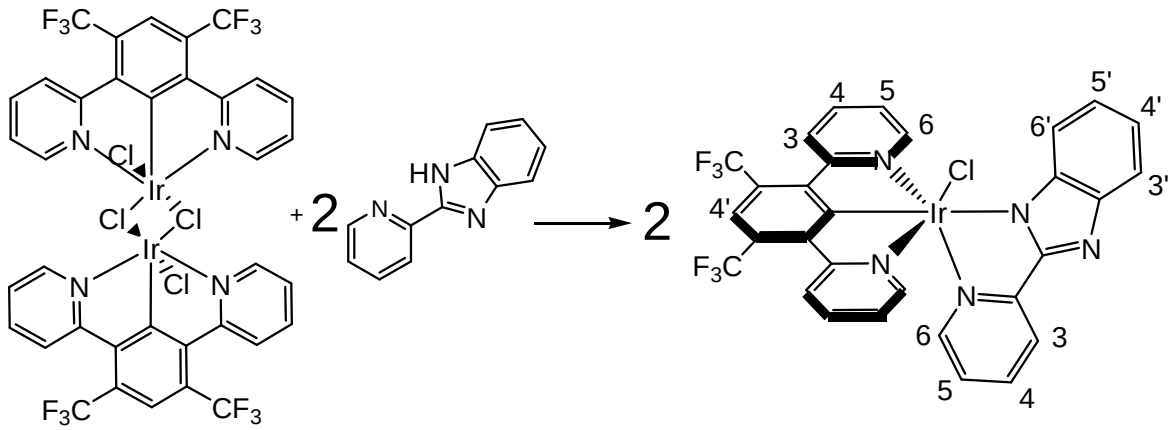

A mixture of [Ir(**L3**)Cl(μ-Cl)]$_2$ (30 mg, 0.024 mmol), pbiH (12 mg, 0.06 mmol) and silver triflate (30 mg, 0.1 mmol) in 4 ml of toluene was heated at reflux temperature, using the same synthetic method as for Ir(**L1**)(pbi)Cl **(17)**. The product was purified via silica gel chromatography (from 100% DCM to 99% DCM; 1% MeOH), and obtained as a yellow solid (14 mg, 0.018 mmol, 37%). ^{1}H-NMR ($CDCl_3$, 400 MHz): δ 9.79 (d, 1H, ^{3}J = 5.2, H^6-pbi), 8.61 (d, 1H, ^{3}J = 8.0, H^3-pbi), 8.35 (d, 2H, ^{3}J = 8.4, H^6-NCN), 8.19-8.15 (s+t, 2H, H$^{4'}$-NCN+H^4-pbi), 7.74-7.64 (t+t+d, 5H, H^3-NCN+H^4-NCN+H^5-pbi), 7.45 (d, 1H, ^{3}J = 8.0, H$^{3'}$-pbi), 7.01 (t, 2H, ^{3}J = 7.6, H^5-NCN), 6.85 (t, 1H, ^{3}J = 7.6, H$^{4'}$-pbi), 6.56 (t, 1H, ^{3}J = 7.6, H$^{5'}$-pbi), 5.30 (d, 1H, ^{3}J = 8.4, H$^{6'}$-pbi). ^{19}F-NMR ($CDCl_3$): δ -59.39. Mass Spectrometry (ES+): *m/z* 790 [M+H]$^+$.

Synthesis of [Ir(1,3-di-(2-pyridyl)-4,6-dimethylbenzene-N,C$^{2'}$,N)(2-(2-pyridyl-N-methyl)benzimidazole) chloride]$^{+}$[PF_6]$^{-}$ [Ir(L1)(Me-pbi)Cl]$^{+}$ (20)

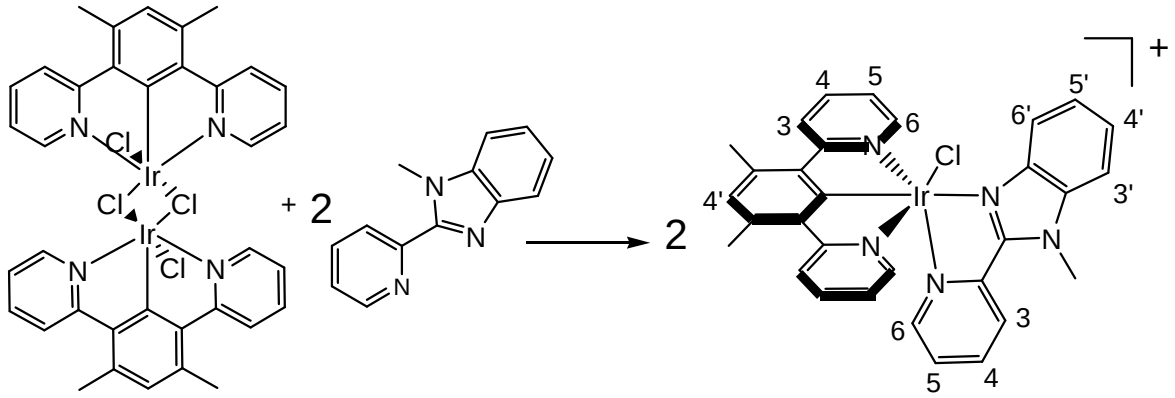

A mixture of [Ir(**L1**)Cl(μ-Cl)]$_2$ (28 mg, 0.027 mmol), Me-pbiH (12 mg, 0.54 mmol) and silver triflate (28 mg, 0.11 mmol) in 4 ml of toluene was heated at reflux temperature. The solution was cooled to room temperature and the precipitated AgCl was removed by centrifuge and washed with acetonitrile. The combined organic layer was dried under reduced pressure, dissolved in the minimum amount of acetonitrile and a saturated aqueous solution of KPF_6 was added, the precipitated complex was isolated by centrifuge, washed with water and dried under vacuum. The product was purified via silica gel separation chromatography (from 100% DCM to 98% DCM; 2% MeOH), and obtained as a yellow solid (12 mg, 0.029 mmol, 53%). ^{1}H-NMR (CD_3CN, 500 MHz): δ 10.06 (d, 1H, ^{3}J = 5.0, H^{6}-pbi), 8.73 (d, 1H, ^{3}J = 8.0, H^{3}-pbi), 8.53 (td, 1H, ^{3}J = 8.5, ^{4}J = 2.0, H^{4}-pbi), 8.21-8.17 (d+t, 3H, H^{5}-pbi+H^{6}-NCN), 7.78 (t, 2H, ^{3}J = 8.5, H^{4}-NCN), 7.64 (d, 2H, ^{3}J = 6.0, H^{3}-NCN), 7.53 (d, 1H, ^{3}J = 8.0, H$^{3'}$-pbi), 7.33 (t, 1H, ^{3}J = 7.0, H$^{4'}$-PBI), 7.23 (s, 1H, H$^{4'}$-NCN), 7.05 (td, 2H, ^{3}J = 7.0, ^{4}J = 1.0, H^{5}-NCN), 6.93 (t, 1H, ^{3}J = 7.5, H$^{5'}$-pbi), 6.87 (d, 1H, ^{3}J = 8.5, H$^{6'}$-pbi), 2.91 (s, 6H, H^{Me}). Mass Spectrometry (ES+): [M]$^{+}$ 696 *m/z*. HRMS (ES+): *m/z* 694.1470 [M]$^{+}$. Calcd for $C_{31}H_{26}N_5Cl^{191}Ir$: *m/z* 694.1506.

Synthesis of [Ir(1,3-di-(2-pyridyl)-4,6-di-(trifluoromethyl)benzene-N,$C^{2'}$,N)(2-(2-pyridyl-N-methyl)bezimidazol) chloride]$^{+}$[PF_6]$^{-}$ [Ir(L3)(Me-pbi)Cl]$^{+}$ (21)

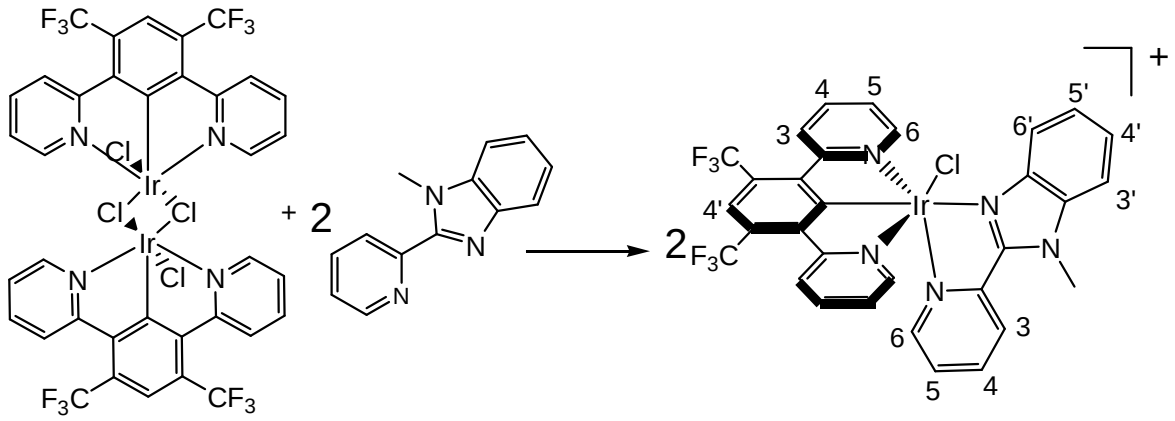

A mixture of [Ir(**L3**)Cl(μ-Cl)]$_2$ (30 mg, 0.024 mmol), Me-pbiH (12 mg, 0.54 mmol) and silver triflate (28 mg, 0.11 mmol) in 4 ml of toluene was heated at reflux teperature. Same procedure was adopted as for [Ir(**L1**)(Me-pbi)Cl]$^{+}$ **(20)**. The product was purified via silica gel chromatography (from 100% DCM to 98% DCM; 2% MeOH), and obtained as a yellow solid (12 mg, 0.025 mmol, 53%). ^{1}H-NMR (CD_3CN, 400 MHz): δ 10.01 (dd, 1H, ^{3}J = 6.0, ^{3}J = 0.8, H^{6}-pbi), 8.74 (d, 1H, ^{3}J = 7.2, H^{3}-pbi), 8.56 (td, 1H, ^{3}J = 4.0, ^{4}J = 1.6, H^{3py}-pbi), 8.31(s, 1H, $H^{4'}$-NCN), 8.21 (td, 1H, ^{3}J = 5.6, ^{4}J = 1.6, H^{5}-pbi), 7.95 (td, 2H, ^{3}J = 7.6, ^{4}J = 1.6, H^{4}-NCN), 7.79 (dd, 2H, ^{3}J = 6.4, ^{4}J = 0.4, H^{3}-NCN), 7.53 (d, 1H, ^{3}J = 8.8, $H^{3'}$-pbi), 7.32 (td, 1H, ^{3}J = 5.2, ^{4}J = 0.8, $H^{4'}$-pbi), 7.26 (td, 2H, ^{3}J = 5.6, ^{4}J = 1.2, H^{5}-NCN), 6.97 (td, 1H, ^{3}J = 5.6, ^{4}J = 0.8, $H^{5'}$-pbi), 5.65 (d, 1H, ^{3}J = 7.6, ^{3}J = 0.4, $H^{6'}$-pbi). ^{19}F-NMR (CD_3CN, 376 MHz): δ -60.15 (6F, NCN), -71.5 and -75.2 (6F, s, PF_6). Mass Spectrometry (ES+): *m/z* 804 $[M]^{+}$. HRMS (ES+): *m/z* 802.0901 $[M]^{+}$. Calcd for $C_{31}H_{20}N_5F_6Cl^{191}Ir$: *m/z* 802.0940.

5.14. Ligand metathesis

Synthesis of Ir(1,3-di-(2-pyridyl)-4,6-dimethylbenzene-N,C$^{2'}$,N)(2,4-(difluorophenyl)pyridine-N,C$^{2'}$) cynide [Ir(L1)(dFppy)CN] (22)

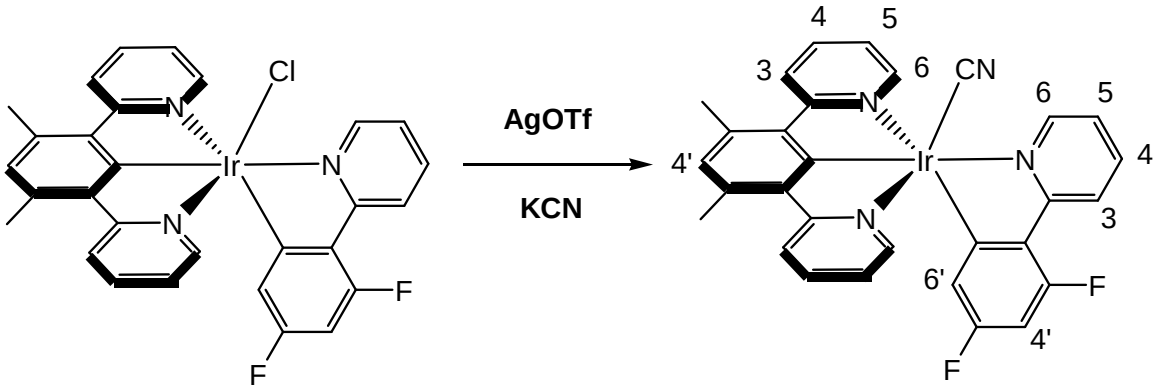

In Schlenk 15mg (0.022 mmol) of Ir(**L1**)(dFppy)Cl **(1)** and 8mg (0.3mmol) of silver triflate were dissolved in 2ml of acetone and refluxed for 6 hours. After cooling to room temperature the precipitated AgCl was removed by centrifuge and the combined organic layers dried under vacuum. The resulting solid was dissolved in methanol and was added to a solution of KCN (3mg, 0.05mmol) in 3 ml in methanol and strirred overnight. The resulting solution was then extracted in dichloromethane and washed with water and dried over $MgSO_4$. The product was obtained as a yellow solid (10 mg, 0.015 mmol, 68%). ^{1}H-NMR ($CDCl_3$, 400 MHz): δ 9.99 (d, 1H, ^{3}J = 5.2, H^{6}-NC), 8.40 (d, 1H, ^{3}J = 9.2, H^{3}-NC), 7.98-7.94 (t+d, 3H, H^{4}-NC+H^{6}-NCN), 7.60 (d, 2H, ^{3}J = 6.0, H^{3}-NCN), 7.53 (td, 2H, ^{3}J = 7.6, ^{4}J = 1.6, H^{4}-NCN), 7.43 (t, 1H, ^{3}J = 5.6, H^{5}-NC), 6.86 (s, 1H, H$^{4'}$-NCN), 6.72 (m, 2H, ^{3}J = 6.8, ^{4}J = 2.8, H^{5}-NCN), 6.15 (dd, ^{3}J = 11.2, ^{4}J = 2.0, 1H, H$^{4'}$-NC), 5.41 (dd, 1H, ^{3}J = 8.0, ^{4}J = 2.0, H$^{6'}$-NC), 2.77 (s, 6H, H^{Me}). ^{19}F-NMR ($CDCl_3$, 376 MHz): δ -109.0 (2F, ^{3}J = 11.6, NCN), -109.7 (2F, NC). Mass Spectrometry (MALDI+): *m/z* 668 $[M]^+$, *m/z* 642 $[M-(CN)]^+$. HRMS (ASAP+): *m/z* 666.1357 $[M]^+$. Calcd for $C_{30}H_{21}N_4F_2{}^{191}Ir$: *m/z* 666.1340.

Synthesis of Ir(1,3-di-(2-pyridyl)-4,6-difluorobenzene-N,C$^{2'}$,N)(2,4-(difluorophenyl)pyridine-N,C$^{2'}$) cyanide [Ir(L2)(dFppy)CN] (23)

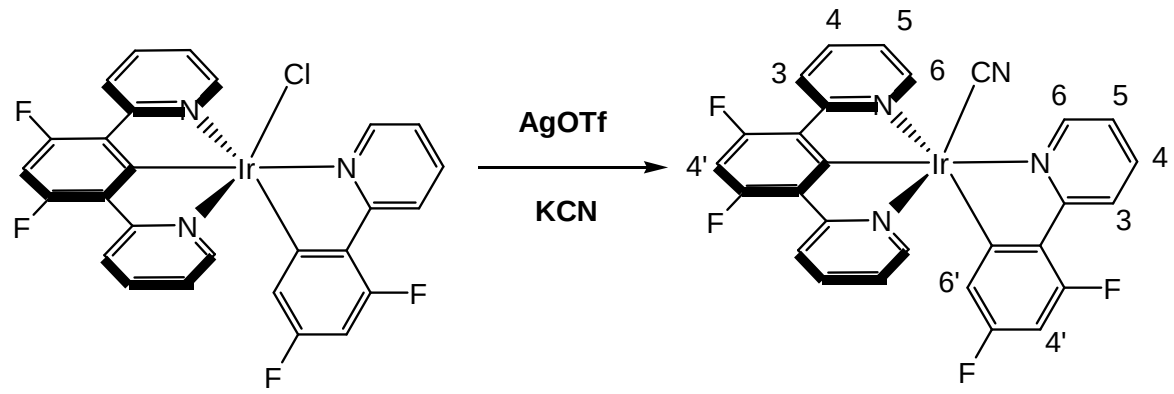

This complex prepared in the same way, starting from Ir(**L2**)(dFppy)Cl **(2)** (36mg, 0.052 mmol) leading to the product (22mg, 0.033 mmol, 63%). ^{1}H-NMR ($CDCl_3$, 700 MHz): δ 10.08 (d, 1H, ^{3}J = 4.9, H^{6}-NC), 8.44 (d, 1H, ^{3}J = 9,1, H^{3}-NC),8.12 (d, 2H, ^{3}J = 7.7, H^{6}-NCN), 8.04 (t, 1H, ^{3}J = 7.0, H^{4}-NC), 7.65 (t, 2H, ^{3}J = 7.0, H^{4}-NCN), 7.60 (d, 2H, ^{3}J = 4.9, H^{3}-NCN), 7.51 (t, 1H, ^{3}J = 6.3, H^{5}-NC), 6.86-6.83 (t+t, 3H, H^{5}-NCN+H$^{4'}$-NCN), 6.20 (m, 1H, ^{3}J = 11.2, ^{4}J = 1.4H$^{4'}$-NC), 5.46 (dd, 1H, ^{3}J = 7.7, ^{4}J = 0.7, H$^{6'}$-NC). ^{19}F-NMR ($CDCl_3$, 660 MHz): δ –107.6 (2F, d, ^{3}J = 6.0, NCN), -108.3 (1F, NC), -109.1 (1F, NC). Mass Spectrometry (MALDI+): *m/z* 676 [M]$^{+}$, *m/z* 650 [M-(CN)]$^{+}$. HRMS (ASAP+): *m/z* 674.0860. Calculated for $C_{28}H_{15}N_4F_4{}^{191}Ir$: *m/z* 674.0862.

Synthesis of Ir(1,3-di-(2-pyridyl)-4,6-difluorobenzene-N,C$^{2'}$,N)(2,4-(difluorophenyl)pyridine-N,C$^{2'}$) cyanide [Ir(L2)(ppy)CN] (24)

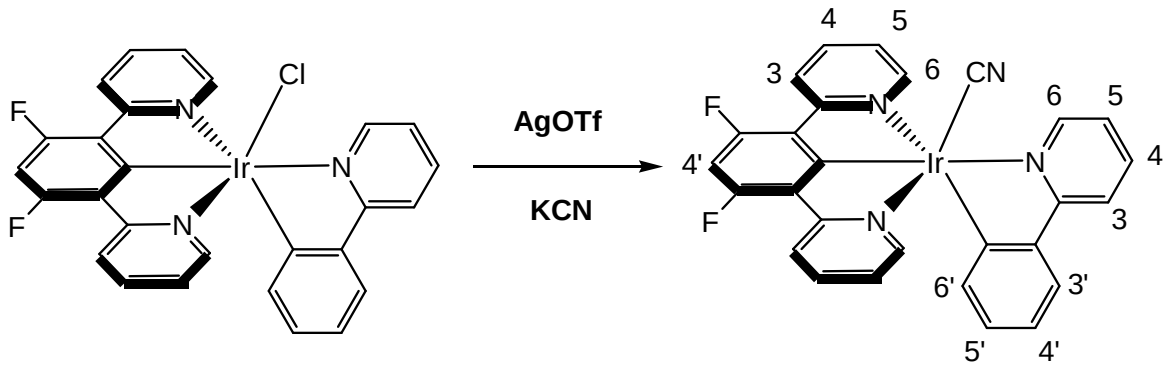

This complex prepared in the same way, starting from Ir(**L2**)(ppy)Cl **(4)** (36mg, 0.052 mmol) leading to the product (22mg, 0.033 mmol, 63%). ^{1}H-NMR ($CDCl_3$, 400 MHz): δ 9.96 (dd, 1H, ^{3}J = 4.8, H^{6}-NC), 8.62 (d, 1H, ^{3}J = 5.2, H^{3}-NC), 8.03(d, 2H, ^{3}J = 5.7, H^{6}-NCN), 7.98-7.91 (td+d, 2H, H^{4}-NC+H$^{3'}$-NC), 7.67 (t, 1H, ^{3}J=6.4, H^{4}-NC), 7.59-7.53 (td+d, 4H, H^{3}-NCN+H^{4}-NCN), 7.46-7.38 (t+t+t, 3H, H$^{4'}$-NC+H$^{4'}$-NCN+H^{5}-NC), 6.75 (td, 2H, ^{3}J = 9.6, ^{4}J = 1.6, H^{5}-NCN), 6.20 (td, 1H, ^{3}J = 6.0, ^{4}J = 1.2H$^{4'}$-NC), 5.46 (dd, 1H, ^{3}J = 7.2, ^{4}J = 0.8, H$^{6'}$-NC). ^{19}F-NMR ($CDCl_3$, 376 MHz): δ –108.6 (2F, d, $^{3}J_{F-H}$ = 12, NCN). Mass Spectrometry (MALDI+): *m/z* 640 [M]$^{+}$.

Synthesis of Ir(1,3-di-(2-pyridyl)-4,6-bis-(trifluoromethyl)benzene-N,$C^{2'}$,N) (2,4-(difluorophenyl)pyridine-N,$C^{2'}$) cyanide [Ir(L3)(dFppy)CN] (25)

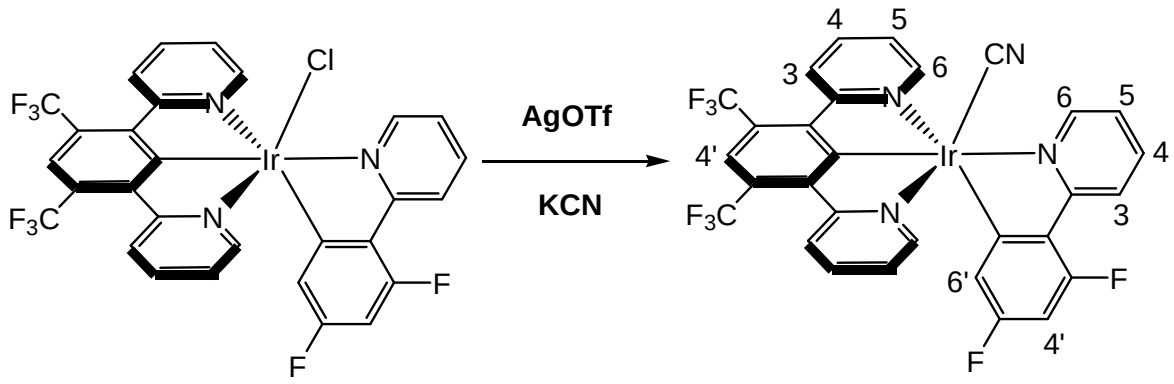

This complex prepared in the same way, starting from Ir(**L3**)(dFppy)Cl **(3)** (15 mg, 0.019 mmol) leading to the product (8mg, 0.010 mmol, 54%). ^{1}H-NMR ($CDCl_3$, 400 MHz): δ 10.03 (dd, 1H, ^{3}J = 4.4, ^{4}J = 0.8, H^{6}-NC), 8.45 (dd, 1H, ^{3}J = 8.4, ^{4}J = 1.6, H^{3}-NC),8.37 (d, 2H, ^{3}J = 8.8, H^{6}-NCN), 8.07-8.01 (t+s, 2H, H^{4}-NC+$H^{4'}$-NCN), 7.77-7.70 (d+t, 4H, H^{4}-NCN+H^{3}-NCN), 7.50 (td, 1H, ^{3}J = 6.0, ^{4}J = 1.2, H^{5}-NC), 6.97 (td, 2H, ^{3}J = 6.3, ^{4}J = 0.8, H^{5}-NCN), 6.20 (m, 1H, ^{3}J= 13.2, ^{4}J = 2.4, ^{5}J = 1.4$H^{4'}$-NC), 5.15 (dd, 1H, ^{3}J= 8.0, ^{4}J=2.4, $H^{6'}$-NC). ^{19}F-NMR ($CDCl_3$, 376 MHz): δ -59.2 (6F, NCN), -70.7 and -83.1 (2F, NC). Mass Spectrometry (ASAP+): *m/z* 775 [M].

Synthesis of Ir(1,3-di-(2-pyridyl)-4,6-dimethylbenzene-N,C$^{2'}$,N)(2-phenylpyridine-N,C$^{2'}$) cyanide [Ir(L1)(ppy)CN] (26)

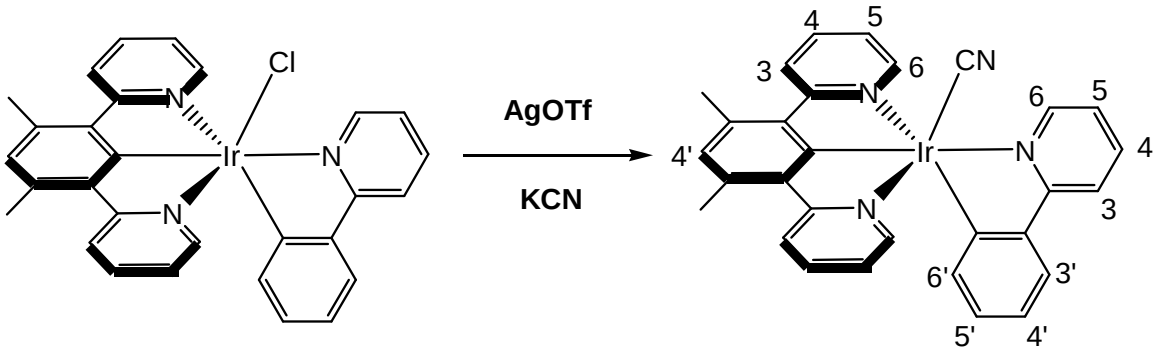

This complex prepared in the same way, starting from Ir(**L1**)(ppy)Cl (10 mg, 0.030 mmol) leading to the product (10mg, 0.016 mmol, 84%). ^{1}H-NMR ($CDCl_3$, 400 MHz): δ 9.84 (d, 1H, ^{3}J = 6.0, H^{6}-NC), 8.03 (d, 1H, ^{3}J = 8.4, H^{3}-NC), 7.97 (d, 2H, ^{3}J = 8.4, H^{6}-NCN), 7.65 (d, 2H, ^{3}J = 4.4, H^{3}-NCN), 7.59-7.49 (t+d, 6H, H^{4}-NCN+H$^{3'}$-NC), 7.43 (td, 1H, ^{3}J = 5.6, ^{4}J = 0.8, H^{4}-NC), 6.88 (s, 1H, H$^{4'}$-NCN), 6.76-6.66 (t+t, 3H, H^{5}-NCN+H^{5}-NC), 6.55 (td, 2H, ^{3}J = 7.6, ^{4}J = 0.8, H$^{4'}$-NC), 6.47 (td, 1H, ^{3}J = 7.2, ^{4}J = 1.2, H$^{5'}$-NC), 5.90 (dd, 1H, ^{3}J=7.2, ^{4}J = 0.8, H$^{6'}$-NC), 2.78 (6H, s, H^{Me}). Mass Spectrometry (ASAP+): 632 *m/z* [M]$^{+}$.

Synthesis of Ir(1,3-di-(2-pyridyl)-4,6-difluorobenzene-N,$C^{2'}$,N)(2,4-(difluorophenyl)pyridine-N,$C^{2'}$) thiocynide [Ir(L1)(dFppy)SCN] (27)

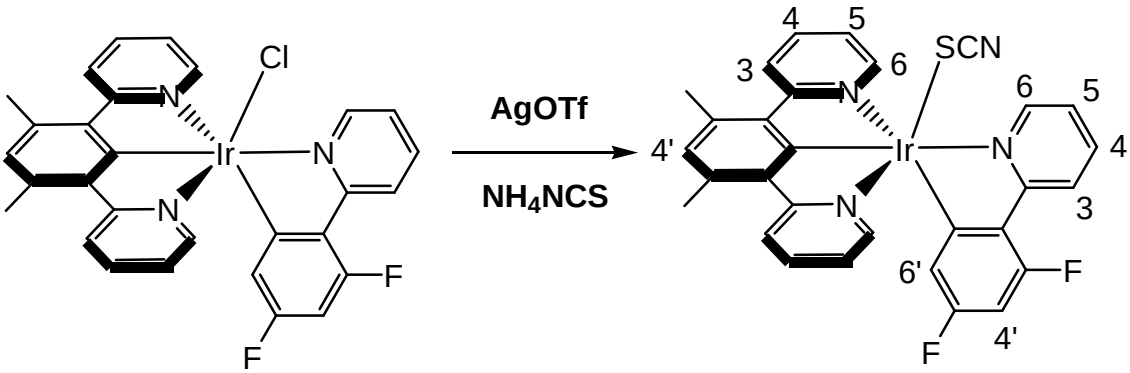

Ir(**L1**)(dFppy)Cl **(1)** (10 mg, 0,02mmol) and silver triflate (10 mg 0.03 mmol) were dissolved in acetone (2 ml) in a Schlenk, and the solution was heated at reflux for 6 hours. After cooling to room temperature, the precipitated AgCl was removed by centrifuge and the combined organic layers dried under vacuum. The resulting solid was dissolved in methanol and was added to a solution of NH_4SCN in methanol (10mg, 0.13mmol in 3 ml) and strirred overnight. Dichloromethane (5 ml) was added, and the solution was washed with NaOH (1M, 3*5 ml) followed by water, and dried over $mgSO_4$. Removal of solvent gave the product as a yellow solid (15 mg, 0.021 mmol, 95%). ^{1}H-NMR ($CDCl_3$, 400 MHz): δ 9.59 (dd, 1H, ^{3}J = 5.6, ^{4}J = 0.8, H^6-NC), 8.44 (dd, 1H, ^{3}J = 8.4, ^{4}J = 1.2, H^3-NC), 8.02-8.00 (t+d, 3H, H^4-NC+H^6-NCN), 7.52 (d, 2H, ^{3}J = 6.0, H^3-NCN), 7.70-7.60 (t+t, 3H, H^4-NCN+H^5-NC), 6.92 (s, 1H, $H^{4'}$-NCN), 6.81 (t, 2H, ^{3}J = 6.4, H^5-NCN), 6.18 (m, 1H, ^{3}J = 13.2, ^{4}J = 2.4, $H^{4'}$-NC), 5.41 (dd, 1H, ^{3}J = 11.2, ^{4}J = 2.4, $H^{6'}$-NC), 2.82 (s, 6H, H^{Me}). ^{19}F-NMR ($CDCl_3$, 376 MHz): δ -108.8 (1F, NC), -109.7 (1F, NC). Mass Spectrometry (MALDI+): *m/z* 700 $[M]^+$, *m/z* 642 $[M-(SCN)]^+$. HRMS (ASAP+): *m/z* 698.1048 $[M]^+$. Calculated for $^{191}IrC_{30}H_{21}F_2SN_4$: *m/z* 698.1034.

Synthesis of Ir(1,3-di-(2-pyridyl)-4,6-dimethylbenzene-N,C$^{2'}$,N)(2-phenylpyridine-N,C$^{2'}$) thiocynide [Ir(L1)(ppy)SCN] (28)

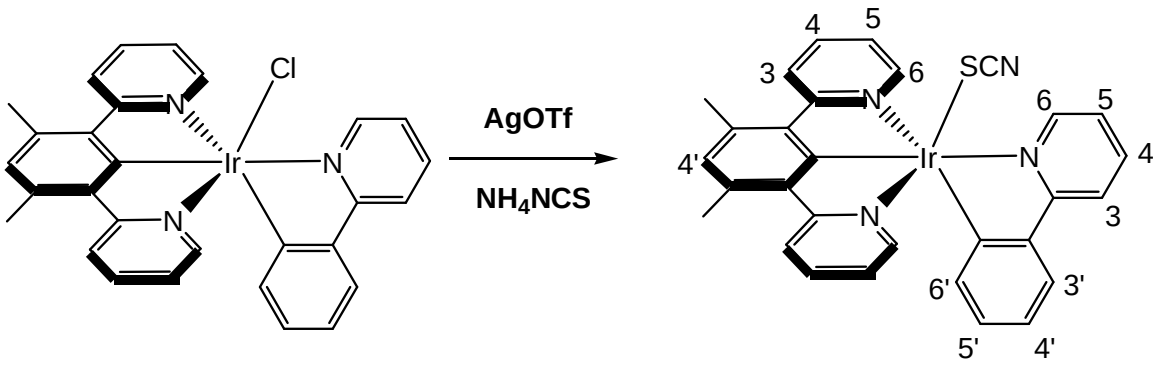

The title complex was prepared from Ir(**L1**)(ppy)Cl (10 mg, 0.016 mmol) using the same procedure, leading to the product as a yellow solid (6 mg, 0.009 mmol, 56%). ^{1}H-NMR ($CDCl_3$, 400 MHz): δ 9.50 (d, 1H, ^{3}J = 5.6, H^{6}-NC), 8.01 (d, 1H, ^{3}J = 8.0, H^{3}-NC), 7.96-7.92 (d+t, 3H, H^{6}-NCN+H^{4}-NC), 7.54-7.50 (t+d+d, 6H, H^{5}-NC+H^{4}-NCN+H^{3}-NCN+H^{3}-NC), 6.85 (s, 1H, H$^{4'}$-NCN), 6.71 (td, 2H, ^{3}J = 5.6, ^{4}J = 2.0, H^{5}-NCN), 6.65 (td, 1H, ^{3}J = 7.6, ^{4}J = 0.8, H$^{4'}$-NC), 6.47 (td, 1H, ^{3}J = 7.2, ^{4}J = 1.2, H$^{5'}$-NC), 5.46 (dd, 1H, ^{3}J = 7.2, ^{4}J = 0.8, H$^{6'}$-NC), 2.78 (6H, s, H^{Me}). Mass Spectrometry (ASAP+): *m/z* 606 $[M-Cl]^+$, *m/z* 663 $[M]^+$.

Synthesis of Ir(1,3-di-(2-pyridyl)-4,6-difluorobenzene-N,C$^{2'}$,N)(2-phenylpyridine-N,C$^{2'}$) thiocynide [Ir(L2)(ppy)SCN] (29)

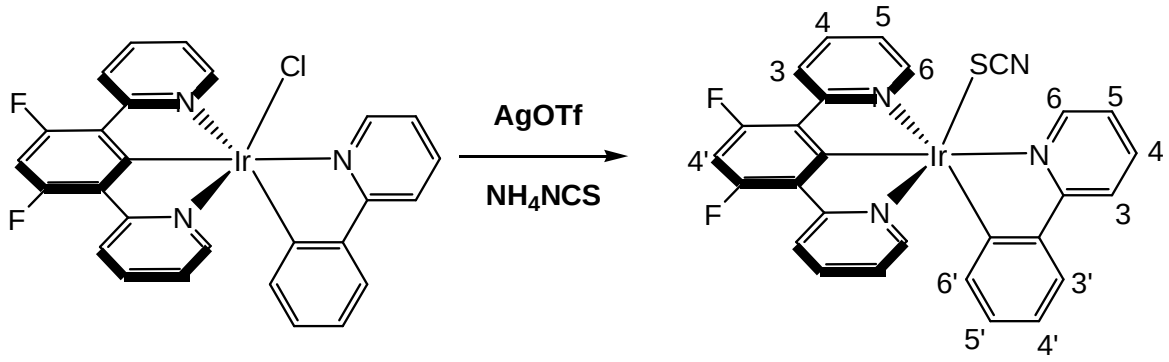

The title complex was prepared from Ir(**L2**)(ppy)Cl **(4)** (16 mg, 0.025 mmol) using the same procedure, leading to the product as a yellow solid (9 mg, 0.013 mmol, 52%). ^{1}H-NMR ($CDCl_3$, 400 MHz): δ 9.50 (d, 1H, ^{3}J = 5.6, H^{6}-NC), 8.01 (d, 1H, ^{3}J = 8.0, H^{3}-NC), 7.96-7.92 (d+t, 3H, H^{6}-NCN+H^{4}-NC), 7.54-7.50 (t+d+d, 6H, H^{5}-NC+H^{4}-NCN+H^{3}-NCN+H$^{3'}$-NC), 6.85 (s, 1H, H$^{4'}$-NCN), 6.71 (td, 2H, ^{3}J = 5.6, ^{4}J = 2.0, H^{5}-NCN), 6.65 (td, 1H, ^{3}J = 7.6, ^{4}J = 0.8, H$^{4'}$-NC), 6.47 (td, 1H, ^{3}J = 7.2, ^{4}J = 1.2, H$^{5'}$-NC), 5.46 (dd, 1H, ^{3}J = 7.2, ^{4}J = 0.8, H$^{6'}$-NC). ^{19}F-NMR ($CDCl_3$, 660 MHz): δ -108.0 (2F, d, J=7.2). Mass Spectrometry (ASAP+): *m/z* 614 $[M-Cl]^+$, *m/z* 672 $[M]^+$.

Synthesis of Ir(1,3-di-(2-pyridyl)-4,6-dimethylbenzene-N,C$^{2'}$,N)(2,4-(difluorophenyl)pyridine-N,C$^{2'}$)(3,5-bis(trifluoromethyl)benzene-1-acetylide) [Ir(L1)(dFppy)(A1)] (30)

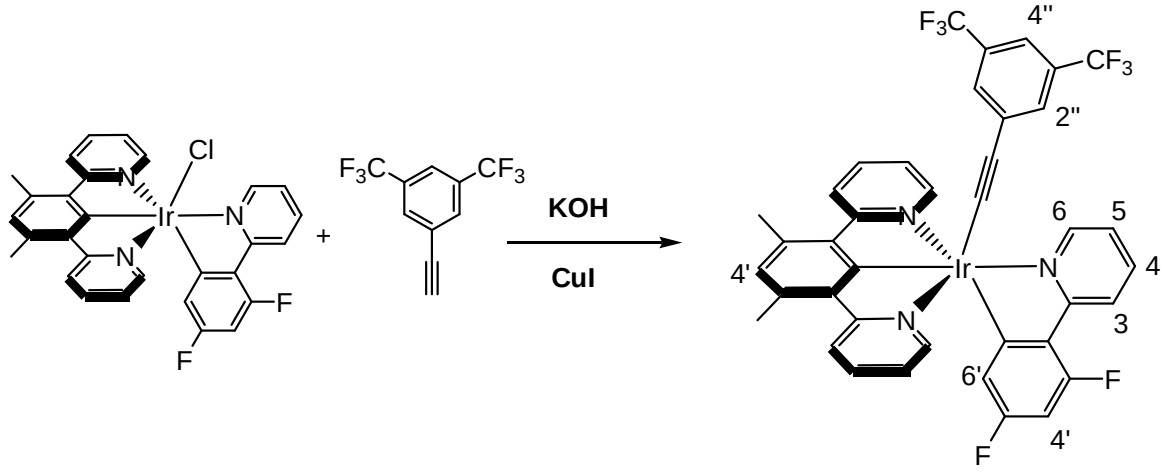

1-Ethynyl-3,5-bis(trifluoromethyl)benzene (8 mg, 0.032 mmol) and KOH (30 mg, 0.5mmol) in 5 ml of methol were stirred for 1 hour. After that a solution of Ir(**L1**)(dFppy)Cl **(1)** (15 mg, 0.022 mmol) and CuI (3 mg, 0.017) in methanol was added and the combined solutions were stirred overnight. The target complex precipitated from the solution and is isolated by cenerfuge and washed with methanol (10 mg, 0.011, 50%). ^{1}H-NMR ($CDCl_3$, 400 MHz): δ 10.18 (dd, 1H, ^{3}J = 4.4, ^{4}J = 1.2, H^{6}-NC), 8.45 (d, 1H, ^{3}J = 8.0, H^{3}-NC) 8.05 (d, 2H, ^{3}J = 8.4, H^{6}-NCN), 7.98 (t, 3H, ^{3}J = 9.6, H^{4}-NC), 7.74 (d, 2H, ^{3}J = 5.6, H^{3}-NCN), 7.59 (t, 2H, ^{3}J = 8.0, H^{4}-NCN), 7.49 (t, 1H, ^{3}J = 6.0, H^{5}-NC), 7.36 (s+s, 3H, H$^{2''}$+H$^{4''}$), 6.91 (s, 1H, H$^{4'}$-NCN), 6.79 (td, 2H, ^{3}J = 7.2, ^{4}J = 1.2, H^{5}-NCN), 6.17 (m, 1H, ^{3}J = 13.2, ^{4}J = 2.4, H$^{4'}$-NC), 5.44 (dd, 1H, ^{3}J = 8.4, ^{4}J = 2.8, H$^{6'}$-NC), 2.86 (s, 6H, H^{Me}). ^{19}F-NMR ($CDCl_3$, 376 MHz): δ -63.5 (6F, ancillary), -110.3 and -110.5 (2F, NC). Mass Spectrometry (MALDI+): *m/z* 879 [M]$^{+}$, *m/z* 642 [M-(dtfmbA)]$^{+}$.

Synthesis of Ir(1,3-di-(2-pyridyl)-4,6-di-(trifluoromethyl)benzene-N,C$^{2'}$,N)(2-phenylpyridine-N,C$^{2'}$)(3,5-bis-(trifluoromethyl)benzene-1-acetylide) [Ir(L3)(ppy)(A1)] (31)

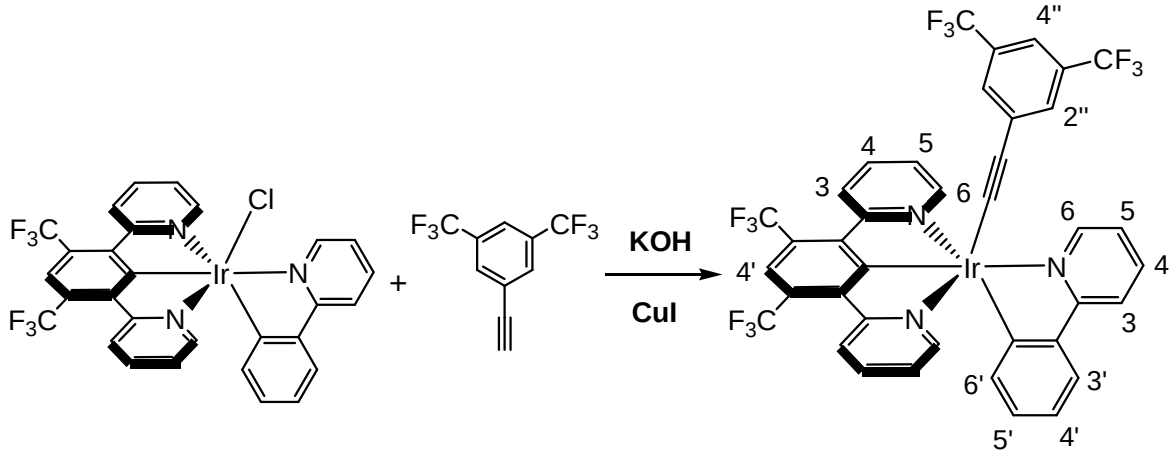

The title compound was prepared from Ir(**L3**)(ppy)Cl **(5)** (20 mg, 0.027 mmol) in the same way as for the previous complex, leading to the target complex (12 mg, 0.012, 47%). ^{1}H NMR ($CDCl_3$, 400 MHz) δ 10.16 (d, ^{3}J = 5.5, 1H, H^{6}-NC), 8.43 (d, ^{3}J = 8.4, 2H, H^{3}-NC), 8.23 – 7.87 (d+t+d, 4H, H^{4}-NC+H$^{4'}$-NC+H^{3}-NCN), 7.79 – 7.45 (t+d+t, 4H, H^{4}-NCN+H$^{6'}$-NCN+H^{5}-NC), 7.37 (s+s, ^{3}J = 13.7, 3H, H$^{2''}$+H$^{4''}$), 6.98 (t, ^{3}J = 7.2, 2H, H^{5}-NCN), 6.80 (t, ^{3}J = 7.5, 1H, H^{5}-NC), 6.63 (t, ^{3}J = 7.3, 1H, H$^{5'}$-NC), 5.72 (d, ^{3}J = 7.4, 1H, H$^{6'}$-NC). ^{19}F-NMR($CDCl_3$, 400 MHz) δ –59.02 (6F, NCN), -63.50 (6F, ancillary). Mass Spectrometry (MALDI+): *m/z* 951 [M]$^{+}$, *m/q* 714 [M-btfmbA]$^{+}$. HRMS (ASAP+): *m/z* 949.1100 [M]$^{+}$. Calculated for $C_{39}H_{20}N_3F_{12}{}^{191}Ir$: *m/z* 949.1072.

Synthesis of Ir(1,3-di-(2-pyridyl)-4,6-di-(trifluoromethyl)benzene-N,C$^{2'}$,N)(2-phenylpyridine-N,C$^{2'}$)(4-methoxy-phenylacetylene)[Ir(L3)(ppy)(A3)] (32)

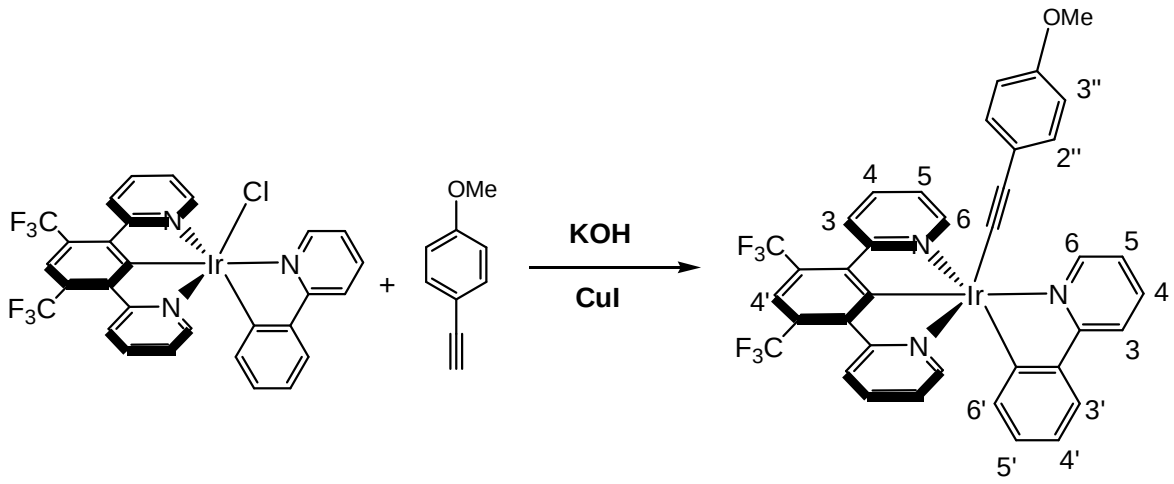

The title compound was prepared from Ir(**L3**)(ppy)Cl **(5)** (15 mg, 0.022 mmol) in the same way as for the previous complex, leading to the target complex (10 mg, 52%). ^{1}H-NMR ($CDCl_3$, 400 MHz): δ 10.18 (d, 1H, ^{3}J = 4.4, H^{6}-NC), 8.45 (d, 1H, ^{3}J = 8.0, H^{3}-NC) 8.05 (d, 2H, ^{3}J = 8.4, H^{6}-NCN), 7.98 (t, 2H, ^{3}J = 8.0, H^{4}-NCN), 7.74 (d, 2H, ^{3}J = 5.6, H^{3}-NCN), 7.59 (t, 2H, ^{3}J = 8.0, H^{5}-NCN), 7.49 (t, 1H, ^{3}J = 6.0, H^{5}-NC), 7.36 (d+d, 4H, H$^{2''}$+H$^{4''}$), 6.91 (s, 1H, H$^{4'}$-NCN), 6.81-6.72 (t+d, 2H , H$^{3'}$-NC+H^{4}-NC), 6.17 (m, 1H, H$^{5'}$-NC), 5.44 (dd, 1H, ^{3}J = 8.4, ^{4}J = 2.8, H$^{6'}$-NC), 2.86 (s, 6H, H^{OMe}). ^{19}F-NMR ($CDCl_3$, 176 MHz): δ -57.0 (6F, NCN). Mass Spectrometry (MALDI+): *m/z* 845 [M]$^{+}$, *m/z* 714 [M-OMeA]$^{+}$.

Synthesis of Ir(1,3-di-(2-pyridyl)-4,6-di-(trifluoromethyl)benzene-N,C$^{2'}$,N)(2-phenylpyridine-N,C$^{2'}$)(phenylacetylene) [Ir(L3)(ppy)(A2)] (33)

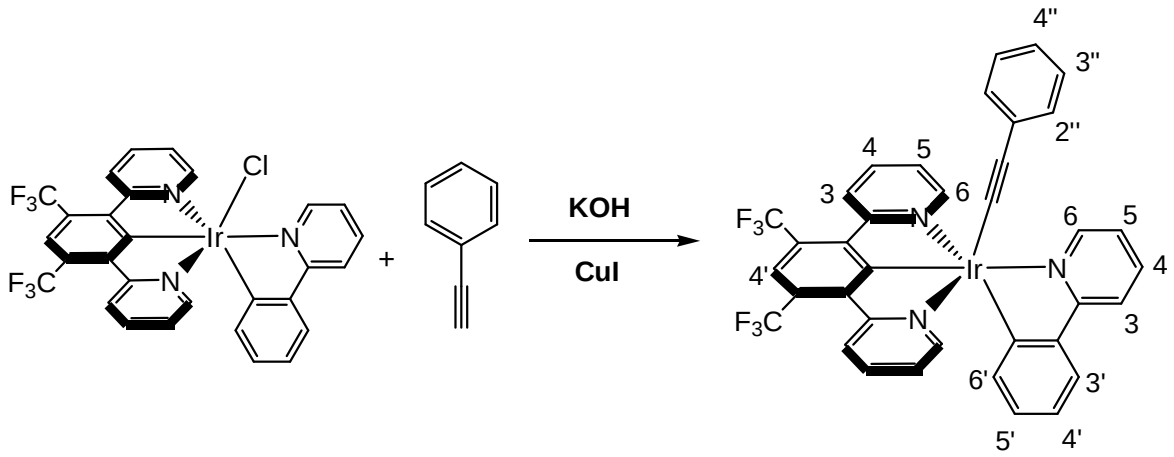

The title compound was prepared from Ir(**L3**)(ppy)Cl **(5)** (15 mg, 0.022 mmol) in the same way as for the previous complex, leading to the target complex (8 mg, 0.011 mmol, 50%). ^{1}H-NMR ($CDCl_3$, 400 MHz): δ 10.18 (d, 1H, ^{3}J = 4.4, H^{6}-NC), 8.45 (d, 1H, ^{3}J = 8.0, H^{3}-NC) 8.05 (d, 2H, ^{3}J = 8.4, H^{6}-NCN), 7.98 (t, 2H, ^{3}J = 8.0, H^{4}-NCN), 7.74 (d, 2H, ^{3}J = 5.6, H^{3}-NCN), 7.59 (t, 2H, ^{3}J = 8.0, H^{5}-NCN), 7.49 (t, 1H, ^{3}J = 6.0, H^{5}-NC), 7.30-7.40 (m, 3H, H$^{2''}$+H$^{3''}$+H$^{4''}$), 6.91 (s, 1H, H$^{4'}$-NCN), 6.79 (t+t, 2H, H$^{3'}$-NC+H$^{4'}$-NC), 6.17 (m, 1H, H$^{5'}$-NC), 5.44 (dd, 1H, ^{3}J = 8.4, ^{4}J = 2.8, H$^{6'}$-NC), 2.86 (s, 6H, H^{Me}). Mass Spectrometry (MALDI+): *m/z* 815 [M]$^{+}$, *m/z* 741 [M-phenA]$^{+}$.

Synthesis of Ir(1,3-di-(2-pyridyl)-4,6-di-(trifluoromethyl)benzene-N,$C^{2'}$,N)(2-phenylpyridine-N,$C^{2'}$)(4-dimethylamino-phenylacetylene) [Ir(L3)(ppy)(A4)] (34)

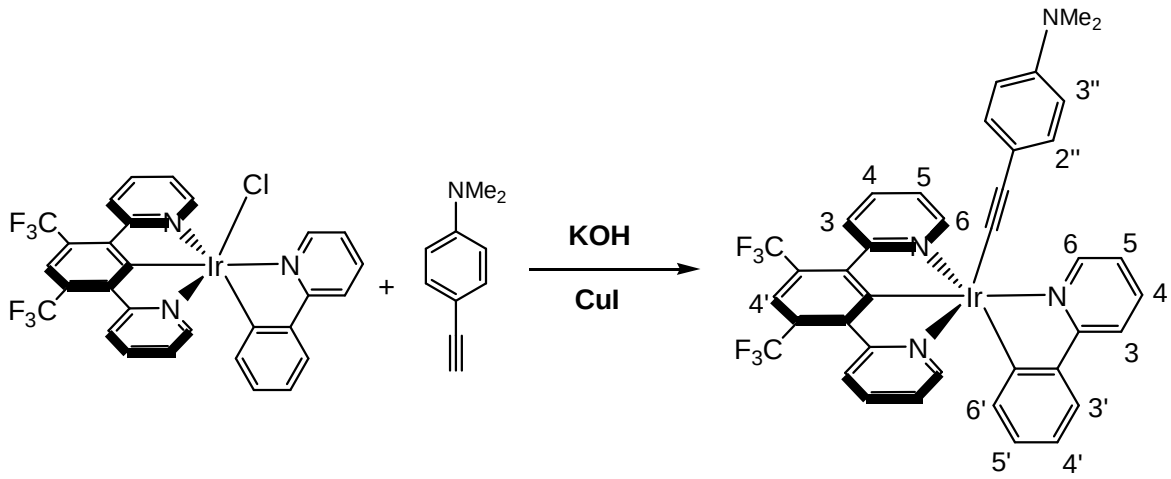

The title compound was prepared from Ir(**L3**)(ppy)Cl **(5)** (20 mg, 0.027 mmol) in the same way as for the previous complex, leading to the target complex (10 mg, 0.014 mmol, 52%). ^{1}H-NMR ($CDCl_3$, 400 MHz): δ 10.18 (d, 1H, ^{3}J = 4.4, H^{6}-NC), 8.45 (d, 1H, ^{3}J = 8.0, H^{3}-NC) 8.05 (d, 2H, ^{3}J = 8.4, H^{6}-NCN), 7.98 (t, 3H, ^{3}J = 8.0, H^{4}-NCN), 7.74 (d, 2H, ^{3}J = 5.6, H^{3}-NCN), 7.59 (t, 2H, ^{3}J = 8.0, H^{5}-NC), 7.49 (t, 1H, ^{3}J = 6.0, H^{5}-NC), 7.36 (d+d, 4H, $H^{2''}$+$H^{4''}$), 6.91 (s, 1H, $H^{4'}$-NCN), 6.79 (t+t 2H, $H^{3'}$-NC+$H^{4'}$-NC), 6.17 (m, 1H, $H^{5'}$-NC), 5.44 (dd, 1H, ^{3}J = 8.4, ^{4}J = 2.8, $H^{6'}$-NC), 2.86 (s, 6H, H^{Me}). ^{19}F-NMR ($CDCl_3$, 376 MHz) : δ -58.2 (6F, NCN). Mass Spectrometry (MALDI): *m/z* 858 $[M]^+$, *m/z* 714 $[M\text{-}OMeA]^+$.

Synthesis of Ir(1,3-di-(2-pyridyl)-4,6-di-(trifluoromethyl)benzene-N,C$^{2'}$,N)(2-phenylpyridine-N,C$^{2'}$)(4-cyano-phenylacetylene) [Ir(L3)(ppy)(A5)] (35)

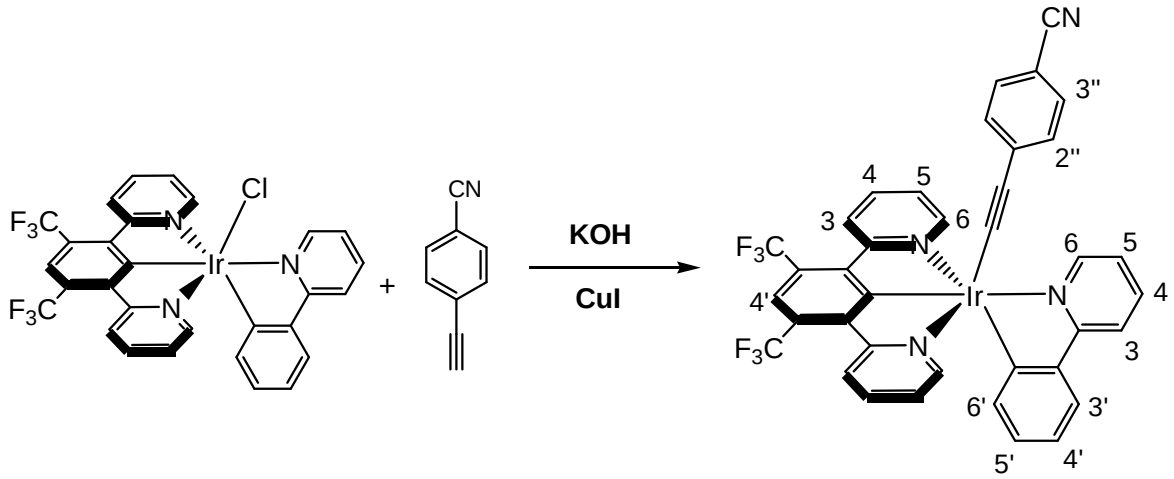

The title compound was prepared from Ir(**L3**)(ppy)Cl **(5)** (15 mg, 0.022 mmol) in the same way as for the previous complex, leading to the target complex (12 mg, 0.014 mmol, 64%). ^{1}H-NMR ($CDCl_3$, 400 MHz): δ 10.09 (dd, 1H, ^{3}J = 4.0, ^{4}J = 0.8, H^{6}-NC), 8.35 (d, 2H, ^{3}J = 8.0, H^{6}-NCN), 8.05 (d+s, 2H, H^{3}-NCN+H$^{4'}$-NCN), 7.96 (td, 1H, ^{3}J = 7.2, ^{4}J = 1.2, H^{4}-NC), 7.88 (dd, 2H, ^{3}J = 5.6, ^{4}J = 1.2, H^{3}-NCN), 7.64 (td, 2H, ^{3}J=8.0, ^{4}J = 1.6, H^{4}-NCN), 7.58 (d, 1H, ^{3}J = 8.0, H$^{3'}$-NC), 7.46 (td, 1H, ^{3}J = 6.0, ^{4}J = 1.2, H^{5}-NC), 7.22 (d, 2H, ^{3}J = 8.4, H$^{2''\text{ or }3''}$), 7.94 (d, 2H, ^{3}J = 8.4, H$^{2''\text{ or }3''}$), 6.89 (td, 2H, ^{3}J = 6.4, H^{5}-NCN), 6.73 (td, 1H, ^{3}J = 7.6, ^{4}J = 1,.2, H$^{4'}$-NC), 6.56 (td, 1H, ^{3}J = 8.0, ^{4}J = 1.2, H$^{5'}$-NC), 5.64 (dd, 1H, ^{3}J = 8.0, ^{4}J = 1.6, H$^{6'}$-NC). ^{19}F-NMR ($CDCl_3$, 376 MHz): δ -58.7 (6F, NCN). Mass Spectrometry (MALDI+): *m/z* 841 $[M]^+$, *m/z* 714 $[M\text{-}OMeA]^+$. HRMS (ASAP+): *m/z* 839.1383. Calculated for $C_{38}H_{21}N_4F_6{}^{191}Ir$: *m/z* 839.1299.

Synthesis of Ir(1,3-di-(2-pyridyl)-4,6-di-(trifluoromethyl)benzene-N,C$^{2'}$,N)(2-phenylpyridine-N,C$^{2'}$)(5-phenyl-tetrazole) [Ir(L3)(ppy)(phtr)] (36)

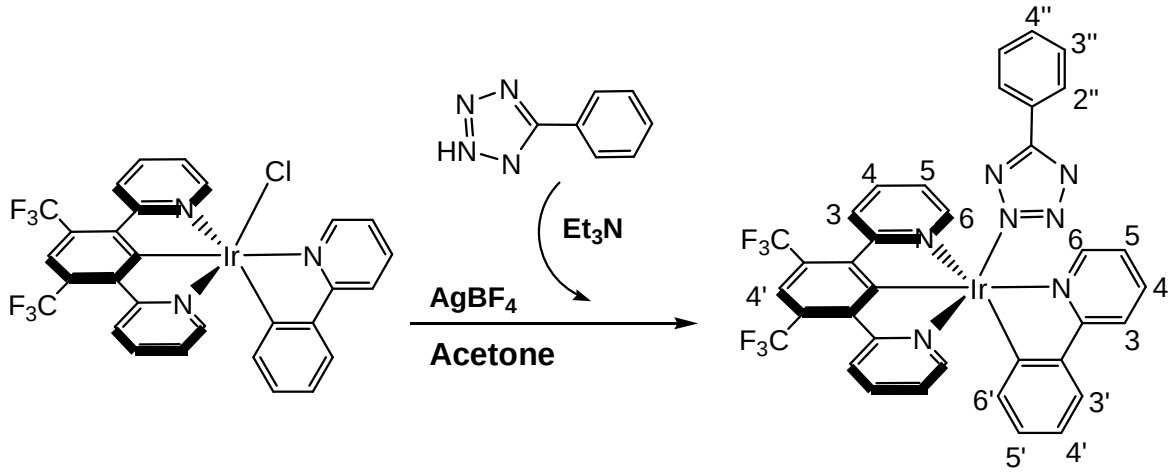

In a schlenk tube were Ir(**L3**)(ppy)Cl **(5)** (50 mg, 0.067 mmol) and $AgBF_4$ (16 mg, 0.073 mmol) in 5 ml of a solution acetone/water 2:1. the apparatus was proteted from light with aluminium foil and the mixture refluxed overnight under nitrogen. After cooling to room temperature, the precipitated AgCl was removed by centerfuge from the solution of the solvate-complex. Meanwhile a solution of 5-phenyl-tetrazole (12 mg, 0.085 mmol) in acetone (3 ml) was treated with few drops of Et_3N and stirred for 30 minutes. The solution containing the deprotonated tetrazole was then added dropwise to the solution containing the solvate-complex. The combined mixture was then refluxed overnight. After cooling to room temperature, the mixture was diluited with 50 ml of dichloromethane and extractions were performed with 100*3 ml of water. The organic layer was dried over $MgSO_4$ and filtered. Purificetion was achieved after silica gel chromatography (DCM/MeOH 95:5). The product was an orange solid (15 mg, 0.019 mmol, 28%). ^{1}H-NMR (CD_3Cl, 400 MHz): δ 8.79 (dd, 1H, ^3J = 5.6, ^4J = 1.2, H^6-NC), 8.30 (d, 2H, ^3J = 8.4, H^6-NCN), 8.08 (d, 1H, ^3J = 8.4, H^3-NC), 8.0-7.92 (s+t+d. 4H, $H^{4'}$-NCN+H^4-NC+$H^{4''}$), 7.73-7.68 (t+t, 3H, H^4-NCN+$H^{2''\ or\ 3''}$), 7.60 (d, 1H, ^3J = 7.2, ^4J = 0.8, $H^{3'}$-NC), 7.36 (t, 1H, ^3J = 6.4, ^4J = 1.2, H^5-NC), 7.25-7.15

(d+t, 3H, H^3-NCN+$H^{2''\ or\ 3''}$), 7.0 (td, 2H, ^3J = 6.4, ^4J = 0.8, H^5-NCN), 6.76 (td, 1H, ^3J = 6.8, ^4J = 1.2, $H^{4'}$-NC), 6.59 (td, 1H, ^3J = 7.2, ^4J = 1.2, $H^{5'}$-NC), 5.76 (dd, 1H, ^3J = 7.6, ^4J = 0.8, $H^{6'}$-NC). ^{13}C-NMR ($CDCl^3$, 700 MHz): δ 199.8, 183.5, 165.4 (C^2-NCN), 152.0 ($CH^{4'}$-NCN), 150.0 ($CH^{2''}$-phtr), 149.7 (CH^6-NC), 148.0, 144.2, 144.1, 142.1, 142.0, 138.4 (CH^4-NC), 137.1, 136.5 ($CH^{3'}$-NC), 136.0, 130.3, 129.8 ($CH^{4'}$-NC), 128.6 (CH^3-NCN or $CH^{3''}$-phtr), 127.9 (CH^3-NCN or $CH^{3''}$-phtr), 126.2, 125.8, 125.6 (CH^4-phtr), 124.9 (CH^6-NCN), 123.9 ($CH^{6'}$-NC), 122.1 (CH^5-NC), 119.1 (CH^3-NC), 119.0. ^{19}F-NMR ($CDCl_3$, 660 MHz): -58.8 (2F, NCN). Mass Spectrometry (MALDI+): *m/z* 860 $[M]^+$, 714 *m/z* $[M\text{-phtr}]^+$. HRMS (ASAP+): *m/z* 858.1535 $[M]^+$. Calculated for $C_{36}H_{23}N_7F_6{}^{191}Ir$: *m/z* 858.1525.

Synthesis of Ir(1,3-di-(2-pyridyl)-4,6-di-(trifluoromethyl)benzene-N,$C^{2'}$,N)(2-phenylpyridine-N,$C^{2'}$)(5-(2-bromophenyl)-tetrazole) [Ir(L3)(ppy)(brphtr)] (37)

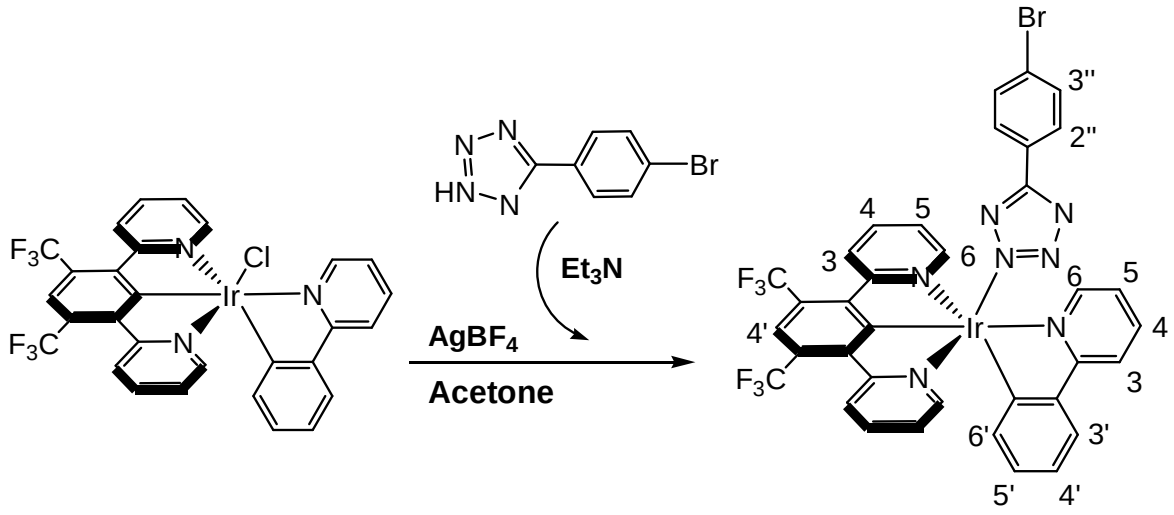

In a schlenk tube were Ir(**L3**)(ppy)Cl **(5)** (50 mg, 0.067 mmol) and $AgBF_4$ (16 mg, 0.073 mmol) in 5 ml of a solution acetone/water 2:1. the apparatus was proteted from light with aluminium foil and the mixture refluxed overnight under nitrogen.

Identical synthetic procedure was adopted as for the synthesis of Ir(**L3**)(ppy)(phtr) **(36)** adding 19 mg, (0.085 mmol) of 1-(4bromo-phenyl)-tetrazole in acetone (3 ml). Purification of the product was achieved after silica gel chromatography (DCM/MeOH 95:5). The product was an orange solid (61 mg, 0.065 mmol, 97%). ^{1}H-NMR (CD_3Cl, 400 MHz): δ 8.79 (dd, 1H, ^{3}J = 5.6, ^{4}J = 1.2, H^{6}-NC), 8.32 (d, 2H, ^{3}J = 8.4, H^{6}-NCN), 8.08 (d, 1H, ^{3}J = 8.4, H^{3}-NC), 7.97-7.92 (s+t+d. 4H, $H^{4'}$-NCN+H^{4}-NC+H^{3}-NCN), 7.72 (t, 2H, ^{3}J = 7.6, ^{4}J = 2.0, H^{4}-NCN), 7.62-7.58 (d+d, 3H, H^{3}-NC+$H^{2'' \text{ or } 3''}$), 7.36 (t, 1H, ^{3}J = 7.2, ^{4}J = 1.2, H^{5}-NC), 7.31 (d, 2H, ^{3}J = 8.8, $H^{2'' \text{ or } 3''}$), 6.99 (td, 2H, ^{3}J = 6.8, ^{4}J = 1.2, H^{5}-NCN), 6.77 (td, 1H, ^{3}J = 7.2, ^{4}J = 1.2, $H^{4'}$-NC), 6.60 (td, 1H, ^{3}J = 7.2, ^{4}J = 1.2, $H^{5'}$-NC), 5.77 (dd, 1H, ^{3}J = 8.4, ^{4}J = 1.2, $H^{6'}$-NC). ^{13}C-NMR ($CDCl^{3}$, 700 MHz): δ 199.8, 183.5, 165.4 (C^{2}-NCN), 152.0 ($CH^{4'}$-NCN), 150.0 ($CH^{2''}$-phtr), 149.7 (CH^{6}-NC), 148.0, 144.2, 144.1, 142.1, 142.0, 138.4 (CH^{4}-NC), 137.1, 136.5 ($CH^{3'}$-NC), 136.0, 130.3, 129.8 ($CH^{4'}$-NC), 128.6 (CH^{3}-NCN or $CH^{3''}$-phtr), 127.9 (CH^{3}-NCN or $CH^{3''}$-phtr), 126.2, 125.8, 125.6 (C^{4}-phtr), 124.9 (CH^{6}-NCN), 123.9 ($CH^{6'}$-NC), 122.1 (CH^{5}-NC), 119.1 (CH^{3}-NC), 119.0. ^{19}F-NMR ($CDCl_3$, 660 MHz): -58.8 (2F, NCN). Mass Spectrometry (MALDI+): *m/z* 938 $[M]^{+}$, 714 *m/z* $[M\text{-phtr}]^{+}$. HRMS (ASAP+): *m/z* 936.0656 $[M]^{+}$. Calculated for $^{79}BrF_6N_7C_{36}H_{21}{}^{191}Ir$: *m/z* 936.0575.

5.15. Synthesis of Rhodium complexes

Synthesis of Rh(1,3-di-(2-pyridyl)-4,6-dimethylbenzene-N,$C^{2'}$,N)(2,4-(difluorophenyl)pyridine-N,$C^{2'}$)chloride [Rh(L1)(dFppy)Cl] (38)

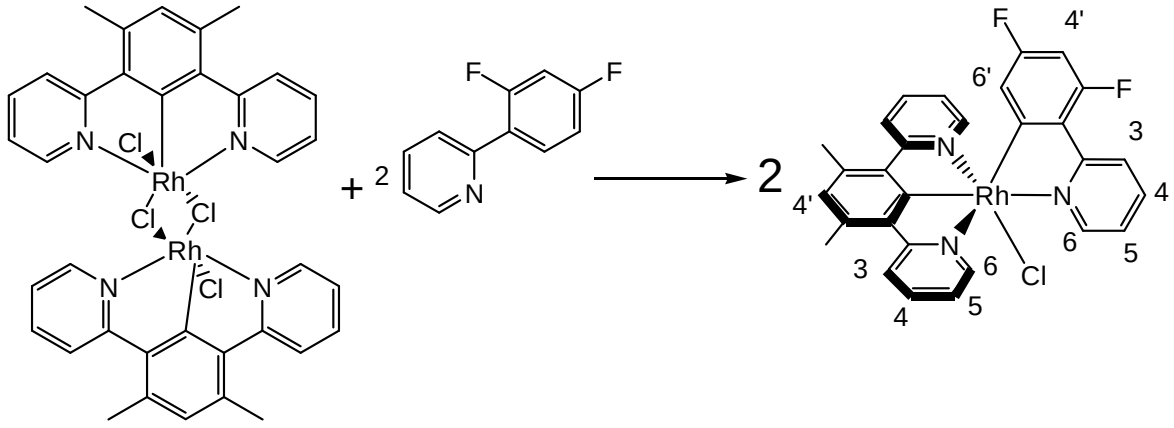

In Schlenk were added 50 mg of [Rh(**L1**)Cl(μ-Cl)]$_2$ (0.058 mmol), 23 mg of dFppyH (0.131 mmol) in 3 ml of ethylene-glykol. The mixture was refluxed for 4 hours and then cooled down to room tempetature. A saturated aqueous solution of KPF_6 was then added and the precipitate collected by centrifuge and washed with acetonitrile. The combined organic layer was dried under reduced pressure. The product was a pale yellow solid (28 mg, 0.046 mmol, 41%). ^{1}H-NMR ($CDCl_3$, 500 MHz): δ 10.18 (d, 1H, ^{3}J = 4.5, H^6-NC), 8.43 (d, 1H, ^{3}J = 7.0, H^3-NC), 8.07 (t, 1H, ^{3}J = 8.0, H^4-NC), 7.98 (d, 2H, ^{3}J = 7.0, H^6-NCN), 7.62 (t, 2H, ^{3}J = 7.5, H^4-NCN), 7.52 (d, 2H, ^{3}J = 6.0, H^3-NCN), 6.92 (s, 1H, $H^{4'}$-NCN),6.86 (t, 1H, ^{3}J = 6.5, H^5-NC), 6.81 (t, 2H, ^{3}J = 6.8, H^5-NCN), 6.25 (m, 1H, $H^{4'}$-NC), 5.72 (dd, 1H, ^{3}J = 6.5, ^{4}J = 0.5, $H^{6'}$-NC), 2.81 (s, 6H, H^{Me}). ^{19}F-NMR ($CDCl_3$, 176 MHz): δ -70.7 and -83.2 (2F, NC). Mass Spectrometry (MALDI+): *m/z* 552 $[M-Cl]^+$, *m/z* 586 [M].

Synthesis of Rh(1,3-di-(2-pyridyl)-4,6-difluorobenzene-N,C$^{2'}$,N)(2,4-(difluorophenyl)pyridine-N,C$^{2'}$)chloride [Rh(L2)(dFppy)Cl] (39)

Synthesis of Rh(1,3-di-(2-pyridyl)-4,6-di-(trifluoromethyl)benzene-N,C$^{2'}$,N)(2,4-difluorophenylpyridine-N,C$^{2'}$) chloride [Rh(L3)(dFppy)Cl]

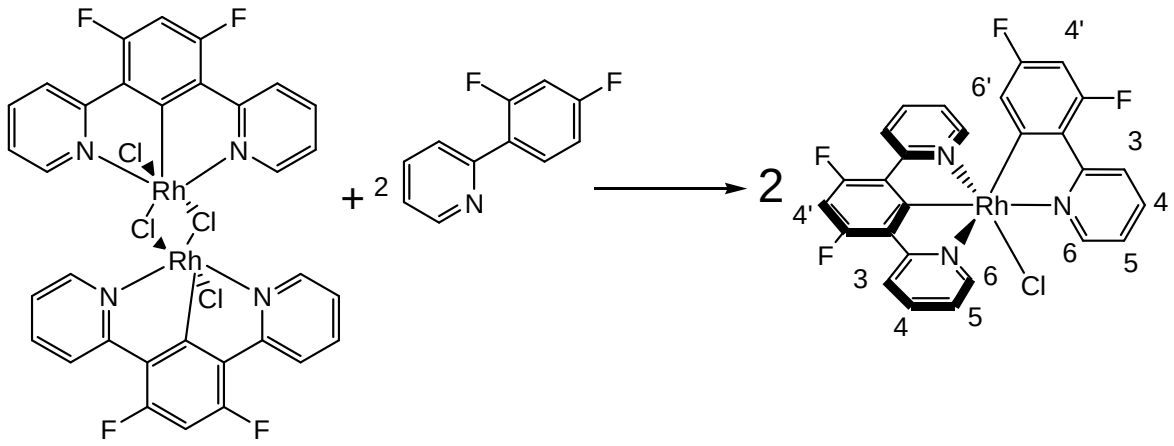

Thiscomplex was prepared from [Rh(**L2**)Cl(μ-Cl)]$_2$ (58 mg, 0.066 mmol), dFppyH (25 mg, 0.130 mmol) and Silver triflate (68 mg, 0.25 mmol) in 3ml of toluene. The same synthetic method was adopted as for the synthesis of Rh(**L1**)(dFppy)Cl **(38)**. The product was a pale yellow solid (12 mg, 0.018 mmol, 16%). ^{1}H-NMR ($CDCl_3$, 400 MHz): δ 10.11 (d, 1H, ^{3}J = 5.2, H^{6}-NC), 8.38 (d, 1H, ^{3}J = 9.2, H^{3}-NC), 8.00 (d, 2H, ^{3}J = 8.0, H^{6}-NCN), 7.62 (td, 2H, ^{3}J = 8.0, ^{4}J = 1.6, H^{4}-NCN), 7.53 (t, 1H, ^{3}J = 6.4, H^{4}-NC), 7.37 (d, 2H, ^{3}J = 6.0, H^{3}-NCN), 7.18 (s, 1H, H^{5}-NC), 6.81 (td, 2H, ^{3}J = 7.6, ^{4}J = 1.2, H^{5}-NCN), 6.72 (t, 1H, ^{3}J = 11.6, H$^{4'}$-NCN), 6.23 (m, 1H, H$^{4'}$-NC), 5.69 (m, 1H, H$^{6'}$-NC). ^{19}F-NMR ($CDCl_3$, 176 MHz): δ -78.80 (1F, NC), -79.0 (1F, NC), -107.90 (2F, d, ^{3}J = 7.2, NCN), Mass Spectrometry (MALDI+): *m/z* 560 [M-Cl]$^{+}$. HRMS (ASAP+): m/z 594.9959 [M–Cl]$^{+}$. Calcd for $C_{27}H_{15}N_3F_4Cl^{108}Rh$: *m/z* 594.9945.

(40)

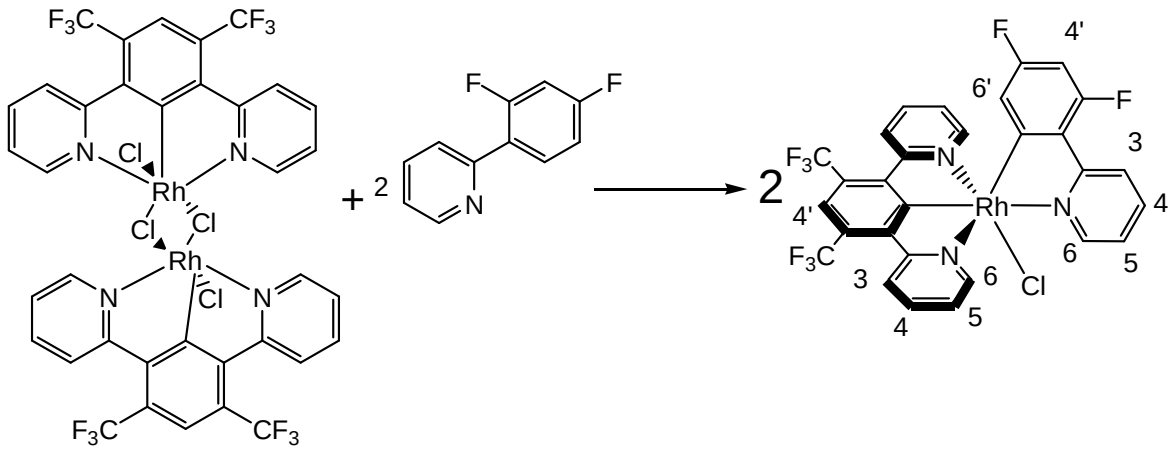

This complex was prepared from [Rh(**L3**)Cl(μ-Cl)]$_2$ (42 mg, 0.038 mmol) and dFppyH (15 mg, 0.079 mmol) in the presence of silver triflate (35 mg, 0.14 mmol) in toluene (4 mL), as described above for Ir(**L1**)(dFppy)Cl **(1)**. The crude product was purified by chromatography (silica gel, CH_2Cl_2/MeOH, gradient elution from 100/0 to 99/1), giving an orange solid (15 mg, 56%). ^{1}H NMR ($CDCl_3$, 700 MHz): δ 10.12 (1H, d, ^{3}J = 5.2, H^6-NC), 8.30 (1H, d, ^{3}J = 8.4, H^3-NC), 8.04 (3H, t+s, H^4-NC+H^4-NCN), 7.74 (2H, td, ^{3}J = 9.2, ^{4}J = 1.6, H^6-NCN), 7.58 (3H, d+t, H^5-NCN+H^5-NC), 6.99 (2H, dd, ^{3}J = 7.6, ^{4}J = 1.2, H^6-NCN), 6.23 (1H, td, ^{3}J = 15.6, ^{4}J = 2.8, H$^{4'}$-NC), 5.32 (1H, dd, ^{3}J = 9.0, ^{4}J = 2.5, H$^{6'}$-NC). ^{19}F NMR ($CDCl_3$, 376.4 MHz): δ –58.7 (6F, s, CF_3), –107.6 and –108.1 (2F, NC). Mass Spectrometry (MALDI+): *m/z* 660 [M–Cl]$^+$. HRMS (ES+): *m/z* 660.8973 [M–Cl]$^+$. Calcd for $C_{29}H_{15}N_3F_8Rh$: *m/z* 660.01932.

5.16. Synthesis of multimetallic complexes

Synthesis of bis[Ir(1,3-di-(2-pyridyl)-4,6-di-(trifluoromethyl)benzene-N,$C^{2'}$,N)(2-phenylpyridine-N,$C^{2'}$,N)](4,4'-diethynylbiphenyl-acetylide) [b[Ir(L3)(ppy)]bpha] (41)

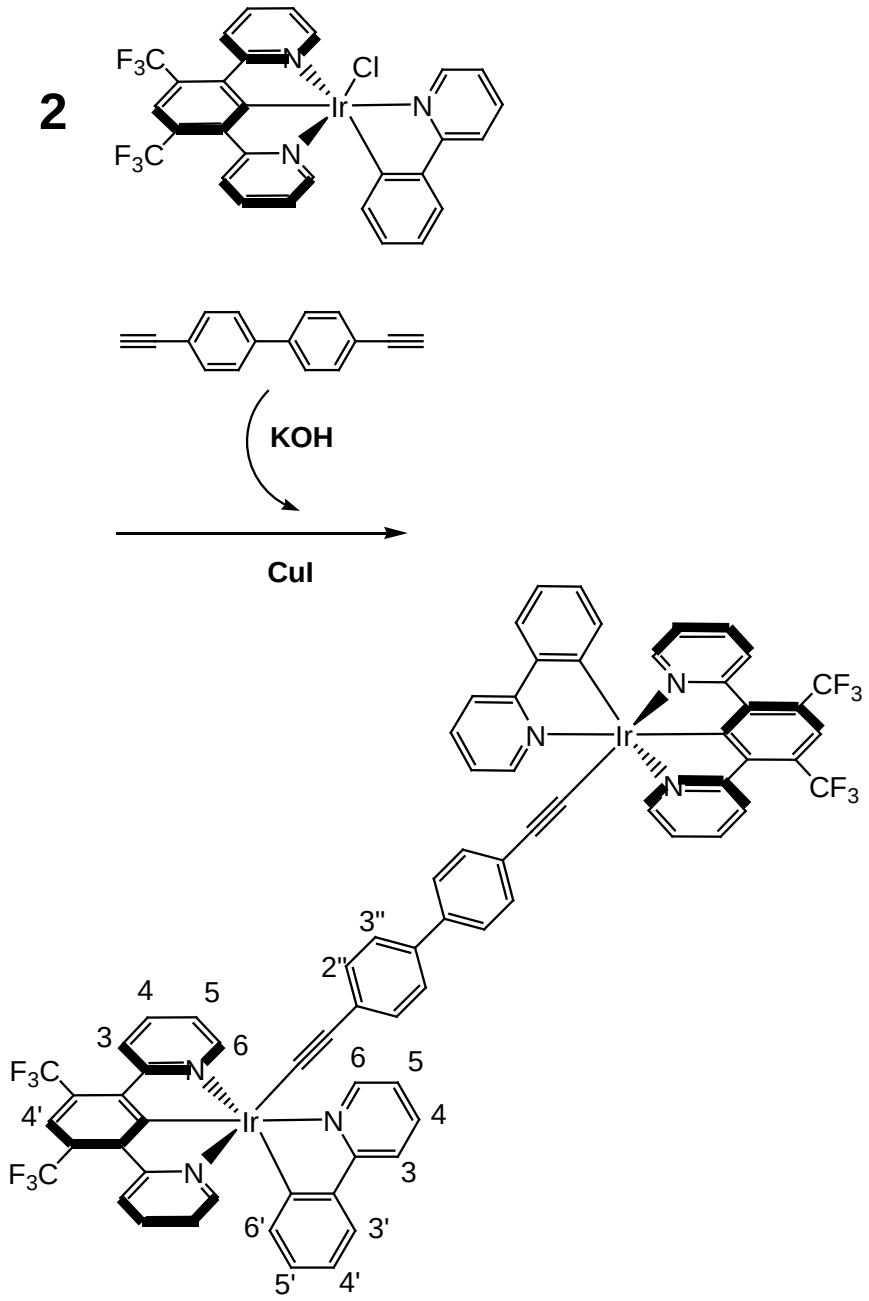

In Schlenk 3mg (0.017mmol) of 4,4'-diethynylbiphenyl and 30 mg(0.5mmol) of KOH in 5 ml of methol were stirred for 1 hour. A solution of Ir(**L3**)(ppy)Cl **(5)** (25mg, 0.033 mmol) and CuI (3 mg, 0.017) in methanol was added and stirred overnight. The target complex precipitated from the solution and is isolated by cenerfuge and washed with methanol (7 mg, 0.005 mmol 53%). ^{1}H-NMR ($CDCl_3$, 400 MHz): δ 10.31 (d, 2H, ^{3}J = 6.0, H^{6}-NC), 8.39 (d, 4H, ^{3}J = 8.0, H^{6}-NCN), 8.10-8.06 (s+d, 4H, $H^{4'}$-NCN+H^{3}-NC), 8.00 (d, 2H, ^{3}J = 5.6, $H^{3'}$-NC), 7.96 (d, 4H, ^{3}J = 4.8, H^{3}-NCN), 7.71-7.63 (t+t, 6H, H^{4}-NCN+H^{4}-NC), 7.50 (t, 2H, ^{3}J = 6.4, H^{5}-NC), 7.16 (d, 4H, ^{3}J = 8.0, $H^{2''\text{ or }3''}$), 6.98 (d, 4H, ^{3}J = 8.4, $H^{2''\text{ or }3''}$), 9.93 (t, 4H, ^{3}J = 6.0, H^{5}-NCN), 6.78 (t, 2H, ^{3}J = 8.0, $H^{4'}$-NC), 6.61 (t, 2H, ^{3}J = 7.2, $H^{5'}$-NC), 5.69 (d, 2H, ^{3}J = 7.2, $H^{6'}$-NC). ^{19}F-NMR ($CDCl_3$, 660 MHz): δ -58.8 (12F, NCN). Mass Spectrometry (MALDI+): *m/z* 714 $[M]^{+}$, = *m/z* 1628 $[M\text{-bridge-}M]^{+}$.

Synthesis of bis[Ir(1,3-di-(2-pyridyl)-4,6-di-trifluoromethylbenzene)(2-phenylpyridine)] 4-4' tetrazolyl-bisphenyl [b[Ir(L3)(ppy)]btrph] (42)

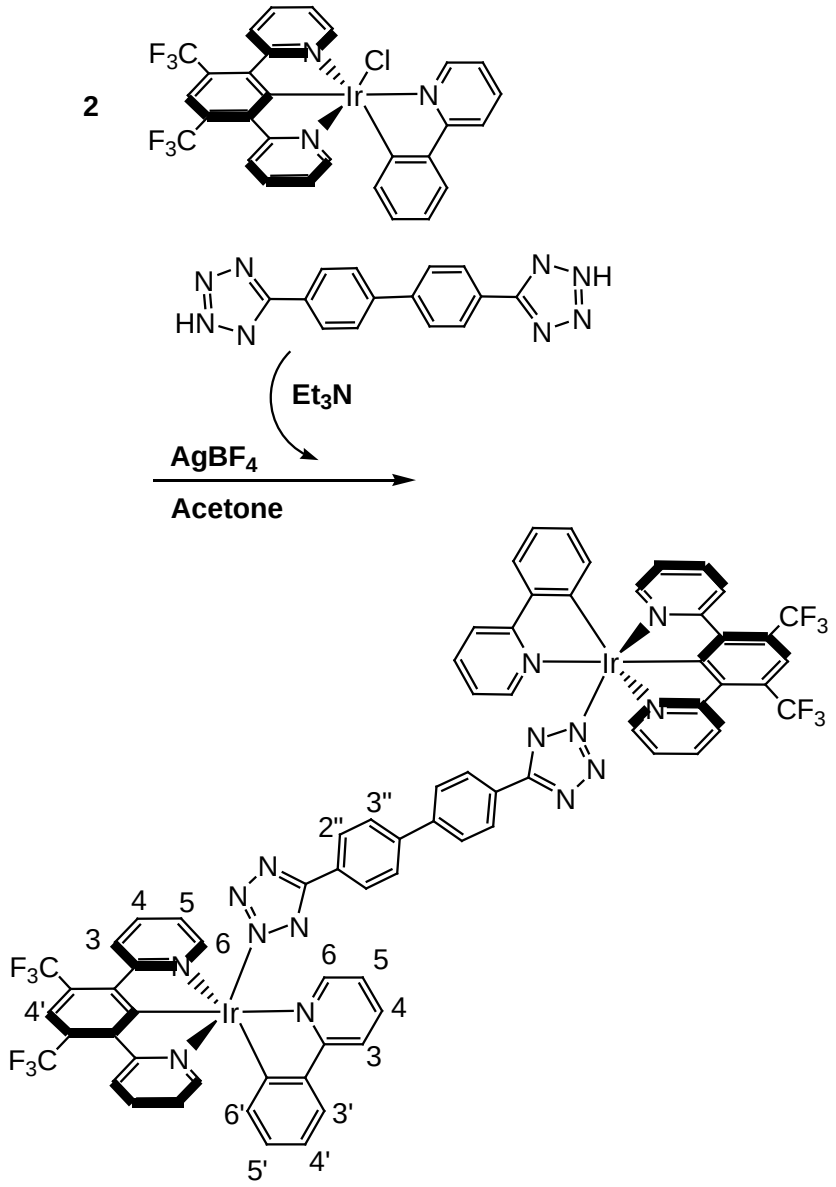

In a schlenk tube were Ir(**L3**)(ppy)Cl **(5)** (50 mg, 0.067 mmol) and $AgBF_4$ (16 mg, 0.073 mmol) in 5 ml of a solution acetone/water 2:1. the apparatus was proteted from light with aluminium foil and the mixture refluxed overnight under nitrogen. After cooling to room temperature, the precipitated AgCl was removed by

centerfuge from the solution of the solvate-complex. Meanwhile a solution of 4-4' tetrazolyl-bis-phenyl (5 mg, 0.033 mmol) in acetone (3 ml) was treated with few drops of Et_3N and stirred for 30 minutes. The solution containing the deprotonated tetrazole was then added dropwise to the solution containing the solvate-complex. The combined mixture was then reflux overnight. After cooling to room temperature, the mixture was diluited with 50 ml of dichloromethane and extractions were performed with 100x3 ml of water. The organic layer was dried over $MgSO_4$ and filtered. Purificetion was achieved after silica gel chromatography (DCM/MeOH 95:5). The product was an orange solid (6 mg, 0.0035 mmol, 10%). ^{1}H-NMR (CD_3Cl, 400 MHz): δ 8.87 (2H, dd, ^3J = 8.8, ^4J = 1.6, H^6-NC), 8.39 (4H, d, ^3J = 8.4, H^6-NCN), 8.14 (2H, d, ^3J = 8.4, H^3-NC), 8.04-7.96 (8H, s+d+t, $H^{4'}$-NCN+H^3-NCN+H^4-NC), 7.85-7.64 (8H, d+td, $H^{2''\text{ or }3''}$+H^4-NCN), 7.65 (2H, dd, ^3J = 8.4, 1.6, $H^{3'}$-NC), 7.48 (4H, d, ^3J = 8.8, $H^{2''\text{ or }3''}$), 7.42 (2H, td, ^3J = 8.4, ^4J = 0.8, H^5-NC), 7.06 (4H, td, ^3J = 7.2, ^4J = 2.4, H^5-NCN), 6.84 (2H, td, ^3J = 7.6, ^3J = 2.4, $H^{4'}$-NC), 6.68 (2H, td, ^3J = 7.6, ^4J = 2.4, $H^{5'}$-NC), 5.85 (2H, dd, ^3J = 7.6, ^4J = 1.6, $H^{6'}$-NC). ^{19}F-NMR: δ -77.6 (12F, NCN). Mass Spectroscopy (MALDI+): *m/z* 714 $[M]^+$, = *m/z* 1717 $[M\text{-bridge-}M]^+$. HRMS (ES+): *m/z* 1713.2852 $[M\text{-bridge-}M]^+$. Calcd for $C_{72}H_{42}N_{14}F_{12}{}^{191}Ir$: *m/z* 1713.2816.

CHAPTER 6

BIBLIOGRAPHY

Bibliography

1. K. Kalyanasundaram, *Photochem. of Polypyridine and Porphyrin Complexes;* Academic Press: London, U.K., 1992.
2. M. Z. Hoffmann, Ed. *Inorg. Photchem., State of the Art. J. Chem. Educ.*1983, **60**, 784.
3. V. Balzani, F. Bolletta, M. T. Gandolfi, M. Maestri, *Top. Curr. Chem.*, 1978, **75**, 1.
4. A. P. De Silva, H. Q. N. Gunaratne, T. Gunnlaugsson, A. J. M. Huxley, C. P. McCoy, J. T. Rademacher, and T. E. Rice, *Chem. Rev.*, 1997, **97**, 1515.
5. V. Balzani, F. Scandola, *Supr. Photochem.; Ellis Horwood: New York*, 1991.
6. E. M. Kober, J. V. Caspar, R. S. Lumpkin, T. J. Meyer, *J. Phys. Chem.*, 1986, **90**, 3722.
7. J. V. Caspar, E. M. Kober, B. P. Sullivan, T. J. Meyer, *J. Am. Chem. Soc.* 1982, **104**, 630.
8. J. V. Caspar, T. J. Meyer, *Inorg. Chem.* 1983, **22**, 2444.
9. J. V. Caspar, T. J. Meyer, *J . Phys. Chem.* 1983, **87**, 952.
10. D. M. Roundhill, *Photochem. and Photophys. of Metal Complexes. Plenum Press, New York and London*, 1994.
11. G. B. Porter, *Intr. to Inorg. Photochem.,* 1983, **60**, 785.
12. P. W. Atkins, *Physical Chemistry, Fifth Edition, Oxford University Press*.
13. R. P. Wayne, *Principles and applications in Photochem., Oxford University Press,* 1988.
14. A. W. Adamson, *Properties of Excited States,* 1983, **60**, 797.
15. G. A. Crosby, R. J. Watts, D. H. Carstens, *Science*, 1970, **170**, 1195.
16. V. Balzani, F. Bolletta, M. T. Gandolfi, M. Maestri, *Top. Curr. Chem.*, 1978, **75**, 1.
17. M. K. De Armond, C. M. Carlin, *Coord. Chem. Rev.*, 1981, **36**, 325.
18. V. Balzani, A. Juris, M. Venturi, S. Campagna, and S. Serroni, *Chem. Rev.*, 1996, **96**, 759.
19. T. J. Meyer, *Pure Appl. Chem.*, 1990, **62**, 1003.

20. W. E. Jones, S. M. Baxter, G. F. Strouse, T. J. Meyer, *J. Am. Chem. Soc.* 1993, **115**, 7363.
21. G. A. Crosby, *Structure, Bonding and Excited States of Coordination Complexes,* 1983, **60**, 79.
22. J. Michl, *Handbook of Photochem..*
23. M. Kasha, *Discuss. Faraday Soc.*, 1950, **9**, 14.
24. V. Whittle, *Synthesis and Luminescence of Iridium and Rhodium Complexes Incorporating NCN-Coordinating Terdentate Ligands,* Durham University, Department of Chemistry, PhD thesis.
25. J. R. Lakowicz, *'Principles of Fluoresence Spectroscopy'*, *Plenum Press,* 1999.
26. A. Gilbert and J. Baggott, '*Essentials of Molecular Photochem.*', *Blackwell Scientific Publications,* 1991.
27. A. Juris, V. Balzani, F. Barigelletti, S. Campagna, P. Besler, A. Von Zelewsky, *Coord. Chem. Rev.,* 1988, **84**, 85.
28. M. J. Cook, A. P. Lewis, G. S. G. McAuliffe, V. Skarda, A. J. Thomson, J. L. Glasper, D. J. Robbins, *J. Chem. Soc. Perkin Trans.*, *2,* 1984, 1293.
29. B. Higgins, B. A. DeGraff, J. N. Demas, *Inorg. Chem.*, 2005, **44**, 6662.
30. K. K. W. Lo, W. K. Hui, C. K. Chung, K. H. K. Tsang, D. C. M. Ng,N. Zhu, K. K. Cheung, *Coord. Chem. Rev.*, 2005, **249**, 1434.
31. F. E. Lytle and D. M. Hercules, *J. Am. Chem. Soc.*, 1969, **91**, 253.
32. D. M. Klassen and G. A. Crosby, *J. Chem. Phys.*, 1968, **48**, 1853.
33. G. A. Crosby, W. G. Perkins, and D. M. Klassen, *J. Chem. Phys.*, 1965, **43**, 1498.
34. J. Paris, W. W. Brandt, *J. Am. Chem. Soc.*, 1959, **81**, 5001.
35. J. N. Demas, G. A. Crosby, *J. Mol. Spectrosc.*, 1968, **26**, 72.
36. D. P. Rillema, D. S. Jones, and H. A. Levey, *J. Chem. Soc., Chem. Commun.*, 1979, 849.
37. C.J. Elsevier, J. Reedijk, P.H. Walton, M.D. Ward, *J. Chem. Soc. Dalton Trans.* 2003, 1869.
38. N. Sutin, *A. Chem. Res.*, 1982, **15**, 275.
39. V. Balzani, A. Credi, M. Venturi, *Molecular Devices and Machines –A Journey into the Nanoworld, Wiley-VCH, Weinheim*, 2003.

40. N. Armaroli, Photochem. Photobiol. *Sci. 2*, 2003, 73.
41. E. C. Constable, C. E. Housecroft, A. M. W. Cargill-Thompson, P. Passaniti, S. Silvi, M. Maestri, and A. Credi, *Inorg. Chim. Acta*, 2007, **360**, 1102.
42. M. Maestri, N. Armaroli, V. Balzani, E.C. Constable, A.M.W. Cargill Thompson, *Inorg. Chem.*, 1995, **34**, 2759.
43. G.J.E. Davidson, S.J. Loeb, P. Passaniti, S. Silvi, A. Credi, *Chem. Eur. J.*, 2006, **12**, 8926.
44. J.P. Collin, S. Guillerez, J.P. Sauvage, *J. Chem. Soc*., Chem. Comm., 1989, 776.
45. P.P. Laine´, F. Bedioui, F. Loiseau, C. Chiorboli, S. Campagna, *J. Am. Chem. Soc.*, 2006, **128,** 7510.
46. V. Balzani, *Ed. Supr. Photochem.y; Reidel: Dordrecht, The Netherlands.*, 1987.
47. F. Scandola, M. T. Indelli, C. Chiorboli, C. A. Bignozzi, *Top. Curr. Chem.*, 1990, **58,** 73.
48. G. Orellana, C.A. Ibarra, J. Santoro, *Inorg. Chem.*, 1988, **27**, 1025.
49. G. Orellana, A. Kirsch-De Mesmaeker, N.J. Turro, *Inorg. Chem.*, 1990, **29**, 882.
50. R. T. Brown, N. C. Fletcher, M. Nieuwenhuyzen, and T. E. Keyes, *Inorg. Chim. Acta*, 2005, **358**, 1079.
51. E. A. P. Armstrong, R. T. Brown, M. S. Sekwale, N. C. Fletcher, X. Q. Gong, and P. Hu, *Inorg. Chem.*, 2004, **43**, 1714.
52. J. R. Winkler, T. L. Netzel, C. Cruetz, and N. Sutin, *J. Am. Chem. Soc.*, 1987, **109**, 2381.
53. J. M. Calvert, J. V. Caspar, R. A. Binstead, T. D. Westmoreland, and T. J. Meyer, *J. Am. Chem. Soc.*, 1982, **104**, 6620.
54. E. C. Constable, A. M. W. Cargill-Thompson, N. Armaroli, V. Balzani, and M. Maestri, *Polyhedron*, 1992, **11**, 2707.
55. F. Barigelletti, L. Flamigni, M. Guardigli, A. Juris, M. Beley, S. Chodorowski-Kimmes, J. P. Collin, and J. P. Sauvage, *Inorg. Chem.*, 1996, **35**, 136.
56. A. C. Benniston, V. Goulle, A. Harriman, J. M. Lehn, and B. Marczinke, *J. Phys. Chem.*, 1994, **98**, 7798.

57. T. S. Arrhenius, M. Blanchard-Desce, M. Dvolaitzky, J. M. Lehn, *Proc. Natl. Acad. Sei.*, 1986, **83**, 5355.
58. S.A. Kugimiya,T. Lazrak, J. M. Lehn, *J. Chem. Soc., Chem. Commun.* 1991, 1179.
59. A. Slama-Schwok, M. Blanchard-Desce, J. M. Lehn, *J. Phys. Chem.*, 1990, **94**, 3894.
60. M. Beley, J. P. Collin, J. P. Sauvage, H. Sugihara, F. Heisel, and A. Miehé, *J. Chem. Soc., Dalton Trans.*, 1991, 3157
61. J. R. Kirchhoff, D. R. McMillin, P. A. Marnot and J. P. Sauvage, J. Am. *Chem. Soc.,* 1985,**107**, 1138.
62. F. Barigelletti, L. Flamigni, M. Guardighi, J. P. Sauvage, J. P. Collin, and A. Sour, *Chem. Commun.*, 1996, 1329.
63. E. C. Constable, R. P. G. Henney, T. A. Leese, and D. A. Tocher, *J. Chem. Soc., Dalton Trans.*, 1990, 443.
64. J. P. Collin, M. Beley, and J. P. Sauvage, *Inorg. Chim. Acta*, 1991, **186**, 91.
65. E. C. Constable, *Adu. Znorg. Chem. Radiochem.,* 1987, **30**, 69.
66. M. D. Dixon, J. Collin, J. Sauvage, L. Flamigni, S. Encinas, F. Barigelletti, *Chem Soc. Rev.*, 2000*,* **29**, 385.
67. R. J. Watts, *Comments Inog. Chem.,* 1991, **11**, 303.
68. M. S. Lowry, S. Bernhard, *Chem. Eur. J.*, 2006**, 12**, 7970.
69. M. Maestri, V. Balzani, C. Deuschel-Cornioley, A. von Zelewsky, *Adv. Photochem.*, 1992, **17**, 1.
70. K.J. Arm and J.A.G. Williams*, Dalton Trans., 2006, 2172*.
71. A. P. Wilde, R. J. Watts, *J. Phys. Chem.* 1991, **95**, 622.
72. N. J. Turro, *Modern Mol. Photochem., Benjamin/Cummings, Menlo Park, CA*, 1978.
73. M. G. Colombo, A. Hauser, H. U. G. Sdel, *Inorg. Chem.*, 1993, **32**, 3088.
74. K. A. King, R. J. Watts, *J. Am. Chem. Soc.*, 1987, **109**, 1589.
75. R. E. DeSimone and R. S. Drago, *Inorg. Chem.*, 1969, **8**, 2517.
76. B. Chiswell and S. E. Livingstone, *J. Inorg. Nucl. Chem.*, 1964, **26**, 47.
77. J. A. Broomhead and W. Grumley, *Inorg. Chem.*, 1971, **10**, 2002.
78. S. C. Rasmussen, M. M. Richter, E. Yi, H. Place and K. J. Brewer, *Inorg. Chem.*, 1990, **29**, 3926.

79. B. Martin and G. M. Waind, *J. Chem. Soc.*, 1958, 4282.
80. C. M. Flynn, Jr and J. N. Demas, *J. Am. Chem. Soc.*, 1974, **96**, 1959.
81. B. P. Sullivan and T. J. Meyer, *J. Chem. Soc. Chem. Commun.*, 1984, 403.
82. G. Morgan and F. H. Burstall, *J. Chem. Soc.*, 1937, 1649.
83. L. M. Vogler, B. Scott and K. J. Brewer, *Inorg. Chem.*, 1993, **32**, 898.
84. N. P. Ayala, C. M. Flynn, L. Sacksteder, J. N. Demas, B. A. Degraff, *J. Am. Chem. Soc.*, 1990, **112**, 3837.
85. J. P. Collin, I. M. Dixon, J. P. Sauvage, J. A. G. Williams, F. Barigelletti and L. Flamigni, *J. Am. Chem. Soc.*, 1999, **121**, 5009.
86. A. Tsuboyama, H. Iwawaki, M. Frugori, T. Mukaide, J. Kamatani, S. Igawa, T. Moriyama, S. Miura, T. Takiguchi, S. Okada, M. Oshino, K. Ueno, *J. Am. Chem. Soc.,* 2003, **125**, 12971.
87. F. Flamigni, A. Barbieri, C. Sabatini, B. Ventura, F. Barigelletti, *Iridium(III) polyammine complexes: spectroscopy, electrochemistry, photophysics and photoinduced procsses in multicomponent arrays, Instituto per la sintesi Organica e la Fotoreattività del Consiglio Nazionale delle Ricerche, ISOF-CNR, Bologna, Italy*
88. W. Leslie, A. S. Batsanov, J. A. K. Howard, J. A. G. Williams, *Dalton Trans.*, 2004, 623.
89. W. Leslie, R.A. Poole, P. R. Murray, L. J. Yellowlees, A. Beeby, J. A. G. Williams, *Polyhedron*, 2004, **23**, 2769.
90. M. Licini, J. A. G. Williams, *Chem. Commun.*, 1999, 1943.
91. J. P. Sauvage, J. P. Collin, J. C. Chambron, S. Guillerez, C. Coudret, V. Balzani, F. Bariglietti, L. De Cola, L. Flamigni, *Chem. Rev.,* 1994, **94**, 993.
92. F. O. Garces, K. A. King, R. J. Watts, *Inorg. Chem.*, 1988, **27**, 3464.
93. M. Nonoyama, *Bull. Chem. Sac. Jpn.*, 1974, ***47,*** 767.
94. J. Dehand, M. Pfeffer, *Coord. Chem. Reu.*, 1976, **18**, 327.
95. K. Dedeian, P. I. Djurovich, F. O. Garces, G. Carlson, R. J. Watts, *Inorg. Chem.*, 1991, **30**, 1685.
96. A. B. Tamayo, B. D. Alleyne, P. I. Djurovich, S. Lamansky, I. Tsyba, N. N. Ho, R. Bau, M. E. Thompson, *J. Am. Chem. Soc.*, 2003, **125**, 7377.

97. M. G. Colombo, T. C. Brunold, T. Riedener, H. U. Gudel, *Inorg. Chem.*, 1994, **33**, 545.
98. V. V. Grushin, N. Herron, D. D. LeCloux, W. J. Marshall, V. A. Petrov, Y. Wang, *Chem. Commun.*, 2001, 1494.
99. J. C. Ostrowski, M. R. Robinson, A. J. Heeger, G. C. Bazan, *Chem. Commun.* 2002, 784.
100. M. Nonoyama, *Bull. Chem. SOC. Jpn*., 1974**, *47,*** 767.
101. P. J. Steel, F. Lahousse, D. Lerner, C. Marzin, *Inorg*. *Chem.*, 1983, **22**, 1488.
102. P. J. Steel, E. C. Constable, *J. Chem. Soc., Dalton Trans*., 1990, 1389.
103. S. Sprouse, K. A. King, P. J. Spellane and R. J. Watts, *J. Am. Chem. Soc.*, 1984, **106**, 6647.
104. M. A. Baldo, M. E. Thompson, and S. R. Forrest, *Nature*, 2000, **403**, 750.
105. F. O. Garces, K. Dedeian, N. L. Keder, and R. J. Watts, *Acta Crystallogr., Sect. C: Cryst. Struc. Commun.*, 1993, **49**, 1117.
106. J. A. G. Gareth Williams, A. J.Wilkinson, V. L. Whittle, *Dalton Trans.*, 2008, 1.
107. A. Mamo , I. Stefio , M. F. Parisi, A. Credi, M. Venturi, C. Di Pietro, S. Campagna, *Inorg. Chem.*, 1997, **36**: 5947.
108. A. J. Wilkinson, H. Puschmann , J. A. K. Howard, C. E. Foster, J. A. G. Williams, *Inorg. Chem.*, 2006, **45**, 8685.
109. J. A. Gareth Williams, *Chem. Soc. Rev.*, 2009, **38**, 1783.
110. M. Maestri, N. Armaroli, V. Balzani, E.C. Constable, A.M.W. Cargill Thompson, *Inorg. Chem.*, 1995, **34**, 2759.
111. J. L. Kahl, K. W. Hanck, K. Dearmond, *J. Phys. Chem.*, 1978, **82**, 540.
112. Y. Ohsawa, S. Sprouse, K. A. King, M. K. Dearmond, K. W. Hanck, R. J. Watts, *J. Phys. Chem.*, 1987, **91**, 1047.
113. J. N. Demas, E. W. Harris, C. M. Flynn, D. Diemente, *J. Am. Chem. Soc.*, 1975, **97**, 3838.
114. H. Yersin, *Top. Curr. Chem.*, 2004, **241**, 1.
115. P. Day, N. Sanders, *J. Chem. Soc. A.*, 1967, 1536.

116. J. Li, P. I. Djurovich, B. D. Alleyne, M. Youssufuddin, N. N. Ho, J. C. Thomas, J. C. Peters, R. Bau, M. E. Thompson, *Inorg. Chem.*, 2005, **44**, 1713.
117. M. G. Colombo, A. Hauser, H. U. Güdel, *Top Curr. Chem.*, 1994, **171**, 143.
118. M. K. Nazeeruddin, R. Humphry-Baker, D. Berner, S. Rivier, L. Zuppiroli, M. Graetzel, *J. Am. Chem. Soc.*, 2003, **125**, 8790.
119. J. Brooks, Y. Babayan, S. Lamansky, P. I. Djurovich, I. Tsyba, R. Bau, M. E. Thompson, *Inorg. Chem.* 2002, **41**, 3055.
120. W. J. Finkenzeller, H. Yersin, *Chem. Phys. Lett.* 2003, **377**, 299.
121. W. J. Finkenzeller, P. Stoessel, H. Yersin, *Chem. Phys. Lett.*, 2004, **397**, 289.
122. A. J. Wilkinson, A. E. Goeta, C. E. Foster, J. A. G. Williams, *Inorg. Chem.*, 2004, **43**, 6513.
123. M. Polson, S. Fracasso, V. Bertolasi, M. Ravaglia, F. Scandola, *Inorg. Chem.*, 2004, **43**, 1950.
124. T. Yutaka, S. Obara, S. Oawa, K. Nozaki, N. Ikeda, T. Ohno, Y. Ishii, K. Sakai, M. Haga, *Inorg. Chem.*, 2005, **44**, 4737.
125. F. W. Vanhelmont, H. U. Gudel, M. Fortsch, H. B. Burgi, *Inorg. Chem.*, 1997, **36**, 5512.
126. S. Lamansky, P. Djurovich, D. Murphy, F. Abdel-Razzaq, R. Kwong, I. Tsyba, M. Bortz, B. Mui, R. Bau, M. E. Thompson, *Inorg. Chem.*, 2001, **40**, 1704.
127. S. Lamansky, P. Djurovich, D. Murphy, F. Abdel-Razzaq, H. E. Lee, C. Adachi, P. E. Burrows, S. R. Forrest, M. E. Thompson, *J. of the Am. Chem. Soc.*, 2001, **123**, 4304.
128. V. V. Grushin, N. Herron, D. D. LeCloux, W. J. Marshall, V. A. Petrov, Y. Wang, *Chem. Comm.*, 2001, 1494.
129. R. Ragni, E. A. Plummer, K. Brunner, J. W. Hofstraat, F. Babudri, G. M. Farinola, F. Naso, L. De Cola, *J. of Mater. Chem.*, 2006, **16**: 1161.
130. C. H. Yang, S. W. Li, Y. Chi, Y. M. Cheng, Y. S. Yeh, P. T. Chou, G. H. Lee, C. H. Wang, C. F. Shu, *Inorg. Chem.*, 2005, **44**, 7770.
131. C. S. K. Mak, A. Hayer, S. I. Pascu, S. E. Watkins, A. B. Holmes, A. Kohler, R. H. Friend, *Chem. Comm.*, 2005, 4708.

132. S. C. Lo, *Chem. Mater.*, 2006, 5159.
133. K. Dedeian, J. M. Shi, N. Shepherd, E. Forsythe, D. C. Morton, *Inorg. Chem.*, 2005, **44**, 4445.
134. P. Coppo, E. A. Plummer, L. De Cola, *Chem. Commun.*, 2004, 1774.
135. E. J. Nam, J. H. Kim, B. O. Kim, S. M. Kim, N. G. Park, Y. S. Kim, Y. K. Kim, Y. Ha, *Bull. of the Chem. Soc. of Japan*, 2004, **77**: 751.
136. C. W. Tang, S. A. Van Styke, C. H. Chen, *J. Appl. Phys.*, 1989, **65**, 3610.
137. R. Pohl,; V. A. Montes, J. Shinar, J. Pavel Anzenbacher, *J. Org. Chem.*, 2004, **69**, 1723.
138. P. J. Steel, E. C. Constable, *J. Chem. Soc., Dalton Trans*., **1990**, 1389.
139. M. S. Lowry, W. R. Hudson, R. A. Pascal, Jr., S. Bernhard, J. Am. Chem. Soc. 2004, **126**, 14129.
140. M. Pope, H. Kallman, P. Magnante, *J. Chem. Phys.*, 1963, **38**, 2042.
141. C. W. Tang, S. A. Van Slyke, *Appl. Phys. Lett.*, 1987, **51**, 913.
142. J. D. Slinker, A. A. Gorodetsky, M. S. Lowry, J. Wang, S. Parker, S. Rohl, S. Bernhard, G. G. Malliaras, *J. Am. Chem. Soc.*, 2004, **126**, 2763.
143. L. S. Hung, C. H. Chen, *Mater. Science and Eng.,* 2002, **39**, 143.
144. E. Holder, B. M.W. Langeveld, U. S. Schubert, *Adv. Mater.*, 2005, **17**, 1109.
145. S. Forrest, P. Burrows, M. Thompson, *IEEE Spectrum*, 2000, **37**, 29.
146. Y. Y. Noh, C.L. Lee, J. J. Kim, K. Yase, *J. Chem. Phys.*, 2003, **118**, 2853.
147. J. H. Burroughes, D. D. C. Bradley, A. R. Brown, R. N. Marks, K. Mackay, R. H. Friend, P. L. Burns, A. B. Holmes, *Nature*, 1990, **347**, 539.
148. M. A. Baldo, D. F. O'Brien, Y. You, A. Shoustikov, S. Sibley, M. E. Thompson, S. R. Forrest, *Nature*, **395**, 151.
149. R. C. Evans, P. Douglas, C. J. Winscom, *Coord. Chem. Rev.*, 2006, **250**, 2093.
150. K. Tandon, S. Ramamsesha, S. Mazumbdar, *Phys. Rev. B: Condens. Mater. Phys. Mater.,* 2003, **67**, 109.
151. C. Adachi, M. A. Baldo, S. R. Forrest, S. Lamansky, M. E. Thompson, R. C. Kwong, *Appl. Phys. Lett.,* 2001, **78**, 1622.

152. T. Sajoto, P. I. Djurovich, A. Tamayo, M. Yousufuddin, R. Bau, M. E. Thompson, R. J. Holmes, S. R. Forrest, *Inorg. Chem.*, 2005, **44**, 7992.
153. S. Lamansky, P. Djurovich, D. Murphy, F. Abdel-Razzaq, H. E. Lee, C. Adachi, P. E. Burrows, S. R. Forrest, M. E. Thompson, *J. Am. Chem. Soc.*, 2001, **123**, 4304.
154. C. S. K. Mak, A. Hayer, S. I. Pascu, S. E. Watkins, A. B. Holmes, A. Kçhler, R. H. Friend, *Chem. Commun.*, 2005, 4708.
155. S. Obara, M. Itabashi, S. Tamaki, Y. Tanabe, Y. Ishili, K. Nozaki, M. Haga, *Inorg. Chem.*, 2006, **45**, 8907.
156. C. Schaffner-Hamann, A. Von Zelewsky, A. Barbieri, F. Barigelletti, G. Muller, J. P. Riehl, A. Neels, *J. of the Am. Chem. Soc.*, 2004, **126**: 9339.
157. M. C. DeRosa, P. J. Mosher, C. E. B. Evans, R., *J. Crutchley, Macromol. Symp.*, 2003, **196**, 235.
158. G. Di Marco, M. Lanza, M. Pieruccini, S. Campagna, *Adv. Mat.*, 1996, **8**: 576.
159. G. Di Marco, M. Lanza, A. Mamo, I. Stefio, C. Di Pietro, G. Romeo, S. Campagna, *An.. Chem.*, 1998, **70**, 5019.
160. Y. Amao, Y. Ishikawa, I. Okura, *Anal. Chim. Acta*, 2001, **445**, 177.
161. M. C. De Rosa, P J. Mosher, C. E. B. Evans, R. J. Crutchley, *Macromol. Symp.*, 2003, **196**, 235.
162. M. C. DeRosa, D. J. Hodgson, G. D. Enright, B. Dawson, C. E. B. Evans, R. J. Crutchley, *J. Am. Chem. Soc.*, 2004, **126**, 7619.
163. M. Kirch, J. M. Lehn, J. P. Sauvage, *Helv. Chim. Acta*, 1979, **62**, 1345.
164. K. Kalyanasundaram, J. Kiwi, M. GrUtzel, *Helv. Chim. Acta*, 1978, **61**, 2720.
165. C. V. Krishnan, B. S. Brunschwig, C. Creutz, N. Sutin, *J. Am. Chem. Soc.*, 1985, **107**, 2005.
166. M. S. Lowry, J. I. Goldsmith, J. D. Slinker, R. Rohl, R. A. Pascal, Jr., G. G. Malliaras, S. Bernhard, *Chem. Mater.*, 2005, **17**, 5712.
167. K. K. W. Lo, D. C. M. Ng, C. K. Chung, *Organometallics*, 2001, **20**, 4999.
168. K. K. W. Lo, C. K. Chung, N. Zhu, *Chem. Eur. J*,. 2003, **9**, 475.
169. K. K. W. Lo, C. K. Chung, N. Zhu, *Chem. Eur. J.*, 2006, **12**, 1500.
170. K. K. W. Lo, C. K. Chung, T. K. M. Lee, L. H. Lui, K. H. K. Tsang, N. Zhu, *Inorg. Chem.*, 2003, **42**, 6886.

171. Q. Pei, G. Yu, C. Zhang, Y. Yang, A. J. Heeger, *Science, New Series*, 1995, **269**, 1086.
172. G. Kalyuzhny, M. Buda, J. McNeill, P. Barbara, A. J. Bard, *J. Am. Chem. Soc.*, 2003, **125**, 6272.
173. Y. Yang, Q. Pei, *Appl. Phys. Lett.* ,1996, **68**, 2708.
174. Y. Yang, Q. Pei, *Appl. Phys. Lett.*, 1997, **70**, 1926.
175. U. Mitschke, P. Bauerle, *J. Mater. Chem.*, 2000, **10**, 1471.
176. S. Welter, K. Brunner, J. W. Hofstraat, L. De Cola, *Nature*, 2003, **421**, 54.
177. H. C. Su, H. F. Chen, F. C. Fang, C. C. Liu, C. C. Wu, K. T. Wong, Y. H. Liu, S. M. Peng, *J. Am. Chem. Soc.*, 2008, **130**, 3413.
178. L. Ghizdavu, O. Lentzen, S. Schumm, A. Brodkorb, C. Moucheron, and A. Kirsch-De Mesmaeker, *Inorg. Chem.*, 2003, **42**, 1935.
179. H. M. Burke, J. F. Gallagher, M. T. Indelli, and J. G. Vos, *Inorg. Chim. Acta*, 2004, **357**, 2989.
180. M. T. Indelli, C. Chiorboli, and F. Scandola, *Top. Curr. Chem.*, 2007, **280**, 215.
181. C. M. Flynn and J. N. Demas, *J. Am. Chem. Soc.*, 1974, **96**, 1959.
182. J. N. Demas and G. A. Crosby, *J. Am. Chem. Soc.*, 1970, **92**, 7262.
183. M. E. Frink, S. D. Sprouse, H. A. Goodwin, R. J. Watts, and P. C. Ford, *Inorg. Chem.*, 1988, **27**, 1283.
184. M. G. Colombo, T. C. Brunold, T. Riedener, and H. U. Güdel, *Inorg. Chem.*, 1994, **33**, 545.
185. E. C. Constable, T. A. Leese, and D. A. Tocher, *Polyhedron*, 1990, **9**, 1613.
186. M. G. Colombo, A. Zilian, and H. U. Güdel, *J. Am. Chem. Soc.*, 1990, **112**, 4581.
187. A. Zilian and H. U. Güdel, *Coord. Chem. Rev.*, 1991, **111**, 33.
188. M. G. Colombo, A. Hauser, and H. U. Güdel, *Inorg. Chem.*, 1993, **32**, 3088
189. J. Slinker, D. Bernards, P. L. Houston, H. D. Abruña, S. Bernhard, G. Malliaras, *Chem. Comm.,* 2003, 2393.
190. A. M. W. Cargill, Thompson, *Coord. Chem.*, Rev., 1997, **160**, 1.
191. H. Hofmeier and U. S. Schubert, *Chem. Soc. Rev.*, 2004, **33**, 373.

192. E. C. Constable, *Chem. Soc. Rev.*, 2007, **36**, 226.
193. M. Beley, J. P. Collin, R. Louis, B. Metz and J. P. Sauvage, *J. Am. Chem. Soc.*, 1991, **113**, 8521.
194. H. Bonnemann, *Angew. Chem.*, *Int. Ed. Engl.*, 1978, **17**, 505.
195. Cardenas D. J., Echavarren A. M., Ramirez de Arellano M. C., *Organometallics,* 1999, **18**, 3337.
196. A. Jouaiti, M. Georoy and J. P. Collin, *Inorg. Chim. Acta*, 1996, **245**, 69.
197. M. D. Sindkhedkar, H. R. Mulla, M. A. Wurth, and A. Cammers-Goodwin, *Tetrahedron*, 2001, **57**, 2991.
198. A. J. Wilkinson, '*PhD Thesis*', University of Durham, 2004.
199. L. Arturo Casado, P. Espinet, *J. Am. Chem. Soc.,* 1998, **120**, 35, 8979.
200. The method used was a modification of that described in Allinson G., Bushby R. J., Jesudason M.V., Pailleud J. L., Taylor N. J., *Chem. Soc., Perkin Trans.*, 1997, **2**, 147.
201. M. Beley, S. Chodorowsky, J. P. Collin, J. P. Sauvage, *Tetrahedron Lett.*, 1993, **34**, 2933.
202. A. Rajca, S. Rajca, J. Wongsriratanakul, C. R. Ross, *Polyhedron,* 2001, **20**, 1669.
203. T. Kaminski, P. Gros, Y. Fort, *Eur. J. Org. Chem.*, 2003, 3855.
204. K. A. King, P. J. Spellane, and R. J. Watts, *J. Am. Chem. Soc.*, 1985, **107**, 1431
205. T. Ishiyama, M. Murata and N. Miyaura, *J. Org. Chem.*, 1995, **60**,7508.
206. D. L. Rochester, S. Develay, S. Za Lisj, J. A. G. Williams, *Dalton Trans.*, 2009, 1728.
207. W. Goodall, K. Wild, K. J. Arm and J. A. G. Williams, *J. Chem. Soc., Perkin Trans.*, 2002, **2**, 1669.
208. J. Crocker, 4th year project report, 2010.
209. Akira, Suzuki, *J. Organometallic Chem.,* 2002, **653**, 83.
210. S. Sprouse, K. A. King, P. J. Spellane, R. J. Watts, *J. Am. Chem. Soc.*, 1984, **106**, 6646.
211. P.J. Hay, *J. Phys. Chem. A*, 2002, **106**, 1634.
212. P. Coppo, E.A. Plummer, L. De Cola, *Chem. Commun.* , 2004, 1774.
213. F. Lafolet, S. Welter, Z. Popovic, L. De Cola, *J. Mater. Chem.*, 2005, **15**, 2820.

214. C. Sabatini, A. Barbieri, F. Barigelletti, K.J. Arm, J.A.G. Williams, *Photochem. Photobiol. Sci*. 2007, **6**, 397.
215. S. C. Lo, C. P. Shipley, R. N. Bera, R. E. Harding, A. R. Cowley, P. L. Burn, D. W. I. Samuel, *Chem. Mater.,* 2006, **18**, 5119.
216. J.A.G. Williams, S. Develay, D.L. Rochester, L. Murphy, *Coord. Chem. Rev.,* 2008, **252**, 23.
217. A.F. Rausch, H.H. Homeier, H. Yersin, *Top. Organomet. Chem.,* 2010, **29**, 193.
218. R.E. Harding, S. C. Lo, C.P. Shipley, P.L. Burn, I.D.W. Samuel, *Org. Electron.,* 2008, **9**, 377.
219. M. Cocchi, J. Kalinowski, L. Murphy, J.A.G. Williams, V. Fattori, *Organic Electronics*, 2010, **11**, 388.
220. S. Bettington, M. Tavasli, M. R. Bryce, A. S. Batsanov, A. L. Thompson, H. A. Al Attar, F. B. Dias, A. P. Monkman, *J. Mat. Chem.*, 2006, **16**, 1046.
221. E. A. Plummer, J. W. Hofstraat, L. De Cola, *Dalton Tansactions,* , 2003, 2080.
222. F. Neve, A. Crispini, S. Serroni, F. Loiseau, S. Campagna, *Inorg. Chem.,* , 2001, **40**, 1093
223. J.H. Vandiemen, R. Hage , J. G. Haasnoot, H.E.B. Lempers, J. Reedijk, J.G. Vos, L. De Cola, F. Barigelletti, V. Balzani, *Inorg. Chem.*, 1992, **31**, 3518.
224. P. Coppo , M. Duati , V.N. Kozhevnikov, J.W. Hofstraat, L. De Cola, *Angew. Chem., Internetional Editinon,* **2005**, **44**, 1806.
225. E. C. Constable, *Chem. Commun.*, 1997.
226. K. Sonogashira, Y. Tohda, N. Hagihara. "A convenient synthesis of acetylenes: catalytic substitutions of acetylenic hydrogen with bromoalkenes, iodoarenes and bromopyridines". *Tetrahedron Letters*, 1975, **16**, 4467.
227. P. Brulatti, *Synthesis and characterisation of novel dinuclear complexes of Ru(II) containing tetrazolyl-thiofene bridging ligands, Master's degree Thesis, Department of Industrial Chemistry, University of Bologna,* 2006.
228. K. Nakamaru, *Bull. Chem. Soc. Jpn.*, 1982, **55**, 2697.
229. J. N. Demas and G. A. Crosby, *J. Phys. Chem.*, 1971, **75**, 991.

230. M. J. Frisch, G. W. Trucks, H. B. Schlegel, G. E. Scuseria, M. A. Robb, J. R. Cheeseman, V. G. Zakrzewski, J. A. Montgomery Jr., R. E. Stratmann, J. C. Burant, S. Dapprich, J. M. Millam, A. D. Daniels, K. N. Kudin, M. C. Strain, O. Farkas, J. Tomasi, V. Barone, M. Cossi, R. Cammi, B. Mennucci, C. Pomelli, C. Adamo, S. Clifford, J. Ochterski, G. A. Petersson, P. Y. Ayala, Q. Cui, K. Morokuma, D. K. Malick, A. D. Rabuck, K. Raghavachari, J. B. Foresman, J. Cioslowski, J. V. Ortiz, A. G. Baboul, B. B. Stefanov, G. Liu, A. Liashenko, P. Piskorz, I. Komaromi, R. Gomperts, R. L. Martin, D. J. Fox, T. Keith, M. A. Al-Laham, C. Y. Peng, A. Nanayakkara, M. Challacombe, P. M. W. Gill, B. Johnson, W. Chen, M. N. Wong, J. L. Andres, C. Gonzalez, M. Head-Gordon, E. S. Replogle, and J. A. Pople, in 'Gaussian 98, Revision A.9', Gaussian Inc., Pittsburgh PA, 1998.

231. M. J. Frisch, G. W. Trucks, H. B. Schlegel, G. E. Scuseria, M. A. Robb, J. R. Cheeseman, J. A. Montgomery Jr., T. Vreven, K. N. Kudin, J. C. Burant, J. M. Millam, S. S. Iyengar, J. Tomasi, V. Barone, B. Mennucci, M. Cossi, G. Scalmani, N. Rega, G. A. Petersson, H. Nakatsuji, M. Hada, M. Ehara, K. Toyota, R. Fukuda, J. Hasegawa, M. Ishida, T. Nakajima, Y. Honda, O. Kitao, H. Nakai, M. Klene, X. Li, J. E. Knox, H. P. Hratchian, J. B. Cross, V. Bakken, C. Adamo, J. Jaramillo, R. Gomperts, R. E. Stratmann, O. Yazyev, A. J. Austin, R. Cammi, C. Pomelli, J. W. Ochterski, P. Y. Ayala, K. Morokuma, G. A. Voth, P. Salvador, J. J. Dannenberg, V. G. Zakrzewski, S. Dapprich, A. D. Daniels, M. C. Strain, O. Farkas, D. K. Malick, A. D. Rabuck, K. Raghavachari, J. B. Foresman, J. V. Ortiz, Q. Cui, A. G. Baboul, S. Clifford, J. Cioslowski, B. B. Stefanov, G. Liu, A. Liashenko, P. Piskorz, I. Komaromi, R. L. Martin, D. J. Fox, T. Keith, M. A. Al-Laham, C. Y. Peng, A. Nanayakkara, M. Challacombe, P. M. W. Gill, B. Johnson, W. Chen, M. W. Wong, C. Gonzalez, and J. A. Pople, in 'Gaussian 03, Revision C.02', Gaussian Inc., Wallingford CT, 2003.

232. M. Ishikawa, K. Nonoshita, Y. Ogino, Y. Nagae, D. Tsukahara, H. Hosaka, H. Maruki, S. Ohyama, R. Yoshimoto, K. Sasaki, Y. Nagata, J. Eiki, T. Nishimura, *Bioorg. Med. Chem. Lett.*, 2009, **19**, 4450.

233. P. J. Hay, *J. Phys. Chem. A*, 2002, **106**, 1634.

234. U. S. Shumbert, C. Eschbaumer, M. Heller, *Org. Lett.*, 2000, **2**, 3373.

235. S. P. McIlroy, E. Cló, L. Nikolajsen, P. K. Frederiksen, C. B. Nielsen, K. V. Mikkelsen, K. V. G. Ogilby, P. R. Ogilby, *J. Org. Chem*, 2005, **70**, 1134.

236. M. Kuroboshi, Y. Waki Y., H. Tanaka, *J. Org. Chem.* 2003*,* **68***,* 3942.

237. K, Koguro, T. Oga, S. Mitsui, R. Orita, *Synthesis*, 1998, 910.